DISS. ETH NO. 18515

UAV Photogrammetry

A dissertation submitted to

ETH ZURICH

for the degree of
Doctor of Sciences

presented by

HENRI EISENBEIß

Dipl.-Ing., University of Technology Dresden

born 31st of December 1977

citizen of Germany

accepted on the recommendation of

Prof. Dr. Armin Grün, examiner
Zurich, Switzerland

Prof. Dr. Impyeong Lee, co-examiner
Seoul, Korea

2009

CONTENT

ACKNOWLEDGMENTS

to Peru for archaeological documentations. He supported me through all our discussions, paper writing, mutual reviewing of the thesis at any time and innumerable common field works in Switzerland and around the world.

Moreover, during the thesis writing, I was particularly supported by Tara Lorencak with English corrections. Her hints helped me to improve my skills over the period of thesis writing. In addition, I'm grateful for the valuable and helpful comments of my cousin Tim Flohrer. Additionally, I thank Daniel Krättli, our UAV-pilot, who supported me in all experiments and field mission conducted with our UAV system (Copter 1B).

At IGP, I like to thank all members, former members, students and academic guests who supported my work through their collaboration and man-power, as well as for the help during the UAV field mission. Furthermore, I want to express my special thanks to Beat Rüedin and Emanuel Baltsavias, as well as Thomas Hanusch, David Novák, Natalia Vassilieva and Kirsten Wolff, who contributed their time and expertise to the present research.

Furthermore I thank my project partners and sponsors. Without their valuable contribution, collaboration and financial support this broad study on UAV photogrammetry would not have been possible.

Project partners:
Heli: *Jacques Chapuis, Christoph Eck, Roland Haarbrink, Lars Zander*; Pinchango Alto: *Johny Isla Cuadrado, Karsten Lambers, Markus Reindel, Martin Sauerbier*; Randa: *Valentin Gischig, Frank Lemy, Simon Löw*; UAV-born LiDAR: *Benedikt Imbach, Hannes Püschel, Peter Rieger, Roland Siegwart, Nikolaus Studnicka*; Maize field: *Peter Stamp, Andre Vogler*; Copan: *Jennifer von Schwerin, Heather Ritchards, Fabio Remondino, Martin Sauerbier*; Gravel pit*: Gabriel Flury, Martin Lötscher, Emil Siegrist*; Sarnen: *Ruth Hug, Hannes Püschel, Martin Sauerbier*; Tachymeter Tracking: *Werner Stempfhuber*; Other UAVs: *Kai Jütte, Michael Kolb, Sina Muster, Uwe Niethammer, Paolo Perona;* SU & FC ETH Zurich*: Anne Katrin Thomas, Roman Windlin*.

Companies and Financial support:
Aeroscout, DAI, ETH Zurich, European Union, Geocopter, Helimap, Lötscher Kies + Beton, omnisight, Riegl, SNF, Swiss-UAV, UNESCO, weControl.

ABSTRACT

UAVs are unmanned aerial vehicles. Hence, UAV photogrammetry can be understood as a new photogrammetric measurement tool. UAV photogrammetry opens various new applications in the close range domain, combining aerial and terrestrial photogrammetry, but also introduces low-cost alternatives to the classical manned aerial photogrammtery. This thesis deals with the challenging task: *"The use of UAV systems as photogrammetric data acquisition platforms"* and the work was conducted by the author at IGP at ETH Zurich from 2003 to 2009.

In this work, a new terminology, *UAV Photogrammetry*, was introduced. UAV Photogrammetry describes photogrammetric measurement platforms, which operate as either remotely controlled, semi-autonomously, or autonomously, all without a pilot sitting in the platform, and the photogrammetric processing of UAV images. The broad definition covers balloons, kites, gliders, airships, rotary and fixed wing UAVs with the capability for photogrammetric data acquisition in manual, semi-automated and automated flight mode. To more clearly define UAVs, a comprehensive literature review on UAVs used in photogrammetry will be given. Using the existing categorizations of UAVs, the outcome of the literature review and our experiments, a new classification for UAVs, with respect on low-cost and high-end systems, the real-time processing capability (based on the integrated sensors and the flight performance, as well as the influence of environmental conditions), was provided. For this work, UAV systems, based on the new classification, will be selected to demonstrate how UAVs can be applied for photogrammetric data acquisition and processing.

In addition to the revised definitions and classifications of UAVs, we have devised a new generic workflow for the photogrammetric UAV flight planning, image acquisition, quality control and data processing. This workflow can specifically be adapted to individual UAV-systems and applications. Thus, specific tools, such as flight planning, are developed. Based on our results, UAV flight control systems and the flight operations were improved and commercial and in-house developed software packages were additionally evaluated for the processing of UAV image data. The proposed workflow allows the combination of office and field work, enabling the first results to be available during the field work for preliminary

analysis.

This dissertation also emphasizes the influence of the manual, assisted and autonomous control of the UAV system on the flight performance during the data acquisition, which in turn influences the results and the feasibility of the photogrammetric data processing. Therefore, an autonomous tachymeter tracking of the flight trajectory was performed firstly with an UAV system. A test field for UAVs was then established at the campus Hönggerberg at ETH Zurich. This test field enables us to assess the flight performance of various UAV systems. Specifically, an UAV system combined with a light weight laser scanner acquired a DSM over our test field.

Complementary to the developed workflow the accomplished real world application, this work has shown the great potential of using UAVs in photogrammetry and upcoming applications. The focus of our applications was particularly on archaeology and environmental applications, which allowed us to prove our established workflow and to underline the high potential of UAV systems for specific photogrammetric tasks, specifically the use of autonomous operated and stabilized UAV systems.

- In the frame of the Nasca/Palpa project, the pre-Inca settlement Pinchango Alto (Peru) was documented with our autonomous flying model helicopter. For the first time an accurate and dense elevation model (10cm resolution) of an archaeological site was generated automatically using our in-house developed software. A detailed analysis of the generated data was done using terrestrial laser scanning data. The comparison of both data sets showed that the mean difference between the elevation models was less than 1cm with a standard deviation of 6cm.

- The world heritage Maya site Copán (Honduras) was documented with our system in 2009. The preliminary results, achieved directly after the data acquisition, underlined the expectations and potentials for up-coming archaeological analysis and investigations.

- The castle Landenberg was documented with 1cm resolution using terrestrial and UAV images.

- In the framework of this dissertation, the rockslide Randa (Switzerland) was documented with LiDAR and image data taken from a manned helicopter. The results from the manned system were compared to the observed data from a UAV for a small part of the rockslide. The elevation model generated from the UAV image data had a substantial higher resolution and showed less occlusions than the LiDAR data. These differences result from the possibility to acquire image data close to the rockslide using an autonomous operated UAV, without endangering human life, and using a specific flight planning tool for UAVs in mountainous areas. This particular application showed also the

limitations of existing UAVs in the data acquisition in Alpine areas, due to the high altitudes. However recent developments of new UAV systems are now ready in future work to operate in Alpine areas.

- Using a quadrotor, equipped with a light weight compact camera, it was possible to generate elevation models of a gravel pit at different time periods (February and April). The image data was acquired in the semi-automated and automated mode, allowing an estimation of the volume dug from the pit over time.

- An UAV was used in a study for the evaluation of genetically modified maize (simulated) on conventional maize. High resolution elevation models and orthoimages were produced from two campaigns. The generated spatial data was integrated into a GIS and then used with measures for the out-crossing in maize, to analyse the inclination, height, distance and wind on the influence of cross-pollination in maize.

Finally, based on the experimental results, a new particular workflow for combination of image and LiDAR sensors on one UAV platform was provided.

ZUSAMMENFASSUNG

Der Begriff UAV steht für unbemannte Luftfahrzeuge, somit kann UAV Photogrammetrie als neue photogrammetrische Aufnahmemethode unter Verwendung von unbemannten Luftfahrzeugen aufgefasst werden. Die Verwendung von UAV Photogrammtrie erlaubt neue Anwendungen im Nahbereich und in der Kombination von Luftbild- und Nahbreichsphotogrammetrie. Mit UAVs ergeben sich low-cost Alternativen zur klassischen bemannten Luftbildphotogrammetrie. Die vorliegende Dissertation beschäftigt sich mit der *„Verwendung von UAV-Systemen (unbemannte Luftfahrzeuge) als photogrammetrische Datenakquisitionsplattform"* und wurde in der Periode von 2003 bis 2009 am Institut für Geodäsie und Photogrammetrie (IGP) der ETH Zürich vom Autor der Arbeit verfasst.

In dieser Arbeit wird der Begriff UAV-Photogrammetrie neu eingeführt. Er beschreibt ein photogrammetrisches Aufnahmesystem, welches manuell, halbautomatisch oder automatisch gesteuert und kontrolliert werden kann und die photogrammetrische Auswertung von UAV Bildern. Das heisst, es ist kein Pilot an Bord des Systems.

Die Systeme beinhalten Ballons, Drachen, Gleitschirme, Luftschiffe, Hubschrauber, Quadkopter und Flächenflieger. In diesem Zusammenhang wird eine umfassende Literaturübersicht gegeben, die UAVs mit Anwendungen in der Photogrammetrie darstellt.

Unter Verwendung vorhandener Klassifizierungen von UAVs anhand der vorliegenden Literaturstudie und den durchgeführten Experimenten für diese Arbeit sind neue Klassifikationsmethoden für UAVs definiert. Diese Klassifikationen unterscheiden zwischen low-cost und high-end Systemen und der Kapazität für den Echtzeitprozess in Abhängigkeit vom implementierten Sensor und Umwelteinflüssen.

Es wurden verschiedene UAV-Systeme für die Untersuchungen auf ihre Anwendbarkeit von UAV-Systeme als photogrammetrische Datenakquisitionsplattformen ausgewählt. Basis bildeten spezifische gegebene Klassifikationen. Die ausgewählten Systeme werden in dieser Arbeit vorgestellt und untersucht. Zudem wurde ein allgemeiner Workflow für die Flugplanung, Akquisition und Prozessierung von UAV-Bilddaten entwickelt. Abhängig vom UAV-System und dessen Anwendung kann der Workflow an die Gegebenheiten vor Ort angepasst werden. Dafür wurden spezielle Tools, wie zum Beispiel Bildflugplanung für

UAVs entwickelt. Basierend auf den erzielten Ergebnissen sind die Flugsteuerungssysteme angepasst, das Flugverhalten verbessert und kommerzielle sowie am IGP entwickelte photogrammetrische Softwarepakete für das Prozessieren von UAV-Bilddaten analysiert worden. Der generierte Workflow ermöglicht die Kombination von Feld- und Büroarbeiten, so dass die Ergebnisse für erste Analysen im Feld verwendet werden können.

Diese Arbeit beschäftigt sich auch mit dem Einfluss von manueller, halbautomatisch und automatisch durchgeführter Steuerung auf die Flugeigenschaften der UAV-Flüge und die photogrammetrische Auswertbarkeit der erfassten Bilddaten. Das Flugverhalten und die Positionierungsgenauigkeit einer UAV-Plattform werden damit erstmalig mittels automatischer Verfolgung und Messen mittels eines Tachymeters durchgeführt. Für diese Analysen wurde ein Testfeld am Campus Hönggerberg der ETH Zürich angelegt. Dieses Testfeld erlaubt die Untersuchung der Flugtrajektorie und –performance von verschiedenen UAVs. Zusätzlich zu der Untersuchung mit dem Tachymeter konnten mit einem Laserscanner integriert an einem UAV ein Höhenmodell vom Testfeld generiert werden.

Ergänzend zum entwickelten Workflow sind im Rahmen dieser Arbeit verschiedene Anwendungen mit UAVs in der Photogrammetrie in den letzten 5 Jahren durchgeführt worden. Die Ergebnisse zeigen das grosse Potential der Plattformen für die Verwendung in der Photogrammetrie und zukünftigen Anwendungen auf. Der Fokus bei den Anwendungen wurde dabei auf die Archäologie und auf die Dokumentation unserer Umwelt gelegt. Die durchgeführten Anwendungen erlaubten die Bestätigung des generierten Workflows und betonten das grosse Potential von UAV-Systemen (besonders für autonome und stabilisierte Systeme) für ausgewählte photogrammetrische Aufgaben.

- Im Rahmen des Nasca-Palpa Projektes wurde die Prä-Inka Siedlung Pinchango Alto (Peru) mit einem autonom fliegenden Modellhelikopter dokumentiert. Zum ersten Mal konnte ein genaues und hochaufgelöstes (10cm Auflösung) Höhenmodel einer archäologischen Siedlung automatisch mit einem am Institut entwickelten Softwarepaket generiert werden. Das berechnete Höhenmodell wurde mittels eines mit terrestrischen Laserscanning generiertem Höhenmodell detailliert analysiert. Die Differenz der beiden Höhenmodelle ergab einen mittleren Offset von weniger als einem Zentimeter und einer Standardabweichung von sechs Zentimeter.

- Die zum UNESCO Weltkulturerbe zählende Maya Tempelanlage Copán (Honduras) wurde mit dem gleichen UAV-System im Rahmen von Feldarbeiten im April 2009 dokumentiert. Die ersten Ergebnisse direkt nach der Datenaufnahme bestätigen das grosse Potential der UAV-Bilddaten für zukünftige archäologische Arbeiten.

- Das Schloss Landenberg wurde mit einer Auflösung von einem Zentimeter mittels kombinierter Auswertung von terrestrischen und UAV-Bilddaten aufgenommen.

- Im Rahmen der vorliegenden Dissertation wurde der Felssturz bei Randa (Schweiz) mit luftgestütztem LiDAR und Bilddaten von einem bemannten Helikopter aufgenommen und ist somit dokumentiert. Die vom bemannten Flug aus generierten Daten wurden für ein kleineres Gebiet zusätzlich auch mittels UAV-Bilddaten aufgenommen. Aufgrund der präzisen Planung in steilem Gebiet erlaubte das verwendete UAV nahe am Objekt zu operieren ohne menschliches Leben zu gefährden. Jedoch zeigte das Projekt unter anderem auch die Grenze von UAV-Flügen in höheren Lagen der alpinen Gebiete. Neuere technische Entwicklungen zeigen jedoch, dass UAV-Systeme verbessert werden können, so dass diese in zukünftigen Arbeiten in diesen Regionen eingesetzt werden können.

- In einem weiteren Projekt wurden mittels Bilddaten, aufgenommen von einer Kompaktkamera von einem Quadkopter, zwei Höhenmodelle einer Kiesgrube zu verschiedenen Zeitpunkten generiert. Die Bilddaten konnten halbautomatisch und automatisch aufgenommen werden. Mittels der generierten Daten ist eine Volumenabschätzung des abgebauten Gebietes durchgeführt worden.

- Ein Beispiel aus der Agronomie beschäftigt sich mit der Untersuchung des Einflusses von genmodifiziertem Mais (simuliert) auf natürlichen Mais. Dafür wurden von Maisfeldern in zwei Messkampagnen Höhenmodelle und Orthobilder generiert. Die erzeugten Daten wurden gemeinsam mit der Auskreuzungsrate in ein GIS (Geographisches Information System) integriert und der Einfluss des transgenen Mais auf natürlichem Mais im Bezug auf Neigung, Höhe, Distanz und Windeinflüsse analysiert.

Abschliessend wurde mit den gewonnen Ergebnissen aus den Experimenten ein Workflow für die Kombination von LiDAR- und Bildsensoren für ein UAV-System gegeben.

I. LIST OF FIGURES

II.   LIST OF TABLES

III. ABBREVIATIONS

2D	2 Dimensional
3D	3 Dimensional
ASCII	American Standard Code for Information Interchange
AT	Aerial Triangulation
BAZL	Bundesamt für Zivilluftfahrt – Federal Office for Civil Aviation (FOCA)
BUN	Bundle adjustment software package at ETH Zurich
CCD	Charge-coupled device
cm	centimeter
CAA	Civil Aviation Authority
CASA	Civil Aviation Safety Authority
CMOS	Complementary metal-oxide-semiconductor
CP	Check Points
DAI	Deutsches Archäologisches Institut – German Archaeological Institute
DG	Direct Georeferencing
DGPS	Differential Global Positioning System
DSM	Digital Surface Model
DTM	Digital Terrain Model
EASA	European Aviation Safety Agency
EU	European Union
FAA	Federal Aviation Administration
GCP	Ground Control Point
GCS	Ground Control Station
GDOP	Geometric Dilution of Precision
GHz	Gigahertz
GIS	Geographic Information System
GNSS	Global Navigation Satellite System
GPS	Global Positioning System
GSD	Ground Sampling Distance

GSM	Global System for Mobile communications; originally from Groupe Spécial Mobile
HazNETH	Research Network on Natural Hazards at ETH Zurich
IC	Inter Commission
IHAH	Honduran Institute of Anthropology and History
IMG	File extension IMG: ERDAS Imagine image file
IMU	Inertial Measurement Unit includes error compensation
INS	Inertial Navigation System includes error compensation and a navigation computer
ISDM	Image Station Digital Mensuration (Z/I)
ISSD	Image Station Stereo Display (Z/I)
KAAK	Kommission für Archäologie Aussereuropäischer Kulturen (Commission for Archaeology of Non-European Cultures)
L-class	Large payload UAVs
LiDAR	Light Detection and Ranging
Laser	The acronym laser stands for Light Amplification by Stimulated Emission of Radiation
Laser-DSM	Digital Surface Model generated out of Laser data
LIP	Late Intermediate Period
LMS-Q240i-60	Type of an Airborne laser scanner (Riegl)
LMS-Z420i	Type of an Terrestrial laser scanner (Riegl)
LPS	Leica Photogrammetry Suite
LS3D	Least Squares 3D Surface Matching
m	Meter
mm	Millimeter
a.s.l.	Above sea level
MAV	Micro Aerial Vehicle
M-class	Micro & Mini UAV systems
MEMS	Microelectromechanical systems
MHz	Megahertz
MMS	Mobile Mapping Systems
MTOM	Maximum Take-Off Mass
NASA	National Aeronautics and Space Administration
OM-class	Open source and manual controlled systems
Pt/m^2	Points per square meter
RC-helicopter	Remote controlled helicopter
Radar	Radio Detection and Ranging

RMAX	Type of a model helicopter from Yamaha (Yahama, 2009)
RMSE	Root Mean Square Error
ROA	Remotely Operated Aircraft
RPA	Remotely Piloted Aircraft
RPV	Remotely Piloted Vehicle
SAT-PP	Satellite Image Precision Processing
SLR camera	Single-lens reflex camera
TBD	To be defined
TIN	Triangulated irregular network
SNF	Schweizer National Font
UA	Unmanned Aircraft
UAS	Unmanned Aircraft System consists of an Unmanned Aircraft (UA), a Control System (CS) -usually a Ground Control System (GCS) - and a communications data link between the UA and the CS.
UAV	Unmanned Aerial Vehicle
UAV BT	Block Triangulation of image data acquired from an UAV
UAV-DSM	Digital Surface Model which was generated out of image data taken from an UAV
UHF	Ultra High Frequency
U.S.	United States
UTM	Universal Transverse Mercator
UV	Unmanned Vehicle
UVS	Unmanned Vehicle System
VRML	Virtual Reality Modeling Language
VTOL	Vertical takeoff and landing
WITAS	The Wallenberg Laboratory for research on Information Technology and Autonomous Systems
WGS84	World Geodetic System 1984
XML	Extensible Markup Language
Z/I	Zeiss Intergraph

1 Introduction

Figure 1-1: Model helicopter flying over the Campus Hönggerberg (ETH Zurich).

1.1   Definition of UAVs

"UAVs are to be understood as uninhabited and reusable motorized aerial vehicles." states van Blyenburgh, 1999. These vehicles are remotely controlled, semi-autonomous, autonomous, or have a combination of these capabilities. Comparing UAV to manned aircraft, it is obvious that the main difference between the two systems is that on the UAV no pilot is physically present in the aircraft. This does not necessarily imply that an UAV flies by itself autonomously. In many cases, the crew (operator, backup-pilot etc.) responsible for a UAV is larger than that of a conventional aircraft (Everaerts, 2008).

The term UAV is commonly used in the Computer Science, Robotics and Artificial Intelligence, as well as the Photogrammetry and Remote Sensing communities. Additionally, synonyms like Remotely Piloted Vehicle (RPV), Remotely Operated Aircraft (ROA) or Remotely Piloted Aircraft (RPA) and Unmanned Vehicle Systems (UVS) can also infrequently be found in the literature. RPV is a term to describe a robotic aircraft flown by a pilot using a ground control station. The first use of this term may be addressed to the United States (U.S.) Department of Defense during the 1970's and 1980's. The terms ROA and RPA have been used by National Aeronautics and Space Administration (NASA) and Federal Aviation Administration (FAA) in the U.S. in place of UAV. Furthermore, the term Unmanned Aircraft System (UAS) is also being used (Colomina, et al., 2008). The FAA has adopted the generic class UAS, which was originally introduced by the U.S. Navy. Common understanding is that the terminology UAS stands for the whole system, including the Unmanned Aircraft (UA) and the Ground Control Station (GCS).

1.1.1 UAV photogrammetry

The new terminology UAV photogrammetry (Eisenbeiss, 2008c) describes a photogrammetric measurement platform, which operates remotely controlled, semi-autonomously, or autonomously, without a pilot sitting in the vehicle. The platform is equipped with a photogrammetric measurement system, including, but not limited to a small or medium size still-video or video camera, thermal or infrared camera systems, airborne LiDAR system, or a combination thereof. Current standard UAVs allow the registration and tracking of the position and orientation of the implemented sensors in a local or global coordinate system. Hence, UAV photogrammetry can be understood as a new photogrammetric measurement tool. UAV photogrammetry opens various new applications in the close range domain, combining aerial and terrestrial photogrammetry, but also introduces new (near-) real time application and low-cost alternatives to the classical manned aerial photogrammtery (see Table 1-1). A detailed study on real-time data collection using airborne sensors including UAVs can be found in Kerle, et al., 2008.

Table 1-1: Features of Aerial, close range and UAV photogrammetry.

	Aerial	Close Range	UAV
Planning	(semi-)automatic	manual	automatic-manual
Data acquisition / Flight	assisted/manual	autonom/assisted/manual	autonom/assisted/manual
Size of the area	km^2	$mm^2 - m^2$	$m^2 - km^2$
Image resolution /GSD	cm-m	mm - dm	mm - m
Distance to the object	100m- 10km	cm - ~300m	m - km
Orientation	normal case, recently also oblique	normal/oblique	normal/oblique
Absolut accuracy of the initial orientation values	cm - dm	mm-m	cm - 10m
Image block size/ number of scans	10 - 1000	1 - 500	1 - 1000
Special applications (examples) and features	large scale areas (Mapping, Forestry, Glaciology, 3D-City modeling)	small-scale areas and objects (archaeological documentation, 3D modeling of buildings)	small- and large-scale areas (archaeological documentation, monitoring of hazards, 3D modeling of buildings and objects)
		architectural and industrial photogrammetry	applications in inaccessible areas and dangerous objects
	aerial view	terrestrial view	aerial view
			real-time applications (monitoring)

Existing UAVs can be used in large-scale and small-scale applications. The system price may vary within some orders of magnitude, depending on the complexity of the system. With costs between €1000 up to several millions of Euro, the system can be similar or even higher priced compared to a standard manned aircraft system. However, the focus of this study is more on low-cost UAV systems for applications. The subsequently presented advantages and limitations of UAV photogrammetry in comparison to the existing methods are thus mostly valid for low-cost systems and small-scale applications, only.

1.1.2 Advantages of UAVs

Major advantages of UAVs compared to manned aircraft systems are that UAVs can be used in high risk situations without endangering a human life and inaccessible areas, at low altitude and at flight profiles close to the objects where manned systems cannot be flown. These regions are for example natural disaster sites, e.g. mountainous and volcanic areas, flood plains, earthquake and desert areas and scenes of accidents. In areas where access is difficult and where no manned aircraft is available or even no flight permission is given, UAVs are sometimes the only practical alternative. Furthermore, in cloudy and drizzly weather conditions, the data acquisition with UAVs is still possible, when the distance to the object permits flying below the clouds. Such weather conditions do not allow the data acquisition with large format cameras integrated into manned aircrafts due to required larger flight altitude above ground. In addition, one fundamental advantage of using UAVs is that they are not burdened with the physiological limitations and economic expenses of human pilots. Moreover, supplementary advantages are the real-time capability and the ability for fast data acquisition, while transmitting the image, video and orientation data in real time to the ground control station.

Most of the (non-)commercially available UAV systems on the market focus on low cost systems, and thus a major advantage of using UAVs is also the cost factor, as UAVs are less expensive and have lower operating costs than manned aircrafts have. But, sometimes as mentioned in the previous section - depending on the application - the cost can be similar to manned systems. As for small-scale applications the expenses for manned aircrafts are not maintainable, projects are quite often not feasible or terrestrial systems have to be used as alternative systems, recognizing not all project requirements are met. Thus, UAVs can be seen as supplement or replacement to terrestrial photogrammetry in a certain area of applications. In the case of combination of terrestrial and UAV photogrammetry, it is even possible to use the same camera system and having the same distance to the object, which simplifies the combined data processing.

In addition to these advantages, the UAV-images can be also used for the high resolution texture mapping on existing DSMs and 3D-models, as well as for image rectification. The rectified images and derivates, like image mosaics, maps and drawings, can be used for image interpretation.

The implementation of GPS/INS systems as well as the stabilization and navigation units allow precise flights, guaranteeing, on the one hand, sufficient image coverage and overlap and on the other hand, enabling the user to estimate the expected product accuracy preflight.

Looking at rotary wing UAVs, the platform allows vertical take-off and landing vanishing the need for an available runway. Furthermore, the use of VTOL (Vertical take-off and landing) systems permits the image acquisition on a hovering point, while the camera is turning in vertical and horizontal direction.

1.1.3 Limitations in the use of UAVs

UAVs, especially low-cost UAVs, limit the sensor payload in weight and dimension, so that often low weight sensors like small or medium format amateur cameras are selected. Therefore, in comparison to large format cameras, UAVs have to acquire a higher number of images in order to obtain the same image coverage and comparable image resolution. Moreover, low-cost sensors are normally less stable than high-end sensors, which results in a reduced image quality. In addition, these payload limitations require the use of low weight navigation units, which implies less accurate results for the orientation of the sensors. Furthermore, low-cost UAVs are normally equipped with less powerful engines, limiting the reachable altitude.

Existing commercial software packages applied for photogrammetric data processing are rarely set up to support UAV images, as through no standardized workflows and sensor models are being implemented.

In addition to these drawbacks, UAVs do not benefit from the sensing and intelligent features of human beings. Thus, UAVs cannot react like human beings in unexpected situations, e.g. unexpected appearance of an obstacle. In general there are no sufficient regulations for UAVs given by the civil and security authorities (Colomina, et al., 2008). Low-cost UAVs are not equipped with air traffic communication equipments and collision avoidance systems, like manned aircrafts. Therefore, due to the lack of communication with the air traffic authorities, UAVs are restricted to the flight in line-of-sight and to operate with a back-up pilot. The flight range of the UAV is also, in addition to the line-of-sight regulation, dependant on the skill of the pilot to detect and follow the orientation of the UAV-system. To take full advantage of the impressive flying capabilities of UAVs, like the fully automated operating rotary wing UAVs, there needs to be a well trained pilot, due to security issues. The pilot should be able to interact with the system at any time and maneuvers.

Based on the communication and steering unit of UAVs, we can state that the operation distance depends on the range of the radio link for rotary and fixed wing UAVs, which is equivalent to the length of the rope for kites and balloon systems used in the past. In addition, the radio frequencies (35 and 40MHz in Switzerland) maybe subject to interferences caused by other systems (remote controlled cars and model aircrafts, as well as citizens' band radio), which use the same frequencies, or may suffer from signal jamming. Thus, depending on the local situation of the area of interest, the frequency for the communication between GCS and UAV has to be selected carefully. Nowadays, UAVs are also controlled via 2.4GHZ radio connection, while the video link has to be shifted to 5GHz.

1.1.4 Categorization of photogrammetric platforms

Recent technological improvements of UAVs during the last years emerged to revisit the categorization of photogrammetric platforms.

Abdulla, 2004 presented in the *Manual of Photogrammetry* the existing photogrammetric platforms, such as airborne, satellite and land-based platforms, as well as auxiliary systems. Thereby, the airborne platforms are subdivided in aircraft platforms such as single and twin engine aircrafts and other platforms like unmanned surveillance and reconnaissance aircraft systems, helicopters and balloons. The unmanned surveillance and reconnaissance aircrafts are basically UAV systems, but in the context of this categorization only high altitude and long endurance UAVs such as the Predator B (United States Air Force) are taken into account. Furthermore, the land-based platforms are partitioned into van-based mobile mapping systems and real-time videogrammetry systems. Looking at aerial based platforms

like, for example, kites, model helicopters, quadrotors[1] and terrestrial based systems such as grains, rope-way, well-bucket and base bars, it is clear that not all platforms available for photogrammetric observations can be categorized using this classification. Furthermore, the category auxiliary systems do not represent the non-classified platforms. This group remains for the positioning systems such as GPS, INS and stabilized platforms, as well as aerial survey flight management systems.

Kraus, 2007 focused in his book *Photogrammetry: Geometry from images and Laser scans* mainly on aerial photogrammetry. He does not explicitly categorize the platforms used in the aerial case. Chapter 3 (Kraus, 2007) concentrates however on photogrammetric recording systems and their applications, where the recording systems are classified into photochemical, photo-electronic, and digitizing systems. In addition, Kraus distinguishes between aerial and terrestrial cameras, while he separates terrestrial and mobile mapping methods.
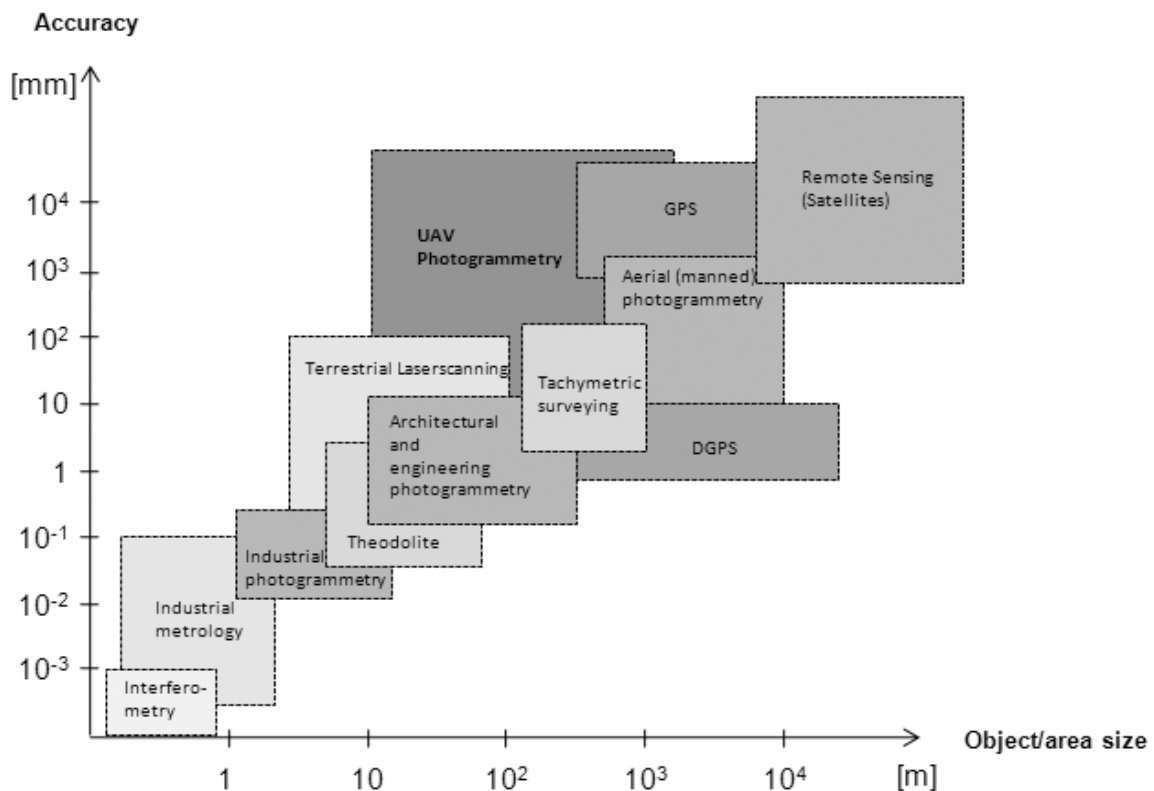
Figure 1-2: The accuracy of measurement methods in relation to the object/area size. Modified from Fig. 1.4 in Luhmann, et al., 2006, p. 4.

Luhmann, et al., 2006 (p. 4, Figure 1.4) introduced a categorization scheme of measurement techniques, which traded the size of the measured object vs. the required measurement accuracy. This categorization comprises almost all techniques, but the chosen graphical

---

[1] Additionally, synonyms like Quadcopter and Quadrocopter are used in the literature.

representation does not address the performance of each system at different conditions. Actually, considering the height dimension of an object, some of the presented methods may not cover the entire object with the presented accuracy. Introducing the transition section between aerial and terrestrial based platforms according to Figure 1.4 in Luhmann, et al., 2006, as well as introducing a new category for aerial based platforms operating in the close range and aerial domain without restriction for the viewing angle, leads to a more complete picture. Accordingly, we added the category "UAV photogrammetry", combining all unmanned aircrafts into a dedicated category, making the classification of photogrammetric platforms more understandable and clearer in the context of the recent developments (see Figure 1-2). Appendix Figure A-1 comprises terrestrial, helicopter and airborne laser scanning and Radar interferometry to UAV photogrammetry in a separate Figure.

1.2   Research goals

The combination of photogrammetric aerial and terrestrial recording methods using a mini UAV (**U**nmanned **A**erial **V**ehicle) opens a broad range of applications, such as surveillance and monitoring of the environment and infrastructural assets. In particular, these methods and techniques are of paramount interest for the documentation of cultural heritage sites and areas of natural importance, facing threats from natural deterioration and hazards. Today, UAVs can be used as a precise, automated and computer controlled data acquisition and measurement platform, thanks to the recent developments of low-cost sensors such as off-the-shelf digital cameras, GPS/INS (Global Positioning System / Inertial Navigation System) based stabilization, navigation units and laser scanners. This work deals with the challenging task: *The use of UAV systems as photogrammetric data acquisition platform.*

The main goal of this study is the identification and automation of a generic workflow using an UAV as a photogrammetric data acquisition platform. This workflow covers the flight planning, the autonomous flight of the UAV-system and the automation of the post-processing, striving to have the first results already available during field work. This work also investigates on real applications, focusing on the precision and resolution of the generated photogrammetric products, like elevation models, orthophoto and textured 3D models. Moreover, our study investigates on the influences of environmental conditions and manual, semi-automated and automated control of the UAV system on the UAV flight trajectory and on the results.

UAVs have not yet been established as a standard photogrammetric measurement platform. This work also documents our achievements and developments of UAVs in photogrammetry accomplished in the past. Moreover, since UAVs are a promising alternative or complement

to the traditional aerial and terrestrial photogrammetry, this work gives an overview on existing UAVs, and in particular highlights some suitable platforms for photogrammetric applications, focusing on low-cost and automated systems.

Autonomously flying UAVs offer the potential for automated data acquisition of complex objects. However, the implementation of efficient data acquisition and processing techniques, avoiding collision with objects, and requiring near real-time processing, makes the development of a special flight planning tool and its integration into the flight control system absolutely mandatory. This work evaluates the data processing capabilities of commercial software packages for UAV image processing. Newly developed tools, such as UAV flight planning, are presented that automate the data processing, shorting the processing time and reducing the overall processing effort. Complementing image data, a LiDAR system is integrated into the UAV-platform in order to improve the quality of the extracted elevation model. Our highly flexible generic workflow is described, that allows replacing and exchanging individual modules of the workflow without influencing the remaining modules, making it suitable for various real applications.

This work documents the application of the developed workflow to a great variety of real world data, and highlights the advantages and identifies limitations in the use of UAVs as a photogrammetric data acquisition platform. In this context, we focus on the extraction of DSM (Digital Surface Model) data from UAV-image data under extreme conditions. The results are compared to manually measured data, comprising LiDAR data acquired from the ground and from manned aircraft systems. Furthermore, exploiting the potential of a new workflow combining LiDAR and image data in UAV-based applications concludes this work.

1.2.1 Rationale

UAVs are increasingly seen as an attractive low-cost alternative or supplement to aerial and terrestrial photogrammetry due to their low cost, flexibility, availability and readiness for duty. In addition, UAVs can be operated in hazardous or temporarily inaccessible locations. UAVs can also provide both a quick overview of a situation, as well as detailed area documentation. However, prior to a successful UAV operation, an extensive mission planning is necessary. This mission planning of course is dependent on the kind of application and in particular on the specifics of the situation at the flight area. In many occasions, no detailed field information is available, only rudimentary maps or limited graphical information.

The main motivation of this study is to generate high-resolution information of in-accessible areas, such as maps, orthoimages, general topography, detailed elevation models, extraction of dangerous obstacles, 3D models of buildings and highly grown vegetation in near real-time

or with limited post processing efforts. Furthermore, the in-depth mission planning requires an overview image of the flight area with corresponding GPS coordinates for map calibration at the ground control station for further mission planning. A typical flight scenario over an unknown area includes the initially assisted flight mode when the operator defines the flight velocities and the flight area with the joystick. The helicopter flies up over the area of interest and acquires one single overview image. The overview image data is geo-referenced using the onboard GPS position and attitude information delivered by the flight control system.

The extraction of the terrain, orthoimages and textured 3D models from UAV-images or other sensor data can be applied to all kinds of hazards, catastrophic or environmental disasters, in any country, in order to instruct and to coordinate urgent response measures, such as building collapse, aircraft accidents, search and rescue operations, fire combat, crop damages, landslides and volcano outburst. Further applications include 3D documentation of the environment, cultural heritage sites, surveying of power lines, pipeline inspection, dam monitoring and recording of cadastral data. The main advantage is to provide detailed area information and area profiles for further detailed mission planning and to facilitate quick response times. Typical customers of such include not only civil security services, but also mapping agencies, real estate companies and environmental organizations. The successful outcome of this study sets a new milestone in civilian use of UAVs, particularly in the less well documented areas world wide.

1.3 Outline

Chapter 2 gives a literature overview of UAV systems and research related to their application in photogrammetry. Chapter 3 focuses on UAV systems. In this chapter a general overview and new classifications of UAVs are given. Additionally we introduce UAV systems, which have been used in our study. The following chapters 4 and 5 focus on the automated photogrammetric data acquisition using UAV systems and the processing of these data. Chapters 6 and 7 comprise of applications of UAV photogrammetry, with an emphasis two main applications. Chapter 6 addresses archaeological applications and cultural heritage documentation of three sites, while chapter 7 gives practical examples of monitoring of hazards and environmental applications. In chapter 8, the results of the given examples as well as applied methods, are summarized and an outlook to future applications is given. Figure 1-3 shows the overview of the content and the relations between the main developments (Chapter 4 and 5) and the applications (chapters 6 and 7).
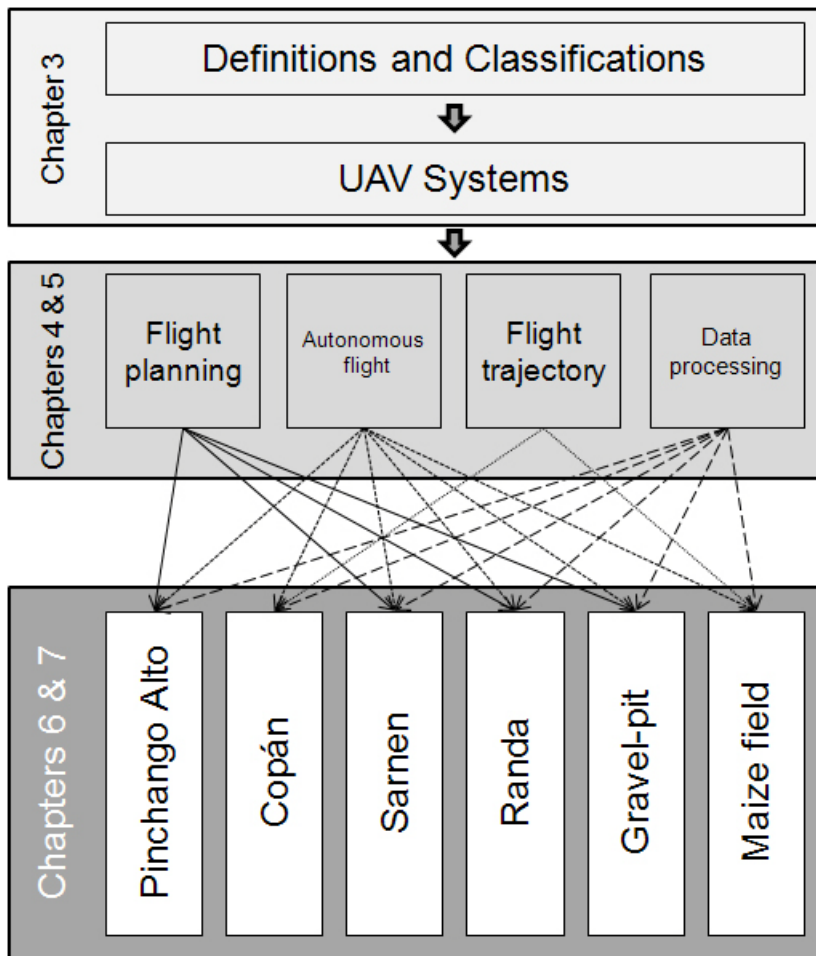
Figure 1-3: Content overview.

2 LITERATURE REVIEW

Figure 2-1: Autonomous flight over campus ETH Hönggerberg in April 2009.

This chapter gives an overview of the evolution of UAVs, which have been used for photogrammetric applications and developments. The review is structured in chronological order. Furthermore, the chapter is subdivided in time periods. Specifically the first section highlights the developments up to 2004 and the second section shows the progress between 2004 and 2007, while the last section illustrates the latest improvements.

2.1 Pre 2004

2.1.1 Early investigations

The first aerial photographs were taken by Gaspard Tournachon in 1858 from a manned balloon in Paris (Newhall, 1969).
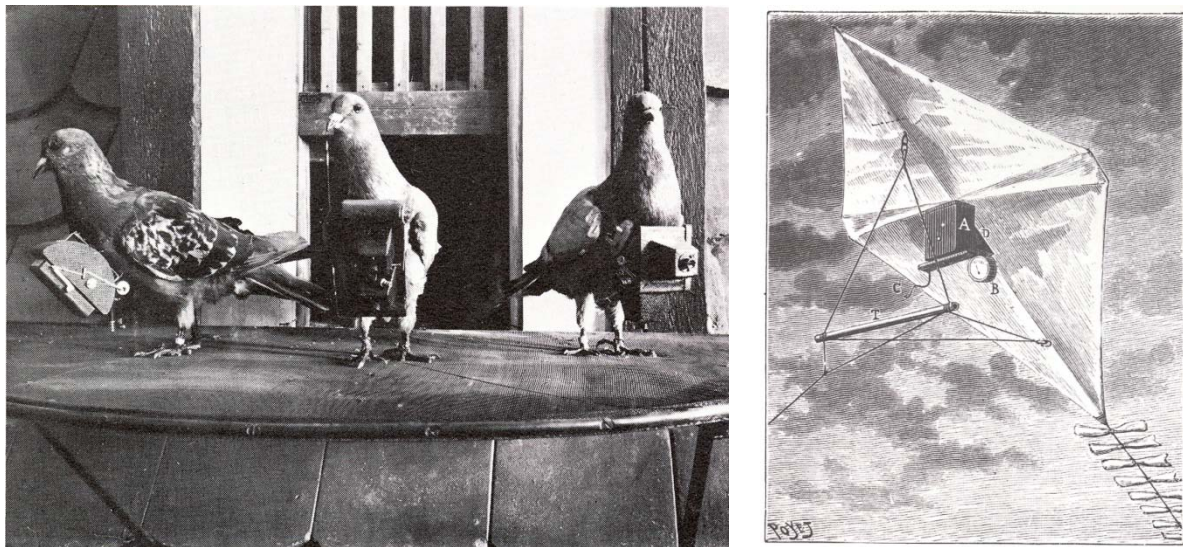
Figure 2-2: The left Figure shows a example for Pigeons, while the right one show a drawing of a dragon (Newhall, 1969).

Over the years, the experiments and evolution of manned balloons were coupled with model balloons. In parallel to the balloons, other systems like kites (Athur Batut, 1888 and Lawrence and Myers, 1906), Pigeons (Neubronner, 1903) and Rockets (Alfred Maul, 1904) were used for spying during the world wars in the last century (see Figure 2-2 and Newhall, 1969). In 1970 Whittlesey reported on the use of a tethered balloon for archaeological documentations, which he started in 1967 (Whittlesley, 1970 and Figure 2-3, Left). For these projects, several cameras were used, for example the Lindhof 6cm x 9cm format with Schneider Kreutsnach wide-angle lens and the Graflex XL with ~6cm x 8cm using the same lens. The cameras were mounted in a gimbal, while the camera unit was 9m below the balloon during the flight. These cameras allowed images to be taken at a distance of up to 50m above the ground. Later on, a Hasselbald 400 FL camera with a Zeiss Distagon 50mm lens was used, which enabled the

radio control for image acquisition (see Figure 2-3, Right). The payload of this particular construction was 2.7kg and the balloon was able to fly up to 600m above the ground. This platform already showed that UAVs can be used in different flying heights: The flying height itself depends on the requirements of the project and system parameters, such as the range of the camera and system control.
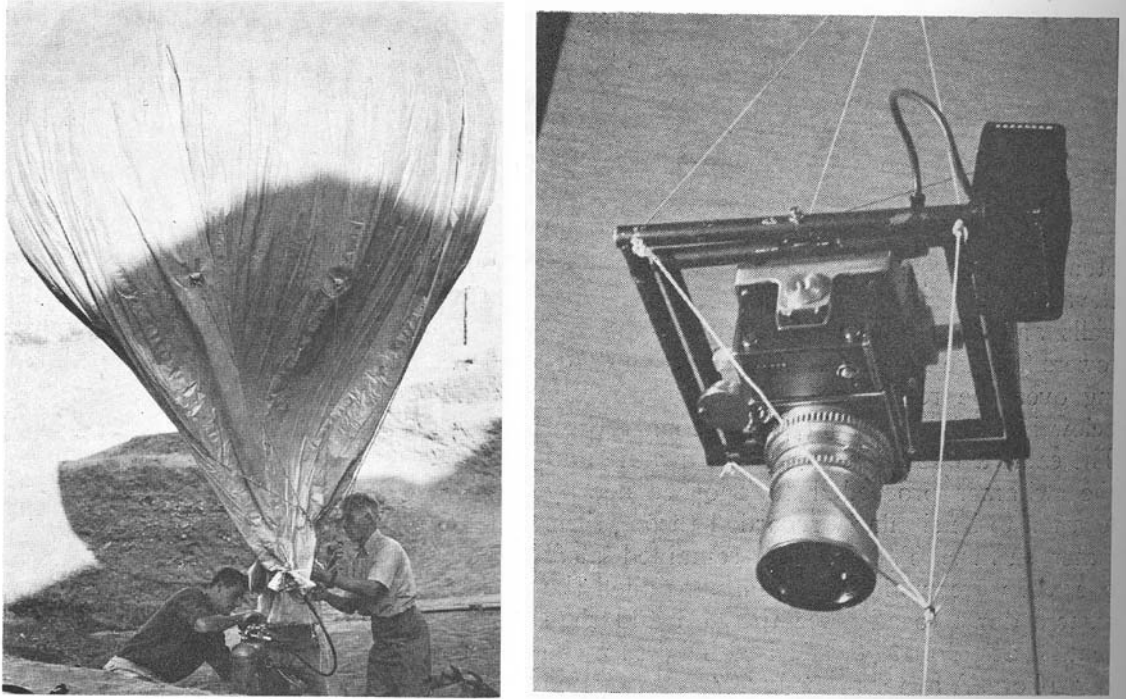
Figure 2-3: Left: Filling of a tethered balloon; Right: The radio controlled Hasselblad El 500 camera hung in its gimbal (Whittlesley, 1970).

In 1979, one of the earliest experiments with fixed wing UAVs in photogrammetry was done by (Przybilla and Wester-Ebbinghaus, 1979). First tests were accomplished using the manually controlled fixed wing UAV of the company Hegi with a flying height of 150m above ground and a velocity of 11m/s (see Figure 2-4).

The airplane was 3m long and had a wing span of 2.6m. The plane could carry a maximum payload of 3kg. The Navigation equipment by Lindhof Technika was used to steer the airplane, while the flying height was determined from the size of the plane in the image viewer. In combination with terrestrial images it was possible to acquire images of an archaeological area for the reconstruction of the architecture of the site. However, the application of this manually controlled airplane was limited by a small runway nearby the object, which was necessary for take-off and landing. Furthermore, the results were not sufficient because of image motion, which was caused due to the velocity of the airplane and the vibration of the engine. Therefore, the authors proposed to use less vibration-sensitive model helicopters (Przybilla and Wester-Ebbinghaus, 1979).

13

Figure 2-4: Model airplane Firma Hegi (Przybilla and Wester-Ebbinghaus, 1979).

Figure 2-5: Model helicopter from Schlüter (Wester-Ebbinghaus, 1980).

In 1980, Wester-Ebbinghaus was the first to use a rotary wing UAV for photogrammetric purposes. The rotary wing UAV was a model helicopter from Schlüter (Bell 222) with a maximum payload of 3kg (see Figure 2-5). The helicopter was able to fly in a height range from 10m to 100m and the predicted height could be kept within 90%, using the same navigation equipment as for the fixed wing UAV in 1979. The system was able to carry a medium format camera like the Rolleiflex SLX. To compensate for the vibration caused by the engine, polystyrene walls were installed on the helicopter and successfully suppressed the vibrations. For flight operation a pilot and a navigator were needed. The pilot controlled the

14

take off, landing and flying, while the navigator had to verify the altitude and activated the camera shutter manually via radio link. Using that system, the Schwebebahn (monorail) Wuppertal, a steel construction dating from 1890, was documented (Wester-Ebbinghaus, 1980).

2.1.2 Balloons

Vozikis, 1983 gave a practical example for a medium format camera mounted on a BCV D4 balloon (with a volume of $15.3m^3$) manufactured by the Delacoste Company. The images were taken by the Institute of Photogrammetry at the Technical University Vienna using a Hasselblad 500 EL/M camera which had a Zeiss (Oberkochen) Distagon wide angle lens (f=50mm). The camera was supported by a cardan mount and was able to rotate around the three principal axes (ω, φ and κ) using a remote control. The angles of the rotation were determined by a theodolite. Six photographs were taken from a height of about 25m and these formed three stereo models. The overlap between the photographs was irregular. However, it was possible to orient the images using the Wild Aviolyt ACl/Aviotab TA2 analytical plotting system and five ground control points (GCPs), with a RMSE (Root mean square error) in planimetry and height of 15 and 40mm, respectively. Finally, it was possible to produce a map of an archaeological site with a scale 1:100 (Vozikis, 1983). These results showed that by using an UAV system (Balloon) equipped with a medium format camera, it is possible to achieve high accuracy for a small size area. However, their results also illustrated that the image block was quite irregular; this was due to the manual control of the platform.

Another balloon platform was built in England by the company Skyscan. Using that system it was possible to photograph sites like New Place Knot Garden at Stratford upon Avon, Warwickshire, Hailes Abbey, Gloucestershire, a 13th century Cistercian foundation and the Tower Bridge in London (Marks, 1989).

In the 1980s, Johnson did some experiments with balloon photogrammetry and medium format images in the Nazca area (Peru). The experiments were not successful, as the system was susceptible to winds (Johnson, et al., 1990).

For the improvement of the road layout, traffic congestion and road repairing plans it is necessary to determine the running speed and position as well as the kind of vehicles driving on the road. In order to meet these needs, a traffic monitoring system based on a balloon platform was proposed by Mori, et al., 1996. However, the method was only partly successful, because the color and the pattern of the road influenced the stereo matching of the vehicles. Furthermore, the quality of the camera as well as the stability of the platform and its position may also have impacted upon the results.

Using a 35mm amateur film camera with a wide-angle lens mounted on a balloon, 12 images were taken from an archaeological site in Athens with abrupt changes in the relief (Karras, et al., 1999). The images were oriented using the Intergraph Image Station SKK system (ZI/Intergraph, 2009). Furthermore, a DSM and an orthomosaic were produced out of the data. The site had a size of 30 by $100m^2$ and the images were taken with an overlap of 80% at a mean flying height of 30m above ground. From the oriented images a surface model was reconstructed manually. The final resolution of the orthomosaic was 7.5mm in object space with an accuracy of 5cm. The achieved accuracy was satisfactory. But, looking at the final resolution, which was 6 times better, the ratio between resolution and accuracy was not selected properly. However, the results of this study showed already at that time, that low-cost system are well suited for the extraction of elevation models and orthoimages out of medium and small format aerial image data.

In 1999, together with a Japanese team from the Keio University (Japan) the Institute of Geodesy and Photogrammetry (ETH Zurich), a balloon photogrammetry mission over Bayon at Angkor (Cambodia) was performed. The main goal of the Bayon field mission was the data acquisition of small format camera balloon images over Bayon for the 3D reconstruction of the complex temple. Balloon images were also taken over the Northern Library of Angkor Wat and over the several Prasat Suor Prat buildings (Gruen, et al., 2001, Visnovcova, et al., 2001). However, due to the wind conditions at the site, the acquired images had not sufficient overlap for a complete processing of the data set.

In 2003, for the monitoring of gully erosion in the Central Ebro Basin in Spain, a remotely controlled blimp was used (Ries and Marzolff, 2003). The blimp had a Zeppelin shape with streamline body and fins for improved stability in wind conditions. The UAV was connected to lightweight tether ropes for flying heights up to 350m above ground.

2.1.3 Airship

Wanzke (1984) presented a hot-air ship, which he had used for stereo photogrammetric documentation. The balloon was designed and constructed by the GEFA-Flug company, under the direction of K. L. Busemeyer. The highlight of this construction was that the elements of the exterior orientation were registered within narrow bounds (1-2m for the position and 5grad for κ). The following observations were made:

- The captivation of the balloon for the exact positioning (X_0 and Y_0) using a focus screen with grid.
- The cardanic suspension of the camera (ω and $\varphi \sim 0$).
- Rotational ability of the camera along the vertical axis (κ).

- Altitude control through a measuring tape hanging down (Z_0).

The platform allowed the montage of a medium format camera (Rolleiflex SLX) or two Nikon motor cameras for stereophotos with fixed base. The balloon was able to operate up to an altitude of ~150m. The system was used for the architectural documentation of a 5000 year old town in Pakistan, while three blocks of aerial images were acquired in a height range of 10m to 150m above ground (Wanzke, 1984).

2.1.4 *Model helicopters*

Miyatsuka (1996) gave an overview of existing terrestrial and aerial based platforms such as grains, rope-way, well-bucket, base bar and balloon, kite, radio controlled model helicopter, hot balloon, light plane, air ship and helicopter. At that time Miyatsuka selected a digital still-video camera from Kodak (DCS 460) with 6 MPixels mounted on a model helicopter. The helicopter was able to fly up to 300m. However, the resolution was not sufficient for the archaeological application, since he had to fly in a high altitude to cover the whole area with a small number of images. Therefore, the author proposed to use a medium format film camera (Miyatsuka, 1996).

1998 Tokmakidis proposed three different methods for the reconstruction of the Tholos in Delphi: The first method used a metal pole construction fitted on a steel plate based on the ground. On the top of the pole a medium format camera (Hasselblad) was mounted on a hanger. The system was maneuverable by several persons at a height of 6m. As a second method, an aerial metric camera (18cm x 18cm) was mounted on a crane. The aerial camera was selected to acquire all the details of two rounded heavy stones and to obtain accuracy up to 1-2mm. Finally, as a third method a manually controlled model helicopter carrying a Hasselblad camera was described (Tokmakidis, et al., 1998).

The manually controlled rotary wing UAV was powered by a reinforced motor, which was able to lift a payload up to 5kg and had a main rotor diameter of 1.64m. Moreover, with a full tank the system was able to fly 20min with a maximum altitude of 500m above ground. Similar to the system proposed by Wester-Ebingghaus, the helicopter was operated by a pilot and an operator. The camera base had a special rubber suspension to absorb vibrations, it also was equipped with a rotation mechanism to turn the camera (Rolleyflex 6006) up to 90 degrees. Therefore, the system was also able to photograph house facades. Furthermore, to aid control of the observation, an electronic view finder was mounted on the camera. The video signal was transmitted through UHF (Ultra-High-Frequency) transmitter to a portable monitor on the ground (Theodoridou, et al., 2000).

In addition, the same system was used for the mapping of an archaeological excavation, where images with a scale of 1:400 were acquired for the purpose of documentation. Finally,

an orthophoto and a 2D plan were produced out of the images (Skarlatos, et al., 2004, Tokmakidis and Scarlatos, 2002).

In 2000, Zischinsky used images taken from a model helicopter partly for the generation of a 3D-model of a historical mill. For the documentation of the building, 82 pictures were taken from the ground and additional 38 images from the helicopter to close the gaps in the model. The small format amateur camera (Kodak DCS460c with 37 and 48mm focal length) mounted on the helicopter took mainly images of roofs and the courtyard. For the exterior orientation of the model, 120 GCPs were determined (Zischinsky, et al., 2000).

The orientation of the images was done with the photogrammetric software package ORPHEUS individually for the terrestrial and the aerial image block. Finally, an average RMSE of 2cm in planimetry and height was obtained for the orientation of both sub-blocks. After that, the object was modeled and textured using ORPHEUS and PHOTOMOD (developed at Vienna University of Technology) respectively with 703 triangles and an image resolution of 5cm. However, on the face of it, the number of GCPs seemed to be a bit excessive. Nevertheless, depending on the number of sub blocks, it was assumed to have this high number of GCPs.

The RMAX rotary wing UAV system from Yamaha (Yahama, 2009) was used as a ground truth measurement system (Hongoh, et al., 2001), which was applied to determine vegetation coverage. Therefore, the sensor took images from different viewing angles, which was the most important aspect of bi-directional reflectance measurements.

Normally, foreigners are not allowed to use manned aeroplanes or helicopters to take aerial images in other countries, however in the same year a mini helicopter was permitted to take Chinese fortress measurements. The Japanese Miyatsuka Institute of Archaeology wanted to acquire high-resolution images of this huge fortress site (3km x 4km). The remote controlled helicopter covers none of both categories and for that reason the UAV-system was used with metric and non-metric cameras (Yasuda and Miyatsuka, 2001).

In 2002, the RMAX system (see Figure 2-6) was used for photogrammetric investigations over two tests sites in Sweden. The goal of the study was to analyze the accuracy of the GPS/INS-system implemented in the UAV. At that time, the RMAX system was already equipped with a DGPS (differential GPS) system, which resulted in a 3D accuracy for the position of 0.3m and 0.1°/0.2° for the orientation (respectively roll and pitch / yaw) of the flight trajectory. The results of the study showed that the stability of the camera mounting, vibrations caused by the main rotors and the accuracy of the GPS/INS system were the main influencing parts for the stabilization of rotary wing UAV-system and the image quality (Eisenbeiss, 2003). The study was done in collaboration with WITAS – Wallenberg

Laboratory for research on Information Technology and Autonomous Systems (Linköping University, Sweden) and the Institute of Photogrammetry and Remote Sensing (University of Technology Dresden). In addition, the flight performance of the system was analyzed. The UAV was flown manually, controlled by a pilot, and in autonomous mode. The results of the flight performance will be discussed more in detail in section 4.3.1.

Figure 2-6: The autonomous flying RMAX system of the Linköping University, Sweden (Eisenbeiss, 2003).

Finally, first investigations on UAV-borne LiDAR systems in the field of robotics started at Carnegie Mellon University. Thrun, 2003 described initial results for a helicopter mapping system combining a SICK LMS laser range finder, a Crossbow IMU, a Honeywell 3D compass, a Garmin GPS, and a Nikon D100 digital SLR camera. The results shown in this study showed for urban and natural terrain already the potential of the spatial detail contained in the 3D point cloud.

2.1.5 Kites

In 1997 several scientific investigations based on kite aerial photography were applied. A fossil forest bed was mapped in the arctic environment (Bigras, 1997) and an archaeological site in Russia was documented (Gawronski and Boyarsky, 1997). Similary, Carlson, 1997 utilized aerial images from a kite from a small rubber raft to document penguin nesting sites in Antarctica.

Aber, et al., 2002 presented a kite platform, which could fly 50-150 m above ground. In the experiments a small airfoil kite ($1.5m^2$) was used, which was well suited for winds of 7 to 11 m/s. The system was tested with the several film, digital, single and stereo camera systems. In addition to the various sensors, the system was used for a variety of applications: Forest cover, wetlands, property surveys, architectural designs, golf course management, cemetery survey and glacial geomorphology. Despite this, the system was mainly used to acquire single images or stereo pairs, which only allows the coverage of a small size area. The kite platform showed that it is easy to adapt several cameras, it belongs to the OM-class UAVs (see chapter 3.2) and the system was well suited to be quickly deployed in the field for various applications (Aber, et al., 2002).

2.1.6 Fixed wing aircraft

In 2002 Herwitz tested two high-resolution digital cameras: A Kodak/Hasselblad system for RGB imaging in the visible spectrum; and a DuncanTech (Auburn, CA) multispectral system for narrow-band imaging in the visible and infrared parts of the spectrum, which later were selected to be mounted on NASA's solar-powered UAV (Unmanned Aerial Vehicle) Helios (AeroVironment, Inc., Simi Valley, CA). Therefore, for the initial evaluation a piloted fixed-wing aircraft was chosen to test the new commercial "off-the-shelf" wireless technology. The hope was to improve the performance significantly to reduce the cost of line-of-sight telemetry for imaging payloads on UAVs. This test was quite important to demonstrate that via broadband wireless Ethernet it is possible to transfer Error-free 16 MB Kodak/Hasselblad digital images, without data dropouts, to the ground-based laptop computer at transfer rates ranging from 1 to 4 Mbit/sec for a distance of up to ~20km (Herwitz, et al., 2002). This technique is therefore quite promising for the image downlink of fixed wing UAVs, which normally acquire more data, given these systems are able to fly longer distances than rotary wing systems.

In this section early studies of UAVs in photogrammetry already showed the high potential of low-cost platforms for photogrammetric applications. However, the UAV systems at this time were mainly controlled manually via radio link or with ropes. Since the manual control did not allow the precise steering of the systems, quite often only few images could be used for the post-processing. We now turn to more recent developments.

2.2 Developments from 2004 to 2007

2.2.1 IGP ETH Zurich

In the period 2004-2007 Eisenbeiss, 2004, Eisenbeiss, 2007, Eisenbeiss, et al., 2007, Eisenbeiss, et al., 2005, Eisenbeiss and Zhang, 2006, Sauerbier, et al., 2006 investigated using autonomous flying rotary wing UAVs like the Copter 1B from the company Surveycopter (Surveycopter, 2009), equipped with a flight control system from the company weControl (weControl, 2009). Using these particular platforms, the following aspects were evaluated:

- The flight autonomy of predefined flight paths.
- Autonomous image acquisition using various low-cost still-video cameras.
- Extreme environmental conditions like desert, alpine and vegetation, urban areas in winter and summer time.
- Image orientation using commercial software and in-house developed packages.
- Accurate DSM and orthophoto generation.
- Evaluation of the achieved results with reference data.

Given that these particular aspects are a major topic of this thesis, we will describe them in more detail in the following chapters.

2.2.2 ISPRS Congress 2004 (Istanbul, Turkey)

At the ISPRS congress 2004 in Istanbul a new ISPRS IC Working Group was initiated. Most of the literature reviewed in this section was published in the proceeding of the ISPRS congress or mid-term symposia (ISPRS, 2004, ISPRS, 2006). The IC Working Group I/V *Autonomous Vehicle Navigation* aim was to focus on the emerging technology of autonomous vehicle navigation. Since the development of the digital cameras, low-cost GPS/INS systems and other sensors have meant, the technology has now advanced toward the automation of the vehicle operations and the acquisition of high resolution images using off-the-shelf cameras. The working group also includes all aspects of navigation of spacecraft, aircraft, UAV, land vehicles, robots, ships, and underwater vehicles.

2.2.2.1 UAV-borne LiDAR

In 2004, at the ISPRS congress and at the ISPRS workshop in Pitsanoluk, Nagai proposed a system, which integrates a LiDAR system and CCD-cameras with GPS/INS data for digital surface model generation. The system used a Subaru helicopter with a payload of 100kg and a main rotor diameter of 4.8m. So far, similar helicopter systems were classified as Mini-UAV system. However, this larger helicopter is not covered by the micro to medium size UAVs because of the mass of 330kg. Based on the range and altitude, the helicopter can be defined

as a mini or close range UAV. The platform also has an operational radius of 3km, flight autonomy of 1h and could fly up to 2,000m above mean sea level (Nagai, et al., 2004).

2.2.2.2 Balloons

Altan, et al., 2004 presented a system consisting of Olympus Camedia 4040 with a 4 Mega-Pixels camera, a balloon with approx. 2.5m main diameter and 8m^3 volume, a control monitor and a mechanic stabilization. The company Topotech developed a similar balloon system carrying a medium format analog camera (Fotinopoulos, 2004).

2.2.2.3 Model helicopter

Jang, et al., 2004 used a rotary wing UAV-system for the acquisition of ancient towers and temple sites in China. The helicopter was selected for the replacement of high camera tripods and ladder trucks, which are uneconomical both in cost and time. The selected helicopter Hirobo & Eagle 90 (Hirobo, 2009) had a main rotor diameter of 1.8m and a payload capability of 8.5kg. The helicopter was able to acquire images from the upper part covering all sides of the temple, while the images of the lower part were taken from ground. Onboard the system, a small video camera was installed too, which was connected to the ground station transmitting the images to a monitor in real time.

2.2.2.4 Fixed wing UAV

Everaerts, et al., 2004, Fransaer, et al., 2004 and Fransaer, et al., 2004 described the fixed wing UAV-system Pegasus, which is a long endurance UAV system for remote sensing. This kind of system has the capability to be airborn for a long time, because solar energy was used as its power supply. It can carry a payload of about 300 kg.

The Chinese Academy of Surveying and Mapping developed a fixed-wing Mini-UAV system. It was intended to reconstruct 3D models of buildings out of the images. However, because of the environmental conditions such as wind it was difficult to control the vehicle manually and to take images on the predicted acquisition points. Accordingly, it was not possible to use the images for stereo image processing and an algorithm had to be developed. This allowed the use of one image and a 2D GIS database for the reconstruction of 3D models of buildings (Jizhou, et al., 2004).

2.2.3 Applications of rotary and fixed wing UAVs

In the same period research groups focused on applications using rotary and fixed wing UAVs for natural resource management and monitoring (Horcher and Visser, 2004), use of stereo images for the generation of crop maps (Kise, et al., 2005, Rovira-Más, et al., 2005), vegetation monitoring (Sugiura, et al., 2005), classification of hyperspectral UAV imagery (Laliberte, et al., 2007) and precision farming (Reidelstuerz, et al., 2007). Several research groups concentrated on environmental monitoring/inspection such as traffic monitoring (Haarbrink and Koers, 2006, Puri, 2004), road following (Egbert and Beard, 2007), vehicle detection (Kaaniche, et al., 2005), car accident and flare inspection of an industrial flue (Haarbrink and Koers, 2006), forest fire monitoring (Zhou, et al., 2005), river monitoring (Masahiko, 2007), recording of large scale urban and suburban sites (Spatalas, et al., 2006) and bridge inspection (Metni and Hamel, 2007). In 2007, fixed and rotary wing UAVs were used for the mapping of archaeological sites (Bendea, et al., 2007, Patias, et al., 2007).

The results of these studies showed, that it was quite easy to acquire images from the area of investigation, but still the flight performance and the image block configuration were not as ideal as in standard aerial photogrammetry cases. The limitation of these parameters is mainly dependant on the flying mode, the navigation unit implemented in the UAV-system and the flight planning as well as the calibration between both of their components. Furthermore, depending on the payload, a low-cost camera with high or low stability and quality can be mounted into the system. Therefore, it is essential to calibrate the cameras beforehand, after the flight or through the flight mission. Hongxia, et al., 2007 presented a paper which focused on the calibration of a low-cost camera used in the UAV system. Hongxia used a self-calibrating bundle adjustment using an indoor 3D test field.

In the field of robotics and artificial intelligence various research groups were focusing on the exploration of unknown urban areas using laser scanner, such as the SICK (Sick, 2009) and Fiberteck (Fiberteck, 2009), for the detection of obstacles (D. Shim, et al., 2005, Scherer, et al., 2007).

Niranjan, et al., 2007 gave an overview about civilian applications, like Precision Agriculture, Disaster Management, Oil and Gas Pipeline Monitoring, Construction Work, Earth Movement and Excavation, Laying of Pipes and Cables, Erection of Buildings, Soil Upheaval and Erosion, Water Logged Surfaces, Plantation of Shrubs and Trees, Discoloring of Vegetation, Forest Fire Detection / Forest Management, Atmospheric Sampling Missions, Landscape Mapping. Niranjan also proposed a prototype for a fixed wing UAV which should have a maximum flight radius larger 2500km, an endurance of greater than 24h, while the operational altitude varies from 100m – 6000m. This spectrum for flying heights allows several applications, but fixed-wing UAVs are not predestinated to be used for all of these

applications. The GSD (ground sampling distance) of one Pixel varies significantly between 100m and 6000m above ground. Therefore, some other platforms like satellites or manned aircrafts are more suitable for some of these applications, while VTOL platforms are more suitable for areas where the take-off of fixed wing platforms is not possible.

Figure 2-7: A quadrotor Md4-200 from the company Microdrones.

In 2007 the Photogrammetry group of the University of Applied Sciences Northwestern Switzerland presented investigations related to rotary wing UAVs. Nebiker and Eugster focused in their studies on model helicopters and quadrotors (see Figure 2-7) for the georegistration of images (Eugster, 2007, Eugster and Nebiker, 2007) and augmented monitoring (Nebiker, et al., 2007b).

2.2.4 Low-cost systems

Low cost drones, like powered paragliders are an alternative for rotary and fixed wing UAVs for individual applications. The kite system from the University of Bonn (Germany) is a manually controlled ~4.1 kW strong 2-stroke engine. The weight of the system varies between 8 kg and 12kg, while up to 5kg can be attached to the system. The frame of the UAV is mounted on a paraglider which serves as a wing. Therefore, a slow stable flight is guaranteed and the system provides high security in case of a failure of the motor. The platform also allows the mount of different sensors. The field of view is transmitted to the operator and can be seen in special goggles or video screens, laptops etc. While image acquisition is triggered via remote control, the position is determined by a low-cost GPS system and transmitted to

the operator. The system is restricted to fly under wind speeds smaller than 6m/s. A maximum flight height of 4,500m and an operation distance of up to 5km are possible. For take-off and landing a runway with a length of 5m to 25m is needed (Thamm and Judex, 2006).

2.2.5 GSM based flight planning

In addition to the studies presented so far, Wzorek, et al., 2006 proposed the GSM technology as a communication media for an autonomous aerial vehicle. This work was done at WITAS. Using a Sony Ericsson mobile phone and the RMAX UAV, it was possible to edit the flight plan online, switch to the camera view, display log messages, insert and remove no-fly zones. Furthermore, the system allowed the sending of fly commands, like fly to position or waypoint, mission start, take-off and landing etc., to the UAV-system. The flight tests and empirical evaluation showed the practicability of this type of technology. Furthermore, it permits the operation of UAVs at large distances, out-of-sight from the operator. It provides a good redundant system alternative in the case where other communication frequencies jam. It also gives access to low price use of the internet. This is an important point since there will be an increasing demand for using information on the internet in real-time during mission execution (Wzorek, et al., 2006).

2.2.6 Summary

The results of the presented studies in the period 2004-2007 showed, that it is quite easy to acquire images from UAVs using off-the-shelf cameras. However, the quality of the results varied, mainly depending on the integrated navigation and stabilization system onboard of the UAV system and the system itself. Therefore, the classical classification of UAVs, which is mainly related to the maxima flying height and endurance, must also include a quality of performance value. This value should indicate, what would be the most suitable applications of the system. This new composition will be explained in chapter 3. We have also shown that in this period the trend for the use of low-cost and small size systems, integrating various sensors, was evident.

2.3 2008 until present

We will now review several studies presented 2008 until present. These studies were mostly published in the IC Working Group I/V at the ISPRS congress in Beijing. The work presented represents the present state of the art and show the demand of research on UAVs (UVS) in photogrammetry.

Everaerts gave an overview of UAV systems used in photogrammetry in the period 2004-2008 (Everaerts, 2008). A second comprehensive overview on "Low-altitude Aerial Photography" was given by Verhoeven, 2009 with the focus on archaeological prospection. These literature studies can be seen as supplement to the literature review presented here.

2.3.1 UAV-borne LiDAR

Nagai, et al., 2004 showed the latest results based on his investigation related to multi sensor integration. In his paper, the system and the multi sensor integration were described. Furthermore, the workflow for the geo-processing and the first results generated from LiDAR data were presented. The geo-processing was done using a "hybrid IMU", which combines the GPS/IMU data, using the image orientation resulting from bundle block adjustment, with a Kalman Filter.

Choi, et al., 2008 provided an overview of a similar system, which was developed as a light and flexible system to perform rapid mapping for emergency responses in South Korea. In a follow up study, Choi, et al., 2009 introduced a improved rapid mapping system for emergency responses. This project was sponsored by the Korean government, with an overall budget of 6 million US dollars and a time period of four years. At the current stage of the project, two configurations of UAV systems, a medium and a high grade system, are described. In a simulation, both configurations are verified and using a synthetic data set, the initial accuracy is compared to the results of aerial triangulation.

Figure 2-8: The scout B1-100 equipped with the Riegl airborne LiDAR scanner LMS-Q160.

A model helicopter from the company aeroscout (Aeroscout, 2009) equipped with a compact and lightweight airborne laser scanner LMS-Q160 from Riegl (Riegl, 2009) was firstly described by Imbach and Eck, 2009. This system is described in detail in chapter 3.4.1.

2.3.2 Rotary wing UAVs

Coppa, et al., 2008 presented the results of a flight simulation system, which was developed to analyze the setup of the servos, which were used for the guidance of the system. The system allows the evaluation before starting the real flight, avoiding the damage of fragile and expensive instruments. On the other hand, it has to be balanced if an already existing system (compare Table 3-8, Table 3-9 and Table 3-11) is cheaper than the development and the simulation of an own system. From our point of view, already several low-cost systems are available at the market. Therefore, the main research in the photogrammetry community should focus more on the integration of the sensors like camera units and LiDAR system as well as the communication with navigation and control unit.

Nebiker, et al., 2008 continued their investigation on rotary wing UAVs. The project MSMS (Multi Spectral Micro Sensor) concentrated on the use of mini and micro UAVs in agricultural applications. For the assessment of plant health, a grapevine field was selected. The site was documented using two platforms: Copter 1B and the md4-200. While for the Copter 1B the Canon D20 was selected, an in-house developed light-weight multi-spectral sensor was used for the md4-200. The system consists of two cameras using a full frame CMOS (Complementary Metal Oxide Semiconductor) sensor element (752 x 480 Pixel), a camera controller and 8mm c-mount lenses. The total payload of the system was 350g, which was well over the official payload limitation of the platform. Therefore, it turned out that data acquisition was only possible in the absence of any wind. This made the system not applicable under real conditions. However, the first result of the study showed the potential of UAV platforms for agronomical applications.

Eugster and Nebiker, 2008 presented the progress and showed the first results of the study on augmented monitoring. The success of the integration of the video data into the 3D-viewer (i3D-viewer, 2009) depended mainly on the achievable accuracy for the geo-referencing. Moreover, the accuracy was correlated with the quality of the available flight attitude and the synchronization between video and flight data stream.

Zhang proposed a rotary wing UAV-based photogrammetric mapping system for the monitoring of unpaved road conditions (Zhang, 2008). The preliminary results of 2D analysis of the road imagery showed that UAV images are suitable for extracting many of the parameters needed for monitoring the condition of unpaved roads. While the 2D image analysis is under further development and refinement, the project is currently focusing on the

development of 3D analysis of images by exploring Photogrammetry techniques. Additionally, Zhang showed results of the photogrammetric processing and UAV-based remote sensing of road conditions (Zhang, 2009a, Zhang, 2009b) using the weControl (weControl, 2009) system for the navigation and stabilization of the helicopter.

Some other recent developments presented in Beijing included Gerke, 2008, who discussed a matching technique for video sequences. Also Steffen and Förstner, 2008 used a quadrotor as a platform for image acquisition under the condition of real time computation of trajectory and surface information. Colomina, et al., 2008 presented a follow up study of their UAV-based photogrammetry and remote sensing system, which were focusing on technical and regulatory issues related to UAVs. The variety of the presented papers showed the need of research related to the topic UAV Photogrammetry. Furthermore, depending on the application and the requested accuracy level different kind of UAV platforms can be used for the photogrammetric data acquisition.

2.3.3 Balloons

Scheritz, et al., 2008 presented at the 9th International Conference on Permafrost a tethered helium filled balloon equipped with a Nikon camera D200. In this study an accurate land cover, such as meso-scale to high-resolution DSM, is needed to obtain reliable inputs for modeling the hydrology and the exchange between the surface and atmosphere. The DSM will be the foundation for modeling meso-scale hydrological processes on the island and to identify locations of discharge. Therefore, the whole island was covered with images taken from heights between 600 and 800m. All points of the DEM, with a ground resolution of 10m, had a horizontal and vertical accuracy better than 1.0m. This study showed the need of high accurate and dense elevation model for hydrological analysis on the meso-scale and the limitation of manual controlled system, as well as the limitations of the available commercialized software packages for the DSM generation. The achieved resolution and accuracy was not sufficient, and so a new flight was conducted in 2008. The results of this study will be presented in chapter 4.3.2, where we focus on manual flights of UAV systems for the photogrammetric data acquisition.

Gomez-Lahoz and Gonzalez-Aguilera, 2009 used for the reconstruction of two archaeological settlements located in Castile (Spain) - the Roman city of Clunia (Burgos) and the Celtic settlement of Las Cogotas (Avila) - a blimp UAV system. The outcomes of the studies were well accepted by professional archaeologists, since the accuracy attained with this approach was ~0.03m in planimetry and ~0.05m in height. With relation to the field work and its logistic, the set-up of the system took about 45–60min and after this, the operations of changing the batteries or downloading the images from the memory card took approximately

less than ten minutes. However, the proposed methodology is quite efficient, reaching a productivity of 3ha/h approximately. This factor is especially important for the reconstruction of large areas, like complete settlements. The system has to be handled however, by two people: one to drive the blimp and another one to control the image acquisition. Therefore, the number of involved persons was the same as for the state of the art fixed and rotary wing UAVs, which need one operator and one backup pilot.

2.3.4 Open source systems

Recently, Niethammer, et al., 2009 used an open source UAV system (Mikrokopter, 2009) for the monitoring of slow moving landslides. The special feature of this UAV system is that it works with four or eight individual powered propellers, allowing the safe landing even if one of the motors fails.
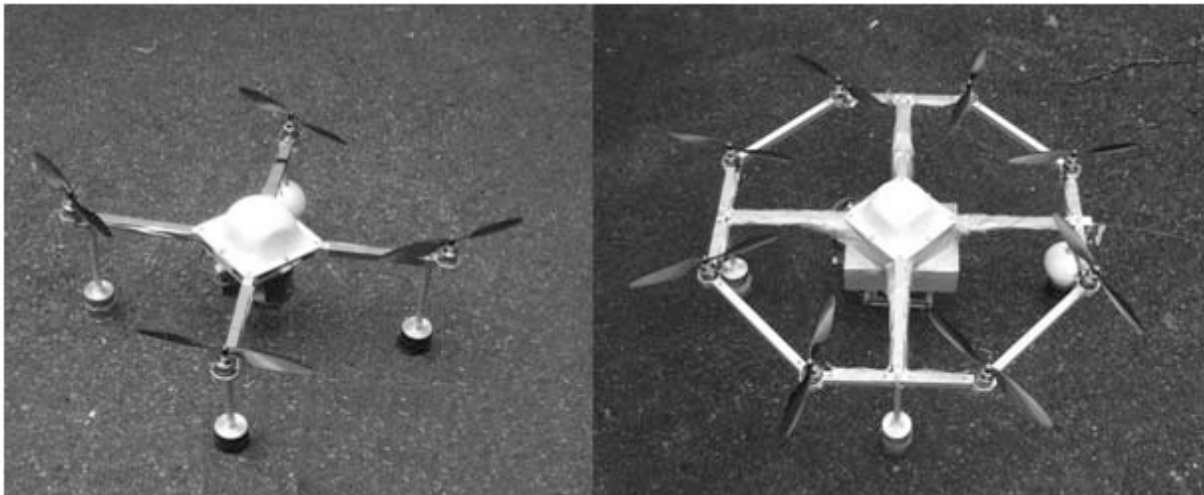
Figure 2-9: Example of a Quadrotor and an Octocopter of the open source system Microkopter (Niethammer, et al., 2009).

2.3.5 Further applications and developments

The China Institute of Surveying and Mapping and the Chinese Academy of Science showed results of three different kinds of UAVs. The investigation used an unmanned helicopter, a fixed wing aircraft and an airship. The study compared the systems based on the security component, quality of the results and efficiency for the data acquisition (Cui, et al., 2008, Yundong, et al., 2008).

Model helicopters, compared to airships and fixed wing, are more complex systems in terms of their technical onboard equipment. The authors came up with the hyphothesis that the unmanned helicopters had the highest failure rate probability. This was rather simplistic, since the evaluation did not take into account the maturity and the quality of the components of the

system. However, the issue considering the safety of human life is quite considerable, as the main rotor of the helicopter could produce the most harm and injury. The quality of the produced product was quite similar, taken into account the flying height and the camera parameters. Looking at the efficiency, two factors were evaluated. The first factor examined the local adaptability, while the second explored the cruise duration. The helicopter systems were most suitable, if only vertical take-off and landing was possible, while the fixed wing system and the airship were preferable due to the long flight autonomy (up to 2.5h) (Yundong, et al., 2008).

Nackaerts, et al., 2008 described a calibration strategy for the MEDUSA (Monitoring Equipment and Devices for Unmanned Systems at high Altitude) camera system and Zhao and Qi, 2008 focused on the altitude data analysis of UAV Remote Sensing images. Lin, 2008 finally presented two more UAV platforms, which are used at the Chinese Academy of Surveying and Mapping.

Figure 2-10: Powered paraglider „Susi" (Source Jütte, 2008).

An overview of the potential of several low-cost UAVs in forestry and agriculture was given in Grenzdörffer, et al., 2008b. In this study, results of the photogrammetric processing of image data taken with a fixed wing *Carolo P330* (Mavionics, 2009) and a powered paraglider *Susi* (Jütte, 2008 and Figure 2-10) were described. The results for the bundle adjustment

varies between, half a meter and centimeter accuracy level. The study described in detail which source of errors influenced the direct georeferencing and showed possibilities to compensate and correct these parameters (Grenzdörffer, et al., 2008b). Furthermore, the system is currently used for the determination of forest border lines, for the documentation of tree damage and the forest stand, as well as the conservation of evidence of illegal forest clearance.

2.3.6 IGP ETH Zurich

Eisenbeiss presented three papers related to different kinds of applications in Photogrammetry. The first paper concentrated on Agriculture/Precision Farming and Geology, where dense elevation models in a complex environment were needed (Eisenbeiss, 2008a). The second paper focused on the 3D modeling and photorealistic texture mapping of a medieval castle based on close range imagery acquired with a mini-UAV and in terrestrial mode (Pueschel, et al., 2008). Finally, the third paper investigated the accurate DSM production using images taken with two kinds of rotary wing UAVs (Haarbrink and Eisenbeiss, 2008). The content and the outcome of these publications will be discussed in detail in the following chapters. Furthermore, the mini UAV system was used in the labs of the Master and Bachelor program in Geomatics at ETH Zurich (see Figure 2-1).

2.4 Conclusions

The presented literature reflects on one hand a chronological review about UAV systems used in photogrammetry, while on the other hand it also highlights the main applications and research in photogrammetry using UAV systems. The results of these studies show, that it is quite simple to acquire images from the area of investigation, however the flight performance and the image block configuration are still not as accurate as in standard aerial photogrammetry cases. The limitation of these parameters mainly depends upon the flying mode, the navigation unit implemented in the UAV-system and the flight planning, as well as the calibration between both these components. Furthermore, depending on the payload, a low-cost camera with high or low stability and quality can be mounted into the system. The presented studies also reflect two main focuses in current UAV photogrammetry research. One central focus is on the use of existing platforms just as a data acquisition platform. A second focus is on the implementation, integration and synchronization of different sensors used in photogrammetry into a UAV platform. The recent investigations focus on applications that require high resolution and accuracy, but also on applications that concentrate on fast processing. Most applications just produce orthophotos or maps out of the images for documentation purposes. Investigations on the DSM generation using image data were only

shown in Karras, et al., 1999, Eisenbeiss, 2008a, Eisenbeiss, 2008b, Haarbrink and Eisenbeiss, 2008, Scheritz, et al., 2008.

Balloons and Kites are cost-saving alternatives for some of the presented fixed and rotary wing systems (Thamm and Judex, 2006, Altan, et al., 2004, Fotinopoulos, 2004, Grenzdörffer, et al., 2008a, Scheritz, et al., 2008). However, these kinds of UAVs are more depending on weather and local conditions, since these systems are difficult to control on a predefined path. In addition, most of them are not stabilized, which complicates the hovering on a position.

For the integration of different sensors, the exterior orientation has to be known and therefore the accuracy of the various sensors implemented into the platform has to be investigated. Quite often a quick overview of images acquired using low-cost sensors is sufficient, whereas for accurate measurements more precise methods, e.g. DGPS and bundle adjustment, have to be explored.

In the more recent investigations the trend goes to fast processing like online triangulation and direct georeferencing. In addition, the sensors and systems are getting tinier and several open source platforms are used in photogrammetry.

Since most of the presented studies showed limitations in the flying mode, the acquired data were sub-optimal and it was not possible to process the complete data set, we will focus in the following on the flight performance of UAVs. We will compare the influence of the manual, semi-automated and automated flights on the UAV trajectory and final products. Moreover, the trend goes also to low-cost and open source systems. In our studies we will analyze the existing UAV systems, classify them and select appropriate UAV-systems for our investigation in terms of flight performance and conducting real applications. However, additionally to the low-cost and open source system, there is also a trend to the data integration of various sensors and high precision and resolution of specific applications and near real-time applications.

Due to the need for fast processing and accurate results and various UAV systems being available, in the following chapter we will concentrate on UAVs and classify them. This overview of UAVs will support the selection of the appropriate UAV for data acquisition and processing, depending on the specification of the UAVs, the requirements of the applications and the given flight regulations for UAVs

3 UAV-SYSTEMS

Figure 3-1: Overview of various UAV systems.

3.1 General overview

In the following we will give an overview on existing classifications, regulations and communities of UAVs. These classifications will be extended with new categorizations, taking into account the specific needs for an UAV photogrammetry platform. We will combine the various classes into three new categories, separating Open-source and Manual controlled UAVs (OM-class), Micro and Mini UAVs (M-class) and Large payload UAVs (L-class).

3.1.1 Classification of UAVs

The definition of UAVs encompasses fixed and rotary wings UAVs, lighter-than-air UAVs, lethal aerial vehicles, decoys and targets, alternatively piloted aircrafts and uninhabited combat aerial vehicles. Sometimes, cruise missiles are also classified as UAVs (van Blyenburgh, 1999). Furthermore, UAVs can be categorized using the main characteristics of aircrafts like unpowered or powered, lighter than air or heavier than air and flexible, fixed or rotary wings (see Table 3-1). Table 3-1 shows a classification of the existing UAVs, which can be used for photogrammetric applications. Table 3-2 gives pro and cons of the in Table 3-1 classified systems regarding their range, endurance and weather, wind dependency and maneuverability.

Table 3-1: Classification of UAVs according to the classes unpowered and powered, as well as lighter or heavier than air.

	Lighter than air	Heavier than air		
		Flexible wing	*Fixed wing*	*Rotary wing*
Unpowered	Balloon	Hang glider	Gliders	Rotor-kite
		Paraglider		
		Kites		
Powered	Airship	Paraglider	Propeller	Single rotors
			Jet engines	Coaxial
				Quadrotors
				Multi-rotors

Rotary wing UAVs, also known as vertical takeoff and landing vehicles (VTOL), can be further classified into single-, double-, four- and multi-rotor systems (see Table 3-1). Single-rotor systems have one main rotor and a tail rotor. The main rotor supplies lift and thrust; the tail rotor is used to counteract the yaw motion and the torque. Double-rotor systems, so called

coaxial systems, differ mainly from single-rotor systems because they have an increased payload and they are able to operate at higher absolute altitude for the same engine power. In addition, they are more easily controllable and have a reduced noise level. These systems have approximately 30 percent more degree of efficiency, since all of the available engine powers is devoted in lift and thrust. However, coaxial systems have one main disadvantage: Using two main rotors mounted in the same rotor shaft, which need to rotate in opposite directions, results in an increased mechanical complexity of the rotor hub. In general, the existing single and double-rotor systems have more power than four- and multi-rotor systems. Accordingly, these kinds of systems are able to carry more payloads, which correspond into the number, size and weight of the sensors mounted on the UAV-system.

Table 3-2: Pro and cons of the different type of UAVs (0: Lowest value; +: Middle value; ++: Best).

Type of aircraft	Range	Endurance	Weather and wind dependency	Maneuverability
Balloon	0	++	0	0
Airship	++	++	0	+
Gliders/Kites	+	0	0	0
Fixed wing gliders	++	+	+	+
Propeller & Jet engines	++	++	+	+
Rotor-kite	++	+	0	+
Single rotor (helicopter)	+	+	+	++
Coaxial	+	++	+	++
Quadrotors	0	0	0	++
Multi-copters	+	+	+	++

Since the existing four-rotor systems (Quadrotors, see Figure 3-1) have less payload capacity, they are equipped with lighter sensors as with low cost systems. With their small size and agile maneuverability, these Quadrotors can be flown indoors as well as outdoors (Hoffmann, et al., 2004). However, these systems are more susceptible to environmental conditions like wind and the operation radius is limited more to smaller areas. Nowadays multi-rotor systems (Niethammer, et al., 2009, Vito, 2009), which have usually similar size and weight as Quadrotors, are able to carry a larger payload, are more stable and they are more secure against system crashes, due to the redundancy of the multiple rotors.

The lift of fixed wing aircrafts (see Table 3-1) is not generated by wing motion relative to the aircraft like birds do, but by forward motion through the air. Powered fixed wings are moving forward using propellers or jet engines. In the categories of fixed wing UAV systems,

unpowered aircrafts like gliders can be found. These use the airstream for the forward motion and uplift. In contrast to fixed wings, rotary wing systems can operate closer to objects and have a larger flexibility in the control of flight maneuvers (Bendea, et al., 2007). On the other hand, fixed wing UAVs are usually able to stay for a longer time in the air, can cover larger areas and are able to enter upper air spaces (see Table 3-2).

In contrast to the rotary wing and fixed wing UAVs, the unpowered balloons and gliders are controlled by ropes. This feature means the systems are limited in their flying altitude and distance to the operator, while the horizontal movement of the system corresponds to the walking of the operator or the movement of the car, to which the system is adapted. Moreover, the influence of wind is greater than for the rotary and fixed wing UAVs.

Compared to the previous mentioned systems, powered airships have due to their uplift the advantage of staying longer in the air than the fixed and rotary wing platforms. Therefore, these systems can be used for long term monitoring tasks. Besides of this advantage, powered airships, as well as powered gliders, have as a drawback that these systems are more dependent on the environmental conditions. In addition the overhead obstructions in particular limit the usage of GPS sensors on these platforms for purpose of navigation.

UAVs can also be classified using the size/weight, endurance, maximum flying height and the flight duration into micro, mini, close, short, medium and long range classes as well as low, medium and high-altitude (van Blyenburgh, 1999 and Figure 3-2). The endurance of the UAV is influenced by the availability of the radio link to control the aircraft and the up- and downlink of the telemetry and image data. Furthermore, the endurance is also dependent on the flight autonomy, which is related to the capacity of batteries for electro motors and the amount of fuel taken as additional payload for gasoline and turbine engines.

An additionally existing classification is given by the Australian Civil Aviation Safety Authority (CASA, 2001). CASA distinguishes between three classes (see Table 3-3), using only the weight of the system for the classification.

Table 3-3: Classification of the CASA for UAVs.

Class	Class I Micro UAVs	Class II Small UAVs	Class III Large UAVs
Specifications	Take-off weight of 100g	Take-off weight of less than 150kg	Take-off weight of more than 150kg
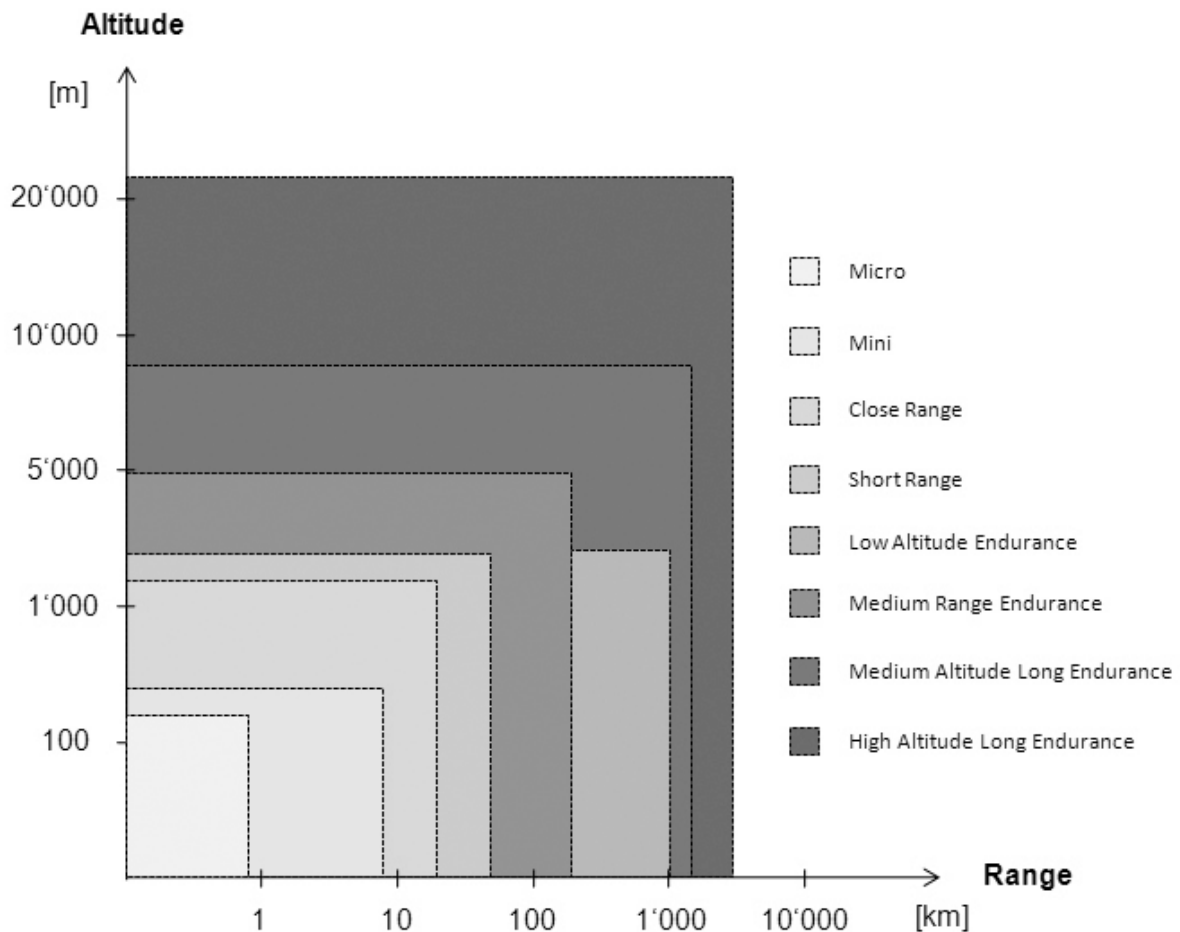
Figure 3-2: Classification of UAVs by range and altitude based on Figure 1 in van Blyenburgh, 1999.

Since the classification of UAVs varies from one country to another (see Table 3-3, Table 3-6 and Section 3.1.2) and no standardized categorization for UAVs in the ISPRS exists, we have adopted the existing classification of UAVs by van Blyenburgh, 1999 (see Figure 3-2) and incorporated the UAV systems used in this thesis. In the following we distinguish between **O**pen source and **M**anual controlled systems (OM-class), **M**icro & **M**ini systems (M-class) and **L**arge payload UAVs (L-class) (see Table 3-4). Open source are non commercialized systems, while low cost stands for a price for the hardware of not more than 5000 Euro. The M-class merges the Micro and Mini UAVs defined by van Blyenburgh, 1999 into one class, while the payload is limited to max. 5kg. The L-class stands for UAVs which correspond to a maximum payload over 5kg (without the payload for petrol).

Using the given categorization in Table 3-4, the system can be amended by two quality values. One value is related to the flight performance: Manual, assisted or autonomous flight, while the second value is related to the quality of the navigation unit. Therefore, we distinguish if no GPS, GPS and DGPS is used for the processing of the navigation data (see

Table 3-5). Combining these two factors, quality measures of the existing UAVs can be given, taken into account the flight performance and the quality of the navigation data.

Table 3-4: Categorization with respect to price and payload of UAV systems.

Category	Explanation	Limitation [e.g. price or payload]
OM-class	**O**pen source and **M**anual controlled systems: Limited commercial use and cost for the hardware of open-source systems not more than 5000 Euro	Manual controlled <5,000 Euro for Open source systems
M-class	**M**icro & **M**ini systems	<5kg
L-class	**L**arge payload UAVs	>5kg

Table 3-5: Classification of UAVs regarding to the type of georeferencing, real time capability and application requirements.

Sensors	Georeferencing	Real-time capability	Application requirement	UAV category
No GPS/INS	post	0	Low accuracy [m]	OM-class
GPS and consumer-grade INS	post/direct	+	Moderate accuracy [dm-m]	M- & L-class
DGPS/ navigation- and tactical grade INS	post/direct	++	High accuracy [cm]	M- & L-class

Additionally, UAV platforms can be classified according to their integrated sensors and real-time capability, which influence directly the data processing. Low-cost sensors will imply post georeferencing, while high-end sensors, such as DGPS and navigation-grade IMUs (see Appendix Figure E-1) have the potential for direct georeferencing. Depending on the implemented sensors and type of processing, specific UAVs will only be suitable for particular applications (see Table 3-5). The given accuracy levels in Table 3-5 for the application requirements can vary for the classified UAVs, according to the method applied for georeferencing.

3.1.2 Regulations

Due to security and insurance constraints UAV flights in the civilian domain have to be flown with backup pilot in line of sight (LOS). The backup pilot (UAV pilot/UAV-p) is the person who has at any time the direct control of the system. He is a qualified person who actively exercises remote control of a non-autonomous flight, or monitoring an autonomous flight. As

a general rule, the UAV operator or the UAV-system overtakes only partly the control of the system, while the UAV-p can overtake the control of the system at any time. In addition, for larger systems the UAV commander is the qualified person responsible for the safe operation. So far the regulations for UAVs differ from one country to another. However, the EASA (European Aviation Safety Agency) defined those UAVs with a "Maximum Take-Off Mass" (MTOM) over 150kg have to be certificated by EASA. UAVs with a MTOM less than 150kg are regulated by the national authorities.

For example, in Switzerland the BAZL (*Bundesamt für Zivilluftfahrt BAZL* – Federal Office for Civil Aviation FOCA) is the responsible federal authority. They categorized UAVs in classes with a take-off weight below and above 30 kg (BAZL, 2001 and Table 3-6). UAVs with a weight more than 30 kg need to have an official authorization by BAZL, while for the second category the authorization depends on the type of the UAV (Kite, balloon or model aircrafts). The responsible air navigation services, like Skyguide (Swiss air navigation service ltd) in Switzerland, are allowed to define exceptions and to give permission for special flights. Moreover, before doing an autonomous flight in Switzerland, permission from the owner of the land, and depending on the application confirmation from the insurance company, is obligatory.

Table 3-6: Regulation for UAVs in Switzerland (BAZL, 2001).

Category	Unpowered UAVs		Powered UAVs
	Gliders and captive balloons	Free balloon	
Unmanned Aircrafts > 30 kg	Need to have the permission of BAZL		
Unmanned Aircrafts < 30 kg	< 60m above ground	max. Payload 2kg or less than 30m^3 volume	Distance to the airport more than 5km
	3km distance to any airport	with more than 1m^3 distance to the airport must be more than 5km	In control zones, the height above ground is max. 150m

To give a second example, in the United Kingdom (UK) the Civil Aviation Authority (CAA) published a comprehensive guide called the "Unmanned Aerial Vehicle Operations in UK Airspace" in 2004 (CAP, 2004). This guide gives, amongst others, a good overview of legal considerations, certifications, registrations, maintenance and inspection, security flying operations relating to UAVs. For example, it even distinguishes between recreational and commercial use in 4 weight categories (<7kg, 7-20 kg, 20-150 kg and < 150 kg). In the future, because of security issues, similar regulations will be defined at national and/or European level in all countries.

3.1.3 UAV communities

In the past the developments of the UAV systems were primarily driven by the military and the artificial intelligence communities, while in the last few years further developments have

also been driven by the progress in the civilian sector of UAVs. An overview of the current variety of research groups, companies and societies working with UAVs is given in Appendix B-1. Table 3-7 also provides an overview of societies, which are working on UAVs or which have recently focused their work on UAVs or their applications. The table should not be interpreted as an all-inclusive overview of existing societies. It is more a collection of the main civilian societies focusing on UAVs. A more detailed study can be found in the UAV Industry report (Visiongain, 2009). Societies such as robotics and electrical engineering, artificial intelligence, unmanned vehicles, vertical take-off and landing and Photogrammetry and Remote Sensing, however are included in Table 3-7. For example, the Association for the Advancement of Artificial Intelligence (AAAI) focuses in general not only on UAVs, rather considers autonomous vehicles in general such as land based, underwater, air and outer space. So in addition to these platforms, the AAAI community is focusing generally on "… *advancing the scientific understanding of the mechanisms underlying thought and intelligent behavior and their embodiment in machines."* (AAAI, 2008).

Table 3-7: Overview of societies and conferences related to UAVs.

Society	Division/ Working Group	Webpage
Robotics and Electrical Engineering		
The IEEE Robotics and Automation Society	IEEE Division X	http://www.ieee-ras.org
The International Association for Automation and Robotics in Construction		http://www.iaarc.org/
Artificial Intelligence		
Association for the Advancement of Artificial Intelligence (AAAI)		http://www.aaai.org/home.html
Unmanned Vehicles		
Association for Unmanned Vehicle Systems International		http://www.auvsi.org/
Unmanned Vehicle Systems International		http://www.uvs-international.org
UAV forum		http://www.uavforum.com/
UAV world		http://www.uavworld.com/
Vertical take-off and landing		
American Helicopter Society (AHS) International		http://www.vtol.org/
Photogrammetry and Remote Sensing		
International Society for Photogrammetry and Remote Sensing	ICWG I/V	http://www.commission1.isprs.org/icwg1_5/
DGPF - Deutsche Gesellschaft für Photogrammetrie und Fernerkundung	UAV Session	http://www.fh-oow.de/3dtage/vortragsprogramm19.php
Remote Sensing and Photogrammetry Society		http://www.rspsoc.org
SGPF - Schweizerische Gesellschaft für Photogrammetrie, Bildanalyse und Fernerkundung	Swiss Geomatic Day 2009	http://www.sgpbf.ch/content/view/72/lang,de/

Since the societies of robotics, electrical engineering and artificial intelligence focus more on the construction and mechanism of UAVs, as well as the steering of autonomous flights, the

ISPRS Working group I/V *UVS for Mapping and Monitoring Applications* has focused on the use and applications of such systems as a photogrammetric data acquisition platform, as well as a tool for Remote Sensing instruments prototyping and for teaching, as well as for the research of onboard processing of image data and the control of the platform integrating GPS/INS and image observation for automated navigation.

3.2 Open Source and Low Cost UAV Systems: OM-Class

Several open source systems exist on the market. In Europe systems like UAVP and Mikrocopter are available for rotary wing systems (Eisenbeiss, et al., 2009b, Mikrokopter, 2009, UAVP, 2009), while the Paparazzi project focused on fixed wing UAVs (Paparazzi, 2009). These open source systems are only allowed to be commercialized, within certain limitations. The members of the open source community developed already high end systems, which allow manoeuvres of complex tasks like the *autonomous stabilized flight, follow me, coming home, and way point navigation*. The *follow me* modus allows a systems to follow another one in the automated flying modus, while the coming home option is essential if the radio link to the system is intermitted. Furthermore, in particular the *way point navigation* function is a valuable tool for photogrammetric applications. Using the own flight planning permits the image acquisition in a photogrammetric block configuration.

Since these kinds of UAV systems are low cost and have a high potential for research and testing purposes, in the following section open source project will be described and two examples for realized systems will be highlighted. After describing the open source system, an example for a low cost UAV such as a powered paraglider will be provided (Grenzdörffer, et al., 2008a, Jütte, 2007, Thamm and Judex, 2006).

3.2.1 Mikrokopter

The open source project Mikrokopter (Mikrokopter, 2009) was initiated by two electrical engineers from Germany in 2006. In contrast to most of the commercially available systems, the cost of the hardware of approximately €1000 is clearly lower. However, the amount of work for the self-construction should not be underestimated.

The required basic components for the construction of a Mikrokopter are four brushless motors including a brushless speed controller, two counter rotating propeller pairs, LiPo-Akku, a radio receiver, a frame-set as well as the Flight-CTRL, which is a micro size flight controller.

Figure 3-3: A Mikrokopter photo flight at Hönggerberg, ETH Zurich (Eisenbeiss, et al., 2009b).

All sensors needed for the flight are mounted on the Flight-Ctrl main board. The four main components are the following:

- A master control unit AVR Atmel ATMEGA644@20MHz,
- 3 gyroscopes ENBC-03R (±300°/s, -5 to 75°C),
- 3 acceleration sensors (ACC) LIS3L02AS4
- Optionally a barometer MPX4115 (15-115 kPa, -40 to +125 °C, max. error of 1.5%).

Furthermore there are more optional components available, which are necessary for the autonomous flight:

- The Navi-Ctrl contruction set including a ARM9-Mikrocontroller,
- A 3-axis magentometer (MK3Mag), which is used for the minimization of the drift in Yaw-direction,
- A GPS-receiver (MK-GPS) LEA-4H from the company u-blox (position accuracy of 2m for 50 % of the position fixes).

Table 3-8: Overview of OM-class systems.

Quad- and Multicopter				Powered Kite
OM-Class Systems				
Feature	*Microkopter ETHZ*	*Microkopter Stuttgart*		*"Susi"*
UAV category	Micro UAV	Micro UAV	Micro UAV	Mini UAV
Special feature of the system	Open Source	Open Source	Open Source	In-house developed & 4500 m m.s.l.
Size / Length	0.3-0.5m	0.6m	0.7m	0.7m
Motortyp	Gearless brushless electro motor	Gearless brushless electro motor	Gearless brushless electro motor	Two-stroke engine
Number of main rotors	4	4	8	
Main rotor Ø / Wing span	0.25 / 0.3m	0.25m	0.25m	~2.5m
Max. take-off weight	0.5-1.2kg	2kg	3.2kg	5-7kg
Payload capacity	0.2-0.5kg	0.5kg	1.5kg	5kg
Flight autonomy	5-20min	12min	12min	3h

An quadrotor Mikrokopter was built by Michael Kolb at ETH Zurich (Eisenbeiss, et al., 2009b), while Niethammer, et al., 2009 built two different Mikrokopter systems, such as a Quadrotor and an Octocopter (see Table 3-8). As mentioned previously, this system has been used for geological documentations at the University of Stuttgart.

3.2.2 Manual controlled system „Susi"

The system "Susi" was developed by the remote sensing group at the University of Bonn (Jütte, 2008, Thamm and Judex, 2006 and Figure 2-10). The system was already successfully used by Kai Juette at the forestry department in Mecklenburg-Western, Pomerania (Germany). The low cost system is a powered paraglider, which stands out from other systems due to its long endurance (up to 3h). The system is also currently used in the project REstored COrridor Dynamics (Record), sponsored by CCES and Cantons Thurgau and Zurich at ETH Zurich (Record, 2009).

The UAV system Susi can be equipped with a still-video camera, such as the Sony DSC-R1 or the multispectral camera TetraCam ADC. Moreover, the system contains a single GPS system and a video camera, which allows the transmission of the actual position and the online video signal via radio link.

The system can be controlled manually. For changing the height above ground the system has to increase the speed and the frame as well as the parachute of the system has to have a steep angle (see Figure 3-4). If the speed above ground is low, the climbing will take a longer period. Furthermore, if the angle of the system is to steep, the system is getting uncontrolled and can cause damage or failure of the system.
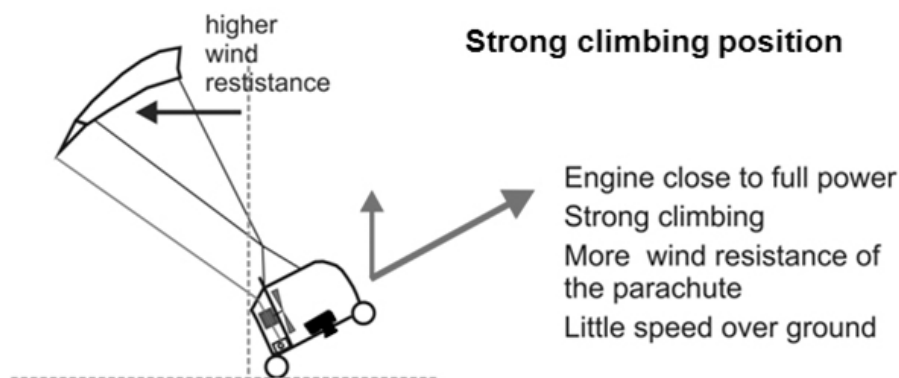
Figure 3-4: UAV SUSI showing the strong climbing position (Modified from Susi manual, 2009).

For changing the flight direction, the system must be controlled carefully, since the reaction of the system is delayed. In addition, depending on the wind direction, the left and right turns are different to control. Therefore, the manual control of the system without stabilizer and advanced fight control system is one of the mayor disadvantages compared to some of the M-Class and L-class systems.

3.3 Micro & Mini UAV Systems: M-Class

This class combines the UAV Systems, which are available for commercial applications and the payload of the system is limited to 5kg. Most of the systems currently available on the market are equipped with low-cost navigation sensors like GPS/INS, stabilized and have the capability to fly completely autonomously or with a predefined flight path. In the following section, a selection of helicopter, quadrotors and multicopter are described, while two systems, which have been used for this study, are explained in more detail.

3.3.1 Quadrotors

Table 3-9: Overview of a selection of existing commercial quad- and multicopter M-Class systems.

Quad- and Multicopter				
M-Class Systems				
Feature	**Microdrones MD4-200**	**Microdrones MD4-1000**	**Astec Falcon 12**	**AirRobot AR100-B**
UAV category	Micro-UAV	Mini-UAV	Mini-UAV	Micro-UAV
Special feature of the system	Carbon-chassis	DGPS and GSM waypoint navigation	Flight up to a wind speed of 10m/s	
Size / Length	1m		1.25m	1m
Motortyp	Gearless brushless electro motor	250W flatcore brushless motors	Information available middle 2009	Gearless brushless electro motor
Number of main rotors	4	4	8	4
Main rotor Ø / Wing span	0.37m	0.5m	0.35m	~0.35m
Max. take-off weight	900g	5.1kg	4.9kg	<1kg
Payload capacity	200g	1kg/0.3kg	1.5kg	200g
Flight autonomy	20min	30min/70min	20min	30min
Max. flying height	3500m (tested at Jungfraujoch 2009)			

Quadrotors are mainly light weight systems, which have normally a maximum take-off weight of up to 5kg. The limitation is mainly due to the payload limitations of some national authorities, like the maximal take-off weight of 5kg in Germany. These systems have a size of 0.5-2m and they are powered by four electro motors. Several commercialized systems are

available on the market, as shown in Table 3-9. Due to the weight limitations, these systems are highly dependent on the wind conditions and the absolute flying height (a.s.l.) will be limited. Moreover, most of the systems can only fly in the manual or assisted flight modus.

Recently, the Microdrones MD4-200 was upgraded by a flight control system, allowing the autonomous flight with a predefined flight path. Therefore, this system was used in this work for the analysis of the influence of the autonomous flight modus to the efficiency and accuracy of photogrammetric data acquisition and processing. Besides of the Microdrones system the companies Ascending technologies GmbH and the Airrobot company are manufacturers for commercialized quadrotors and multicopter platforms. While the company Airrobot is more focusing on military applications, the ascending systems offers systems, which diversify from a hobby line to a professional line. In particular, the Falcon 12 system of Ascending, which is an octocopter, allows a payload up to 1.5kg having flight autonomy of up to 20min (see Table 3-9).

3.3.1.1 Microdrones

Figure 3-5: Left: A detail view of the system showing the adapted camera. Right: Ground Control Station.

The company microdrones GmbH was founded in October 2005. The motivation of the founders was the development and production of VTOL systems such as Micro UAVs. The first unit of the quadrotor system MD4-200 was available in April 2006, which can be operated by one person. The MD4-200 (see Figure 3-5, left) includes the UAV system consisting of accelerometers, gyroscopes, magnetometer, barometer, hygrometer, thermometer and GPS sensors and a whole package of software. The software contains the following components: Flight simulation, way point editor (see Figure 3-6) and flight control, as well as a tool for the analysis of the system parameters post flight.

Figure 3-6: Screenshot of the waypoint editor of mdCockpit showing a plan of an autonomous flight at the campus ETH Hönggerberg.

The *waypoint editor*, shown in Figure 3-6, allows the definition of the image acquisition points based on a rectified map or orthophoto integrated into the waypoint editor. Therefore the position in the map and the height above ground has to be defined. In addition to the way point position, the *vector yaw options* are composed: Camera orientation azimuth and zenith angle, as well as the horizontal, vertical flying speed and the yaw movement speed. Finally, *way point actions* like activating the image triggering, camera zoom and multi or single triggering, as well as the time interval between the single image acquisitions are defined. All attributes of a waypoint are given in chapter 4.2.2.3. The interactive map allows, by clicking on one image point in the map, the preview of the image coverage and the additional parameters mentioned above. As an alternative, the flight path may also be created in Google Earth (GoogleEarth, 2009) and imported manually into the waypoint editor. However, this procedure still requires the definition of the additional parameters in the editor.

The maximal take-off weight of the system is 900g, while the payload is limited to 200g. The weight of the camera is limited thus to 200g. The adapted camera (see Figure 3-5, right) can be controlled via integrated data link through to the ground control station (see Figure 3-5, left). The flight autonomy is limited to 20 min with a flight radius from the flight control station of 500m and the maximal take-off height is restricted to 1500m a.s.l. However, the system was already tested at 3,800m a.s.l. (Klein Matterhorn, Switzerland) and in a separate test with a maximal payload of 350g (Nebiker, et al., 2007a), where the main limitations were given by the local wind conditions. The system contains four rotors, which are connected to 1

Lipo batteries (4 cells) with 2,300mAh. The MD4-200 can operate up to a humidity of 80% and can fly in a temperature interval of 0-40°C (see Table 3-9 and microdrones, 2009b, Nebiker, et al., 2007a).

Recently, Microdrones introduced a new quadrotor MD4-1000 too, which will have a maximum take-off weight of 5.1kg and a payload capacity of either 1kg or 300g, with flight autonomy of 30min and 70min respectively. This system allows, in comparison to the MD4-200, the use of a camera with factor five more weight or the data acquisition longer than 1h (see Table 3-9 and Microdrones, 2009).

3.3.2 Model helicopter

The model helicopter Copter 1B (Surveycopter, France) using the navigation and stabilizing unit wePilot1000 of weControl was primarily used in our study. Moreover, the flight performance was analyzed in our studies and could be improved through our feedback to the system manufacture. Therefore, in the following the helicopter and the navigation unit we will describe in more detail.

3.3.2.1 The Copter 1B

The Copter 1B is operated by 2 people and combines an extra-quick system deployment. The Copter 1B (see Figure 3-7) uses the flight control system wePilot1000 from weControl, which allows for the stabilization of the platform and for an autonomous flight following a predefined flight path for image acquisition. In addition, the system consists of a ground control station (see Figure 3-8: A laptop with monitoring software (weGCS)), a still-video camera, communication links, power supply, video link (incl. video camera) for visual control for monitoring image overlap, and transport equipment. The maximum tested flight height above ground level was 2300m a.s.l. at Flüelapass (Switzerland; see Eisenbeiss, 2008a).

The helicopter itself is powered through a 26ccm petrol engine allowing a maximum payload of 5kg with flight autonomy up to 30min. The size of the helicopter including the main rotor is approximately 2m. In addition the helicopter features a GPS antenna, INS, barometer, compass, camera gimbal, etc. (see Table 3-11 and Figure 3-7).
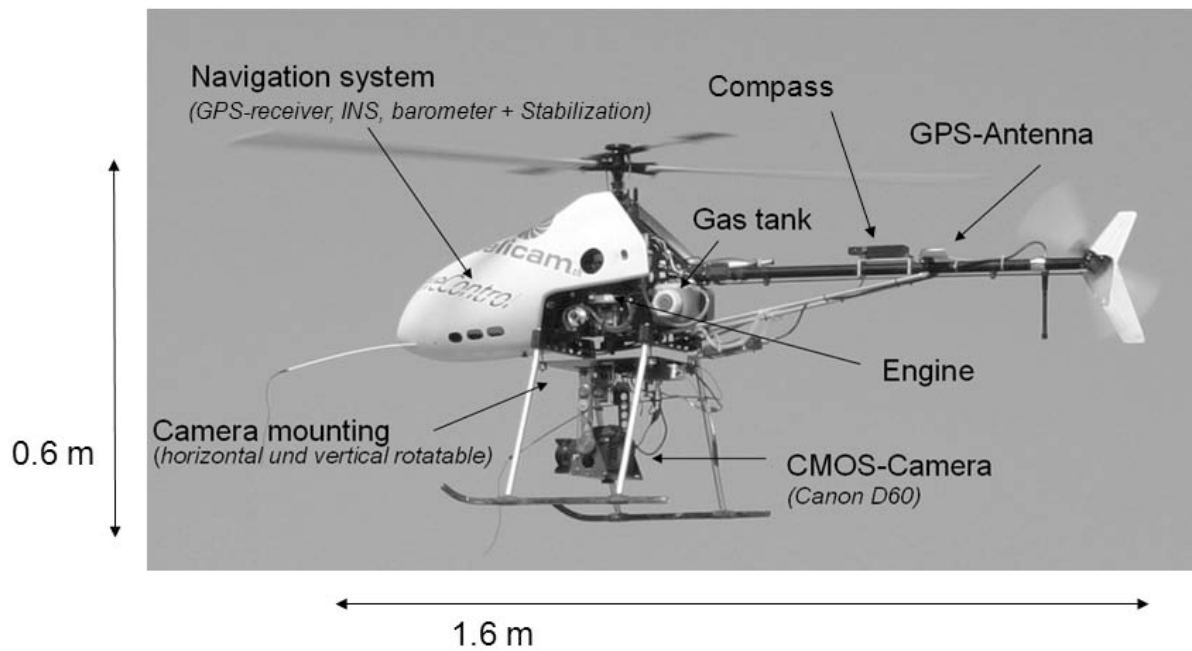
Figure 3-7: Copter 1B from the company Surveycopter and the integrated wePilot (weControl).

Figure 3-8: The flight control station (weGCS) operated by the operator and the pilot in the background during a field mission 2009 in Copan (Honduras).

3.3.2.2 The Flight Control System "wePilot 1000"

The wePilot1000 is intended for professional applications. The wePilot1000 (see Figure 3-10) is a so called "on-demand system", which means that the pilot controls the helicopter with directional commands (forward/lateral/vertical/heading velocity) from the joystick connected to the ground control station or by the geographic coordinates given by the flight path

(waypoints). A combination of both operations is possible in order to interrupt, modify, or continue a specific mission. The wePilot1000 features the following main characteristics:

- Altitude stabilization and velocity control,
- Position and RC transmitter sticks interpreted as velocity commands,
- Integrated GPS/INS system,
- Barometric altimeter,
- Compass,
- Payload intensive flight controller,
- Built-in data logger and telemetry capability,
- Programmable hardware for rapid customization,
- Flight control software weGCS and
- Embedded computer system.
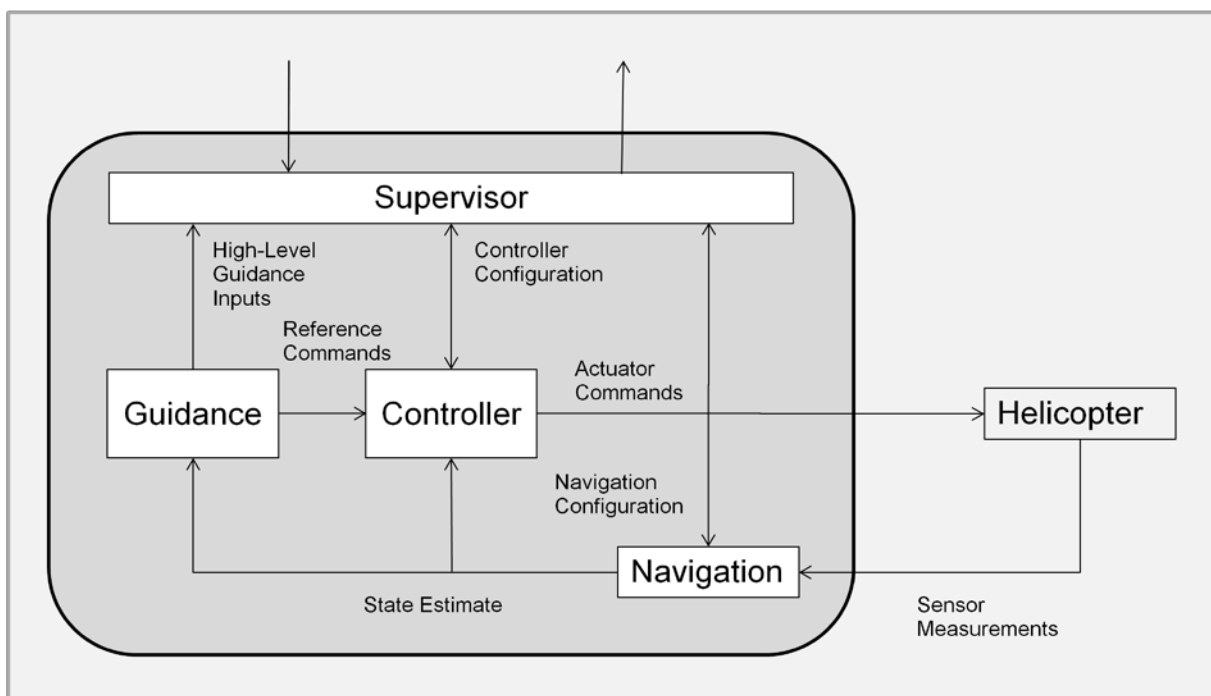
Figure 3-9: Scheme for the flight control system wePilot1000.

The wePilot1000 also provides safety enhancements in case of loss of data communications or failure of the ground control station. Specifically, the wePilot1000 supports a fully autonomous homing process to a previously defined home location. Furthermore, the flight control system can stabilize the helicopter under severe weather conditions, including persistent strong wind and wind gusts. The stabilization performance of the wePilot1000 is an important feature, which allows the use of the system for aerial photography, aerial video recording, or infrared night operations.

The flight control system interacts with the helicopter as shown in Figure 3-9. The helicopter and its integrated sensors provide the navigation unit with input. Using an extended Kalman Filter the system calculates the position, orientation, speed and acceleration of the system on-line (Eck, 2001). These values are transmitted to the Controller, which checks the differences to the given values. Identifying the differences, the Controller sends new action commands to the helicopter to correct the actual values. In addition the navigation data are transmitted to the Guidance, which checks the position to the predefined flight path, which is or can be defined and modified by operator of the system. The Guidance unit gives reference commands to the controller as well, which are transferred to the helicopter again as actuator commands.

Moreover, the computer board allows data communication with various payloads such as gimbals, video and photo cameras. It also includes "black box" data recording capability for post-flight data processing in case of detailed flight analysis. The wePilot1000 electronics is also well isolated against high frequency engine vibrations.

3.3.2.3 Ground Control Station Software (weGCS)
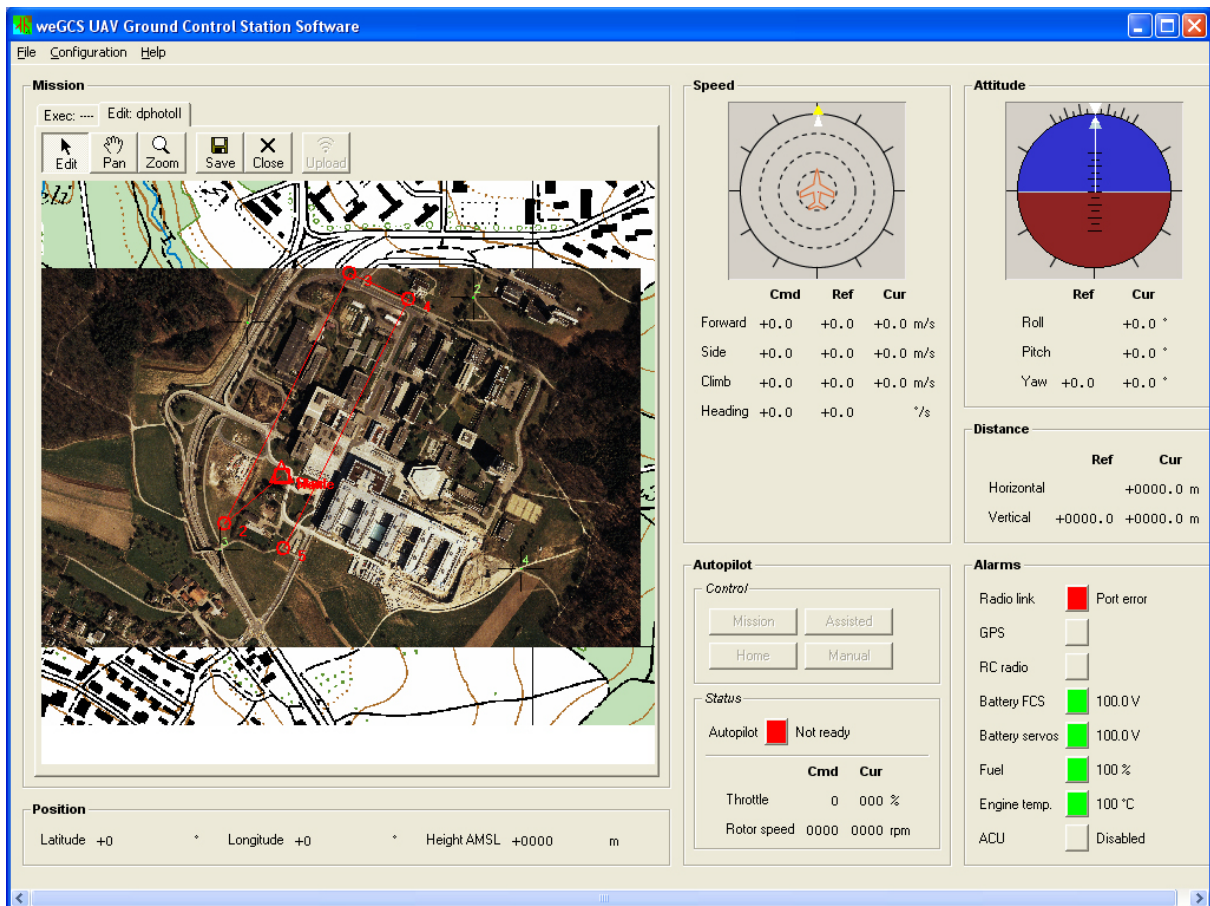
Figure 3-10: Screenshot of the wePilot 1000 showing a mission at the campus ETH Hönggerberg.

The weControl Ground Control Station Software (weGCS) allows, similar to the WayPoint Editor of the MD4-200 system, the definition of the way points using a referenced map, integrated into the weGCS software (see Figure 3-10). Thereby, the image acquisition points can be defined as cruising or stop points, while for cruising points only the start and the end point of a image strip has to be defined and the corresponding baseline between the sequenced images. Moreover, a start and home point has to be defined. The start point permits the set up of the mission relative to the start point, without knowing the exact 3D coordinates. The home point is defined for loss of connection to the helicopter. After 30s without radio connection to the system, the helicopter starts hovering and after an additional 30s without connection, it flies automatically to the home point. The helicopter then hovers at the home point for 180s, before commencing the landing maneuver. Thus, the home point has to be defined in a way that no obstacles are situated between the flight bath and the home point itself.

The weGCS has also a control and steering function during the autonomous flight. All maneuvers can be activated through the flight control station, while in the meantime the reference values for the position, attitude and speed, as well as alarms for the radio link, GPS signal availability, batteries, fuel and engine temperature are monitored through a traffic light system are monitored. The colors of the traffic light are configured as follows: Green is ok and yellow stands for a warning, while red symbolized the trespass of the given limit values (see Figure 3-10). For details on the flight planning integration see paragraph 4.2.

3.3.2.4 Measurement components of the wePilot1000

The flight control system wePilot1000 of our system is based on an integrated navigation solution with redundant sensor information from GPS receiver µ–blox TIM-LP, an INS Crossbow IMU400CD 100, a barometer and a magnetometer from Honeywell HMR2300. The integrated GPS sensor is a C/A Code based single frequency GPS receiver, which also allows differential pseudorange corrections to be considered. The IMU is based on Micro-Electro-Mechanical-System (MEMS) and is therefore categorized as a low quality IMU system. Recently, in 2008 our wePilot 1000 was upgraded to the wePilot1000-10g/N (see Table 3-10). The upgrade consisted of weControl's proprietary IMU (10g accelerometers (Colibrys), 100°/s gyroscopes (Silicon Sensing)) and Novatel's OEMV1 GPS receiver. The upgrade of flight control software include, in addition, a collective limiter in case of engine power loss (auto-rotation), attitude/altitude control in case of GPS loss and the new IMU and GPS receiver fits in the current wePilot housing. The Novatel receiver has a superior performance (not in precision but in terms of robustness and delay) than the µ-blox receiver and is better suited for aerospace applications.

Table 3-10: Given accuracy measures of the three wePilot1000 systems which have been used in our studies (weControl, 2009).

Accuracy measures	wePilot1000 (1-Sigma)	wePilot1000-10g/N (1-Sigma)	wePilot1000 (Scout B1-100)
Horizontal position	2.5m	1.8m	2cm
Vertical position	5.0m	2.0m	2cm
Roll/Pitch	1.0deg	0.1deg	~0.1deg
Yaw	1.0deg	1.0deg	~0.5deg

All given accuracy measures in Table 3-10 are based on characteristic numbers of the integrated sensors and the achieved performance of the flight control systems.

3.3.3 Fixed wing UAVs

In the current study, the focus of our work is mainly on rotary wing UAVs. To give a more complete overview, in the following an example for a fixed wing UAV, which was already used for photogrammetric applications (Grenzdörffer and Engel, 2008), is given.

Figure 3-11: Left: Carolo T200 (Source: Mavionics, 2009); Right: Sky-Sailor solar airplane (Noth, et al., 2007, Fig. 12.10.).

The company Mavionics (Mavionics, 2009) developed a fixed wing UAV, which allows the autonomous flight for different fields of civilian applications. The systems Carolo P330 or Carolo T200 (see Figure 3-11, left) are standard model airplane, which features an autopilot system developed by Mavionics GmbH, mission control software (MCS) and a remote control for manual maneuvers. The standard payload is a Canon Powershot S60. More technical parameters are given in Table 3-11. Similar two the system described so far, the MCS features a georeferenced map, where the flight strips are defined by the start and end point of a flight line. The turn from one line to its successor, is flown in a constant radius, while the minimum radius is limited to 30° in the roll angle by the MCS in order to avoid an instability of the system. After the manual take-off the system changes to the autonomous mode, while the

airplane is close to the first way point. After the mission, the pilot takes over the control and lands the system safe on the ground. More details describing the system and its autopilot and a practical example can be found under Grenzdörffer and Engel, 2008, Grenzdörffer, et al., 2008b, Mavionics, 2009.

Additionally to the fixed wing system above also solar and high altitude long endurance system have a high potential for photogrammetric and remote sensing applications (Noth, et al., 2004, Noth, et al., 2007).

Table 3-11: Overview of fixed-wing, single rotor and coaxial M- and L-class systems.

	Fixed-wing	Single rotor and Coaxial Systems			
	M-Class System		L-Class System		
Feature	Carolo T200	Surveycopter Copter 1B	Aeroscout Scout B1-100	Geocopter GC 201	Swiss-UAV KOAX X-240
UAV category	Mini-UAV	Mini-UAV	Mini-UAV	Mini UAV	Mini-UAV
Special feature of the system		In use since 2003	Laserscanner	Two engines	Usable in alpine areas
Size / Length	1.8m	1.6m	3.3m	2.9m	1.8m
Motortyp	Twin-engine aircraft (Electro motor)	Petrol engine, 26ccm	Petrol engine 100ccm	Turbine engine,	Turbine engine, 8kw
Number of main rotors	2 Propeller	1	1	1	2
Main rotor Ø / Wing span	2.0m	1.80m	3.2m	3.3 m	2.40m
Max. take-off weight	5.6kg	15kg	75kg	80 kg	30kg
Payload capacity	1kg	5kg	18kg	30kg	8kg
Flight autonomy	45min	30min	60min	240min	40min
Max. flying height		2400 (tested at Flueelapass 2007)			

3.4 Large Payload UAV Systems: L-Class

The L-class described in the following is characterized through their capability of carrying a larger payload as the OM- and M-class systems mentioned above. Thus, the L-class systems are able to carry more fuel, which elongate the flight autonomy up to 240min. The larger payload capacity permits also the combination of various sensors into one platform, as well as the integration of more sophisticated sensors result in a high accuracy and stability of the navigation data of the UAV system.

3.4.1 Aeroscout

The Scout B1-100 (Aeroscout, 2009) is a completely autonomous flying model helicopter. A main feature of the scout B1-100 is the large payload of 18-20kg and 10 liters of additional fuel, which allows a maximum flight autonomy of 90 min. The Scout B1-100 is designed to

carry the Riegl airborne LiDAR scanner LMS-Q160 (Aeroscout, 2009, BACS, 2009, Imbach and Eck, 2009, Riegl, 2009 and Figure 3-12).

The LMS-Q160 has an approximate weight of 4.5kg, which is, in comparison to other airborne scanners, extremely lightweight. Despite this, the scanner is robust enough to withstand the shock and vibration load caused by the UAV-system. The maximum measurement range for wire targets is up to 60m, while for flat targets the maximum range goes up to 200m. The scanning range is 80deg, whereas the scanning rate is 5 to 60scans/s. The maximum angular resolution of the scanner is 0.01deg (9mm point sampling distance at 50m flight height). The company Riegl gives an accuracy of 20mm (1 sigma) for a measurement distance of 50m under Riegl test conditions (Riegl, 2009). Using the LMS-Q160 at a flying height of 50m we can achieve a resolution of 50pt/m^2.
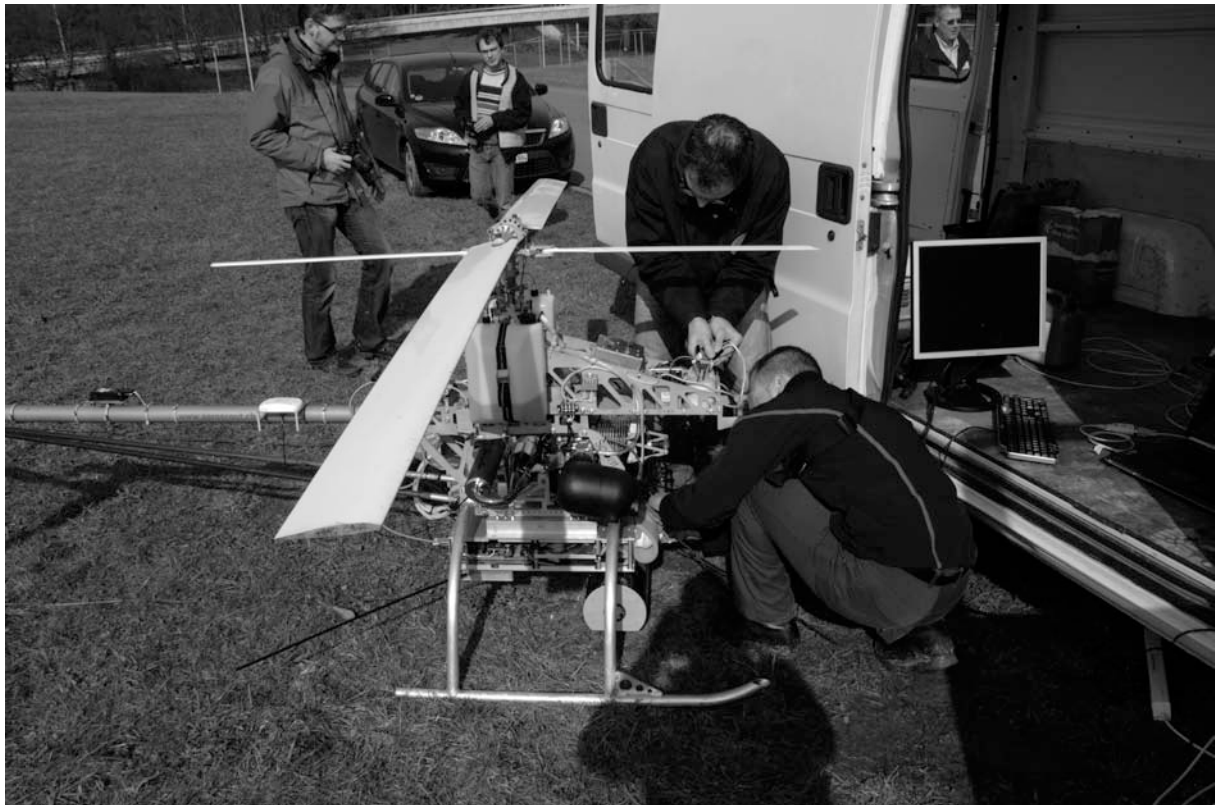
Figure 3-12: Scout B1-100 equipped with the airborne laser scanner LMS-Q160 showing the preparation for the first flight at the Campus Hönggerberg (ETH Zurich).

So far the position and orientation values, observed by the wePilot, were only used for the navigation of the UAV system. For the integration of the airborne scanner on the Scout B1-100, the navigation unit from weControl integrated into the Scout B1-100 has to have a higher accuracy, since these values are used for georeferencing of the LiDAR data.

In addition, the system requires the storage of the binary data stream in real-time, the data has to be synchronized using the UTC time stamp and the electronic components have to be damped to reduce the influence of the vibrations of the system. Therefore, a box for the

electronic equipment is mounted between the skids of the UAV. Since the box is connected to the body of the UAV via shock-mount, all components like IMU and airborne scanner are mounted on or into the box.

3.4.2 Geocopter

The company Geocopter (Geocopter, 2009) is located in the Netherlands. The main focus of Geocopter is on turbine based model helicopter systems (Geocopter GC 201). The system is able to carry up to 30kg payload, which allows also the implementation of medium format cameras or airborne LiDAR systems. Furthermore, the larger payload results also in a higher absolute flying height above mean sea level. In theory up to 4000m a.s.l. The company is also working on a two engines aircraft, which would give an extra safety of the system. This system would also lead to aerial survey flights over urban areas. Details of the system are given in Table 3-11.

Figure 3-13: Geocopter GC 201 during a flight mission in the Netherlands (Source: Geocopter, 2009).

3.5 Conclusions

In this chapter, we have provided an overview of existing classifications, regulations and communities dealing with UAVs and developed a new classification for UAVs (see section 3.1.1). Our new classification allows the selection of an UAV system for a photogrammetric application based on the available project money for hardware and the requested resolution and accuracy of a photogrammetric product. Moreover, the given classifications allow us to select UAVs depending on their endurance, range, weather dependency, maneuverability,

payload capacity and the type of motorization of the UAV system. Giving an example: An application which emphasizes on the monitoring of animals, will be conducted by an UAV with less noise, a long endurance and range capacity. The evaluated UAV systems used in this study were explained in detail and the main functionalities of these systems were provided.

In the following chapter we will now apply the new classifications of UAVs and evaluate some of the provided classifications, like the maneuverability, the control of the UAV system (manual, semi-automated, automated).

4 PROJECT WORKFLOW AND IMAGE DATA ACQUISITION

Figure 4-1: Flight plan for an UAV flight over Campus ETH Hönggerberg visualized in Google Earth (Source: Bare ground and DSM (Google Earth) and 3D Model of Campus Hönggerberg (IGP, ETH Zurich)).

First, an overview of the overall workflow for the processing of UAV images will be given. After that we will concentrate on three aspects. First, we will focus on the flight planning of UAVs, which varies due to the autonomous flight capability, the large spectrum of existing UAVs and the combination of close range and aerial photogrammetry with to the classical flight planning of large-format aerial cameras. The second focus will be on the influence of manual and autonomous flights on the performance of photogrammetric flights and thereby on the quality of the results. In this particular section, examples for manual flight are given, which highlights the need for autonomous photogrammetric flights. Thirdly, we will concentrate on the consistency and accuracy of autonomous flights and a method for the flight performance and accuracy analysis of the 3D trajectory is given. Considering these aspects of autonomous flights, we will apply them in our applications and show the improvements, such as the change from stop to cruising points for the data acquisition (see chapter 6 and 7).

4.1 Workflow

All processing steps of the workflow are categorized in modules, which link each with each other via interfaces. The modules have attributes, which can be defined or modified depending on the procedures specific to individual tasks. The attributes of the modules are generated in the first module "Project Parameter (PP)".

The interfaces will be established in a way that for the individual module the attributes can change, depending on the PPs. Additionally, the interfaces will have functionality for data transformation and formatting. Therefore, with our proposed workflow several UAV applications can be handled.

The main modules are defined as follows:

- o Project parameters (PP)
- o Flight planning (FP)
- o Autonomous photogrammetric flight (APF)
- o Quality check of the data (QCD)
- o UAV Block Triangulation (UAV BT)
- o DSM, Orthophoto, 3D Model (DO3D)

The individual procedures of a module can be a process or a part of a process from commercial or in-house developed software. Figure 4-2 shows which modules were developed by IGP and which were evaluated using existing in-house and commercial

available software packages. Additionally, the figure explains which part of the work is conducted during or after the field work or both.
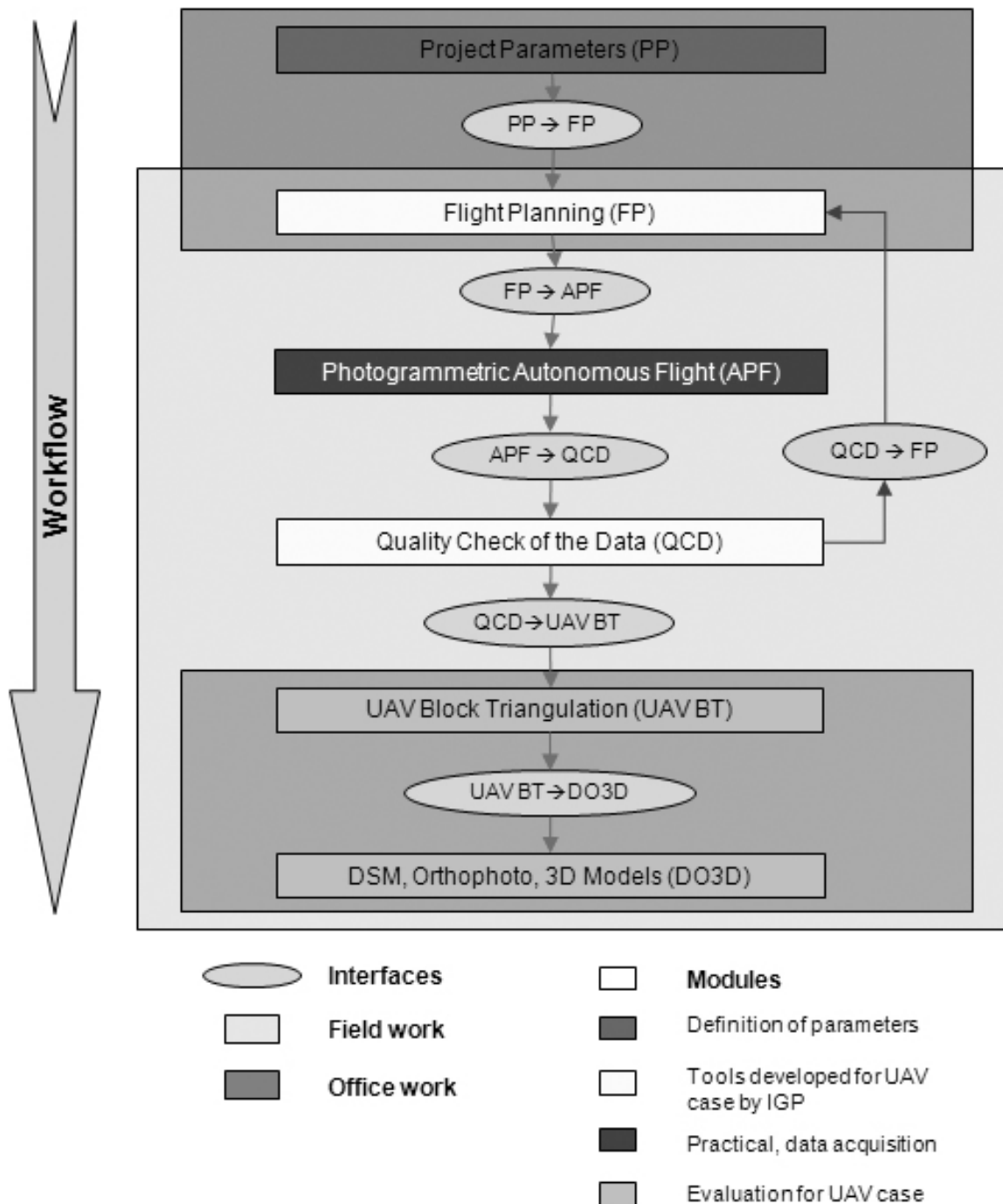
Figure 4-2: Modular Workflow for processing of UAV data showing the main functionalities.

For communication and data transfer between the modules, interfaces are developed and workflows are established. The interfaces have the main functionality to speed up the

communication between the individual working steps (modules). Depending on the application, the interfaces provide the required information from each of the modules.

(a) Design of a flight planning algorithm (FP)

For the automated image acquisition, the flight trajectory of the UAV has to be calculated in advance. PPs like object type, output data, camera sensor, type of model helicopter and flight restrictions are standard project parameters. These parameters can vary from one application to another. Therefore, in depth flight planning, based on the PPs is essential. We define three scenarios in the flight planning module:

- o Documentation of a surface with flat or moderate terrain.
- o Exposure of a rough/ mountainous terrain like hazard areas.
- o 3D modelling of buildings and other objects.

(b) Automation of the photogrammetric flight and improvement of field work (APF)

For the automation of the flight, the following features of the wePilot 1000 system were modified.

- o Autonomous triggering of images and autonomous take-off and landing.
- o Functionality for the camera rotation and measurement of these rotations
- o Increase of the accuracy of position and orientation
    - New GPS and INS sensors with higher accuracy and performance.
    - Triggering and storage of orientation data with image data.
    - DGPS for the LiDAR data acquisition.

The needs for the modification of the flight planning tool were formulated through our studies and implemented by the company weControl.

The enhancement of accuracy of the orientation values can reduce the required number of GCPs (compare Cramer, 2001). For areas, where marked control points cannot be distributed, special natural features such as intersecting lines at street junctions will be used as control points. These points can be determined before or even after the flight using a total station or DGPS.

(c) Quality check of the data (QCD)

Real time quality checking of the data is an important task, since the data acquisition is often time limited and repetition not possible. For quality control of image processing, we provided downsampled stitched overview images directly at the site for a quick quality check. The quality check therefore consisted of the following components:

- o Comparison of defined and acquired positions.

- o Generation of first results during or after the field work.

A table for an additional image flight is generated, when the following circumstances occur and a new flight will be completed.

- o Acquired position does not fit to the predefined acquisition point.

- o An image is not acquired.

- o The footprint comparison shows gaps or the required overlapping interval is not fulfilled.

- o The intermediate results show errors.

(d) UAV Block Triangulation (UAV BT)

An additional focus of this study is on the existing software packages, which can be used for the processing of UAV images. The integration of position and orientation data generated by the navigation unit of the UAV, will lead to a reduction of the number of control points required for the orientation (see Cramer, 2001 pp. 15-17). The use of different independent sensors integrated into the platform will also reduce the time and cost for image measurements and bundle adjustment.

(e) DSM, Orthophoto, 3D Model (DO3D)

For this module we will use commercial software packages and existing inhouse-developed tools. Because of the wide variety of photogrammetric processing software, we categorize them into three classes based on their capability for processing of aerial, terrestrial and a combination of aerial and terrestrial data. We will generate a list for the categories and will evaluate a selection of software packages for UAV data processing (chapter 5) and use them in our applications (see chapters 6 and 7).

In the following sections the modules explained above are described in detail.

4.2 Flight Planning

Since the earliest works with analogue aerial images, flight planning before image acquisition is essential for the aerial image orientation and the generation of photogrammetric products. The most important parameters and formulas for mission planning of an aerial survey are described below and can be found in the literature (amongst others in Kraus, 2007 pp. 144-150, Warner, et al., 1996 pp. 173-193, Schwidefsky and Ackermann, 1976 pp. 131-137). In order to determine the flight path, the main parameters needed are listed in Table 4-1.

The image scale factor is defined by the flight height above ground H_g and the focal length of the camera systems:

$$m_b = \frac{H_g}{f} \qquad \text{4-1}$$

The ground distance of an image side can be calculated with S' or s' respectively if an analogue or digital camera is used:

$$S = \frac{S' \times H_g}{f} \qquad \text{4-2}$$

The length of the baseline is given with p% forward overlap

$$B = S\left(1 - \frac{p}{100}\right) \qquad \text{4-3}$$

and the distance between two neighbouring flight lines with q% side lap can be calculated

$$a = S\left(1 - \frac{q}{100}\right) \qquad \text{4-4}$$

The covered model area is product of

$$F_m = S^2 - S \times B \qquad \text{4-5}$$

The expected accuracy in height can be calculated with the measurement accuracy in planimetry s_x and the ratio of flight height and baseline in image space, while s_x is defined through the measurement method and the pixel size (p_x). Manually measured points can be defined with an accuracy as low as to 0.5 Pixel, while automatic measurement methods allow an accuracy of down to 0.1 Pixel for natural targets for flat terrain and good texture (Heipke, 1999). In alpine areas the point measurement accuracy increases to 0.5 Pixel (Kersten, 1999). However, for UAV images it can be expected to achieve approximately 0.5 Pixel. The accuracies then calculate as:

$$s_x = s_{x\,(Mes)} \times p_x \qquad\qquad 4\text{-}6$$

$$s_z = s_x \times \frac{H_g}{b} \qquad\qquad 4\text{-}7$$

Table 4-1: Flight parameters for the mission planning of photogrammetric aerial flights.

Description	Parameter
Image scale factor	m_b
Focal length	f
Flight height	H_g
Dimension of the analog image and sensor size for digital cameras	s' (x,y)
Scanning resolution for analogue images and the pixel size for digital cameras	p_x and p_y
Sensor diagonal	d
Ground distance of the image	S (X,Y)
Along and across track overlap	p and q
Baseline in image and object space	b and B
Distance between the flight lines	a
Length and width of area to be covered	L_p and L_q
Model area (Stereo coverage)	F_m
Position of the Area	$P_{1..4}\,(X,Y)$
Average terrain height	H_T
Accuracy in planimetry and height	s_x and s_z
Measurements accuracy (Pixel)	$s_{x\,(Mes)}$
Ground velocity	V_g
Velocities of the UAV (Translation and angular velocity)	$V_{X,Y,Z}$ and $V_{\Psi,\,\Theta,\,\Phi}$
Image motion	w
Shutter speed	Δt
Time between two acquisition points	dT
Field of view	FOV
Image acquisition point	P (X, Y, Z)

For the standard large format digital and analogue aerial cameras, appropriate software packages are provided by the camera manufacturers (Intergraph/ZI, 2009, Leica, 2009,Vexcel, 2009). Similarly, for the medium format cameras available on the market, such as DigiCAM quattro (IGI-Systems, 2009) and AIC-x1 (RolleiMetric, 2009), and companies like IGI and Aerotopol (Aerotopol, 2009), manufacturers have developed their own mission planning software.

The commercial mission planning packages for aerial images allow, after the set up of the main project parameters like flight height, coordinate system and camera parameters, the definition of the area of interest in a graphical interface. Similar to a GIS environment, it is possible to load a map and elevation. Some packages also allow the integration of existing 3D-CAD models. After the definition of these parameters, the software calculates the coordinates of the image acquisition points of the flight lines. In addition, the parameters like number of images, expected amount of hard disk memory, accuracy in planimetry and height can be checked and adapted in the software. Finally, the coordinates can be exported and integrated in the flight control system. The flight control system transforms the coordinates and the additional parameters into control commands, which are realized through the servos controlling the UAV.

4.2.1 Flight planning for UAVs

Existing tools for flight/path planning for UAVs to date have been developed for military, robotics, computer vision and artificial intelligence applications. The main research focus has been on extravagant flight manoeuvres like flips and rolls (Abbeel, et al., 2007), collision avoidance (Bellingham, et al., 2003 and Pettersson and Doherty, 2004), automated target tracking (Nordberg, et al., 2002) and operations like the "follow me" modus (Mikrokopter, 2009). Hence, tools have been developed, which work in a local 3D environment, where static and passive mobile obstacles are known. Thus, local path planners are able to produce fast collision-free trajectories (Sasiadek and Duleba, 2000).

Nowadays, in these communities, point navigation for UAVs is a standard tool (Niranjan, et al., 2007). Thus, the autonomous flight based on defined points in a global coordinate system is possible for most of the M- and L-Class UAV systems, while for the OM-class UAVs the control is mostly done in the manual or assisted flight modus. Though, there is a need of the integration and adaptation of photogrammetric flights into the UAV path planning.

In general, UAV mission planning software requires some additional functions integrated, such as the photogrammetric aerial flight planning tools. For the autonomous flights of UAVs, a start and a home point have to be defined (see Chapter 3.3.2.3). Based on the start point, the mission is set up relative to its coordinate. Moreover, some packages allow in addition to the way points, the definition of lines, paths, boundaries and no go areas (Gonzalez, et al., 2006 and Wzorek, et al., 2006). This is especially the case, if the UAV mission is completely autonomous, like in military applications or for vision recognition based flights.

Trisirisatayawong and Cheewinsiriwat, 2004 developed a GIS-based flight planning system, which includes parameters like altitude, aircraft position, viewing angle etc. for UAV flight planning. This system depends on the existing GIS software. Our workflow, described in the following section, is a standalone tool, which easily can be integrated into different software packages, as well as operating systems. It also allows the integration into various UAV operating systems.

Table 4-2: Flight tools for UAVs showing the specification and possible application of the tool.

Flight tool	Specifications	Applications
2/2.5D	Map/Orthoimage & DSM	Flat and moderate terrain
3D	DSM	Mountainous and steep areas
Circle	Map/Orthoimage & Object	Single objects/buildings

Combining both the photogrammetric flight planning and the mission planning of UAVs leads to flight planning for UAVs. Since UAVs operate in a transition section between aerial and terrestrial photogrammetry, where the various camera views are available for data acquisition, we propose the following classification of flight tools depending on the applications (see Table 4-2). As outlined in Table 4-2, we distinguish between flat and moderate terrain, which is the situation for most of the standard applications and mountainous and steep areas, as well as single objects. The documentation of cities can be done with the 2/2.5D flight planning tool, while the flight planning of the data acquisition of the facades of streets can be combination of the 2/2.5D and the circle tool.
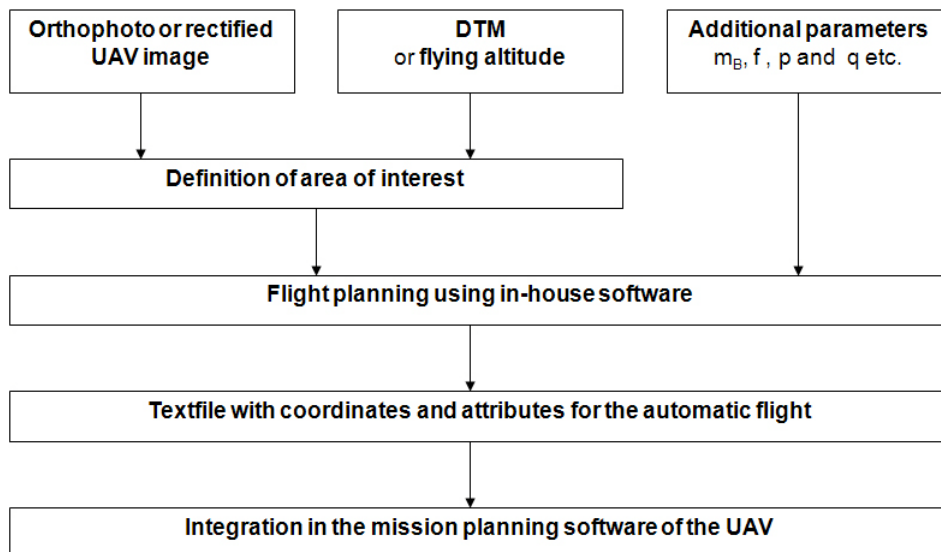
Figure 4-3: Workflow for the flight planning of photogrammetric UAV flights in the 2D and 2.5D case.

The area of interest can be defined in a map or orthoimage using a GIS system, as well as in a 3D world viewer like Google Earth, Virtual Earth etc. or just the given coordinates of the boundaries describing the area of interest. However, if no information about the area is available, the UAV system can acquire its own overview image. This image can be rectified and used for the mission planning. With the defined borders of the area and the additional flight parameters, the flight planning is generated by an in-house developed tool. The outcome of the flight plan are the coordinates of the image acquisition points and attributes for the automatic flight, which finally can be integrated into the mission planning software of the UAV and visualized in a 3D world viewer, such as Google Earth (GoogleEarth, 2009; see Figure 4-27).

In addition to the flight planning for the 2 &2.5D case, there is also a need for the 3D case. Particularly, in steep areas the nadir view would generate a lot of occlusions in the data set. Therefore, a camera view orthogonal to the surface helps to avoid the major occlusions in the data set.

In the 3D case the area of interest is selected in an existing elevation model, and, accordingly, the area is separated into sections. For each particular section a plane is defined in a way that the average 3D distance of the surface to the plane is reduced to a minimum. While looking perpendicular to the surface, we assume to reduce the occlusion in the images. With the given flying distance to the surface, a parallel plane is defined (see Figure 4-4). In the new plane the area of interest is projected and the inclined flight lines for the helicopter flight are generated.
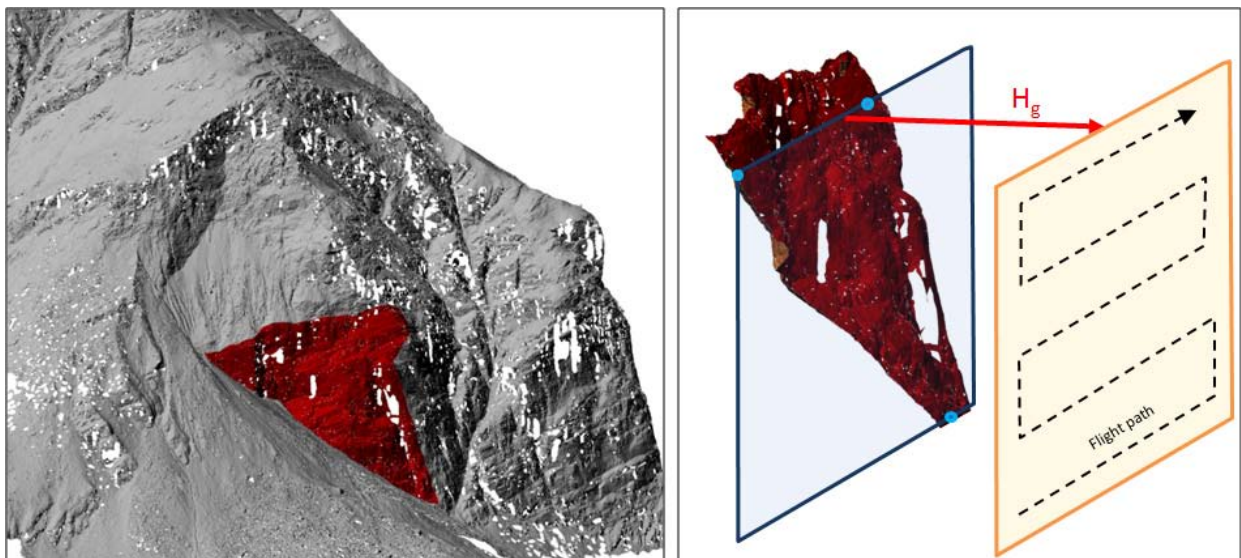
Figure 4-4: Left: Example for a 3D case showing the existing DSM. Right: Fitted plane for the area of interest and a parallel plane with a distance H_g to the fitted plane.

The flight tool, so called Circle (see Table 4-2), was developed for single objects like buildings. In this case, a flight line defined as a circle or ellipse is set around an object. For the flight the camera will be turned in a way that the façade and the roof of the object are visible in the image. While most of the mission planning software for UAVs doesn't allow the integration of the circle, the circle is subdivided into sections. Thus, for the start and end point of a section the coordinates are calculated and integrated as cruising points into the flight planning software.

4.2.2 Integration into the mission planning software

In the following section we will describe the integration of the defined coordinates into the mission planning software packages weGCS (weControl, 2009) and MdCockpit (microdrones, 2009b). Before describing the mission planning tools, the coordinate systems used are defined.

4.2.2.1 Definition of coordinate systems

For the mathematical description of objects, we have to define them within a reference system. In the following section, the coordinate systems needed for the photogrammetric processing of UAV data are described.
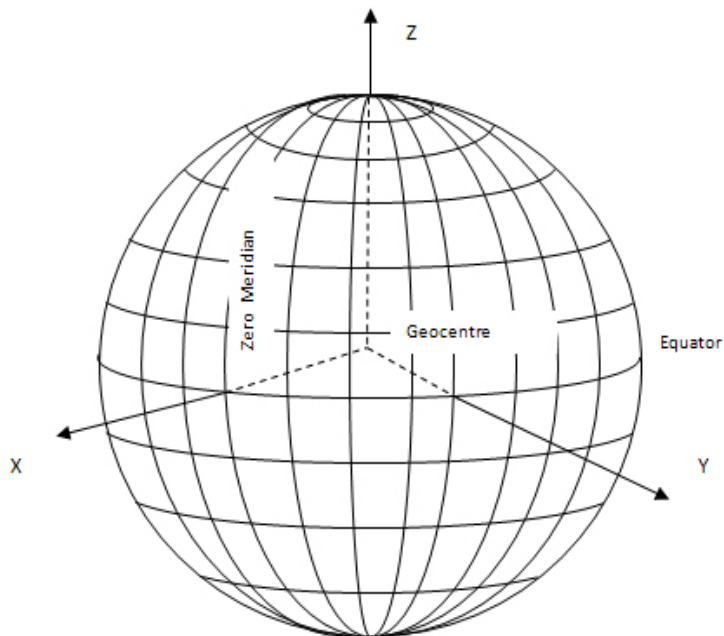
Figure 4-5: Model of the geocentric coordinate system WGS84.

Global coordinate system:
Global coordinate systems are, in general, described as solar or earth fixed coordinate system, where the coordinate axis are for example defined by means of VLBI (Very long baseline

interferometry), SLR (Satellite Laser Ranging), GPS measurements or observation to quasars. These systems have a defined origin; for the geocentric coordinate systems this is the centre of gravity of the earth.

GPS measurements use the WGS84 (World Geodetic System 1984), which is a geocentric coordinate system. The centre of gravity results from the global equipotential model of the earth. The X-axis is defined through the intersection point of the null meridian and the equator, the Z-axis is equal to the rotation axis of the earth, while movements of the pole are taken into account, the Y-axis completes a right handed coordinate system (see Figure 4-5).
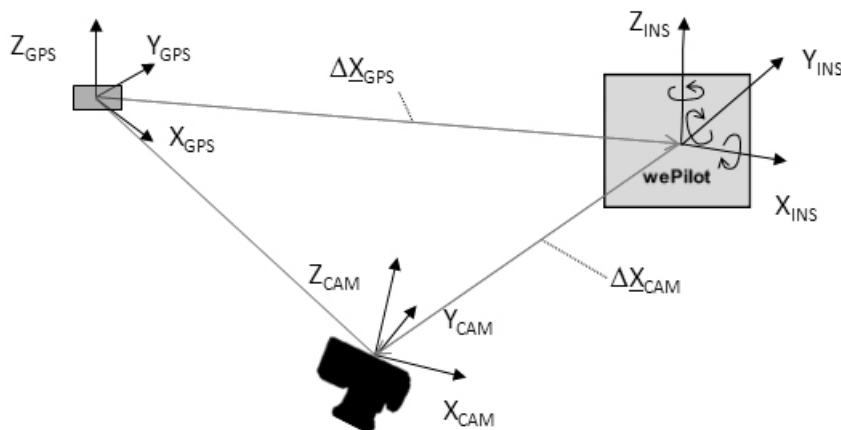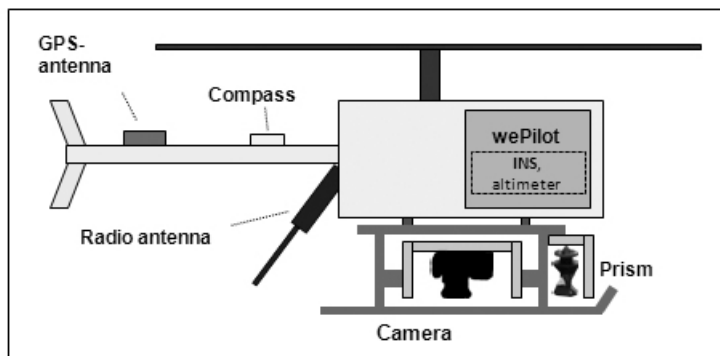
Figure 4-6: Scheme of the main navigation sensors and camera integrated in the Copter 1B.

Local coordinate system:

In contrast to a global coordinate system, local coordinate systems are only valid for a small area. In general, these systems are right-handed systems centered at a chosen point P, with the X-axis being a tangent to the local parallel and looking toward East. The Y-axis is tangent to the local meridian and looks toward North, while the Z-axis is directed upwards using orthometric heights (geoid). An example for a local coordinate systems is the Swiss LV03 system.

Platform and device coordinate systems:

The devices mounted on the UAV are shown in the upper schema of Figure 4-6. UAV, INS and camera systems are local 3D Cartesian coordinate systems. The INS system of the copter 1B determine also the coordinate system of the navigation and stabilization unit (wePilot) of our Copter 1B system. With respect to the inertial reference frame, the rotation angles are defined as: Yaw angle (Ψ) around Z-axis, pitch angle (Θ) around Y-axis and roll angle (Φ) around X-axis.

The camera coordinate system depends on the orientation of the camera mounted on the UAV. In the standard configuration, the X-axis of the camera is mounted parallel to the bow direction of the UAV (flight direction), the Z-axis is parallel to the acquisition axis with the normal to the baseline and the Y-axis completes the right-hand-coordinate system. The centre of origin is defined by the projection center of the camera.

Image coordinate systems:
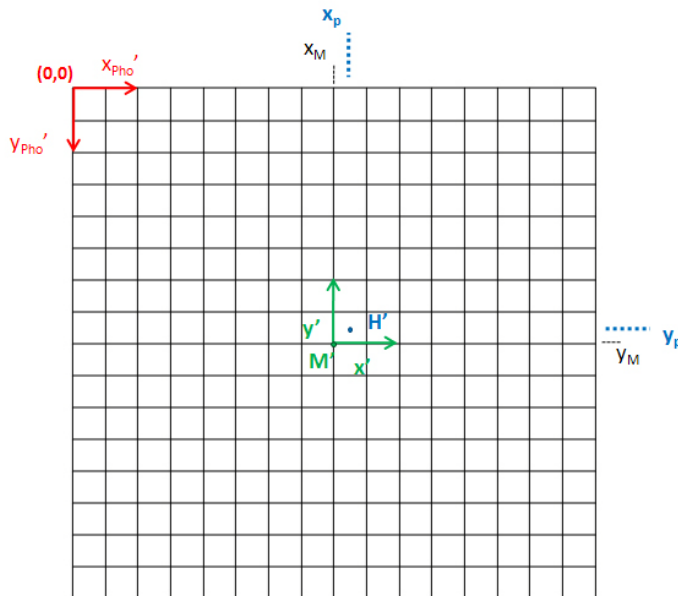
Figure 4-7: Definition of sensor (x_{pho}' and y_{pho}'; e.g. CCD and CMOS) and image (x'and y') coordinate systems.

The sensor coordinate system is a 2-dimensional system, where the y_{Pho}'-axis (rows) is parallel to the acquisition axis and the x_{Pho}'-axis (columns) is defined lateral (see Figure 4-7). The center of the image M' (x_M and y_M) is defined by means of reference or fiducial points (film based system) or the pixel array (electronic systems). The principal point H' (x_p and y_p) is defined as the intersecting point of the optical axis and the image plane. The sensor coordinates (Pixel for digital cameras) can be transformed into metric coordinates using the pixel size p_x and p_y (see equation 4-8).

$$x' = (x'_{Pho} - x_M)p_x$$
$$y' = -(y'_{Pho} - y_M)p_y$$

<div align="right">4-8</div>

4.2.2.2 Direct georeferencing

The direct georeferencing is defined as the direct measurement of the exterior orientation parameters for each image or scanning line of line sensors and aerial laser scanners. Thus, the exterior orientation parameters are observed through the GPS and INS sensors integrated into the platform (Cramer, 2001). In contrast to manned aerial platforms (Haala, 2005), UAVs mostly have integrated low-cost sensors (Eisenbeiss, 2003, Wendel, et al., 2006). Haala, 2005 and Ellum and El-Sheimy, 2006 give a comprehensive overview about the data integration strategy for the computation of the exterior orientation.

Using the coordinate systems defined in paragraph 4.2.2.1, for each point observed in the image (P), the relation between camera and ground coordinate system (Ob) can be described with the following equation 4-9.

$$\begin{pmatrix} X \\ Y \\ Z \end{pmatrix}_{Ob} = \begin{pmatrix} X_0 \\ Y_0 \\ Z_0 \end{pmatrix}_{Ob} + \lambda R_P^{Ob}(\omega, \varphi, \kappa) \begin{pmatrix} (x' - x_p) \\ (y' - y_p) \\ -f \end{pmatrix}_P$$

<div align="right">4-9</div>

The parameters of the interior orientation are the principal point (x_p and y_p) and the focal length f, while the parameters of the exterior orientation consist of coordinates of the projection centre in the object coordinate system and the rotation matrix $R_P^{Ob}(\omega, \varphi, \kappa)$. R_P^{Ob} is the rotation matrix from image coordinate into the object coordinate system. λ is a scale factor.

Considering the position of the camera, GPS and INS in the UAV, which are similar to components mounted in manned aircrafts (compare Cramer, 2001), equation 4-9 can be expanded to equation 4-10.

$$\begin{pmatrix} X \\ Y \\ Z \end{pmatrix}_{Ob} = \begin{pmatrix} X_0 \\ Y_0 \\ Z_0 \end{pmatrix}_{Ob} + R_{INS}^{Ob} \left(\lambda R_P^{INS} \begin{pmatrix} (x' - x_p) \\ (y' - y_p) \\ -f \end{pmatrix} + \begin{pmatrix} \Delta X_{cam} \\ \Delta Y_{cam} \\ \Delta Z_{cam} \end{pmatrix} + \begin{pmatrix} \Delta X_{GPS} \\ \Delta Y_{GPS} \\ \Delta Z_{GPS} \end{pmatrix} \right)_P$$

<div align="right">4-10</div>

The single terms are defined as follows:

$P = \begin{pmatrix} X \\ Y \\ Z \end{pmatrix}_{Ob}$	Object point in object coordinate system (Global or local coordinate system) Ob.
$\begin{pmatrix} X_0 \\ Y_0 \\ Z_0 \end{pmatrix}_{Ob}$	GPS/INS position in the object coordinate system Ob.
$\begin{pmatrix} \Delta X_{cam} \\ \Delta Y_{cam} \\ \Delta Z_{cam} \end{pmatrix}$	Vector between INS and the projection center of the camera, defined in the INS coordinate system.
$\begin{pmatrix} \Delta X_{GPS} \\ \Delta Y_{GPS} \\ \Delta Z_{GPS} \end{pmatrix}$	Vector between GPS (antenna phase center) and INS, defined in the INS coordinate system.
R_{INS}^{Ob}	Rotation of the INS coordinate system into the object coordinate system Ob. The rotation angles are defined through the GPS/INS modul.
R_P^{INS}	Rotation of the image coordinate system P into the INS coordinate system.

4.2.2.3 WeGCS – weControl Ground Control Station

As input for weGCS, a text file with 3D coordinates of the acquisition points, parameters for flying velocity and the definition of point status (stop, crossing or turning point) is generated. These coordinates can be transferred into the weGCS-Mission file (XML-file). For each way point the attributes are defined (Table 4-1).

The first and the second way point define the start and way point respectively, while the following numbers stand for a mission point. The class identifies the point absolutely or relatively with respect to the start point. Behavior of the point stands for cruising or stop, while the payload enables or disables the payload function.

Table 4-3: Attributes used for a waypoint in the weGCS software.

Waypoint
Number
Class
Behavior
Speed
Payload
RelativeData (Northing, Easting, Height)
AbsoluteData (Longitude, Latitude, m a.s.l. Height)

The *RelativeData* and *AbsolutData* are the X, Y, Z or Lo, La, H_{ortho} coordinates of the way point (See Table 4-3). The maximum speed v_{max} is limited through v_{max} (UAV) and v_{max} (w). v_{max} is defined as:

$$v_{\max(w)} = v_G \times \Delta t \times m_b \qquad \text{4-11}$$

$$v_{max} < v_{max}(w) \cap < v_{max}(UAV) \qquad \text{4-12}$$

The *AbsoluteData* can be calculated with respect to a starting point P_1 using the following parameters

$$AbsoluteData(X,Y,Z) = P(X,Y,Z)_i = f\left(P_1, L_p, L_q, f, H_g, H_T, p, q, S'\right) \qquad \text{4-13}$$

The *RealtiveData* of a point can be calculated from the difference of the coordinates of the start point and the *AbsoluteData*.

$$relativeData\,(dX, dY, dZ) = start\,point\,(Y,Y,Z) - AbsoluteData(X,Y,Z) \qquad \text{4-14}$$

The acquisition of the images using the wePilot1000 is possible in different modi: The images can be acquired through manual triggering on a stop point during the manual, as well as the autonomous, flight (see Figure 4-9). The image acquisition can also be automatically enabled after arriving a predefined stop or cruising point.
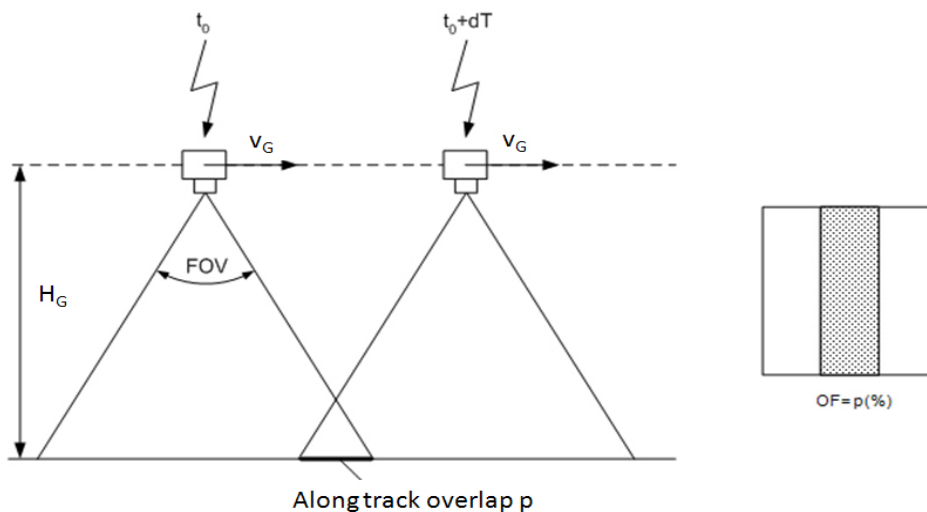
Figure 4-8: Definition of the overlap using the field of view function in the weGCS software.

From the definition of the field of view (FOV; see equation 4-15 and Table 4-1) of the camera and the along track overlap (see Table 4-1), the complete images can also be obtained without manual control using the autonomous flight modus. For this modus, a second option enables one to define the baseline. With a predefined velocity the time interval for the image triggering is calculated. Using these two options for the autonomous mode, the coordinates for image acquisition are indirectly given from the defined start and end point of a flight line (see Figure 3-10).

$$FOV = 2 \times \tan^{-1}\left(\frac{d}{2f}\right) \qquad 4\text{-}15$$
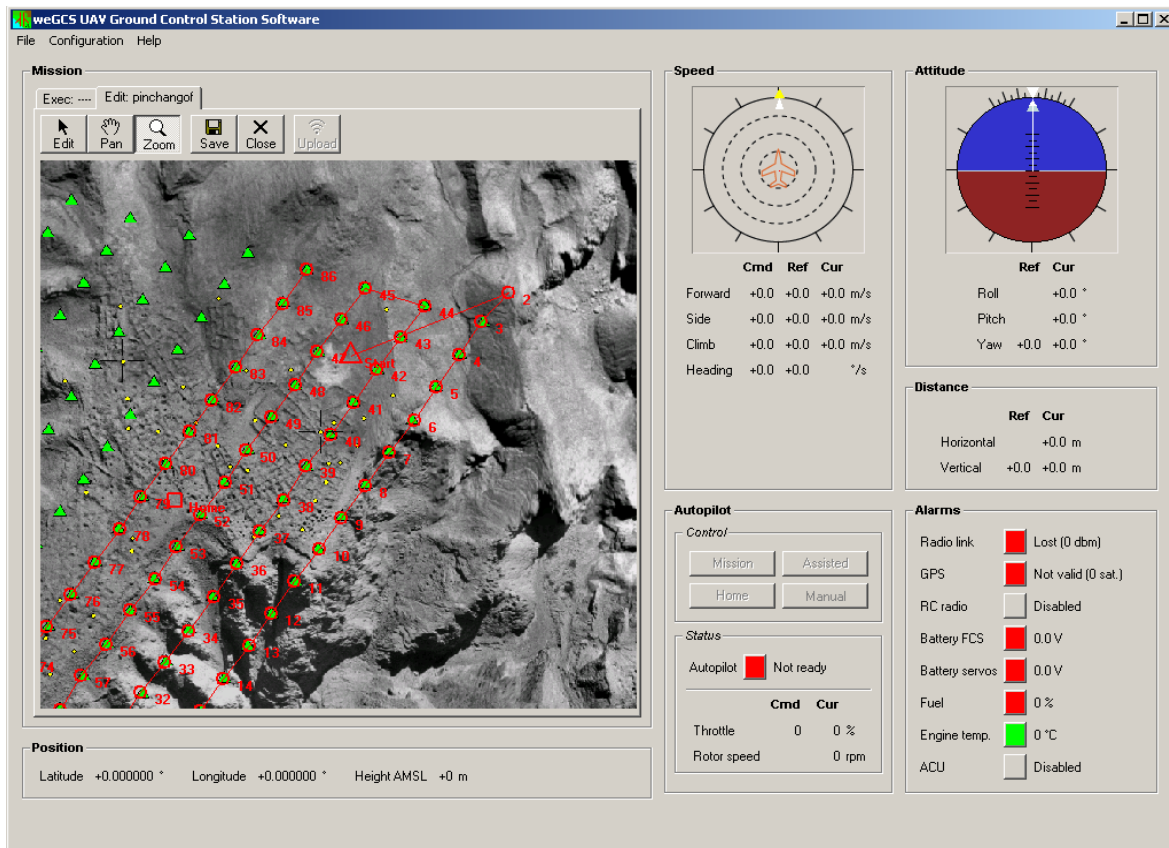
Figure 4-9: WeGCS software showing the flight planning in Pinchango Alto. The image acquisition centres were defined as stop points.

During the image acquisition the wePilot saves image number, position, orientation, date and time of image acquisition (UTC time), the relative height to the start point and the number of the observed GPS satellites (see Figure 4-10). An example of the metadata saved for each camera position is shown in Figure 4-11.

When hotshoe of camera triggers, the flight control system records the following data:
- image number
- UTC year
- UTC month
- UTC day
- UTC hours
- UTC minutes
- UTC seconds (resolution 20ms)
- camera roll angle [deg]
- camera pitch angle [deg]
- camera yaw angle [deg]
- UAV latitude [rad*10^8]
- UAV longitude [rad*10^8]
- UAV altitude (mean sea level) [m]
- relative altitude with respect to takeoff location [m]
- number of GPS satelites:
    – 0x0s = s satelites
    – 0x10 = no valid GPS solution

Figure 4-10: Description of the Metadata of the wePilot1000 (Source: weControl, 2009).

```
1,2009,4,23,13,4,4300,-0.72,-1.85,-177.65,25896600,-155581032,603.50,0.06,9
2,2009,4,23,13,13,3700,-5.42,-2.05,167.50,25897143,-155580067,690.33,86.89,11
3,2009,4,23,13,13,3800,-3.72,1.20,167.90,25897065,-155580054,690.50,87.05,11
4,2009,4,23,13,13,4000,0.32,0.19,172.43,25896990,-155580034,690.61,87.17,11
5,2009,4,23,13,13,4200,0.03,-0.95,178.94,25896912,-155580028,690.56,87.12,11
6,2009,4,23,13,13,4300,-2.69,-0.30,-179.08,25896832,-155580036,690.47,87.03,11
7,2009,4,23,13,13,4500,-2.83,-0.01,179.90,25896753,-155580041,690.41,86.97,11
8,2009,4,23,13,13,4700,-1.67,-0.70,-179.98,25896674,-155580041,690.42,86.98,11
9,2009,4,23,13,13,4800,-2.11,-0.61,-179.27,25896594,-155580044,690.45,87.00,11
10,2009,4,23,13,13,5000,-2.53,-0.30,-179.87,25896515,-155580053,690.43,86.99,11
11,2009,4,23,13,13,5200,-2.32,-0.52,179.03,25896436,-155580057,690.38,86.93,11
12,2009,4,23,13,13,5300,-2.25,-0.66,178.90,25896357,-155580061,690.22,86.78,11
13,2009,4,23,13,13,5500,-3.22,-0.25,178.42,25896278,-155580065,690.39,86.94,11
14,2009,4,23,13,13,5700,-2.56,-0.61,177.87,25896199,-155580069,690.42,86.97,11
15,2009,4,23,13,13,5800,-2.68,-0.69,178.00,25896119,-155580070,690.45,87.00,11
16,2009,4,23,13,14,0,-2.31,-0.34,178.23,25896040,-155580071,690.40,86.96,11
17,2009,4,23,13,14,200,-2.55,-0.69,179.51,25895961,-155580073,690.40,86.96,11
18,2009,4,23,13,14,300,-2.38,-0.18,179.56,25895881,-155580075,690.38,86.94,11
19,2009,4,23,13,14,500,-3.42,-0.41,-179.89,25895803,-155580081,690.51,87.07,11
20,2009,4,23,13,14,700,-2.34,-0.75,179.34,25895724,-155580081,690.42,86.98,11
```

Figure 4-11: Example of the Metadata of the wePilot1000.

Finally, after the image acquisition the metadata, which are saved in the global coordinate system (WGS84), can be transformed using formula 4-16 into a local coordinate system, like the Swiss LV03 (see Figure 4-12).

Image	Y	X	H	Distance	Roll	Nick	Yaw	#Sat
1	-9275309.52	3701903.88	603.50	0.00	-0.72	-1.85	-177.65	9
2	-9275231.86	3701834.33	690.33	104.25	-5.42	-2.05	167.50	11
3	-9275237.50	3701831.28	690.50	6.41	-3.72	1.20	167.90	11
4	-9275242.65	3701827.71	690.61	6.27	0.32	0.19	172.43	11
5	-9275248.55	3701825.26	690.56	6.38	0.03	-0.95	178.94	11
6	-9275255.11	3701823.97	690.47	6.69	-2.69	-0.30	-179.08	11
7	-9275261.48	3701822.45	690.41	6.55	-2.83	-0.01	179.90	11
8	-9275267.68	3701820.50	690.42	6.49	-1.67	-0.70	-179.98	11
9	-9275274.06	3701818.78	690.45	6.61	-2.11	-0.61	-179.27	11
10	-9275280.58	3701817.60	690.43	6.63	-2.53	-0.30	-179.87	11
11	-9275286.91	3701815.99	690.38	6.54	-2.32	-0.52	179.03	11
12	-9275293.25	3701814.38	690.22	6.54	-2.25	-0.66	178.90	11
13	-9275299.59	3701812.77	690.39	6.54	-3.22	-0.25	178.42	11
14	9275305.93	3701811.16	690.42	6.54	2.56	0.61	177.87	11

Figure 4-12: Example of the transformed Metadata of the wePilot1000 into the LV03 system.

4.2.2.4 MdCockpit

Table 4-4: Attributes used for a waypoint in the mdCockpit software.

Waypoint	
Waypoint options	*Point number*
	Description
	Height above ground H_g
	Speed horizontal and vertical (v_H, v_V)
	Camera control
Waypoint position	*Absolute (Longitude, Latitude)*
	Relative (Northing, Easting)
Waypoint interest	*Absolute (Longitude, Latitude, Altitude)*
Vector yaw options	*Yaw angle*
	Yaw continuous move
	Yaw movement direction
	Auto adjust to Point of interest/next waypoint
	Yaw movement speed
Waypoint action	*Task*
	Dwell
	Auto adjust to Point of interest/next waypoint
	Yaw continuous move
	Yaw movement direction
	Camera servo pitch,
	Camera servo zoom
	Camera servo trigger
	Photo interval

The software mdCockpit (microdrones, 2009b) allows detailed individual flight planning prior to the flight mission. Image acquisition points are manually defined in the map. Thus, points defined previously, have to be manually integrated into the software. The attributes of a waypoint defined in mdCockpit are given in Table 4-4.

The absolute and relative coordinates defined in mdCockpit can be generated using Equation 4-13. The additional attributes have to be defined manually. However, mdCockpit allows the definition of a point of interest where the camera automatically acquires images, while the field of view is directed to the point of interest. This function supports the flight tool "Circle", defined in the previous section. Moreover, the task panorama can be used for the initial flight

planning, if the area is completely unknown. Therefore, only one point is defined and the camera automatically generates images for a panorama view.

Finally, for the analysis of the predefined flight path, the trajectory can be exported to GoogleEarth in the KML data format. This procedure allows one to check the flight path for possible collisions in the local environment (see Figure 4-13).
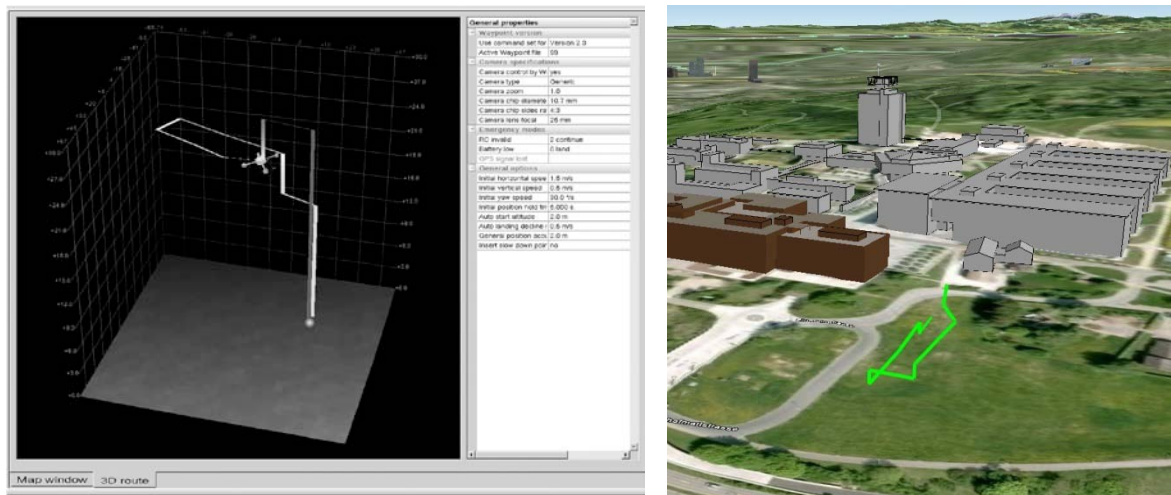
Figure 4-13: Left: Screenshot of the 3D view in the waypoint editor showing the same flight plan at ETH Hönggerberg as Figure 3-6. Right: Exported trajectory shown in Google Earth.

Similar to the weGCS package, mdCockpit is suitable for manual and autonomous flights. Thus, images can be manually triggered in the manual or assisted flight modus, while the autonomous flight follows the actions defined in the waypoint editor. All actions of a waypoint are described in detail in the mdCockpit manual (Microdrones, 2009a).

4.3   Manual versus autonomous flight

Over the last years, the trend for image acquisition is heading towards autonomous flights. However, some systems can only be controlled manually and, because of security reasons, in some areas autonomous flights are not permitted. In the first initial tests carried out in this study, the evaluated systems were only able to operate manually or in a semi-automated way. The improvements of the flight modi and the transition towards autonomous flights would not have been accomplished without the results of this study. In the following examples for manually and autonomous flights we highlight the main differences and improvements.

The first investigations on the influence of the manual flight modi compared to the autonomous of model helicopters were done by Eisenbeiss, 2003. This investigation was done at WITAS (WITAS, 2009). An example of two flights, manually and autonomously

controlled, are explained below. Two more recent examples of manually controlled Kites and Zeppelins are provided in section 4.3.2. The results, given in section 4.3.2, show the practical problems of manual controlled flights as well as demonstrate the capability of low cost systems for specific applications.

4.3.1 Example model helicopter

In the flight test in Sweden 2003 the main focus was on the integration of a differential GPS into the UAV system (Eisenbeiss, 2003). Given our current study, has focused on the importance of using autonomous flights for appropriate data processing, the outcomes of the comparison of manual and autonomous flight in Eisenbeiss (2003) are described below.
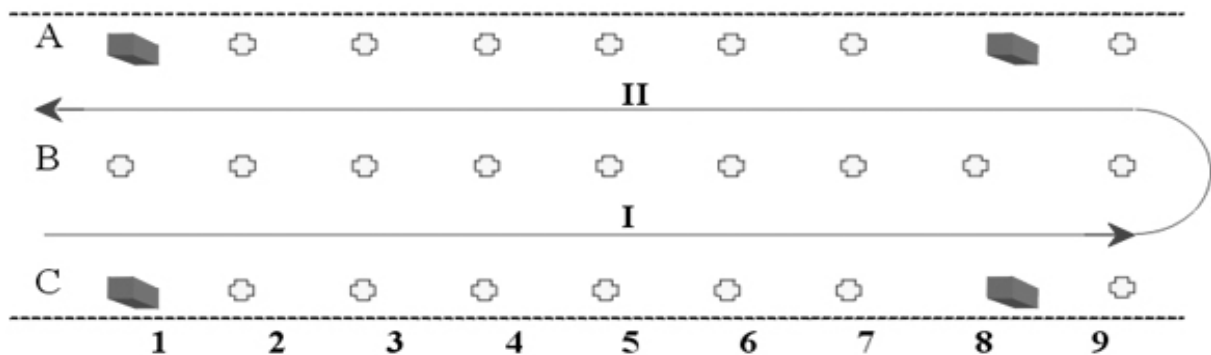
Figure 4-14: Predefined flight path showing the flight lines, runway markings (grey blocks) and control points (Test Motala, Eisenbeiss, 2003).
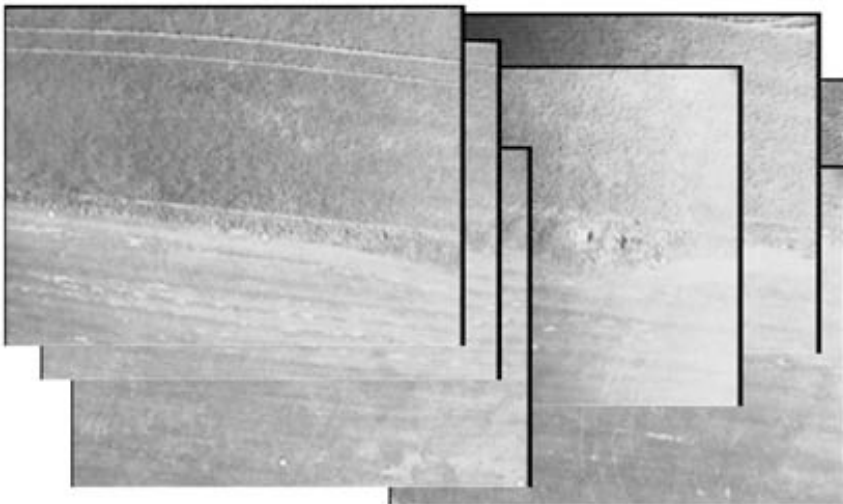
Figure 4-15: Image cover of the first flight line (I) shown in Figure 4-14.

Figure 4-16 shows an example of a manual controlled flight under extreme wind conditions. An experienced pilot controlled the system, attempting to fly two flight lines (see Figure

4-14). Figure 4-15 and Figure 4-16 show clearly that without stabilization, it is impossible to fly a precise block configuration under such wind conditions. Therefore, the results of the image orientation were not successful.
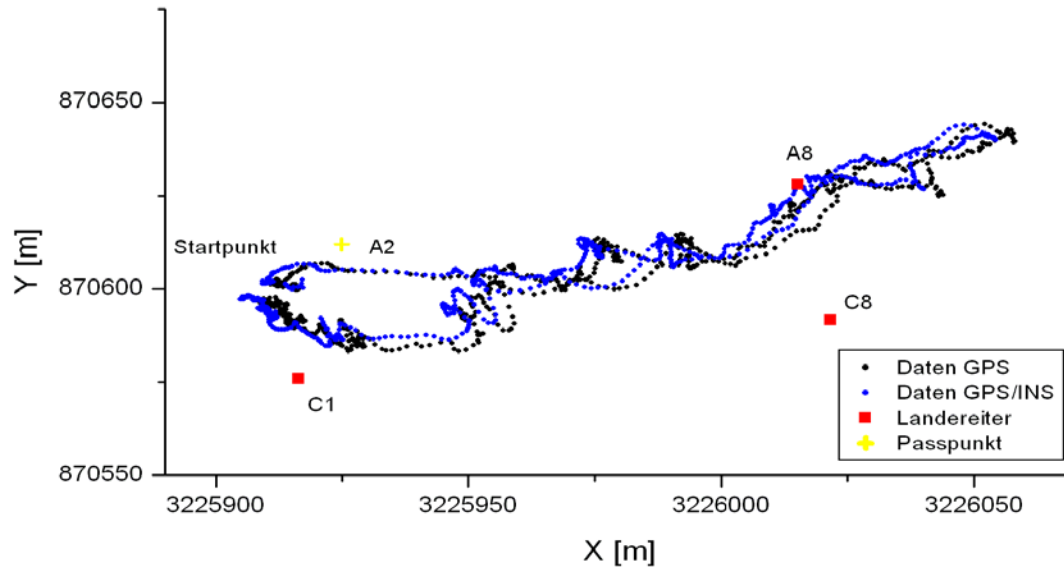
Figure 4-16: Trajectory of the manually controlled flight (Test Motala, Eisenbeiss, 2003).

After this test, the helicopter was stabilized using a GPS/INS system from C-MIGITS II (Rockwell, 1996), which enabled the data acquisition to be in an optimal block configuration (see Figure 4-17).
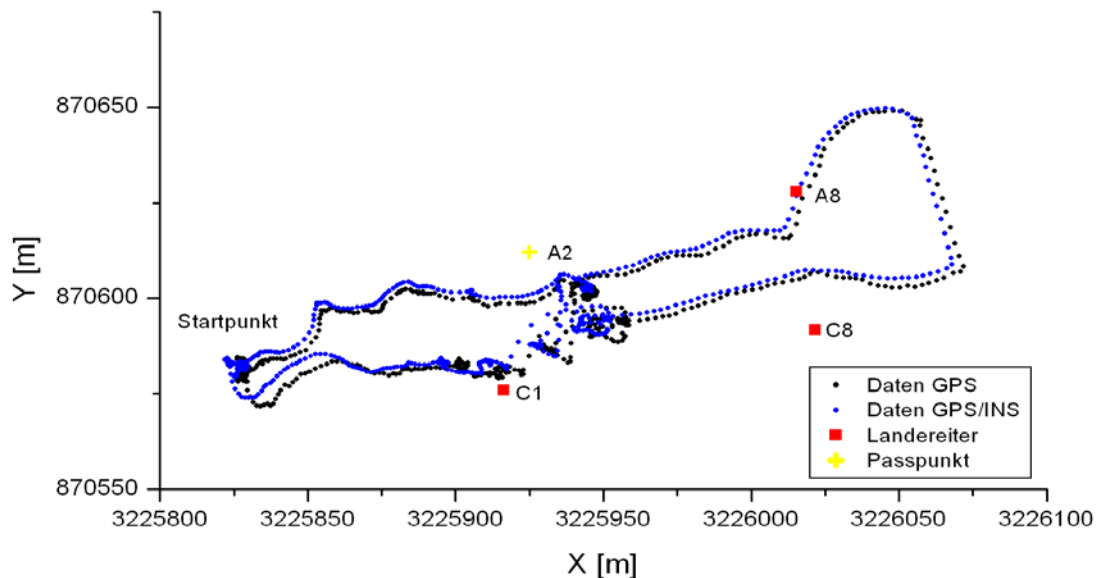
Figure 4-17: Trajectory of the autonomous controlled flight (Test Motala, Eisenbeiss, 2003).

Figure 4-17 shows that the helicopter was able to follow the predefined flight path in the autonomous mode, while the starting and landing phase was controlled manually. Moreover,

the turbulent part of the flight trajectory indicate the transition between manual and autonomous control, where the helicopter tried directly to move towards the desired position. However, at the time of this test, the action commands of the helicopter for transition areas were not defined probably, which resulted into the turbulent trajectory.

4.3.2 Manually controlled Kites and Zeppelin

4.3.2.1 Kites

The system Susi described in chapter 3.2.2 is already used for the production of orthoimages of forest areas in the forestry department Mecklenburg-Western Pormania (Germany). An example of a typical block configuration is shown in Figure 4-18. The images are distributed irregular over the area of interest, while also the image cover varies significantly from one to next image. Furthermore, the orientation and the shape of the images are changing in almost all images, which forebode the change of the orientation angle. Thus, the block configuration is not sufficient for an optimal image orientation.
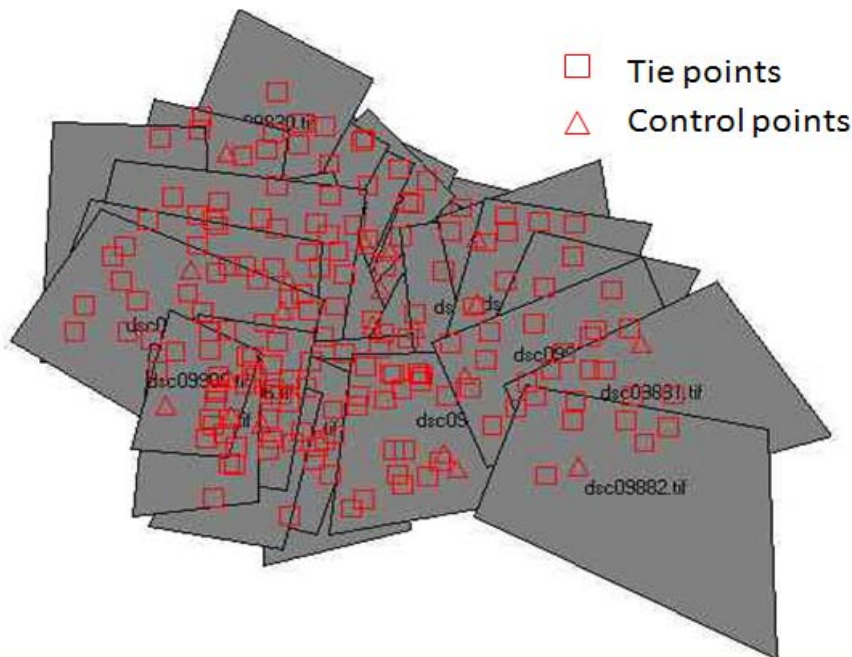
Figure 4-18: Typical block configuration of the motorized kite Susi over a forestry area (Source: Forestry department Mecklenburg-Western Pormania).

However, for economic reasons the data acquisition and the analysis of these data are worthwhile. Quite often, the areas of interest are too small for commercial photogrammetric flights, since the cost-value ratio is not arguable. In addition, frequently during the relevant time frame for forestry analysis, the weather does not allow manned flights, while in the area of interest the weather conditions had been sufficient enough. The manual measurement

effort, which is conditional through the non ideal block configuration, is maintainable. Even though, since the photogrammetric flight companies quite often change their operating system. Finally, the establishment of new workflows for the new systems, also results into more manually work for.

The same system is also currently used at the Hydrology and Water Resources Management group at ETH Zurich. The system is applied in the CCES project RECORD (REstored COrridor Dynamics; Record, 2009). The goal of this work is on the influence of vegetation roots on the morphodynamics processes that shape the river morphology as the restoration progresses. A detailed DEM is need at any time there, when relevant changes due to big floods occur. The purpose of having a manual controlled UAV was to check if this kind of image data is a valuable low cost alternative to LiDAR and large format aerial images in such an environment (i.e., in the presence of flowing water). The acquired images of the first flight were oriented using the software Leica Photogrammerty Suite (LPS, see section 5.1). The significant changes of H_G (see Table 4-1) and the Yaw angle showed that the systems are strongly influenced by local wind conditions (see Figure 4-19). Apparently, from the image configuration, problems in the image orientation and matching occur due to the fact that half of the images are covered from the water surface.
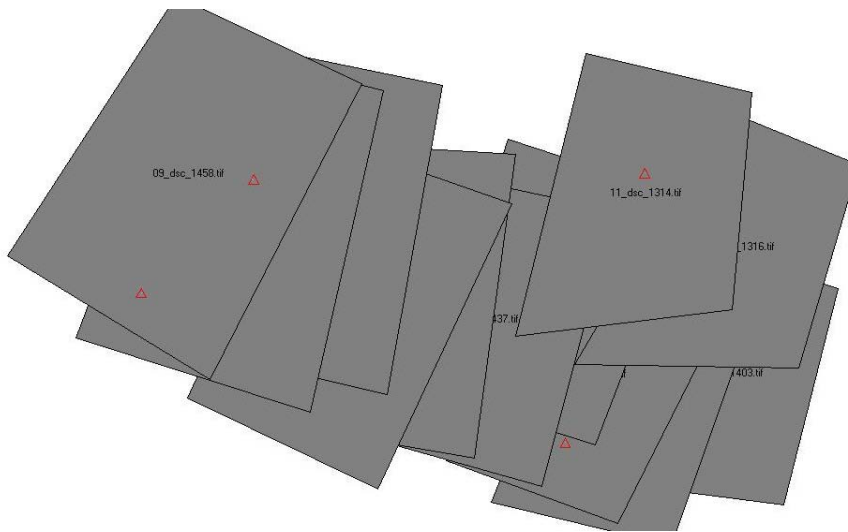
Figure 4-19: Block configuration of the motorized kite Susi used in the RECORD project at ETH Zurich (Hagenbach and Wanner, 2009).

4.3.2.2 Zeppelins
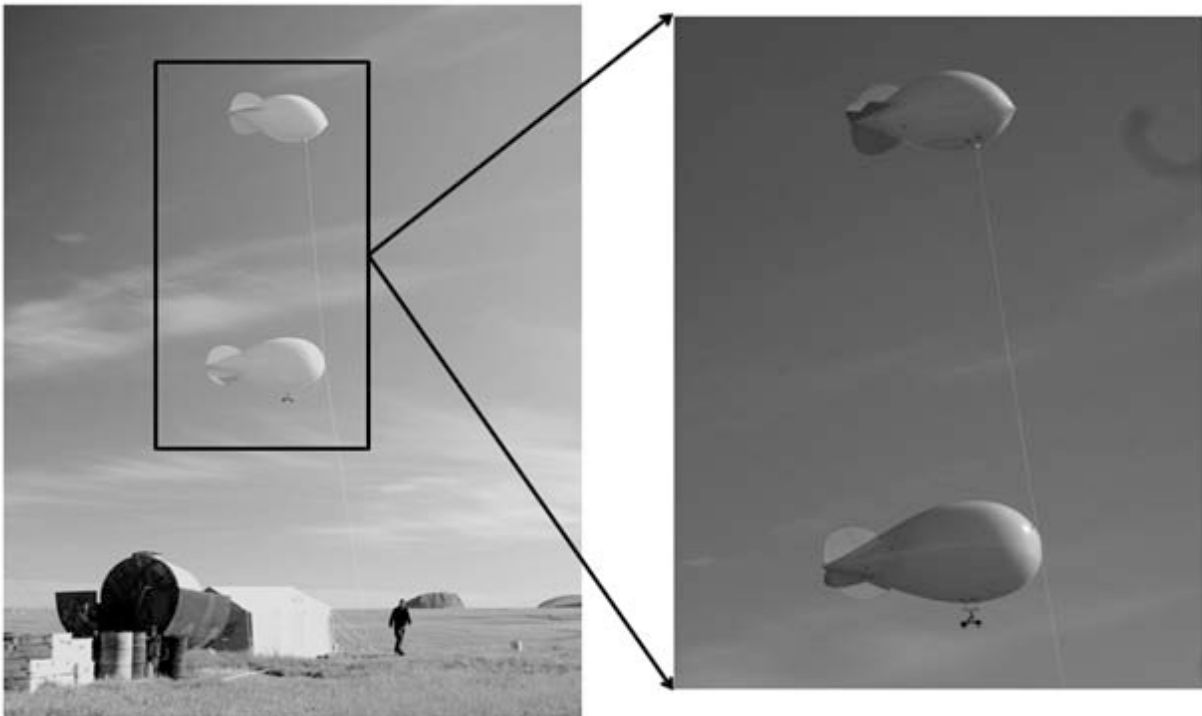
Figure 4-20: Example of a Zeppelin used at Samoilov island (Source: AWI, 2009).

A Zeppelin has a similar concept to the balloon. The main difference between the systems is the shape of a zeppelin. It is more like an airship and, thus, is easier to control and keep stable on a flight trajectory. Usually just one wire is necessary for manual control and the flight trajectory is easier to keep on line. The system used at Samoilov island was constructed from two Zeppelins. Two Zeppelins were necessary to carry the payload (Ries and Marzolff, 2003).

Because of the inaccessibility of Samoilov island, it was not possible to define flight lines for a complete coverage of the area. The connecting flight lines had also only minimal overlap, which meant the orientation of the whole image block was not possible at once (see Figure 4-21). These circumstances prolonged the processing of the data significantly. However, it was possible to orient the images taken from the Zeppelin at Samoilov island in separate image blocks, and to produce orthoimages of the area of interest (the workflow of the image orientation and the generation of photogrammetric products using UAV-images are described in Chapter 5). Since the height differences of the area were not significant, the DSM was reduced to a planar surface using the average height of the terrain.
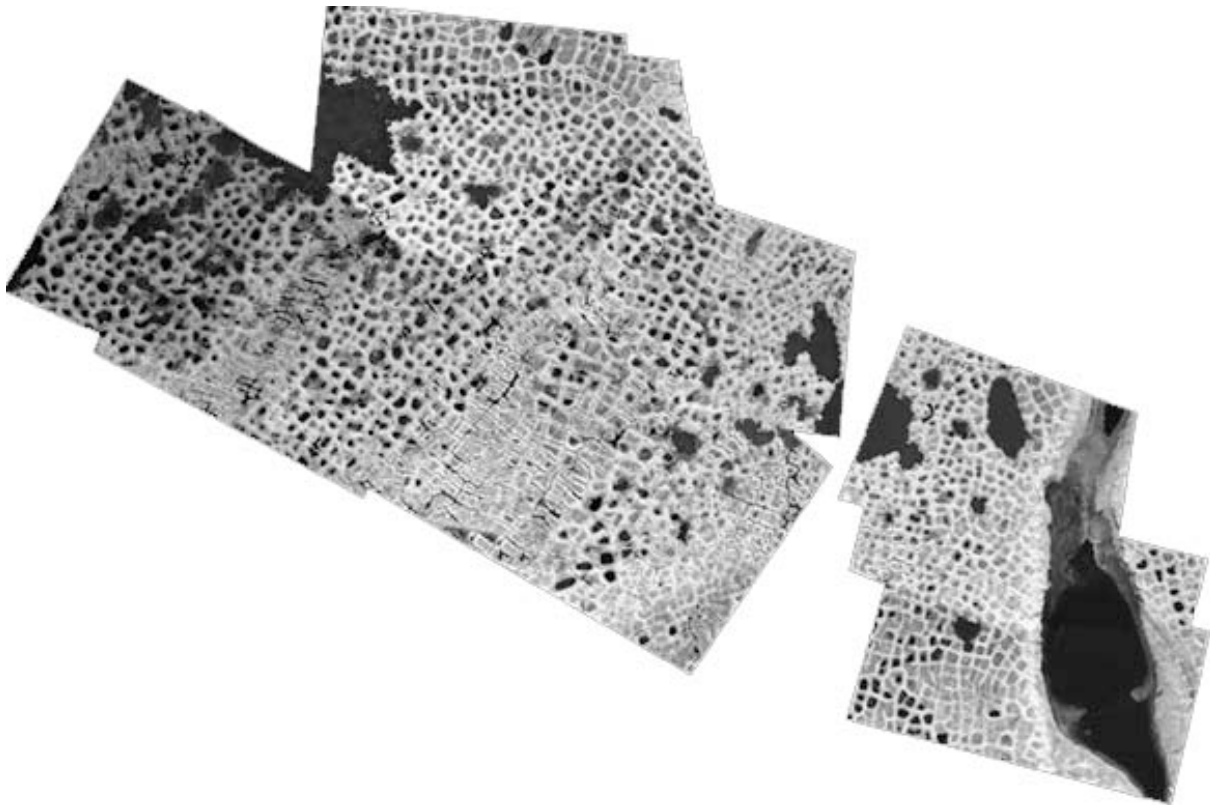
Figure 4-21: Orthoimage generated out of the images acquired during the manual controlled Zeppelin flight at Samoilov Island (Roeoesli, 2009).

4.4   Analysis of the trajectory of autonomous UAV flights

Due to the problems with manually controlled systems mentioned above, the following paragraph highlights the quality and accuracy of the flight path of autonomously flying systems. Since most of the autonomous systems are stabilized, it can be expected that the flight trajectory of the autonomous systems is more stable. Thus, for the automation of the workflow, the orientation values coming from the navigation units can be used as approximation for the image orientation and for the fast production of overview images. Here a new measurement method will be described, which allows the evaluation of the flight trajectory and also yields accuracy measurements. In particular, for economic reasons the influence of the flight modus, such as stop or cruising points, will also be investigated.

For the evaluation of the accuracy of the 3D trajectory of mini-UAVs the following system components have to be analysed: The mounting, the synchronisation and the calibration of the GPS, INS, barometer, compass and the camera, as well as the initial orientation of the IMU unit (Skaloud, 1999).

The ideal position and orientation of sensors on a platform is not a trivial task. The effects, which result from the calibration error of the offsets between the various sensor axes of the

position and orientation, have to be minimized. In addition, movements of the sensors should be avoided and the influences of vibrations have to be reduced. Vibrations of the platform can result in image blurring, while synchronization errors of the sensors can influence the absolute accuracy of the position. However, since the absolute accuracy of low-cost sensors is in the range of several meters, position offsets between camera und GPS sensors less than half meter can be neglected for most of the OM- and M-class UAVs. For systems of the L-class like the Scout B1-100, which is using DGPS, the offset has to be taken into account. The rotation matrix (orientation offset) between the INS body frame and the GPS mapping frame can be calculated in two steps (coarse and fine alignment). Considering the sensed Earth rotation and the gravity, the coarse alignment parameters can be estimated using the raw sensor output. This information can be refined for navigation grade strapdown INS in a fine alignment using a Kalman filter with 'misalignment states' and zero velocity as updates. For integrated systems the alignment parameters can be calculated using the GPS position and the velocity (Poli, 2005, Skaloud, 1999). In addition, the vector between GPS/INS and the camera centre, as well as the rotation matrix between camera frame and INS body frame, can be calculated through a test field calibration. Thus, the UAV system could fly over a test field. The position and orientation determined by from the GPS/INS will be used as initial values for the bundle adjustment, where the corrections can be determined and the offsets derived (Cramer, 2001, Gruen, et al., 1993).

4.4.1 *Flight trajectory versus predefined flight path*

For the comparison of the flight trajectory and the predefined flight path, the coordinates of the image acquisition centres have to be transformed onto the same coordinate system. This transformation has to be done, since the most navigation units use the geographic coordinate system WGS84, while the flight planning is done in a local coordinate system (national coordinate systems), such as the Swiss LV03. The formulas for the transformation are given in a documentation for coordinate transformation (swisstopo, 2005).

$$P\begin{pmatrix} X \\ Y \\ Z \end{pmatrix}_{LV03} = f(WGS84 \rightarrow LV03)\, P\begin{pmatrix} X \\ Y \\ Z \end{pmatrix}_{WGS84} \qquad \text{4-16}$$

These formulas were incorporated into in-house software and adopted to the structure of the wePilot output. An example for the output of the metadata of the wePilot 1000 is shown in Figure 4-12.
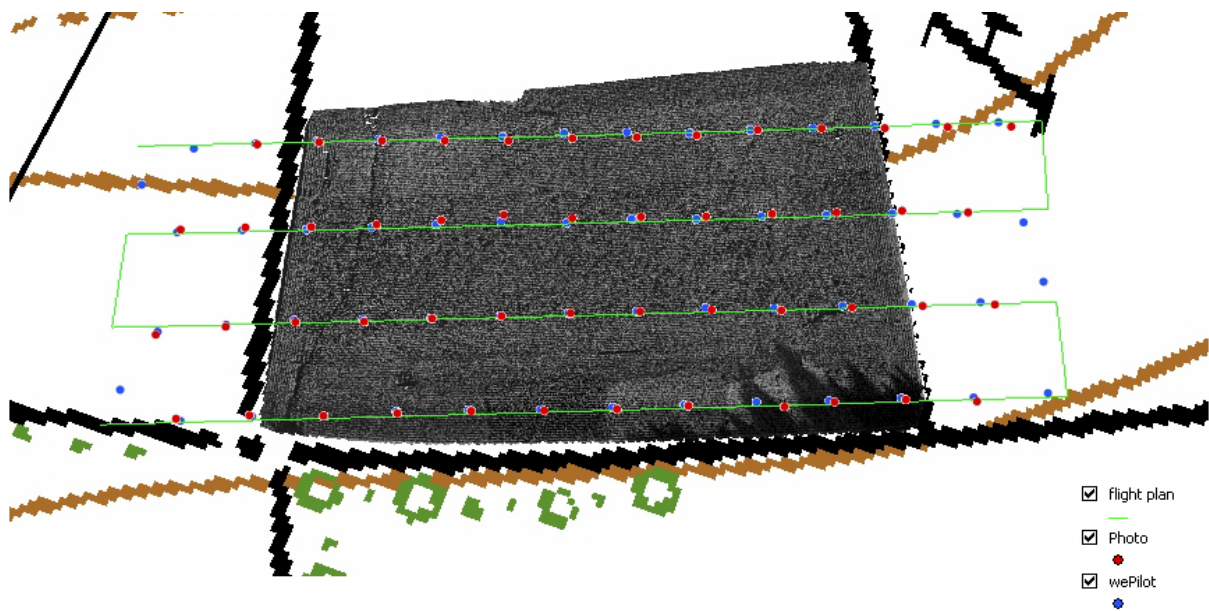
Figure 4-22: Comparison of the trajectory of the flight in 2006 to the predefined flight path.

A typical flight scenario of an autonomous flight is shown in Figure 4-22. This Figure shows the planned trajectory and the measured (wePilot), as well as the computed (Photo) image acquisition points of the example maize field 2006 (see section 7.3). Figure 4-22 shows that the measured (wePilot) and computed (Photo) image acquisition points compare quite well with the given flight plan. The planned and the measured centers have an average distance of approximately 1m in planimetry, while the height components have an offset of 4m (see Table 7-6). The differences in this flight are comparable to the expected accuracy of the wePilot1000 (see Table 3-10 left column).

A second example, which compares the planned and the measured trajectory, is illustrated in Appendix Figure D-2. Figure D-2 shows the flight of the tracking tachymeter experiment (Flight 2, see section 4.4.3). Similar to the maize field experiment, the trajectory visually fit quite well, except that the influence of the wind is clearly evident in the flight data.

4.4.2 Influence of the flight modus

The flight trajectory of our Copter 1B can be analyzed with the Matlab tool Watson (weControl, 2009). Figures such as Figure 4-23 and Figure 4-24 were produced using the Watson tool in this thesis.

The flight modus of the system, manual, assisted or autonomous, influences the stability of the system and the orientation data. Figure 4-23 and Figure 4-24 show the rotation angles and the velocity measured by the INS and GPS respectively of the three flight modi during one

flight of our Copter 1B system, which was stabilized with the wePilot 1000. In the first seconds after turning on the platform, the system was in the initial phase. The UAV then took off manually. Approximately 160 seconds after the start, the system switched from manual mode into the assisted mode, which was especially visible in the vertical velocity component of the velocity (see Figure 4-24). 100 seconds later, the system reached the first mission point, while the UAV switched into the autonomous flight mode. After finishing the flight line, evident at the end of the graph, a turning of the platform to the next strip can be recognized. The discontinuity of the yaw angle in the lower graph of Figure 4-23 result from the transition from -π to π.
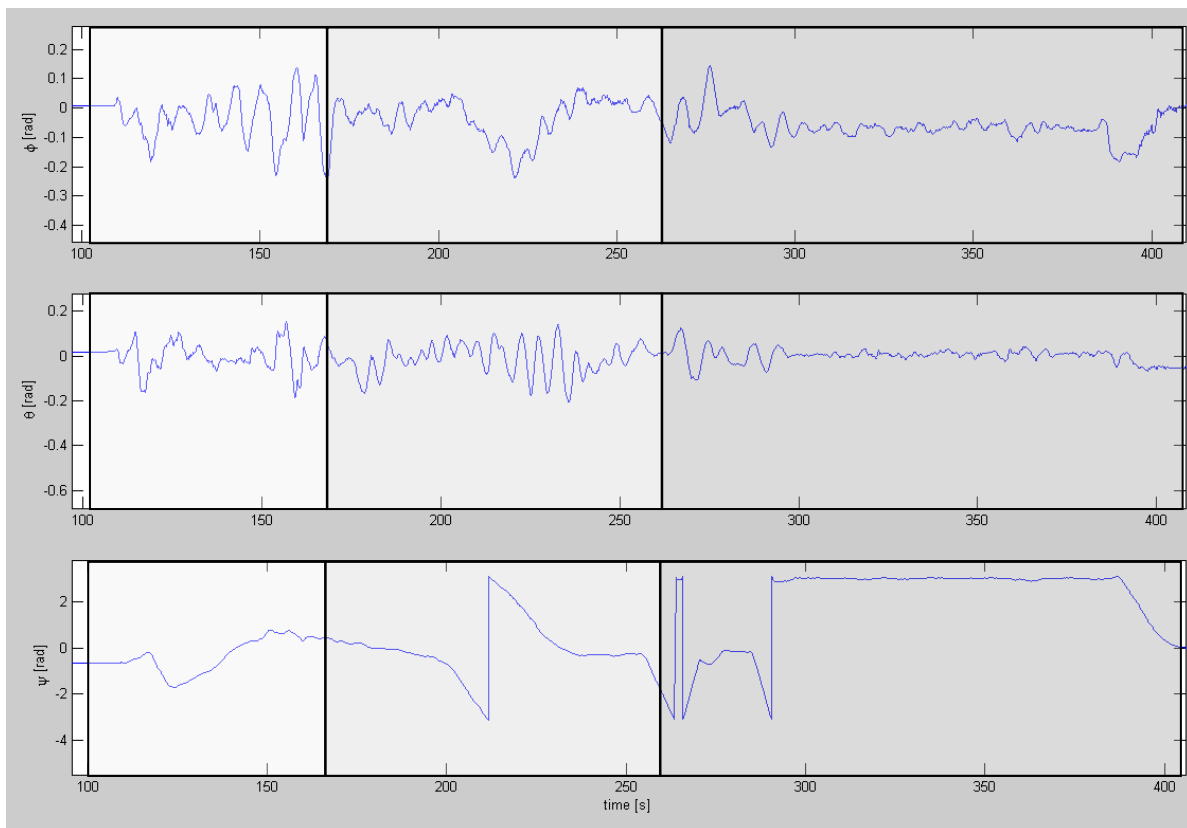
Figure 4-23: Example for the transition between manual (white), assisted controlled (light gray) and autonomous (gray) flight. Upper graph: Roll (Φ) angle around x-axis; Middle graph: pitch (Θ) angle around y-axis; Lower graph: yaw (Ψ) angle around z-axis.

During the autonomous part of the flight the angles were fairly stable. Figure 4-23 shows a variation of the roll and pitch angle in the range of 2° maximum and for the yaw angle of less than 1°. We observed this stability of the rotation angles of the Copter 1B system in most of the flights where there was a normal wind condition. In section 6.3.2.1 an example for extreme wind conditions is provided.
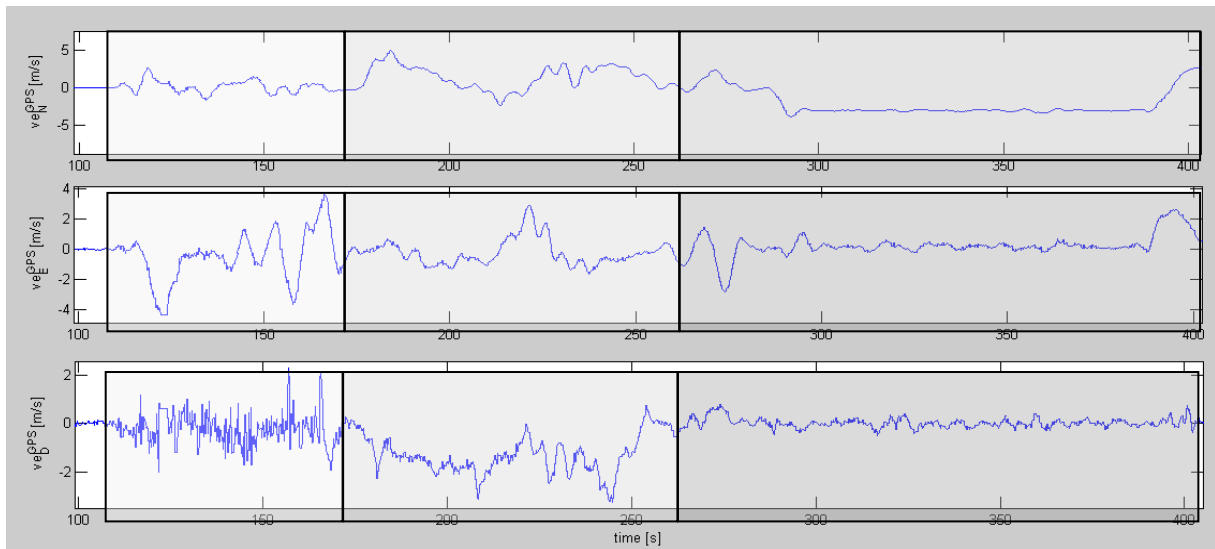
Figure 4-24: Example for the transition between manual (white), assisted controlled (light gray) and autonomous (gray) flight. Upper graph: Velocity v_N (North component); Middle graph: Velocity v_E (East component); Lower graph: Velocity v_D (Height component).

Figure 4-25 and Figure 4-26 show the reference velocities and the measured velocities generated from GPS measurements, acquired during the whole autonomous flight in Copan (Honduras) of the East and West Court in 2009 (see Chapter 6.3). Initially the system was controlled manually and then followed by the assisted mode. Seven parallel strips and one returning line were flown autonomously, while the landing was controlled in the assisted and manual mode. Focusing on the vertical velocity component, again the Z component shows clearly the transition between the manual and the assisted flight modus. In the following autonomous section, the turnings of the UAV are clearly visible. The measured values (Figure 4-26) match the plotted given reference values (Figure 4-25).
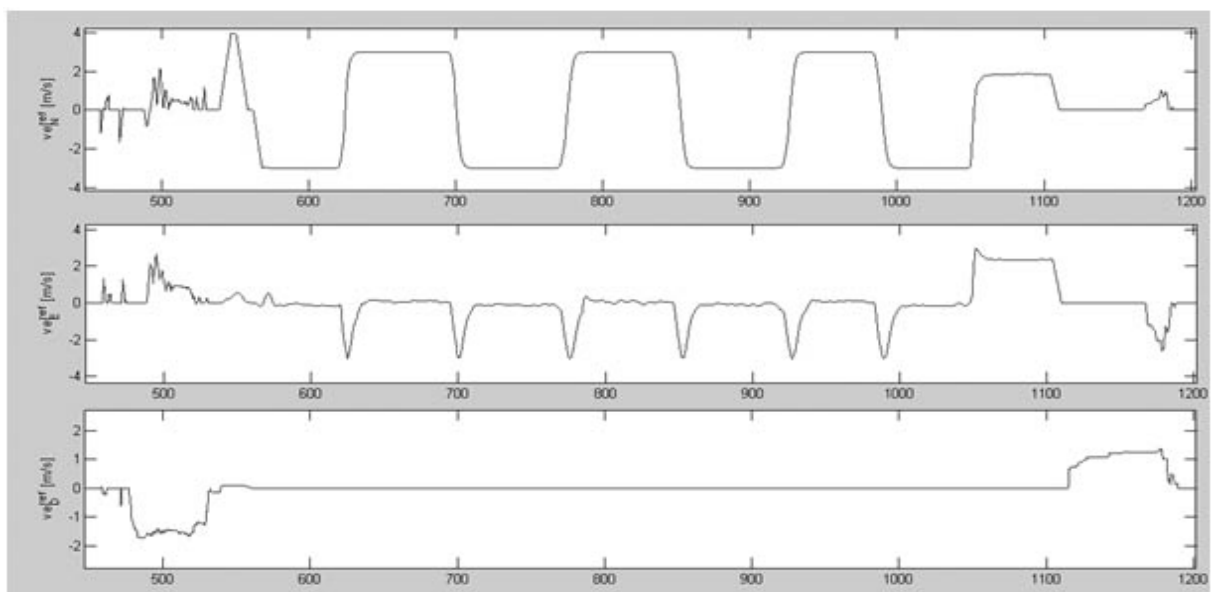
Figure 4-25: Reference velocity values of a flight in Copan (Honduras).

Similar analysis of the flight trajectory would be also possible with the flight control system of the MD4-200. Appendix Figure C-1 and Figure C-2 illustrate examples of the functionalities of the tool integrated into mdCockpit. However, since the autonomous flight mode was implemented into the system only in spring 2009, a detailed analysis of the flight modi of the MD4-200 is beyond the scope of this study.
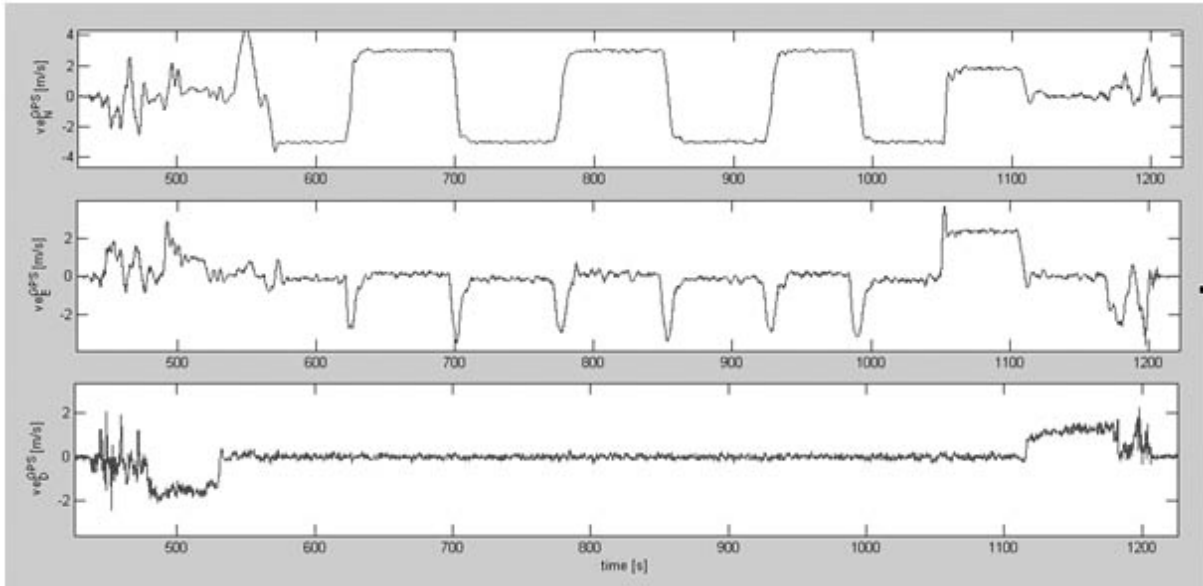
Figure 4-26: Measured GPS velocity values of a flight in Copan (Honduras).

The results presented above show clearly the differences between the flight modi of our UAV system Copter 1B. For independent analysis of the flight trajectory we analyzed the trajectory by tracking the position of the system through a tachymeter. The method and experimental results are described in the following section.

4.4.3 Tracking tachymetry

The precise reconstruction of the 3D-trajectory of mini-UAVs in real time can be determined with several geodetic measurement methods. In order to achieve real-time 3D measurement data with accuracy better than 1 cm and high temporal resolution (≥5Hz) , only tracking total stations can be used (Stempfhuber and Kirschner, 2008). This kind of technology is particularly well suited for applications, which require millimeter accuracy in planimetry and height for object distances up to 300 m, which is a normal distance of an UAV image strip. The polar coordinate measurement system determines, using the 3D-distance as well as the horizontal and vertical angle, the XYZ-position of a moving 360° prism with respect to a certain time stamp. In the last years, all serious manufacturers of geodetic measurement systems worked on the optimization of kinematic observations of total stations. GNSS, Lasertracker, INS-systems, Interferometer and LiDAR-Systems however do not meet the

requirements for this particular task. Additionally, the tracking of the helicopter using high speed cameras could be applied in small areas, while for larger areas, due to the limitation of the field of view of the camera, a new construction for the automatic target tracking would be necessary. Thus, we decided to use the available tracking tachymeter.

The tracking tachymeter is mainly used for the control of construction machines and surveying in the one-man mode. It is also used for kinematic measurements in road construction, where grading, milling off existing layers, compaction and, above all, installation of road surfaces has to be carried out to a level of precision of a few millimeters. Applications such as tunnel and airport construction require a comparable precision (Kirschner and Stempfhuber, 2008).

Considering the influence of different parameters like:
- the maximum tracking speed,

- the precision of the 360°-prism,

- the dynamic behavior of the integrated two-axis tilt sensor,

- the synchronization of the angle and distance measurements, as well as the latency and dead times and

- the behavior of the target tracking,

it is possible to achieve an absolute accuracy of few millimeters. This is not particularly required for the analysis of the flight trajectory of image data acquisition. However, the potential accuracy would help to analyze the flight trajectory of an UAV with an implemented LiDAR system in future work. More parameters and detailed information about their influence on accuracy are described in Kirschner and Stempfhuber, 2008.

4.4.3.1 Experimental setup and data collection

The evaluation of the accuracy of the 3D-trajectory of the Copter 1B was conducted at the campus Hönggerberg of ETH Zurich (see Figure 4-27).

Initially, the control points of the test field were defined in the Swiss coordinate system LV03. It meant, all measurements using the tracking tachymeter could be connected to the LV03. In addition, using the GPS-module, the tracking time was synchronized with the UTC (Coordinated Universal Time) time, which was used as time standard for the analysis.

The flying heights of the image strips were defined 25 and 30 m respectively for strip 1 and 2. For the image acquisition, a still-video camera Nikon D2Xs with an 18 mm lens was selected. The predefined flight parameters were integrated into the weGCS software as described in section 4.2.2.3.
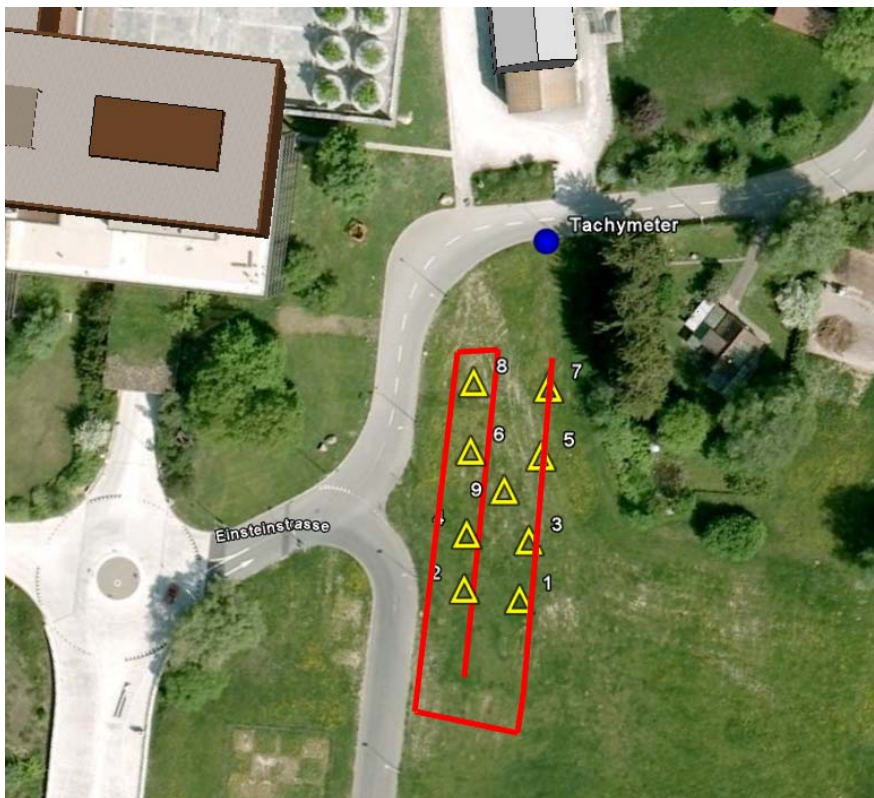
Figure 4-27: Test field configuration at ETH Hoenggerberg for the evaluation of the accuracy of the 3D trajectory visualized in GoogleEarth®.

After the manual take-off and check of the helicopter parameters, the flight mode was changed to the automated flying mode. The first point in the flight path defined as a stop point was used to initiate the measurements of the tracking tachymeter. The second point was a stop point as well, allowing the yaw angle of the helicopter to be aligned parallel to the direction of the first flight line. After finishing the first strip, the helicopter increased the flight height and did a transition to the start point of the second strip. Following the flight path, the helicopter flew the second strip and then a pilot controlled landing. This experiment was repeated 3 times, however for the second and third repeat, the length of the strips was enlarged (see Appendix Figure D-2). Finally, a maximum distance to the tracking tachymeter of 110 m was reached. The results of the each experiment therefore allowed us to draw a more general conclusion of the absolute accuracy of the system.

The survey of the 3D-trajectory of the model helicopter was realized using the calibrated and verified SmartStation TPS1200+ from Leica (Leica, 2009). Using the onboard-application "AutoPoints", the kinematic measurements were registered with a frequency of 5-7 Hz. Before starting the tracking of the helicopter, the SmartStation monitored some GNSS observations, which were used for the synchronization with the UTC time standard. The observations of the tachymeter were done with a precision in time of 150ms. The drift of the

tachymeter time however has to be taken into account in the post-processing (Stempfhuber, 2004). The synchronization with the UTC time is only possible in the initial phase, since the SmartStation does not allow GNSS and TPS measurements at the same time.

4.4.3.2 Analysis

The positions for the image acquisition of the helicopter were compared to the generated 3D-trajectory of the tachymeter. The H_{ortho} (GPS) was corrected for the offset (9m), which resulted from the difference of the defined and measured height of the start point. Afterwards, the coordinates taken from the 3D-trajectory were interpolated to the time of image acquisition. The difference between the GPS and tachymeter position are shown in Figure 4-28 and Appendix D-1.

Table 4-5: The mean value (x_M), the mean corrected standard deviation σ_{Xdiff} and the RMSE of the offset between GPS and tachymeter position at the same time (UTC).

		Strip 1			Strip 2		
		X [m]	Y [m]	H [m]	X [m]	Y [m]	H [m]
	x_M	-2.32	0.64	1.53	1.65	-1.36	1.38
	$\sigma_{X_{diff}}$	0.74	0.40	0.19	0.90	0.42	0.14
Flight 1	RMSE	2.42	0.74	1.54	1.85	1.42	1.39
	x_M	-2.93	0.74	-0.17	-2.84	0.71	0.03
	$\sigma_{X_{diff}}$	0.56	0.39	0.07	0.74	0.33	0.11
Flight 2	RMSE	2.98	0.83	0.18	2.93	0.78	0.11
	x_M	-2.30	0.41	2.24	1.23	-1.62	2.06
	$\sigma_{X_{diff}}$	0.50	0.32	0.16	1.15	0.49	0.11
Flight 3	RMSE	2.35	0.51	2.26	1.66	1.69	2.07
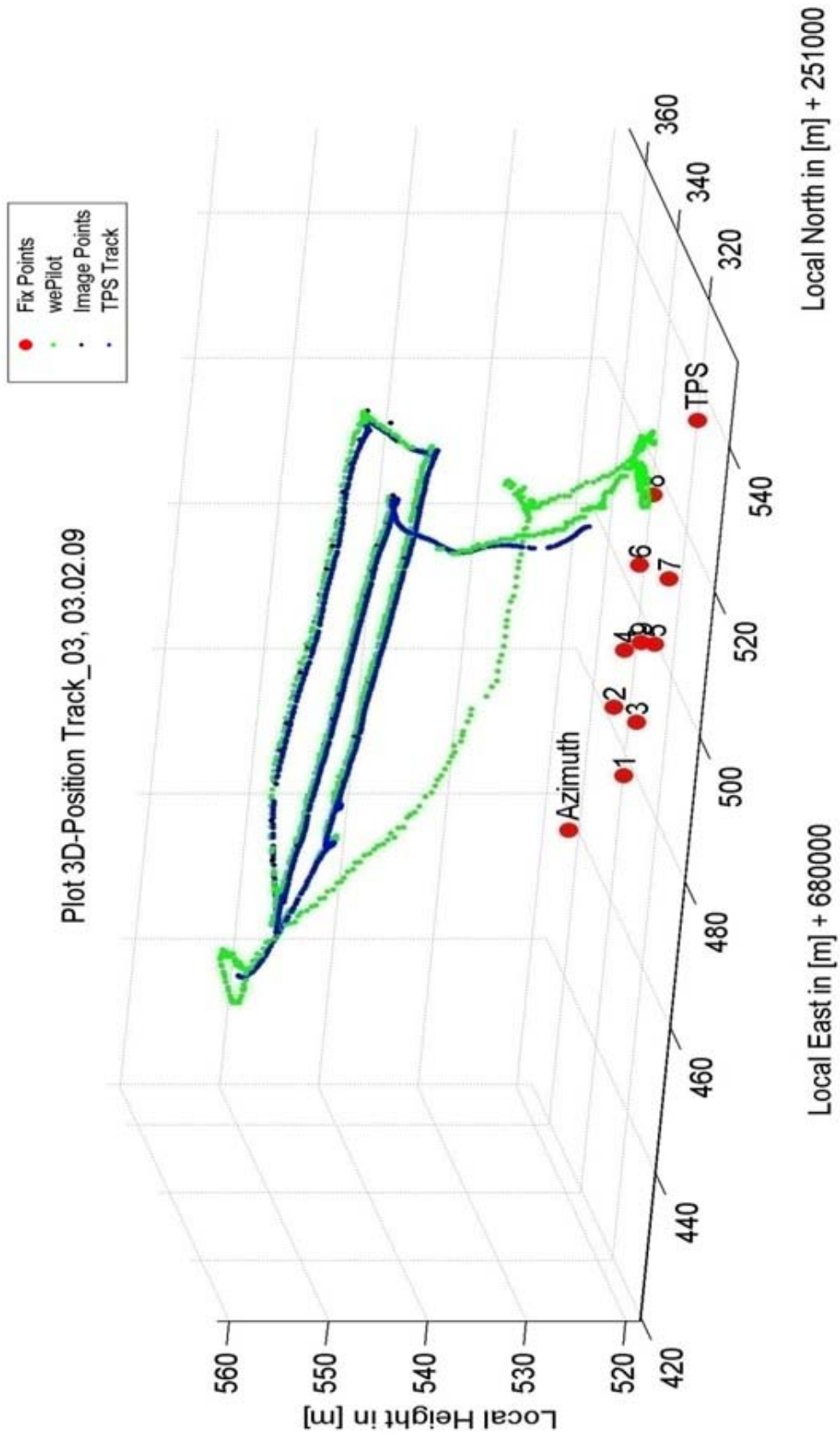
Figure 4-28: 3D-Plot of the trajectory showing the GPS and tachymeter trajectory.

The mean value (x_M), the standard deviation ($\sigma_{X_{diff}}$) and the RMSE of the offset between GPS and tachymeter position were calculated as follows:

$$x_M = \frac{1}{n}\sum_{i=1}^{n} x_i \qquad\qquad 4\text{-}17$$

$$\sigma_{X_{diff}} = \sqrt{\frac{\sum_{i=1}^{n}(x_i - x_M)^2}{n-1}} \qquad\qquad 4\text{-}18$$

$$RMSE = \sqrt{\frac{\sum_{i=1}^{n}(x_{Tach} - x_{GPS})^2}{n}} \qquad\qquad 4\text{-}19$$

The outcomes of all three flights show similar results. The accuracies are of the order of few meters, which is consistent with the manufacturer's data. The offset of the height component in the first and third flight are similar to the expected value. However, the difference of the height component in the second flight is significantly smaller and therefore shows a too optimistic result. The large RMSE values can be presumably explained with the accuracy level of the time synchronization between the components integrated on the UAV and/or the tachymeter measurements. The Euclidian distance between the wePilot observation (GPS, INS and Kalman filterirng) with respect to the 3D-trajectory is significantly smaller than the offset at the same time stamp (see Figure 4-29). This result confirms the assumption, that the main part of the offset is related to the time synchronization and therefore, the maximal offset can be expected in our experiment in the main flight direction X. Moreover, the results show a higher relative accuracy than absolute accuracy. Thus, the accuracy values bring us to the conclusion, that the positioning resulting from low-cost sensors might be usable as approximation for the orientation of the UAV-image data.

The 3D-Plot of the trajectory (see Figure 4-28) shows also that the helicopter is influenced by the wind on stop points. The helicopter moves in a certain limit around the defined point. On the other hand it is also apparent, that during the continuous flight, the trajectory is smooth. Thus, the continue flight modus is more suitable for the image acquisition following a predefined image strip or circle.
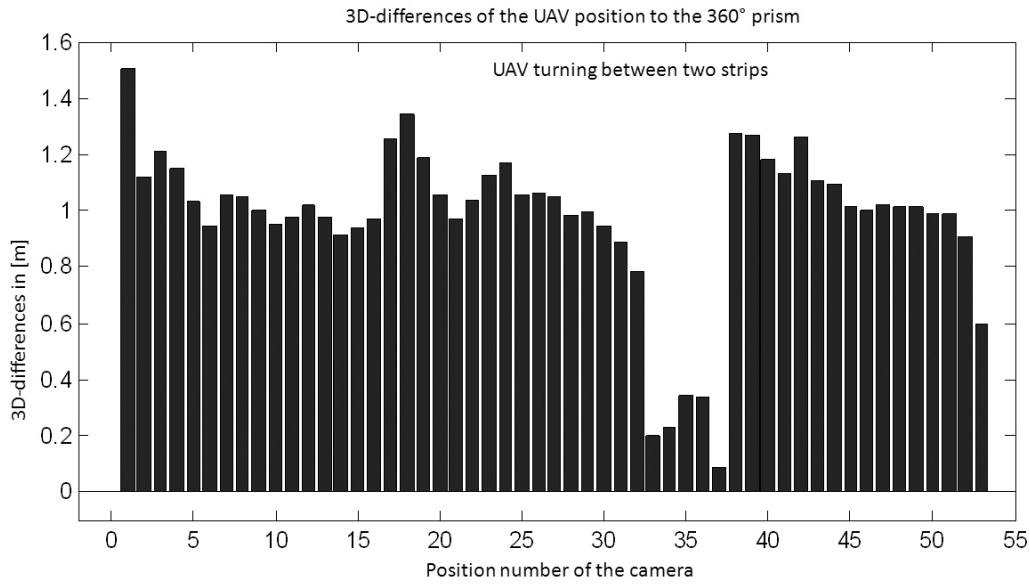
Figure 4-29: Euclidian 3D differences between GPS observation and 3D-trajectory from Tachymeter measurements (Flight 3).

4.5 Main achievements for the autonomous flights

In this chapter we have presented our developed generic workflow of UAV Photogrammetry and concentrated on the modules Project Parameters, Flight Planning, Autonomous Flight and Quality Check of the data. Moreover, in this chapter the manually, assisted and autonomously controlled flights for several UAV systems, which have been investigated in this study, were compared. The autonomous flight is most suitable for photogrammetric data acquisition, since the planned flight trajectory can be flown even under wind conditions. Three flight planning tools were developed, which allow the planning of autonomous flights for scenarios such as flat terrain, steep cliffs and buildings. We described our implementation of the planned flights into the mission planning software weGCS and mdCockpit. The observed flight trajectories of autonomous flights of UAVs were compared to the planned trajectories. Moreover, for the analysis of the 3D trajectory a new method was introduced and adapted for the tracking of the helicopter. For this purpose, a tachymeter was successfully used for the first time the automated tracking of the 3D trajectory of an UAV system.

After accomplishing the autonomous flight we now turn in the following chapter to the processing of UAV images, focusing on image orientation and DSM extraction.

5 PHOTOGRAMMETRIC DATA PROCESSING
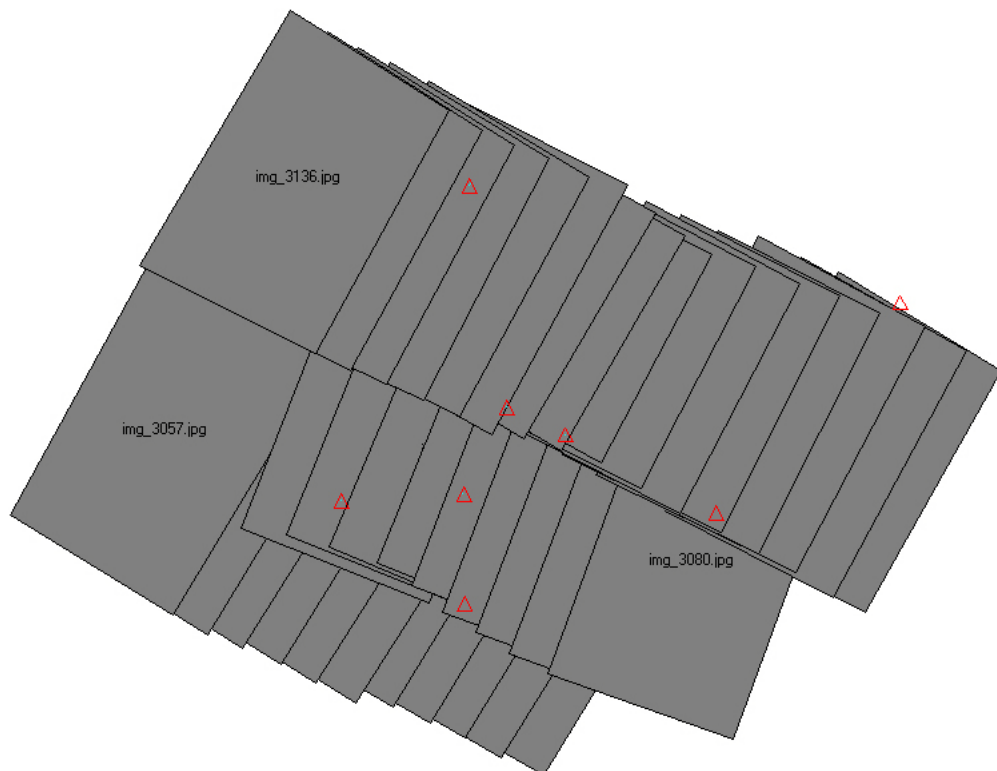
Figure 5-1: Typical block configuration of UAV-images covering an area of 250m x200 m with a GSD of 3cm.

Here we focus on the UAV image orientation and photogrammetric products like DSM, orthoimages. Subsequent to a brief description of the "UAV Block Triangulation", we will focus on the DSM generation and on an alternative or supplementary to the generated DSM using only image information. Thus, we will present the existing UAV-borne laser scanning systems and give the first results of the UAV-borne laser scanning system of ETH Zurich, acquired at the Campus Hönggerberg (ETH Zurich). The study on UAV-borne laser scanning system has been done in collaboration with the Autonomous System Lab at ETH Zurich (ASL, 2009), the companies aeroscout (Aeroscout, 2009) and Riegl (Riegl, 2009). Additionally, we will present the results which have been acquired with a Riegl light-weight airborne scanner and a L-class UAV system.

5.1   Image orientation

5.1.1 Commercial software packages

For the orientation of the images software packages, like LPS (Leica Photogrammetry Suite 8.9-9.2), the embedded ORIMA (Orientation Management Software, ORIMA-LPS-M Rel. 9.10), ISDM (Z/I Imaging, Image Station Digital Mensuration Version 04.04.17.00) originally developed for the processing of aerial images and Photomodeler 6 (EosSystemsInc, 2009), which has its origin in close range photogrammetry, were evaluated.

LPS allows processing imagery from a wide variety of sources and formats (e.g. satellite, aerial and close range images). It contains modules for data import, input and export, image viewing, camera definitions, GCP and tie point measurements, triangulation, orthorectification and DEM generation. Ground control points (GCPs) have to be measured manually.

The tie point measurement method depends on the input data and the terrain. Under good conditions the automatic measurement tool can be used. The LPS standard point measurement uses a screen with two triple tiled windows showing different zoom levels for each image. In ISDM, such windows (usually two per image plus possibly one in stereo) can be freely arranged. The disadvantage of this system is that each window has a title bar of its own that takes up valuable display space. A big difference is that ISDM can simultaneously display more than two images[2] while LPS only allows multi-image display in the stereo measurement tool of V9.1 or higher. Thus, most of the blunders can be detected during the relative

---

[2] This appears to be restricted by the available memory, as too many simultaneously opened images can cause crashes.

orientation process in ISDM. When a point is displayed in five different images simultaneously, it can be corrected in all the images at the same time. Moreover, if an erroneous measurement occurs only in one image, it is not possible to determine which one is false with an image display of only two images at the same time.

ISDM includes a matching algorithm directly implemented in the point measurement process. When the algorithm is activated by clicking on an image, ISDM tries to match the currently active point in the displayed images by taking the cursor position as an initial value. The results are usually usable, and inexperienced users especially profit from this feature. The possibility to calculate a relative orientation in ISDM is also advantageous for blunder detection or reaffirmation that there are currently no blunders. In LPS, a blunder can be detected only by manual checking until the project has proceeded to the point where a bundle adjustment (minimum datum is necessary) is possible. After finishing just one model in ISDM, a relative orientation can confirm whether the measured points are correct and accurate.

The "low cost" software package Photomodeler allowed so far only the manual measurement of tie points for image orientation, thus for a large image block this manual afford was not negligible. Additionally, the software package was not designed for the processing of aerial images. However, nowadays using UAV images, which combines the terrestrial and aerial image acquisition, and lately implemented tools for the automated extraction of tie points sound quite promising. As the development of photogrammetric software packages is moving so fast, it is beyond the scope of this thesis to describe all of the currently available packages.

Table 5-1: Comparison of the software packages.

Software packages	Oblique	Aerial	Combination	Tie points	GPS/INS
LPS Core	x	xx	0	auto. /manual	x
LPS Orima	x	xx	0	auto. /manual	xx
Z/I	x	xx	0	auto. /manual	xx
Photomodeler	xx	x	x	manual	0

A comparison of some of the major characteristics of the software packages for the processing of UAV images is given in Table 5-1.

5.2 Photogrammetric products

In this paragraph, we will describe two commercial and one in-house developed software packages, which have been used for the generation of DSM data from UAV images. The main difference of the presented packages is not only in the algorithm implemented into the

software, it is more the frame given by the whole software package and the adjustable input parameters for the matching process used for the DSM generation.

5.2.1 Generation of digital surface models

5.2.1.1 LPS

The LPS matching strategy implemented in version 9.1 is a combination of feature and area based matching. For the feature point matching, first interest points are extracted and matched by cross-correlation. The area based matching is also based on cross-correlation, refined by least squares matching using a coarse to fine approach through the image pyramids.

In the newer DSM packages, integrated into LPS V9.2 and higher, it is also possible to adopt, in addition, an adaptive matching approach. In this package, it is possible to select the number of pyramid levels used for the processing, to integrate an existing elevation model, to give a range for the DEM and finally define a Z search range either for the whole image block or a selected stereo pair. Moreover, as additional parameters, the percentage of overlapping images can be defined, which allows stereo image matching between images from different strips and non direct image neighbors. These percentages also influence the number of image pyramids used for the image matching. In the area selection sub-window inclusion and exclusion areas for the processing can be defined. The included areas can also be associated with strategy parameters for the matching. These include for example: Default, high mountains, rolling stones, flat areas, urban and forest areas. A detailed overview of the matching parameters for these defined areas is given in the manual of LPS. Finally, as 3D reference information for the DSM generation, information on the accuracy of GCPs, check points and tie points can be selected as input information for the processing.

The extracted DSM can be saved in various data formats, including the software internal format IMG. This is a DEM (Digital elevation model), where the elevation is saved as color coded information. In addition, it allows one to generate TIN- (Triangular Irregular Network) data, 3D shape information and ASCII (American standard code for Information Interchange) data formats. This functionality allows the direct export into software package family like ArcGIS and so forth.

5.2.1.2 SAT-PP

For DSM generation, a hybrid image matching algorithm was used (for details see Zhang, 2005). The method can accommodate images from very high resolution (1mm - 2cm) close range images, over 3cm - 10cm airborne Three-Line-Scanner images and 5cm - 50cm analog aerial images and up to 0.5m - 15m high resolution satellite images like Worldview 1,

IKONOS, QB, SPOT-5 and Aster. It can be used to produce dense, precise and reliable results for DSM/DTM generation. The final DSMs are generated by combining the matching results of feature points, grid points and edges. Matching is performed using cross-correlation and image pyramids. A TIN-based DSM is constructed from the matched features (where edges are used as breaklines) at each level of the pyramid, which in turn is used in the subsequent pyramid level for approximations and adaptive computation of the matching parameters. The modified MPGC (Multiphoto Geometrically Constrained Matching) algorithm (Baltsavias, 1991, Gruen, 1985) is employed to achieve sub-pixel accuracy for all points matched (if possible in more than two images) and to identify inaccurate and possibly false matches. Finally, a raster DSM can be interpolated from the original matching results.

The procedure mainly contains the following features:
It is a combination of feature point, edge and grid point matching. The grid point matching procedure can bridge-over areas with no or little texture through local smoothness constraints. The search for the match of a given grid point has a higher possibility of yielding an ambiguous match and even no matching candidate. In the proposed implementation, the matching candidates for the grid points are firstly computed by the MPGC algorithm and their final match is determined by imposing a local smoothness constraint through the relaxation-based relational matching procedure.

The adaptive determination of the matching parameters results in a higher success rate and less blunders. These parameters include the size of the matching window, the search distance and the threshold value for cross-correlation and MPGC. For instance, the procedure uses a smaller matching window, larger search distance and a smaller threshold value in rough terrain areas and vice versa in smooth terrain. The roughness of the terrain can be computed from the approximate DSM on a higher level of the image pyramid.

Linear features are important for preserving the surface discontinuities. A robust edge matching algorithm, using the multi-image information and adaptive matching window determination, through the analysis of the image content and local smoothness constraints along the edges, has been integrated into our procedure.

Edges (in 3D) are introduced as breaklines when a TIN-based DSM is constructed. This DSM provides good approximations for matching in the next pyramid level. The computation of the approximate DSM in the highest pyramid level uses a matching algorithm based on the "region-growing" strategy (Otto and Chau, 1988), in which the measured seed points are used.

If more than two images are available, the MPGC procedure can use them simultaneously and the matching results are more robust. Here, the resulting DSM from an image pair can be used as an approximation for the MPGC procedure.

Through the quality control procedure, e.g. using the local smoothness and consistency analysis of the intermediate DSM at each image pyramid, the analysis of the differences between the intermediate DSMs, and the analysis of the MPGC results, blunders can be detected and deleted.

For each matched feature, a reliability indicator is assigned. This is based on the analysis of the matching results from cross-correlation and MPGC. This indicator is used for assigning different weights for each measurement, which are used when a regular grid is interpolated (Zhang, 2005).

During this study, the in-house developed software SAT-PP was intensively evaluated and for the processing of UAV-images additional parameters of the interior orientation were integrated: for example the 10 Brown (Brown, 1971) parameters implemented in BUN and LPS and the 12 Ebner parameters (Ebner, 1976) used in Z/I.

The software SAT-PP allows similar to LPS, the definition of excluded areas, while the adaptive parameters are generated automatically during the matching process. So far, the output DSM formats are limited to the ASCII formats ArcASCII (ESRI) and XYZ.

5.2.1.3 NGATE and Match-T

During the most recent years, more and more commercial software packages, which combine various matching strategies for the DSM generation, have become available on the market. In the following section we will briefly describe two promising software packages.

Next-Generation Automatic Terrain Extraction (NGATE) is a tool implemented into SocetSet (BAE-Systems, 2009) and provides automatic generation of elevation models by multi-image-matching and correlation. NGATE combines area and feature based matching algorithms. The feature based matching also includes edge matching, similar to SAT-PP.

In addition to NGATE, also Match-T DSM from Inpho (Inpho, 2009b) combines different matching techniques in a multi-image-matching approach. Several features like an intelligent multi-image matching through on-the-fly selection of the locally best suited images for DTM generation or the consideration of pre-measured morphological data (breaklines, 2D and 3D

exclusion areas, borderlines) and the elimination of outliers, e.g. trees, houses, by robust finite element interpolation are available with this software (Inpho, 2009b).

The practical experiments shown in the following chapters have been mainly processed using the software packages SAT-PP and LPS. In addition, one practical experiment using NGATE is given in section 6.2.5.1.

5.2.2 Orthoimage and 3D Visualization

In contrast to LiDAR sensors, image data do not only allow one to extract surface models, one can, using the texture information, generate orthoimages and textured 3D visualization in combination with elevation data such as DSM and 3D-models.

An existing image may be resampled to produce a new image that conforms to specific geometric properties, such as the production of a vertical view from oblique images. The orthorectification is therefore a special case of image resampling. During the orthorectification, the effects of image perspective and relief displacement are removed, so that the resulting orthoimage has uniformly scaled pixels, similar to a map (Agouris, et al., 2004).

In our study the software packages LPS and SAT-PP were used for the orthoimage generation. While LPS allows the definition of more parameters, such as definition of the terrain, resampling method and the mosaicing of several orthimages, SAT-PP only allows the production of single orthoimages using the extracted DSM.

For the combined visualization of the extracted DSMs and 3D-models, and the rectified images in the examples given in chapter 6 and 7, the 3D-visualization software packages ArcScene (ESRI, 2009), Blender (Blender, 2008), Maya (Autodesk, 2009), Irrlicht (Eisenbeiss, et al., 2009a, Irrlicht, 2009) and Skyline Terra Explorer (Skyline, 2009) were used and in-house developed tools (Sauerbier, et al., 2006).

ArcScene and Skyline Terra Explorer are commercial visualization packages allowing the display of textured 2.5D data. The software Maya was developed mainly for the control of 3D workflows and pipelines in applications such as film, television, game development and design industries; it also allows the visualization of textured 2.5 and 3D DSM data. Blender and Irrlicht are open source software packages, which are able to build and visualize textured 3D models. While Blender is an open source 3D content creation suite, Irrlicht is an open source realtime 3D engine. More details about the visualization packages used in this study can be found in the above references and Sauerbier, 2009, Sauerbier, et al., 2006.

5.3   UAV-borne laser scanning

Laser scanners are active measurement systems, which can generate point clouds with 3D-coordinates for each point. Laser scanners produce distance images. Additionally, some types of these scanners are able to provide intensity images. Depending on the observation platform, laser scanners are classified into airborne and terrestrial laser scanners. Since airborne laser scanners need a precise GPS/INS system onboard of the airplane or helicopter, the complete system is quite expensive in comparison to terrestrial laser scanners. Thus, our motivation, with respect to UAVs, has been to perform first investigation of a light weight and cost UAV-borne laser scanning system (see section 3.4.1).

Using an airborne laser scanner, the earth surface can be scanned in 3D. A laser pulse is transmitted to the ground, where the pulse is diffusely reflected and received again on the scanner. Using the time of flight and the velocity of the laser pulse, the distance to the surface can be calculated. The position of the footprint is determined based on the attitude range and position of the laser system, provided by the GPS/INS sensors. A comprehensive overview of airborne laser scanning is given in Lee, 2002.

Presently only two operating UAV-LiDAR systems are available for photogrammetric data acquisition (Nagai, et al., 2008 and Imbach and Eck, 2009). However, Choi, et al., 2009 has recently proposed an UAV based mapping system, which will integrate also LiDAR and image sensors on one platform. Addionally, other groups from the field of photogrammetry intend to work on this topic in future work.

The aeroscout system combined with a Riegl laser scanner, used for our first investigation, is described in section 3.4.1. The expected accuracy of the orientation elements of the system include 2cm (1 sigma) for the DGPS (Novatel RT2) and a bias of 1mg for the INS (Honeywell HG1700), a misalignment factor of 0.1mrad and an axis gyro drift of 1deg/hr (see Table 3-10). The influence of the bias, misalignment and gyro drift to the position error after 10s and 1000s is given in Appendix Figure E-1. A more detailed analysis of this system is beyond the scope of this study and therefore will not be reported here.

5.3.1 Test field Campus Hönggerberg

The need for a test field for UAVs was recommended in the ISPRS IC Working Group I/V, since nowadays more UAV-platforms are available and the new platforms are getting increasinly more attractive, because of the low-cost of acquisition compared to the cost of conventional manned flights. Moreover, so far only test fields such as the photogrammetric

test sites Uster (Switzerland; Gruen, et al., 1993) Vaihingen/Enz (Germany; ifp, 2009) for large and medium format cameras exist and evaluated in large scale projects (DGPF, 2009, EUROSDR, 2009).

- Laserdaten H$_G$=50m,& 42m
  swath @ 14cm foootfrint
- Image flight at H$_G$=100m,
  3strips with p=q=80%
- Image flight at H$_G$=150m,
  1strip L$_p$=400m and p=80%

Figure 5-2: Set up of the test field for the evaluation of LiDAR and image data showing the planned flights and the GCPs level 1 (see also Appendix F-1).

The test field Hönggerberg (Campus ETH Zurich) with a size of 400m x 250m was set up, around and on top of, the building HIL, where the Institute of Geodesy and Photogrammetry is located. Therefore, it was important to have a test field, based on the regulations for UAV flights in Switzerland, which allows autonomous flights over an uninhabited area (see Table 3-6). The 12 control points of level 1 were well distributed over the test field and the points were measured with a Leica Total Station TPS 1201. To ensure that the test field would maintain a permanent character, the points of level 1 were marked with nails. An overview of these points is shown in Figure 5-2 and Appendix Figure F-1. Having the first level of control points marked permanently, it is easy to enlarge the number of control points and to measure temporally used reference objects, depending on the task of the UAV test. Furthermore, the test field was created in a way that in addition to the evaluation of cameras mounted on the UAV, UAV-borne LiDAR systems can also be tested and evaluated.

5.3.2 First test flights 2009

In March and April 2009 two flights were accomplished. The first flight was an image flight, which was used for the generation of reference data for the LiDAR flight. The second flight

was the first UAV-LiDAR flight at the campus Hönggerberg[3]. For this flight the Scout B1-100 was used, enabling a reference station for DGPS to be set up in the test field. In addition, 13 targets were distributed in the test field and the coordinates of these targets were measured with the TPS1201 (Leica-Geosystems, 2009). The inclined targets were turned, such that each surface pointed in a different direction to ensure a maximum of coverage. The goal of this flight was to evaluate the performance of the built system and to extract a point cloud from the acquired data. The first results of a scan line, acquired during the test flight at Campus Hönggerberg are shown in Figure 5-3.
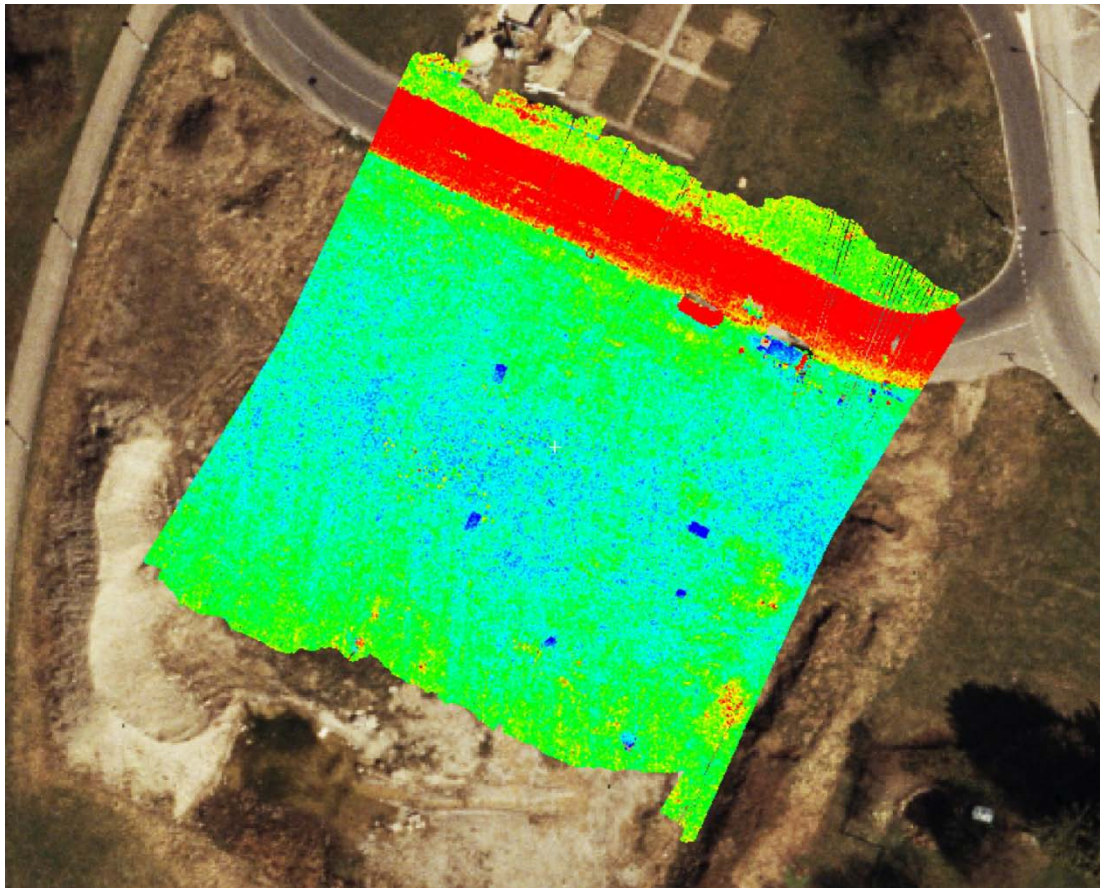
Figure 5-3: Visualization of one scan line of the UAV-born LiDAR showing the intensity values of the scanning. The orthoimage in the background was generated out of analog aerial images.

From the acquired data, objects like the street, a white car (dark blue cluster close to the street), a black car (red cluster on the street border) and the targets (dark blue clusters in the field area) are clearly visible in the point cloud (see Figure 5-3).

---

[3] This work has been supported by the EC under contract number FP6-IST-027140-BACS.
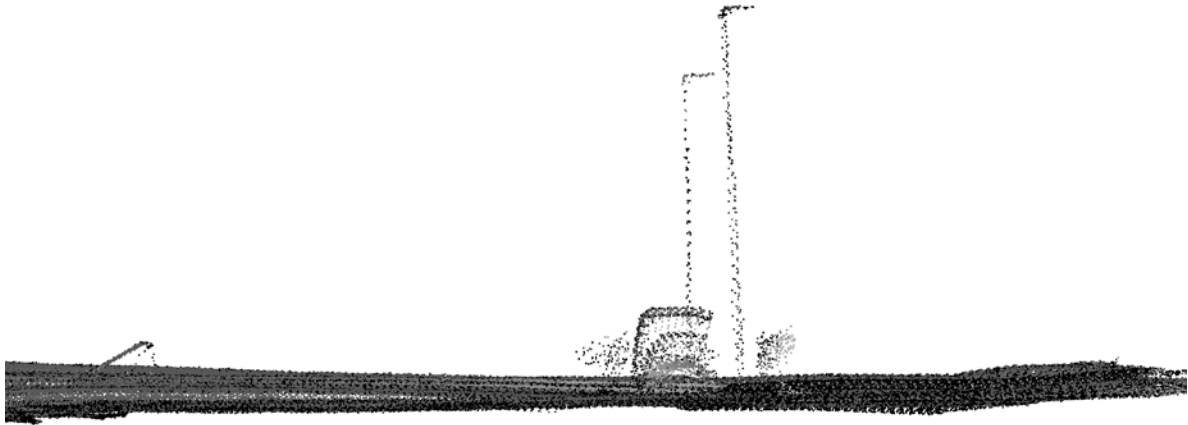
Figure 5-4: Side view of the 3D point cloud of the UAV-born LiDAR flight.

The 3D point cloud showed also clearly the objects of the test field, such as targets, cars and street lights (see Figure 5-4 and Figure G-2).

5.4 Conclusions

In this chapter, the part of our workflow for the processing of UAV images was described. Commercial and in-house developed software packages used in this thesis were explained, with the focus on available software packages for DSM extraction using UAV images. In the frame of this work, our in-house software SAT-PP was adopted to the processing of UAV-images and additional parameters for the interior orientation were implemented by Zhang, 2005. Additionally, the establishment of a test field for the assessment of UAV images and LiDAR data was highlighted and the first LiDAR data produced from a L-Class UAV-system of ETH Zurich was described. The generated point cloud showed the great potential of a LiDAR system mounted on an UAV in terms of the acquired details. Since the flight trajectory data of the first LiDAR flight was suboptimal, this topic will need to be investigated in more detail in future work. In particular, the Kalman filtering of the navigation unit was developed at a time, when the flight trajectory data had been used solely for navigation purposes for the UAV. Thus, the weighting factors for the Kalman filtering using DGPS, in combination with low-cost INS-systems, will need to be optimized. Additionally, the time synchronization of the navigation sensors with the LiDAR system has to be improved.

With the developed workflow presented in chapters 4 and 5 we will now turn in the following to the applications accomplished in this study. We will show that UAVs are flexible and can be applied successfully in the field.

6 ARCHAEOLOGICAL APPLICATIONS AND CULTURAL HERITAGE DOCUMENTATION

Figure 6-1: Maya site Copan (Honduras), overview image showing the ball court (Main Plaza).

6.1 Motivation

In this section real world applications will be demonstrated. In particular in our first example, Pinchango Alto, we will compare the generated elevation data from UAV images to terrestrial laser and manual accomplished data. Moreover, we will focus on the improvement of the autonomous flight and the influence of the flight modus of the UAV on the acquired data.

Many of the existing archaeological and cultural heritage sites worldwide are rarely or not documented at all. Quite often the local authorities are aware of the decomposition of these sites, but there is not enough time or money to protect all of them. Throughout the world archaeologists are looking for fast and low-cost methods, which can be used for the documentation of such venerable site. It is not only the documentation, which has to be done, there is also a need for the reconstruction of the objects for scientific or tourism purposes. Thus, the objects have to be documented quite often with high resolution and accuracy.
Therefore, the focus of our work was on documentation techniques for archaeological and cultural heritage sites. The selection of the examples was based on the complexity of the sites, on the accessibility, the maximum resolution and accuracy of the documentation technique, as well as the comparison and combination of the various techniques. The use of UAVs, the development of workflows for data processing of UAV data and the proof of practicability of UAVs in these applications are the major topics in the current chapter.

In the following section, we will describe three different examples of archaeological and cultural heritage sites, which were successfully documented using our stabilized model helicopter (Copter 1B) with and without a combination of terrestrial images and laser scanning.
The first example, Pinchango Alto (Peru), represents a demolished site, which may not be reconstructed any more. The example Copan (Honduras) is a good example for a combination of well-preserved and fast wheathering, which has to be documented in a way that the structures can also be modeled and reconstructed out of the retrieved data. The third example, castle Landenberg (Switzerland), represents an object with minimal damage. It is still in use and is an important relict of medieval times.

6.2 Pinchango Alto (Peru) a pre-Inca settlement

Pinchango is located in the Palpa region submontane of the Cerro Pinchango. The settlement was documented as part of the long-term Nasca-Palpa Archaeological Project, directed by Markus Reindel and Johny Isla. The site is surrounded by the Rio Grande and Palpa valleys at the horizontal spur of the Cresta de Sacramento. Pinchango is subdivided into a lower and an

upper part (Bajo and Alto respectively), as shown in Figure 6-3.[4] Both parts form the largest and also one of the best preserved sites from the LIP (Late Intermediate Period) in the Palpa region. The size of the region is approximately 20 ha.

Figure 6-2: Pinchango Alto (Peru), a settlement from the Late Intermediate Period (approximately AD 1000-1450).

The upper part is situated about 150m above the valley floor (~490m a.s.l.), while the lower part extends along the northwestern slope towards the Grande valley. It is extremely difficult to access the Pinchango Alto site. The access from the north is only possible along a steep trail leading over a ridge. At the same part of the site a large number of defensive walls are situated. To the south and east, the hilltop site is flanked by a deep gorge. The only direct access to Pinchango Alto is from the northwest via Pinchango Bajo. Unfortunately, a modern irrigation channel now cuts through the whole length of the site, and the so called access path no longer exists.

---

[4] *Our investigation on recording techniques for the documentation of archaeological sites concentrates mainly on Pinchango Alto. However, at this point both parts are introduced, since Pinchango Alto (PV66-137) and Pinchango Bajo (southern part PV66-136 and northern part PV66-138) form the site Pinchango. How the local measurements of both sites were integrated into one data base will be described in the following section.*
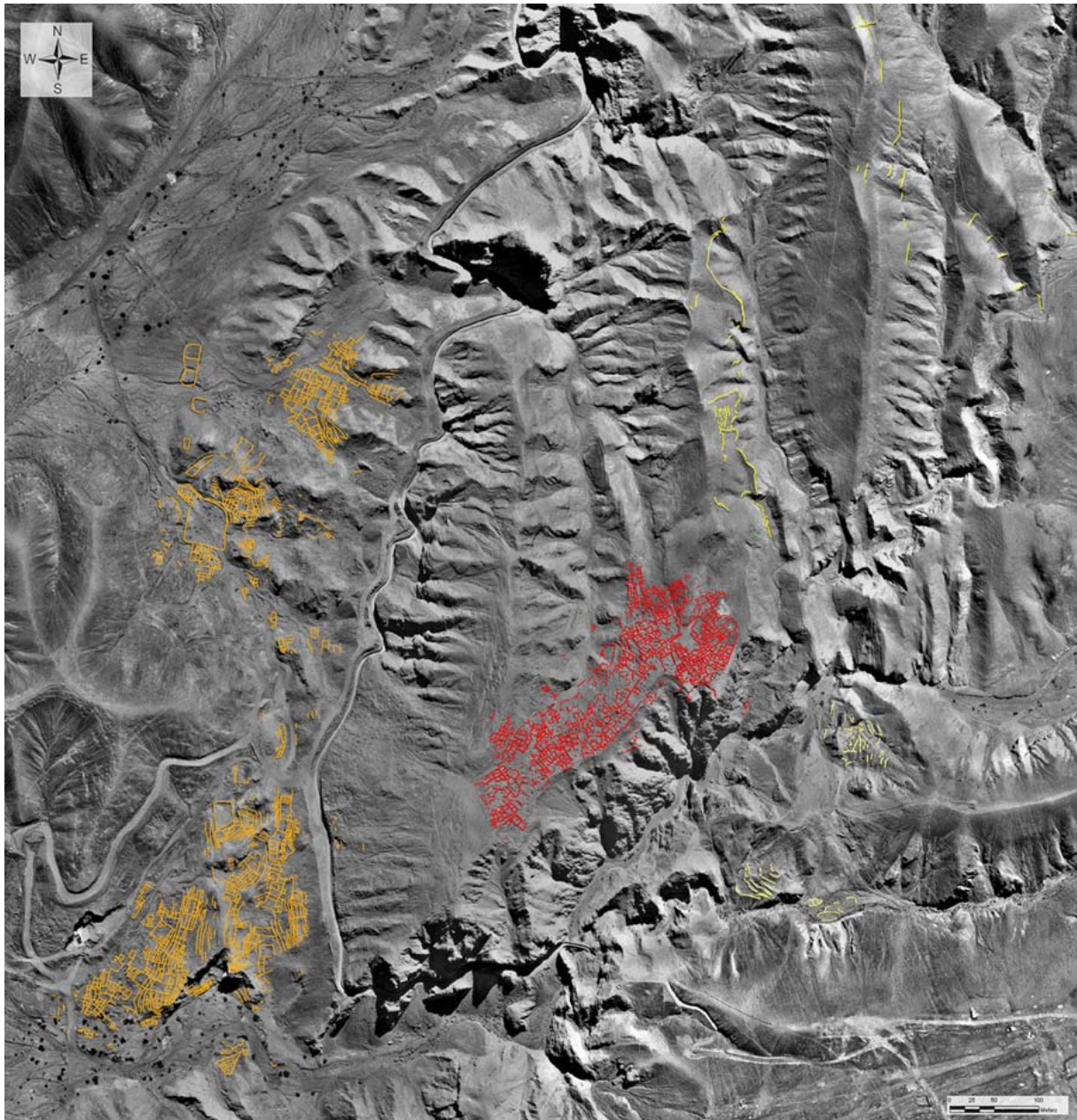
Figure 6-3: A cut-out of the orthoimage from aerial images which shows the entire Pinchango site (14_3002700 S, 75_1100300 W). The orange lines indicate Pinchango Bajo, while the red lines indicate Pinchango Alto. The yellow lines show the defensive walls of the settlement and small settlement structures, which belong to Pinchango too.

The preserved wall height is about 40 to 70cm but can reach a maximum of 1.5m (Figure 6-2). The wall's structure divide the site in small and large rooms, open squares and narrow paths, which are laterally bordered by long slabs. In the central part of Pinchango Alto, a series of holes were burrowed into the ground and underlying bedrock in ancient times. In addition, close to the holes, grinding stones and accumulations of pebbles out of mica are located. The discovery of grinding stones and the holes, which look like short mine shafts, have led to the assumption that the settlement was a mining and mineral processing centre

(Reindel, 2005, Reindel, et al., 2002 and Figure 6-2). However, the holes may also have served as storage of other goods (Stöllner and Reindel, 2007); this has to be investigated in upcoming archaeological excavations.

6.2.1 Previous work at Pinchango

The earliest aerial images were taken in 1944 over the area of Sacramento, which also include the Pinchango area (Lambers, 2006). Some forty years later, Johnson did some experiments with Balloon Photogrammetry and medium format images taken from a sporting airplane in the Nasca area (see chapter 3 and Johnson, et al., 1990).

In 1999, in the framework of a diploma thesis at ETH Zurich, Zwicker, 2000 completed the first photogrammetric and geodetic observation for the archaeological documentation of the site Pinchango Alto. The surrounding area was accomplished by Zwicker (see Reindel and Isla Cuadrado, 1999 and Figure 6-3), while Pinchango Bajo was recently measured in orthoimages generated from aerial images (Kupferschmidt, 2008). At this time, the structure of the site was surveyed by using two methods, which were established in the last decades. For the first method, a tachymeter TC 600 (Leica) was used. Specifically, for the definition of the coordinate system, four fix points were established. Using these points, the terrain and the walls were recorded using tachymetric survey with an accuracy for the tachymetric measurements of 2cm in planimetry and 3cm in height. However, the accuracy of the measurements of the walls in height was approximately 20cm, since the structure of the walls varies significantly from one stone to the next. In the second method the site was mapped using an analytical plotter by manual measurements in analog aerial images. The average image scale was intended to be 1:5000 (Gruen, 1999). Finally, aerial images were acquired in 1998 in the framework of the geoglyph survey Lambers, 2006 with a scale of 1:7000. Since the aerial images covered a larger area than Pinchango Alto, it was also possible to map the defensive walls. The accuracy for the manual measurements of the walls was 10-20cm. The photogrammetric measurements of the contour lines were done in the framework of the Palpa DSM (see Sauerbier and Lambers, 2003, hereafter aerial-DSM), while the measurements of the settlement structure were done by Zwicker, 2000.

The conclusion of the diploma thesis (Zwicker, 2000s) was that the aptitude of both methods varied significantly inside the site. The contour lines produced from the terrestrial measurements showed high accuracy, but they could cover only a limited part of the area of interest. In contrast, the photogrammetric measurements could cover the complete area, while the accuracy of the measurements was not sufficient enough. However, finally for the general plan the photogrammetric data were used.

For the analysis of the mapping of the settlement structure the area was separated into the area with the best preserved walls and the area with the most damaged parts of the site. Comparing the terrestrial and photogrammetric measurements for the well preserved part, both methods are equivalent, while for the demolished part the destroyed structures were not identifiable in the aerial images. Nevertheless, the surrounded defensive walls were only measured in the aerial images, due to time constraints. Finally, the terrestrially measured walls were combined with the photogrammetric measurements of the contour lines and the far-flung defensive walls. These results allowed the analysis of the settlement structure of Pinchango Alto, including agglutinated rooms, enclosures, corridors, and several large plazas.

Using the experiences from 1999, the archaeologists involved in the Nasca-Palpa project searched for new technologies, which would allow more detailed and accurate data acquisition.

6.2.2 A challenge for new technologies

Pinchango Alto was in the focus of the archaeologists because of its state of preservation and size, Pinchango Alto is well suited for the analysis of a typical LIP site in detail. In addition, due to the demand to do the surveying of the sites over a short time period, the archaeologists were looking for documentation techniques which meet the given time frame. Furthermore, the surveying techniques should be easy to use, easily transportable, should have simple handling, be able to manage large datasets and the costs for the techniques should fulfill the usually limited budgets of archaeological field campaigns.

In archaeology it is common practice for the documentation to be based on classical surveying techniques like single point measurements using tachymetry, leveling or tape measurements. These methods are accurate, but for the recording of larger sites like Pinchango Alto, they are quite time consuming. Furthermore, these methods were used for the production of maps or to put distance measurements in archaeological sketches. Therefore, a high resolution, flexible and mobile recording system was needed to document the terrain and the architecture of the site. The recording of the site was also planned to show the potential of novel surveying techniques in archaeological research in terms of detail, efficiency and accuracy.

Finally, considering the general characteristics of LIP sites in the region of Palpa and Nasca, and Pinchango Alto in particular, three goals for the intended investigation of the LIP in the Palpa region were defined: 1) a spatial analysis of the site in its topographical context focusing on accessibility, visibility, and defensibility; 2) a functional study of the internal structure of the site; and 3) an example for the documentation of LIP stone architecture and masonry. Such a multi-level investigation required 3D models of the site and its surroundings at various levels of resolution (see Lambers, et al., 2007).

Moreover, it was also intended to introduce new technologies for the data acquisition of archaeological sites and to compare and combine for the first time terrestrial laser scanning with UAV image data. Especially the combination of terrestrial laser scanning and UAV images should allow the detailed combination of the walls as well as the ground areas.

6.2.3 Field work 2004

6.2.3.1 Selected technologies

Figure 6-4: Left image shows the selected mini-UAV system, while the right image illustrates the chosen terrestrial laser scanner RIEGL LMS 420 at Pinchango.

Table 6-1: Main features of the Riegl laser scanner LMS-Z420i.

Laser scanner LMS-Z420i	
Main dimension	463 x 210 mm
Weight	16 kg
Power supply	12-28 V DC
Measurement range	Up to 1000 m
Minimum range	2 m
Measurement rate	11000 pts/sec
Beam divergence	0.25 mrad

In 2003, during the planning phase of the Pinchango Alto field work, the mini UAV-system Copter 1b from Surveycopter (see Figure 6-4 and Table 3-11) was selected for the documentation campaign in 2004.

Based on the existing systems on the market in 2004, the Riegl laser scanner *LMS-Z420i* was the most appropriate one (see Figure 6-4 and Table 6-1). The *LMS-Z420i* system, a combined laser scanner system (see Kersten, et al., 2006), has a long scanning range of 1000m, it is robust, it allows working in an extreme environment and the adapted camera allows the combination of several lenses (Gaisecker, 2006); all of which fulfilled our requirements for the documentation of the archaeological site Pinchango Alto. The main characteristics of the laser scanner are listed in Table 6-1 (and Gaisecker, 2006).

6.2.3.2 Preparations

With the existing aerial orthoimage (see Figure 6-3) the dimensions of the settlement was determined. The complexity of the settlement could be appraised from a video footage, which was recorded during the field work 1999. Based on these evaluations, one week of field work for laser scanning was estimated. Moreover, the aerial-DSM and the orthoimage were used for the flight planning of the mini UAV flight. From prior fieldwork experiences with UAVs in Sweden (Eisenbeiss, 2003) the required time for the mini-UAV flight, including system checks, flight tests in the field and data acquisition using the stop point strategy, was assumed to one week.

Based on the separation between the area with the best preserved walls and the area with the most damaged parts of the site from the survey campaign 1999, the site was divided into the same classes (A and B respectively) for the laser scan positions density for the 2004 field work. The area A was covered with factor five more scan positions than for area B. Therefore, it was possible to guarantee both high resolution scan- and image-information on every single wall and to have only minor areas without data acquired (Gaisecker, 2006).

The flight planning was done in the office in Zurich using the existing orthoimage and elevation model of the area. The image scale was defined to 1:4,000 to obtain an average image resolution of 3cm with the still-video camera Canon D60 (Lens: EF14mm f/2.8L USM) mounted on the model helicopter. With a flying height of 56m, an image format of 15 by 22m on the ground and an image overlap along and across track of 75 percent, starting from one corner of the site, the acquisition points were calculated. The flying speed between the image points was set to 2m/s. Finally, the predefined image coordinates and the flying speed was saved into the flight mission file. This planning prior to field work was done with the 2/2.5D flight planning tool described in section (4.2.1).

6.2.3.3 Terrestrial Laser scanning and measurement of the control points

For the laser scanning the entire field-work was carried out within 5 days. The central part (Area A and Figure 6-10) was scanned from 47 scan positions, while the remaining part was scanned from 13 scan positions (see Figure 6-6). For the registration of the scan data, and also for the orientation of the helicopter image data, 80 signalized control points (see Figure 6-6) were put into the site and measured with differential GPS with a 3D accuracy of 2cm in horizontal and 3cm in vertical direction, after net-adjustment. For this purpose, retro-reflecting cylinders were combined with circular white cardboard discs. While the reflectors were clearly marked in the laser scan point clouds, the cardboard discs were easily discernable in the aerial images.

Since the differential GPS measurements of the control points were done on the first two days, the laser data could be already registered during data acquisition stage. Thus, immediately after completion of fieldwork a first result for a registered point cloud, consisting of approximately 270 million single point measurements and 420 digital terrestrial images were available (see Table 6-2).

Figure 6-5: Ground control point marker on a stone wall in Pinchango Alto.
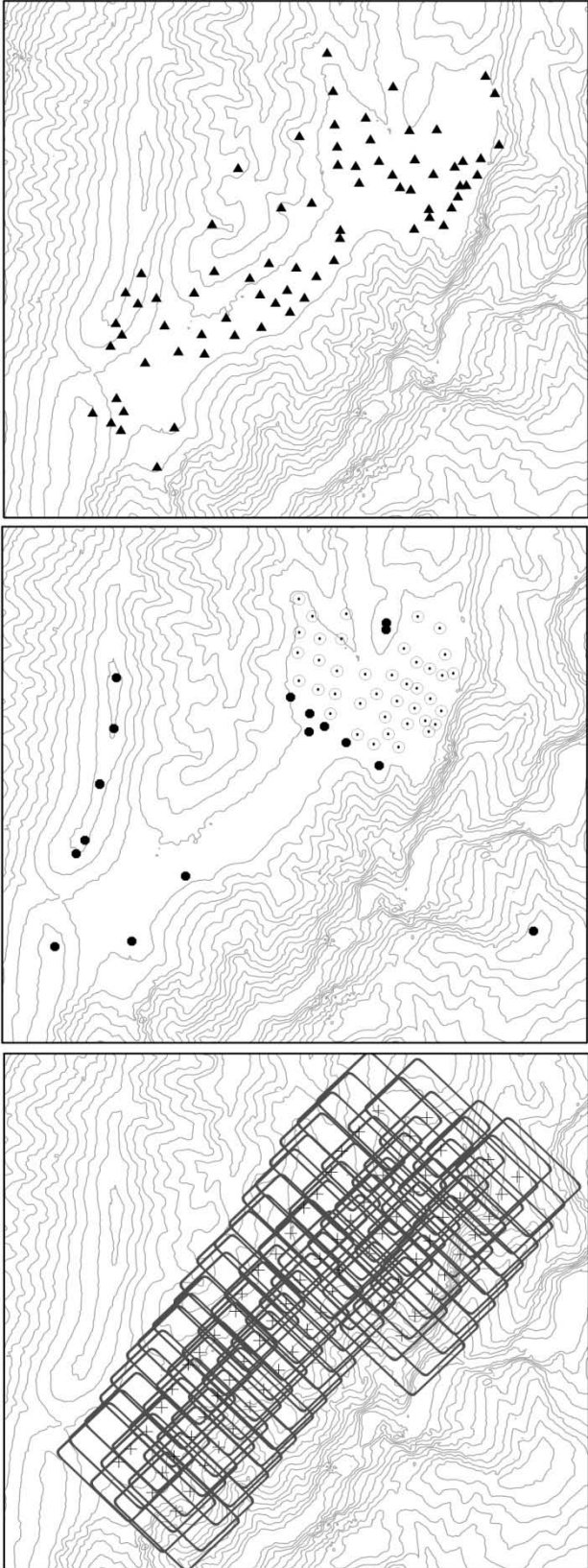
Figure 6-6: Up: Distribution of ground control points over Pinchango Alto; Middle: Distribution of scan positions for the eastern respectively area a (circles) and western (dots) part of the site, Down: Distributions of image coverage of UAV images.

6.2.3.4 Model helicopter

The helicopter flight was navigated both by an operator and a pilot. While take off and landing were controlled by the pilot due to the difficult terrain on the site, the actual flight mission was then controlled by the operator via the flight ground control station. During the flight the operator sent navigation commands to the helicopter to fly to the individual image acquisition points on the predefined flight path. The flight trajectory was controlled via the weGCS software (weControl), while the interface enabled the control of parameters like position, altitude, speed etc. During one flight 1 to 2 image strips could be captured. After which the helicopter had to land to refill gasoline and to recharge the batteries. Therefore, on the first day only 5 out of 8 predefined strips could be flown, resulting in a total of 85 images (see Figure 6-6 and Table 6-2). On the morning of the second day, dusted petrol and sand in the engine caused the helicopter to crash before reaching its normal flight height of 56 m. Due to time constraints it was not possible to repair and relaunch the damaged system. However, 95 % of the site had already been covered on the first day by images suitable for stereoscopic post processing. This was thanks to the precisely predefined flight path, the GPS/INS based stabilizer and the considerable overlap between the image strips (Eisenbeiss, et al., 2005). The complete image acquisition with the model helicopter was 50 minutes, less the time for recharging batteries and flight tests on-site.

6.2.4 Data Processing

6.2.4.1 Mini UAV images

Three different software systems were employed for photogrammetric image processing: the commercial software package LPS (Leica Photogrammetry Suite V8.9, Leica Geosystems) and the in-house software packages BUN and SAT-PP V1.0 (ETH Zurich).

LPS offers the functionality required to accomplish the complete photogrammetric working process from project definition and interior orientation to measurement of tie points (either in manual or automated mode), manual measurement of control points, bundle adjustment, and finally to DSM generation and orthoimage production. The software BUN however allows a more sophisticated aerial triangulation and comprises a robust algorithm for blunder detection during data processing. The adopted workflow for the processing of the UAV images of Pinchango Alto is shown in Figure 6-7.
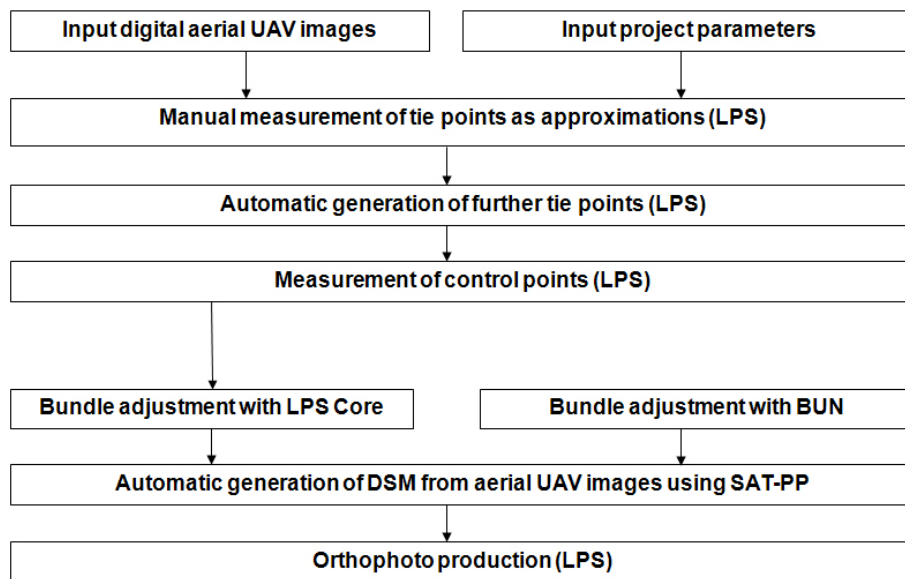
Figure 6-7: Workflow for the processing of the UAV images of Pinchango Alto.

The automatic measurement of tie points in LPS core V8.9 turned out to be time consuming and error prone, as LPS was designed for the standard aerial case, implying the use of calibrated aerial cameras. In Pinchango Alto we used instead an uncalibrated still-video camera with a wide angle lens. These special conditions, in combination with considerably varying terrain elevation not accounted for by the software, change of light conditions, and strong shadows in the images, caused the automatic tie point measurement tool to produce a lot of blunders. Therefore we decided to initially measure a few points manually and then to run the automatic tie point measurement tool. This procedure still yielded a lot of blunders in mountainous areas. These were removed using LPS and BUN, at which BUN detected more blunders than LPS. The image orientation in LPS core resulted in a total image unit weight (σ_0) of 2 Pixel. Finally, using BUN for bundle adjustment with self calibration of selected parameters following Brown's model, an RMSE value of 1/3 pixel (1cm in object space) was achieved (Eisenbeiss, et al., 2005).

For DSM generation from the helicopter images we used the software package SAT-PP (Described in section 5.2.1). The software was initially developed for the processing of satellite images and later adapted enabling it to handle still-video camera and aerial images. Following the workflow of automated image matching in SAT-PP (see Figure 6-8), an interpolated regular DSM (hereafter UAV-DSM) from the matching results with a resolution of 10cm was derived (Table 6-2). The combination of the multiple primitive matching (see Section 5.2.1.2) and the large overlap of 75% in and across flight direction, allowed the generation of a highly detailed DSM out of the still-video image data (see Figure 6-9).
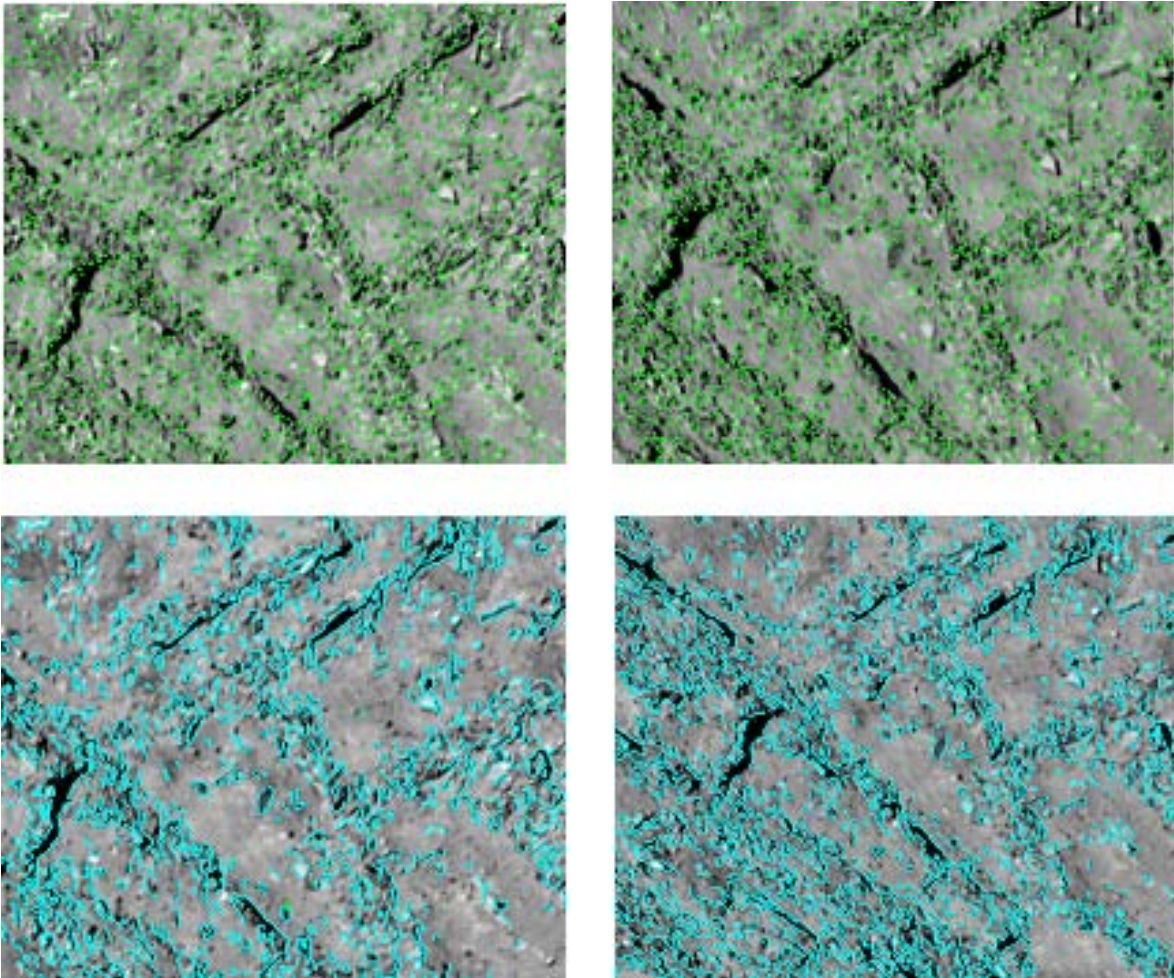
Figure 6-8: Extracted feature points (Up) and edges (Down) of a stereo pairs using SAT-PP.
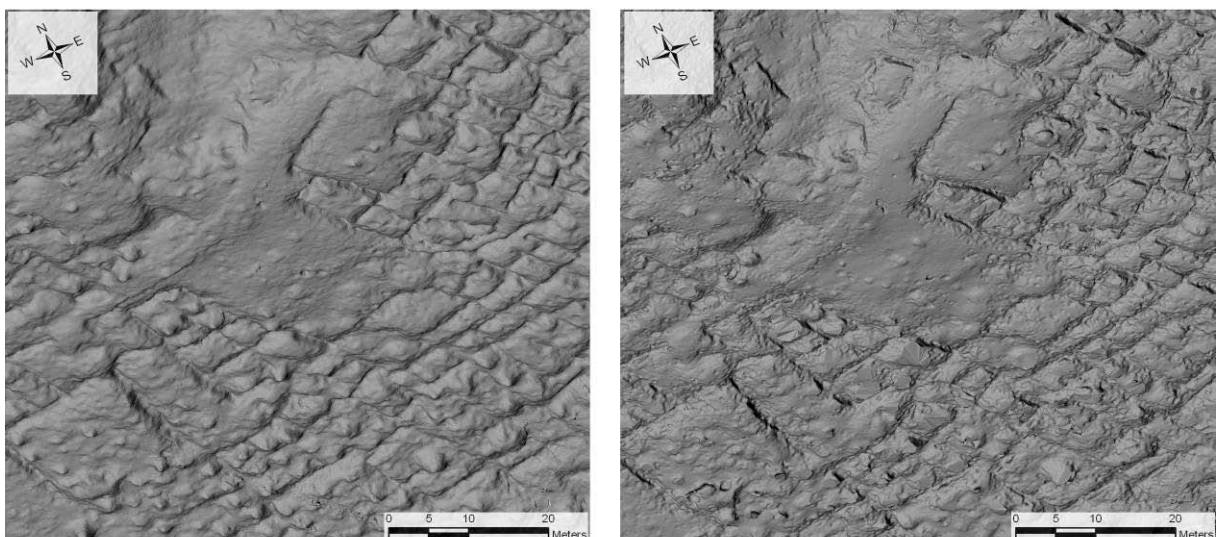
Figure 6-9: Detail view of the centre part of Pinchango Alto. Left: UAV-DSM, Right: Laser-DSM.

Using the image orientation data and the produced UAV-DSM, an orthoimage of the whole site with a ground resolution of 3cm was generated using LPS. The orthoimage was generated

119

from the helicopter images of the first, third and fifth strip. From each strip we selected every other image, resulting in a total of 26 images used for orthoimage production. Cutlines between images were calculated using the weighted cutline function in LPS. In the process of producing the final orthoimage with 3cm ground resolution we applied color balancing and feathering by a distance of three times the pixel size. The processing time for the complete area, about 300m by 200m, was approximately 20min on a 2.8GHz two-processor machine. Verifying check points for accuracy analysis, a mean RMSE value of 3cm for the whole area of Pinchango Alto was achieved.

Finally, for 3D visualization we used the orthoimage and the UAV-DSM. In order to generate a virtual flight through the model we employed Maya (Autodesk, 2009; see Lambers, et al., 2007).

6.2.4.2 Laser data

Using the Riegl RiSCANPRO software the laser data can be post processed in numerous ways. The optimum choice depends strongly on the application and/or the requirements of the end-user. One of the possible output products is a triangulated 3D-model, which can be used for automatically extracting contour lines, profiles, and to perform volume calculations.

In our project, as mentioned above, the registration of the single scans with RISCANPRO to one point cloud was done during the field work with the control points. While the internal registration accuracy of the scan data is about ±1cm, the accuracy for the global registration using control points was about ±5cm. The final registered laser point cloud was reduced from a total number of 270 million points by means of point decimation algorithm implemented in the Riegl software. Outliers were detected manually and semi automatically, again using RiSCANPRO. Finally, for the area A of Pinchango Alto the resolution was set to 10cm. This part of the model covers an area of approximately 130 m x 120m and consists of 1.5 million points and around 3 million triangles generated in Polyworks using a 2.5D Delauney triangulation. For the whole area of Pinchango Alto (200m x 300m), a model with a mesh size of 20cm consisting of 0.5 million points was generated. The result of the triangulation is a digital surface model (hereafter RiSCANPRO-DSM) that allows volume and section calculation (Lambers, et al., 2007).

In contrast to the software provided by Riegl, we applied our in-house surface matching algorithm LS3D for the registration of the point clouds. This software allows the registration of the single scans without using control points. The matching process was performed with an average σ_0 value around 1.0cm, which is consistent with the reported accuracy potential of the LMS-Z420i scanner. After registration the point cloud was georeferenced with 48 well

distributed ground control points (GCPs) to the Laser-DSM (see Figure 6-10 and Table 2). The GCPs were identified on the intensity image of the scans, and a posteriori σ_0 of the adjustment was 4.1cm, which is comparable with the accuracy of the GCP measurements (Akca, 2007).

Before doing the modeling of the surface the point cloud has to be analyzed for outliers. We employed an outlier detection algorithm for laser point clouds, developed by Sotoodeh, 2006. This developed method is based on a density based algorithm. In the laser scan data mainly single and small cluster outliers are detected like people, GPS, bags and boxes.

For the surface modeling, the commercial software package Geomagic Studio 6 (geomagic, 2009) and an in-house method, based on the most advanced sculpturing method using proximity graphs (Lambers, et al., 2007, Sotoodeh, et al., 2008), were selected. For the surface reconstruction of the whole site Geomagic was used, while the in-house method was applied with higher point density for single walls and rooms of the settlement. Using Geomagic the number of points was reduced to 14.8 million points using the "grid sampling" function with a 5cm grid size. The final surface wrapping was done with a medium level noise reduction option. Due to data unavailability some holes occurred on the meshed surface. These holes are mainly the result of occlusions of walls and the invisibility of the "mine shaft" entrances. The holes were filled with the "Fill Holes" function of the software. After the editing, the final model contained 5.8 million triangles. For detailed surface reconstruction of single walls using our method, we selected a wall in area A, where the scan point density was much higher than in the overall area. Although there are some holes in this model, due to under-sampling, the object is completely modeled in the areas that fulfilled the minimum sampling distance criteria. Most of the process was accomplished with only minimal user interaction. In addition, no threshold parameter or predefined values were required.

6.2.4.3 Combined data

After the processing of the helicopter images and laser data we then needed to texture the reconstructed surface models and to combine the various available data to one single data set.

Skyline (Terra Explorer) allowed us to combine the UAV-DSM and the orthoimage and to navigate in near real-time through the textured 3D model (see Figure 6-12). Furthermore, thanks to the automatic registration of the terrestrial image data within the scan data, the triangulated mesh could be textured with the high-resolution image-information. Therefore, using the laser point cloud and the terrestrial images, characteristic bricks from a wall were measured and visualized in the point cloud; the terrestrial images were visualized with the point cloud RiSCANPRO and in a CAD-program at once (Gaisecker, 2006). For the selected wall in area A also in-house software for automated texture mapping was also applied

(Hanusch, 2008). This software calculated the visible parts of the model for every image. For each vertex of the mesh, the image coordinates were calculated. For visualization of the textured model, the open source software Blender was used (Blender, 2008 and Figure 6-11).

Figure 6-10: The Laser-DSM overlaid with the corresponding orthoimage showing the central part of Pinchango Alto.

The derived surface model from laser data was also used for the orthoimage generation and texture mapping of the model helicopter images. The generated surface models from laser data and model helicopter images were also inserted into the 3D model of the surroundings of Pinchango Alto, generated out of aerial images. This enabled reliable studies of the visibility and accessibility of the site in a GIS environment. Figure 6-12 shows a combined textured 3D model for this purpose comprising the UAV DSM that covers Pinchango Alto and the aerial-DSM.

Figure 6-11: Textured 3D-model of a single wall showing a sample of plotted stones forming the walls.
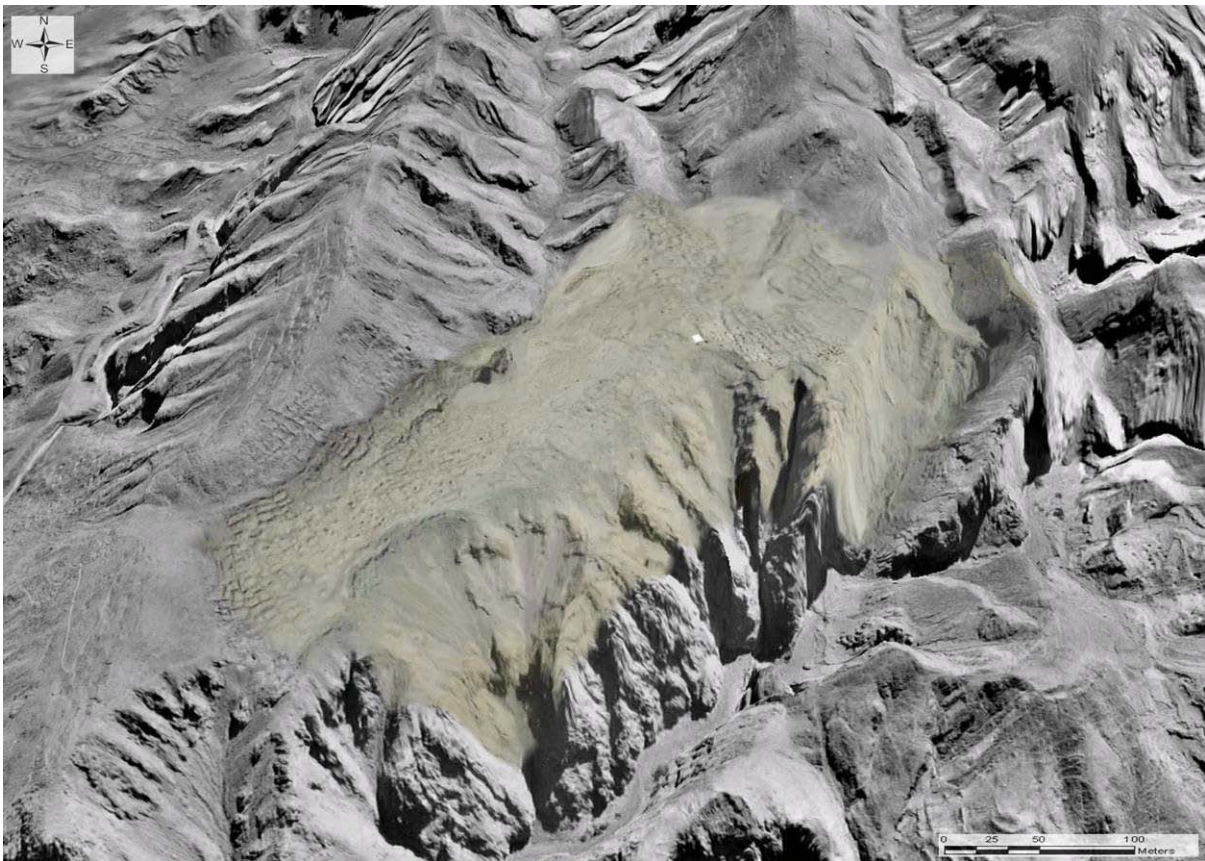
Figure 6-12: Textured 3D-model of Pinchango Alto showing the 3 cm UAV-orthoimage draped over the SAT-DSM with 20 cm resolution. The surrounding areas is presented by the aerial-DSM (2 m resolution) overlaid with the aerial orthoimage (25 cm) (Skyline, 2009; see Sauerbier, 2008).

6.2.5 Results

The application of two highly versatile recording systems, the terrestrial laser scanner and the UAV, allowed the LIP site of Pinchango Alto to be documented with high resolution and accuracy in five days of laser scanning and 50 minutes flight time of the UAV. The acquired

and processed data of Pinchango Alto are a good starting point for a detailed architectural, structural, and functional study of a typical large LIP site in the region of Palpa and Nasca. Table 6-2 illustrates the available data sets for the archaeological interpretations: The oriented UAV- and terrestrial-images, the original laser point cloud, the produced DSMs, orthoimages and texture 3D-models with different resolutions.

Table 6-2: Overview of original data and derived products of the site Pinchango.

Product/Source	Type	Specifications	
		Resolution or Footprint	Amount
ORIGINAL DATA			
Laser scanner (raw data)	Point cloud	1-35 cm	~270 million points
Terrestrial images	Digital Image	Depending on distance to object	427
UAV aerial images	Digital Image	~3 cm	85
Aerial images	Analog Image	~10 cm	4
DIGITAL ELEVATION MODELS			
Laser-DSM	Raster	5 cm	~14.8 million points
UAV-DSM	Raster	10 cm	~4.7 million points
Aerial-DSM	Raster	2 m	~ 1.6 million points
ORTHOIMAGES			
DSMs + UAV images	Orthoimage	3 cm	2
Aerial images	Orthoimage	25 cm	1
TEXTURED 3D MODELS			
Produced with Maya	Video	10/20 cm (Orthoimage/DSM)	1
Visualised using ArcScene	Real time navigation	3/10 cm (Orthoimage/DSM)	1
Produced with Blender	Real time navigation	1-5/5 cm (Texture/3D-model)	2 selected areas
Produced with Skyline	Real time navigation	3/20 cm (Orthoimage/DSM) 25 cm/2 m (Orthoimage/DSM)	1

6.2.5.1 Surface Models

For archaeological analysis, the UAV image data is advantageous, since the image data can be used for the automated generation of elevation models and for manual measurements in stereo viewing mode. For the definition of walls, rooms, forecourts etc., the stereo images provide valuable information for the interpretation by archaeologists. On the other hand the Laser-DSM can be used for interpretation of the architecture of single walls and rooms due to the high point density.

For the quality analysis of the DSMs, a manual-DSM was produced covering only the central part of Pinchango Alto (see Figure 6-10), because the manual measurements were very time consuming. These measurements are well suited to help to identify errors in the Laser- and UAV-DSM. The average distance between the manually stereoscopic measured points were defined to 50cm. The laser model covers the complete Pinchango Alto area, while the UAV-DSM covers 95% of the settlement area, as mentioned in paragraph 6.2.3.4.

Since automatically generated DSMs (Laser and UAV) have a resolution of 5 and 10cm respectively, the manual measurements can aid in trend identification and the results allow one to assess which is close to reality. The manual measurements will not reveal blunders of small features, like single stones, and small modeling problems, but accessorily blunders in the data such as persons in the laser scan or miss-matched points from the matching procedure will be detected.

The 3D comparison of the different elevation models was done with Geomagic Studio. Geomagic Studio has the capability to perform 3D comparison between point to surface or surface to surface models (see Table 6-3, Figure 6-13 (Whole site Pinchango Alto) and Figure 6-14 (Detailed views of two selected areas)).

Table 6-3: Results from the comparison of the different DSM datasets.

	Laser/ SAT-PP	Laser/ Manual	SAT-PP/ Manual	SAT-PP/ NGATE	SAT-PP/ LPS
Std. deviation [m]	0.06	0.11	0.10	0.29	0.50
Mean [m]	< 0.01	< 0.01	< 0.01	0.26	-0.32
Max [m]	0.54	0.66	0.46	~ 3	~ 5

A comparison between the SAT-PP-DSM and those extracted with LPS and NGATE cover only a subset of the best preserved part of the archaeological site. The large standard deviation from SAT-PP /LPS is result of the difference in the orientation of the data. The orientation used in SAT-PP was improved through BUN. Additionally, the discrepancies between SAT-PP and NGATE resulted out of artifacts observed in the NGATE DSM. We should note however that the applied NGATE module was only an evaluation license and therefore the results are preliminary.

The resolution of the laser is higher than in the UAV-DSM, for example single structures like stones can be seen in the Laser-DSM (see Figure 6-9). On the other hand, both data sets contained blunders. The comparison between the Laser- and the UAV-DSM show a mean difference of less than 1cm with a standard deviation of 6cm (Eisenbeiss and Zhang, 2006 and Table 6-3). The differences occurred mainly where the topography changed suddenly, e.g. walls elongated along the flight direction, at the border areas of the settlement and inside the holes (see Figure 6-13). For the UAV-DSM, the main difficulties were on walls and structures with vertical surfaces, which were not covered in different image strips. The laser was unable to acquire points in the holes; therefore, the UAV-DSM fits better in these areas (see Figure 6-9 and Figure 6-14).

The UAV- and the Laser-DSM showed more detail and had higher accuracy in comparison to manual measurements (Eisenbeiss and Zhang, 2006 and Table 6-3) and to the photogrammetric and geodetic measurements obtained in the field campaign in 1999 (Zwicker, 2000). Both, the Laser- and the UAV-DSM, showed similar good results with respect to the manual-DSM. The mean difference was less than one centimeter. The standard deviation was approximately 10cm and the maximum difference was less than 0.5m for the UAV-DSM and 0.7m for the Laser-DSM respectively. The maxima were mainly found in the mining and wall areas. It should be noted that the traditional measurement methods are more time consuming for data acquisition and processing with respect to the proposed methods. Therefore, the new methods were established and will be improved in the near future and can be expected to replace more and more the traditional documentation techniques for comparable applications.

The comparison of the extracted point clouds between LPS V.9.2 and SAT-PP V1.0 shows clearly that SAT-PP was able to extract a denser point cloud (LPS: 230,000 points; SAT-PP: 420,000 points). However, despite this difference, the main structures of the site could be reconstructed in both software packages. In LPS V9.2 the matching algorithm, compared to older versions, had been improved with an adaptive image matching algorithm (see section 5.2.1.1). The main holes in the produced LPS-DSM occurred in the low texture and steep areas, where no points were extracted (see Figure 6-15 and Appendix G-1).
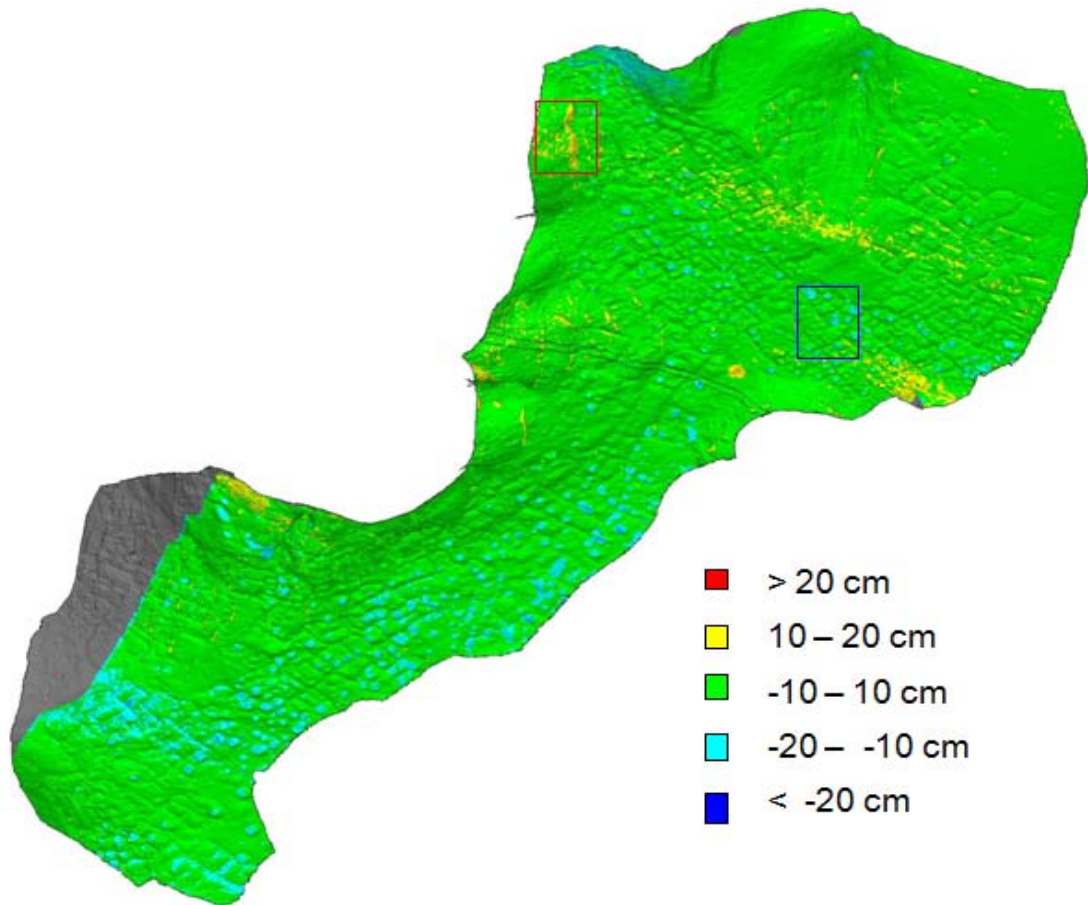
Figure 6-13: Discrepancy map of 3D distances of UAV-DSM and Laser-DSM after registration.
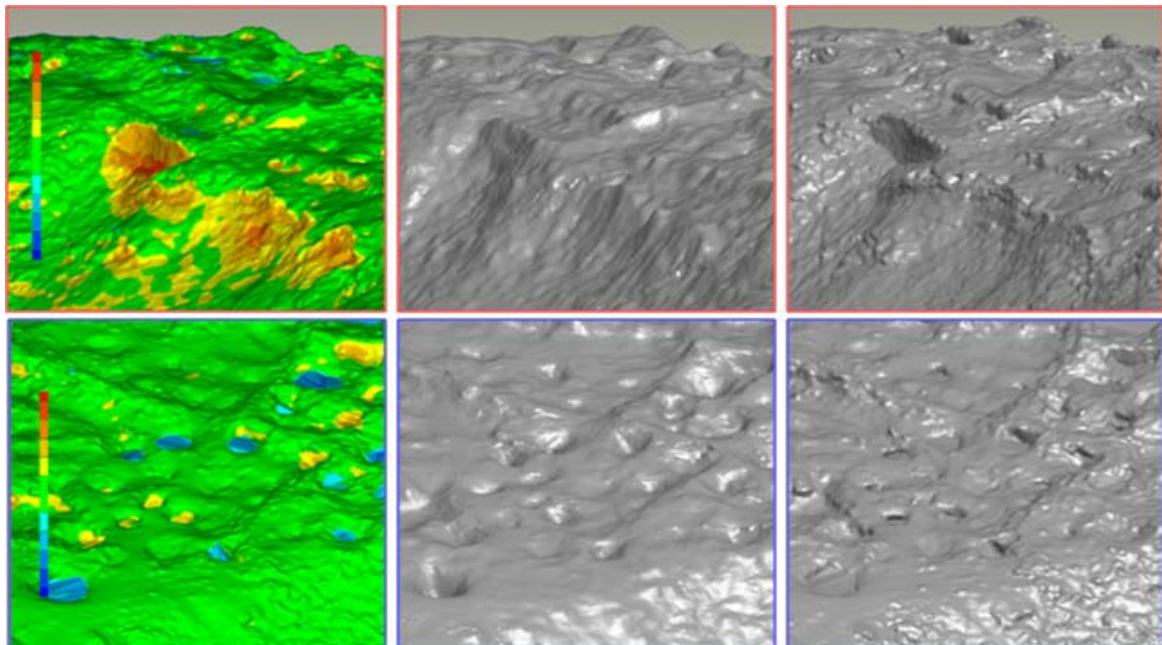
Figure 6-14: Detailed view: Example for the maximum difference of DSMs forthcoming on walls and for mining entrances (holes).
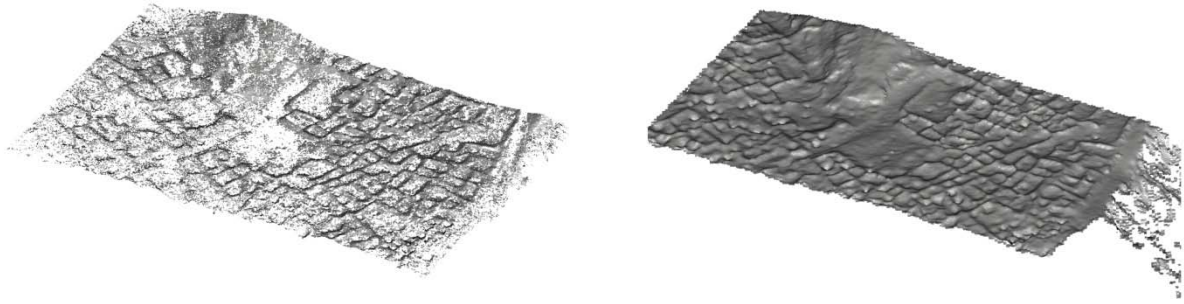
Figure 6-15: Comparison of the matching results out of one stereo pair of the centre of Pinchango Alto. Left: LPS, Right: SAT-PP.

6.2.5.2 Orthophotos and textured 3D-models

Up to now, two high resolution DSMs of Pinchango Alto exist that can be textured with high resolution orthophotos produced from UAV images (see Figure 6-16). This combination is especially well suited for highly accurate measurements of the walls as viewed from nadir direction, and allows the groundplan of the site to be mapped and its internal structure to be studied. The disadvantage of the UAV images is the lack of high resolution texture for the vertical faces of the walls. However, these walls were covered in the laser data and textured using the terrestrial acquired images (see Figure 6-11).
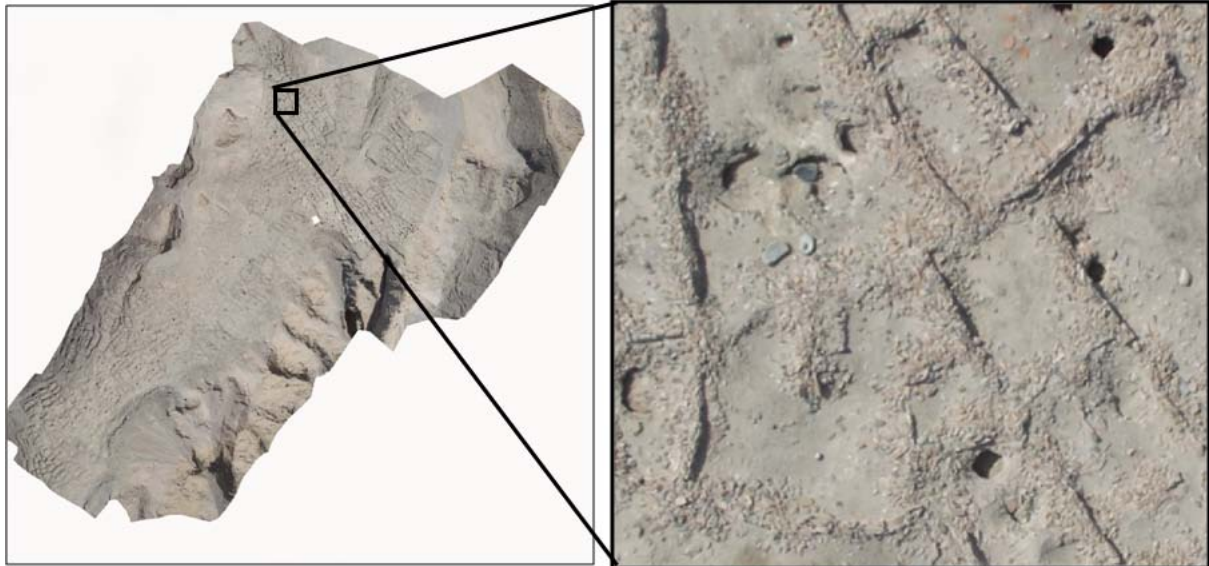
Figure 6-16: Orthophoto with 3cm resolution of Pinchango Alto produced from the UAV-images and – DSM. Left: The complete site. Right: Detailed view of the orthophoto.

The 3D models resulting from the combination of photogrammetry and laser scanning offer many opportunities for future archaeological investigations of the site of Pinchango Alto in particular and the Late Intermediate Period in the Palpa region in general that go well beyond previous studies of prehistoric architecture in southern Peru (see Lambers, et al., 2007).

In order to enable GIS-based studies of the site´s context, the high resolution 3D model was integrated into the textured aerial-DSM (see Figure 6-12). This combined 3D-model allows for example the calculation of access pathways from different directions. It is expected to reveal from which valley the site was most accessible and whether or not a direct access from Pinchango Bajo existed. Also with regards to defensibility, visibility studies taking into account reconstructed wall height may reveal if the site was visible from the valley floors.

6.3 The Maya site Copán (Honduras)

Copán was a Maya city located in the northwest of Honduras near the border to Guatemala and the principal group, which was our area of interest, has a size of 300m by 600m. "Copán was probably the most significant civic center of the southeast region of the Maya lowlands and is mentioned the first in 1576." (Hohmann and Vogrin, 1982, p. 136)

The work presented in the following section was conducted in cooperation with the Honduran Institute of Anthropology and History (IHAH), the University of New Mexico (US) and the B. Kessler Foundation (Italy). The field work itself was accomplished in the frame of the workshop "3D Archaeology and Cultural Heritage Management in Honduras" (IHAH, 2009). Here we will describe the field work accomplished using our UAV system and present first results.

Figure 6-17: Terrestrial Image of the main plaza of Copán showing the ball court in the front (compare Figure 6-1).

6.3.1 Field work 2009

The flight planning of the UAV flights was conducted based on a digital map of the site Copan generated by Richards-Rissetto, 2009 and Figure 6-18, using the 2/2.5D flight planning tool (see Figure 6-18).
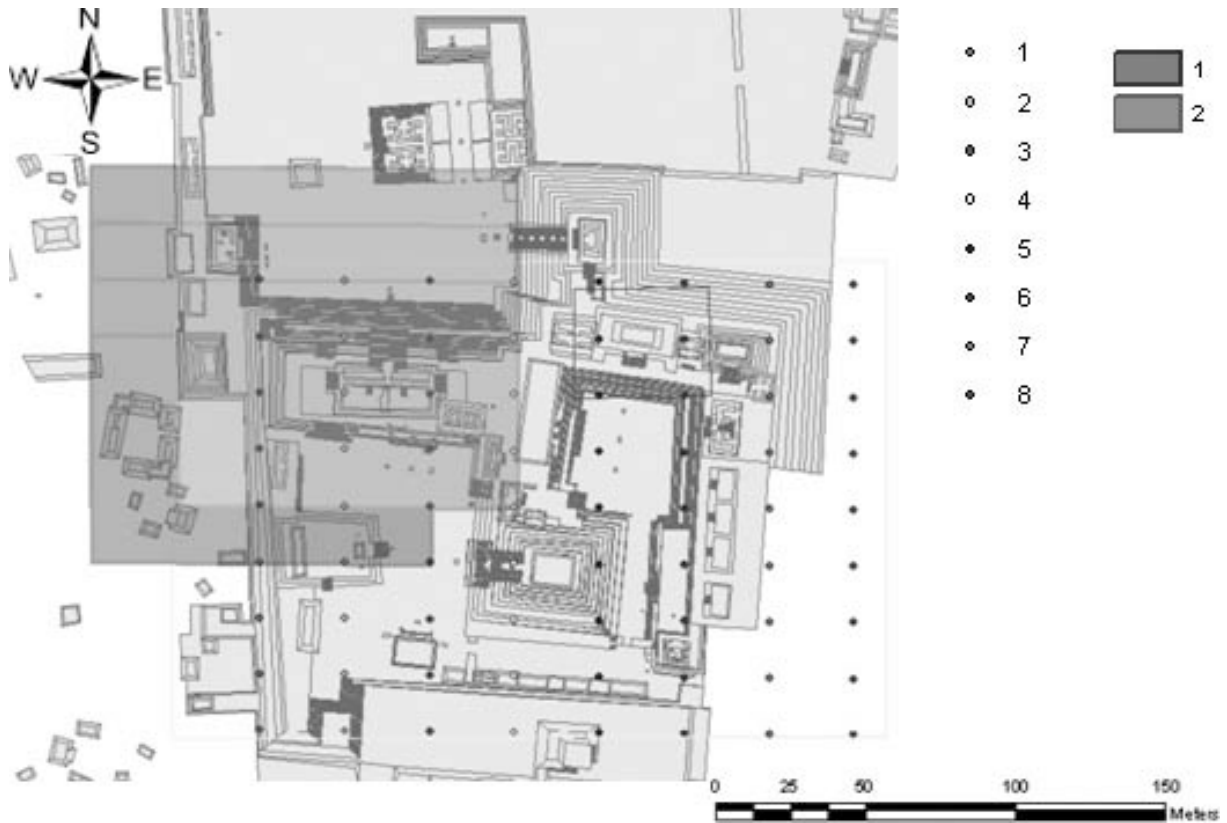
Figure 6-18: Visualization of the flight planning of the east and west court of Copán showing the projection centers of the individual image strips (dots) and exemplary the image coverage of view images.

The image resolution for the east and west court (Area I) was defined to 1cm, while for the main plaza (Area II) the resolution was reduced to 3cm. For the data acquisition the Nikon D2Xs 12 Megapixel still-video camera was selected, using a 35mm and a 24mm lens at 90m and 120m above ground level for the areas I and II respectively. The Nikon camera is a CMOS-sensor with 4288x2848 pixels and a pixel size of 5.5µm. The defined flight parameters are listed in Table 6-4. In contrast to the flight planning in Pinchango Alto, the image acquisition points were defined as cruising points, thus only the start and end point of a flight line were transferred to the flight control software. The image acquisition points between the start and end point were thus calculated through the image baseline.

Table 6-4: Main parameter of the flight planning defined for area I (East and west court) and II (Main plaza).

Area	m_B	H_g [m]	F [mm]	GSD [cm]	Size of the area	p/q [%]
I	2500	90	35	~1	200m x 200m	75/75
II	5000	120	24	3	300m x 200m	75/75

After an initial visit to the site, where the complexity of the objects and the occlusion (see Figure 6-17) caused by the dense tree coverage were clearly evident, it was decided to increase the along track overlap to 87.5%. Thus the number of images for area I was increased

from 80 to 160 images. Since area II was mostly free of trees, the defined overlap was kept and the planned numbers of images of 75 unchanged.

The flights at Copan were conducted in the morning for area I and in the afternoon for area II, with flight times of 12 and 10 minutes respectively. Due to the developing winds in the afternoon, the flight at area II had to be stopped after 3 image strips.

6.3.2 Data Processing

Keeping to the frame work of this thesis, only the images acquired from the east court and temple 22 were oriented; these are the central focus of our project partners. For a quick overview and data checking using the acquired images from both areas, photo stitching was achieved using Photoshop (Adobe, 2009). Moreover, the flight trajectory was analyzed using the flight control data acquired with the wePilot1000-10g/N.

6.3.2.1 Quality control of the flight data

Due to the strong wind, which developed suddenly in the afternoon, we had to stop our flight mission of the main plaza (Area II). Figure 6-19 and 6-20 show the influence of the wind on the observed flight control data.
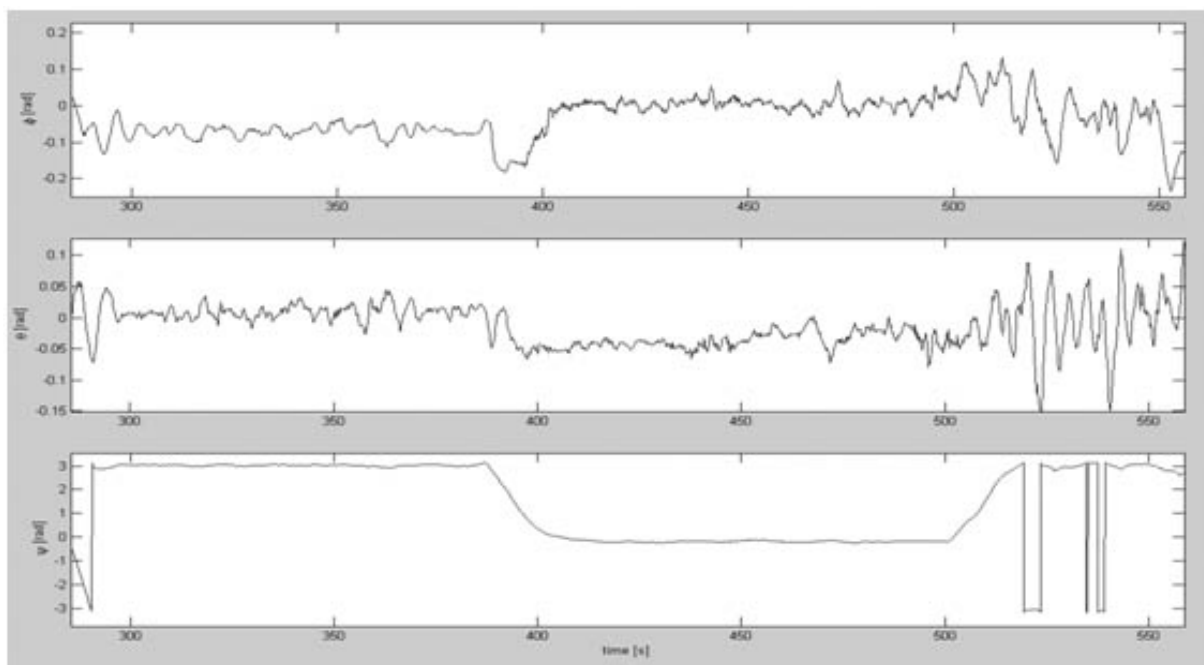
Figure 6-19: Orientation data of the afternoon flight. Upper graph: Φ, Middle graph: Θ, Lower graph: Ψ.
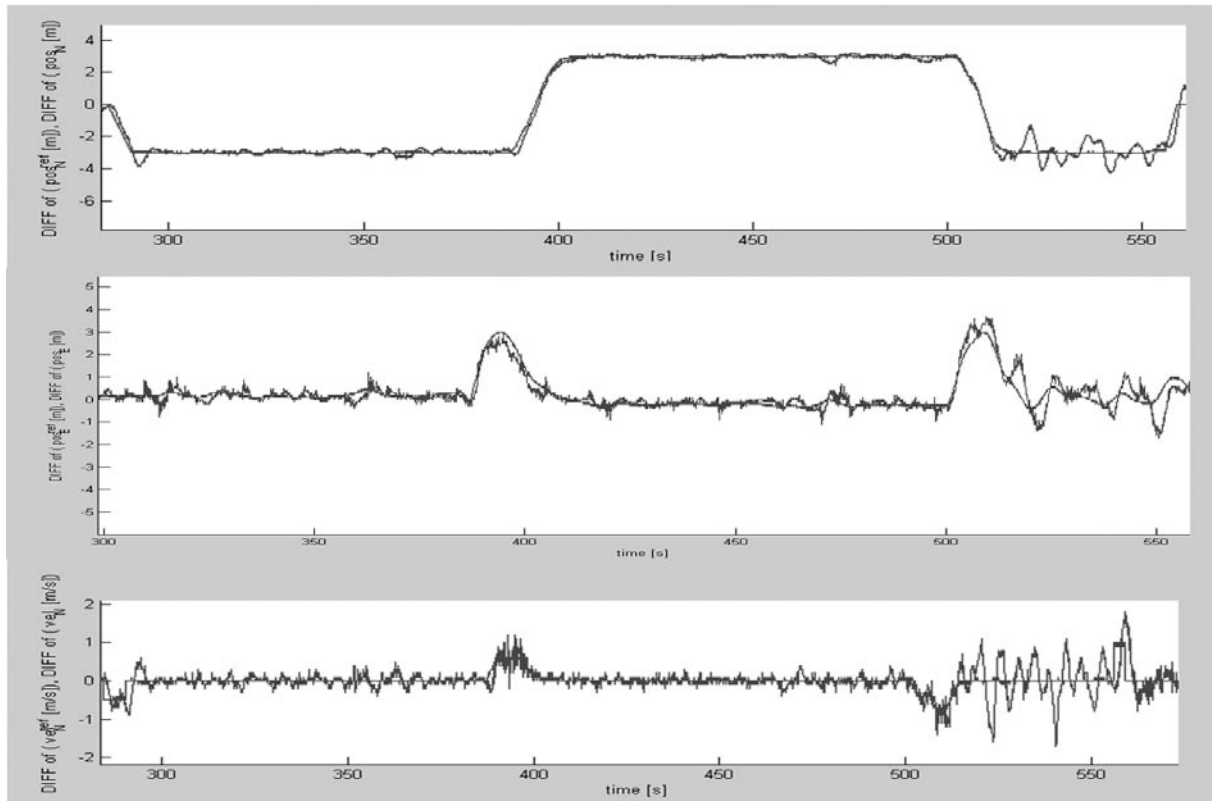
Figure 6-20: Differences of the reference and measured data of the afternoon flight. Upper graph: Position, north component pos$_N$, Middle graph: Position, east component pos$_E$, Lower graph: Velocity, north component v$_N$.

Figure 6-19 illustrates the orientation angles of the flight over area II. The rotation angles are plotted in relation to the flight time. The first and the second line were flown in the interval of 300s to 400s and 400s to 500s respectively. After turning into the third strip, the influence of the wind is visible in the rotation angles. The same effect could also be observed in the difference plots between the reference and the measured GPS coordinates in north and east direction, as well as the velocity values in north direction (see Figure 6-20).

6.3.2.2 First results during field work

After completing data acquisition, the UAV images were stitched to a panorama overview, giving an overview of the site just after the data acquisition (Figure 6-1 and Figure 6-21). Using the unrectified images, it is already possible to identify the main structure and even to recognize features, which were not visible from the ground (see structure in the grassland in Figure 6-1). These identified structures include areas of old excavations, as well as old foundations of buildings which are no longer standing (see Hohmann and Vogrin, 1982).

133

Figure 6-21: Left: Copan Eastcourt, Temple 22 and 16. Right: Overlapping of every second image of one image strip.

6.3.2.3 Photogrammetric processing of the east court data

The first images of our UAV flight in Copán covering the east court and Temple 22 (Ahlfeldt, 2004, Fash, 1991), were oriented using LPS Orima (Rel. 8.0). The results of the orientation of 22 images using 5 GCPs are given in Table 6-5.

Table 6-5: Accuracy values of the image orientation of the east court image block of Copán.

σ_0	RMS changes of control points		
[µm]	X [m]	Y [m]	Z [m]
3.5	0.02	0.02	0.01

6.3.3 Results

With the given orientation values, a DSM of the east court with a point sampling distance of 5cm was produced with SAT-PP V1.0 automatically without any editing. Finally, a first orthoimage with 1cm resolution was generated with LPS (see Figure 6-22).
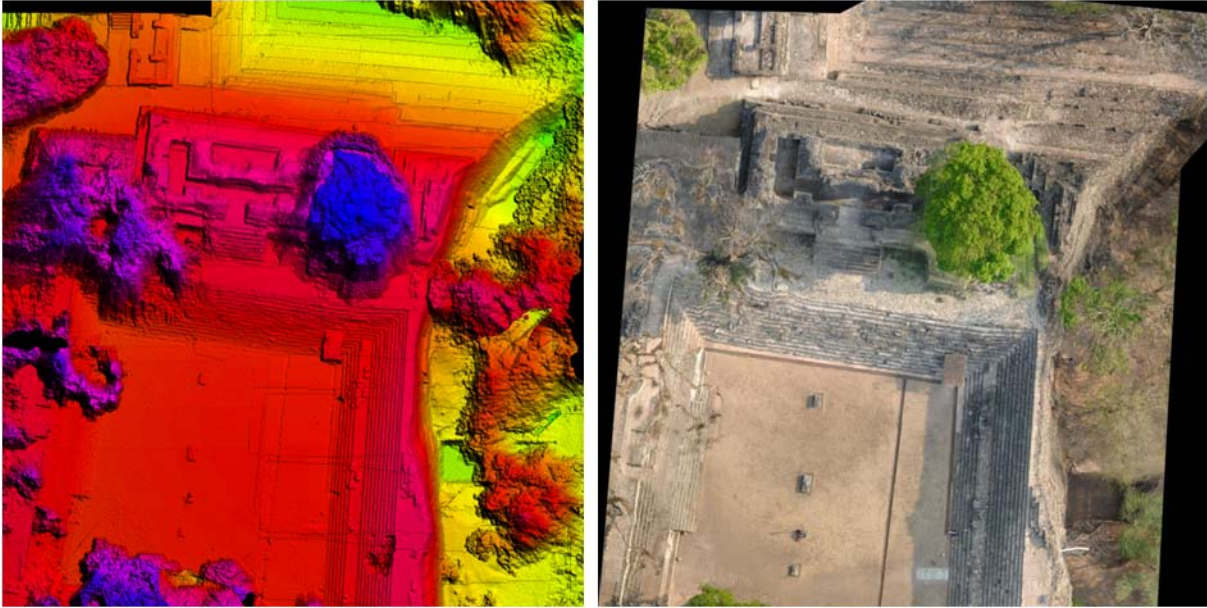
Figure 6-22: First results of the East court and temple 22. Left: DSM with 5cm resolution and Right: Orthoimage with 1cm resolution.

The results shown in Figure 6-22 are preliminary, since the occlusion of the structures through the trees can be observed in the DSM. However, these products were generated in only one day, (including image orientation (4h), DSM generation (6h) and orthoimage production (1h)). This short processing time was possible, due to the good flight performance of the autonomous flight.

6.4 Castle Landenberg (Switzerland)

In this project the goal was to achieve a digital, photo-realistically textured 3D model of the castle Landenberg in Sarnen (Switzerland) by combination of aerial and terrestrial images (Pueschel, et al., 2008).

This work is based on a study undertaken as part of a bachelor thesis at ETH Zurich. The original goal was the documentation of the castle using terrestrial photogrammetry. Already in the planning period it was decided to acquire UAV images, in addition to the terrestrial images. This decision was made due to the exposed position of the castle. Because of occlusions, the front façade was not completely documentable. In addition, for the reconstruction of the structure of the roof and the jutties, images from above the castle were needed. Thus a combination of terrestrial and aerial imagery was chosen to achieve total image coverage of the object.

Figure 6-23: Front view of castle Landenberg. The image was acquired with our UAV-system.

Sarnen is the capital of Obwalden in central Switzerland. The so-called "Schützenhaus" is the town's landmark and lies at an exposed position in the west of the village. The object is not only important for Sarnen, but also for the whole canton Obwalden. In fact the "Schützenhaus" is the symbol of the canton illustrated in the Swiss passport. The "Schützenhaus" is a valuable relict of the medieval castle in Sarnen. It is one of the two buildings which remain of the castle Landenberg. In the 13th century, Castle Landenberg was

built by Rudolf of Habsburg and at that time was the biggest castle in central Switzerland. It remained so until the battles for freedom in 1291, where most parts of the castle were destroyed. From 1646 to 1998 the "Schützenhaus" was the meeting place of the "Landsgemeinde" (provincial assembly), until the public assembly was abolished in Obwalden in 1998. Recently, the castle is used for cultural and social events.

6.4.1 Field work 2007

The image scale for all images was defined to ca. 1:3000, which corresponds to a resolution in object space of approximately 1cm. For the image acquisition of the terrestrial images a distance to the object was defined to 20 to 25 m, which aimed to allow a similar image scale as in the UAV-images. We acquired terrestrial photos from various stations situated around the building and aerial images positioned on a circle, with a radius of 25m around the centre of the building. The flying height was defined to 30m above ground. The centre of the building was defined in the Pixel Map 25 (swisstopo ®). The image acquisition points were defined on the circle with a distance of 25m from one point to the next, which corresponds to an angle between the points on the circle of 15° using the flight planning tool circle (see section 4.2.1). Furthermore, the image acquisition from the helicopter was defined in a way that the camera was looking sidewards with a zenith angle of 70°. Additionally, one image strip was acquired looking perpendicular to the front of the façade of the building.

Figure 6-24: Flight Paths: Circle (left) and frontal strip (right: Orthophoto (GIS-Obwalden, 2009)).

Figure 6-23 shows one example of an image taken from the front façade of the building. The two flights, the circle and the front façade are illustrated in Figure 6-24.

Both, terrestrial and aerial images were acquired with the Nikon D2Xs still-video camera (see section 6.4) with an 18mm lens (Nikon AF NIKKOR 18 mm, 1:2.8 D). Before image

acquisition, the auto focus was set to manual mode, while the focus was fixed to infinity. Afterwards, the focus was locked with scotch tape to avoid unintended movements. The terrestrial images were taken from a tripod to avoid blurred images, since the light conditions did not always allow a short exposure time.

6.4.1.1 Terrestrial Images

Two sets of terrestrial images were acquired. One image set was acquired in foggy weather, while the second set was acquired on a cloud free day. The images taken during sunshine have significant differences in brightness. Due to the inhomogeneous intensity of the light it was difficult to find the optimal shutter speed. Moreover, in the images it was difficult to recognize details in the shadow areas during the photogrammetric processing phase and 3D modeling. The images taken in foggy weather were optimal for our purpose. As a result of the diffuse light, no shadows occurred on the object and therefore the whole façade was distinguishable (Pueschel, et al., 2008).

6.4.1.2 Aerial Images

The coordinates of the waypoints were calculated and imported in the weGCS system. Before the real flight was accomplished, the flight was simulated on the computer using weGCS to verify the waypoints and the flight path. The simulation showed that last point of image acquisition, defined as the stop point, did not allow the automated continuing of the flight to the home point. Therefore, the point was changed to a cruising point.

For safety reasons the starts and landings were flown in manual remote controlled mode, similar to the flights at Pinchango and Copan. As soon as the UAV was in the air, control was taken over by the weGCS navigation unit.

The circle route was flown two times to ensure the acquisition of a sufficient number of high quality images. The horizontal strip from the front, as well as the circle, resulted in images of satisfactory quality. An example of an aerial image from the circle is shown in Figure 6-25 (Left), while a zoom-in of this image is shown Figure 6-25 (Right).

Overall the total terrestrial image acquisition required a few hours and the helicopter was, in total for data acquisition in the air only few minutes. However, in addition to the helicopter flight, the preparation of the flight control station and the helicopter itself, before and after the flight has to be taken in account.

Figure 6-25: Left: Example of an aerial image from the circle route. Right: Zoom-in to the rectangle of the left image.
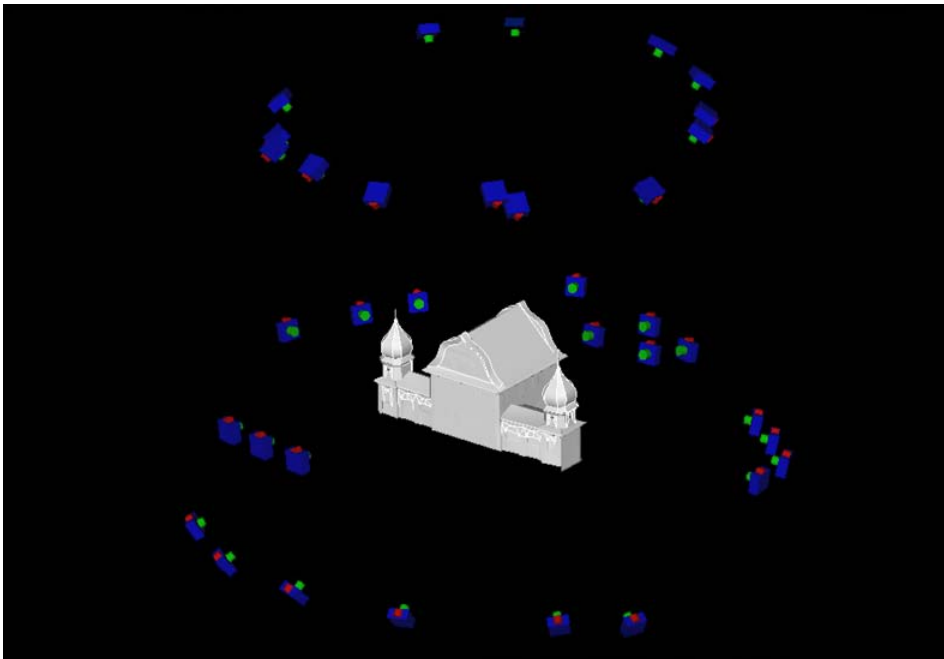
Figure 6-26: Locations of terrestrial and UAV images, which were used for the data model.

6.4.2 Data Processing and 3D Modelling

Before starting the image orientation and modelling, the first step was to select the images that were necessary to achieve a complete coverage of the façade. Due to the complex geometry of the building and the fact that the sight to some parts of the object were obscured because of trees, 18 terrestrial images were needed to ensure a precise and complete modelling of the façade. From the 72 recorded aerial images 14 were selected from the circle and 3 from the linear strip (see Figure 6-26).

The relative orientation was done in PhotoModeler V6. The overall RMS was 0.99Pixel which could be regarded as an acceptable result. After the modeling, which is described in detail in Pueschel, et al., 2008, the project was absolute oriented in the Swiss coordinate

system LV03. Using 12 GCPs we achieved an accuracy of 2.5 cm in object space, which is in the range of the accuracy potential of the DGPS measurement method applied in the project.

6.4.3 Results

Figure 6-27: Castle Landenberg in Irrlicht (Eisenbeiss, et al., 2009a).

Following the described workflow above and in Pueschel, et al., 2008 we were able to produce a geometrically accurate photo-realistically textured 3D model of Castle Landenberg. The overall RMS yielded by bundle adjustment is below 1 pixel, which can be regarded as an adequate result for manual measurements. After texture mapping with the terrestrial and aerial images with a footprint of approximately 1cm, the model of Castle Landenberg could be visualized with high quality.

The textured model was exported to VRML (Virtual Reality Modelling Language) format and can be viewed with any VRML viewer.

The generated model can now serve as a high quality digital representation of Castle Landenberg. On the one hand it is suitable for presentation and visualization purposes, e.g. to promote the site in terms of tourism, while on the other hand it represents an important digital preservation of the castle which allows the user to perform measurements on the model or derive façade plans.

6.5 Conclusions

In this chapter three examples were given. The example Pinchango Alto (Peru) was the first archaeological site which was documented using an autonomously flying model helicopter for the production of accurate and dense elevation models and orthoimage data. The produced elevation data was analyzed and compared to DSMs produced with terrestrial laser scanning and manual measurements. The laser DSM and the UAV-DSM can be fitted together with a mean offset of less than 1cm and a standard deviation of 6cm. Additionally the UAV data was combined with terrestrial laser data and aerial image data. These combinations enable a detailed study of the site at different levels of resolution.

In the second example, initial results from the 2009 field trip to the Maya site Copán (Honduras) were presented. Here the fast processing capability of a specific flight planning and autonomous flight of UAVs was clearly demonstrated. It was possible to produce the first results soon after field work. These showed structures that were not observable from the ground. Here we could show the high potential of stabilized autonomous UAV systems for fast documentation. In this example it was also possible to show the influence of strong wind on the flight data, observed with the flight control system of the UAV. The UAV flights of the first two examples was done under extreme weather conditions, such as hot temperature (up to 40°C) and moderate wind conditions.

Finally, in the third example we were able to document the castle Landenberg (Switzerland) with an image resolution of better than 1cm. Here we introduced a new flight mode "circle", which allowed us to obtain a highly detailed reconstruction of the object, with a combination of terrestrial and UAV images.

After testing UAVs under hot weather conditions and difficult accessible areas, like in Peru and Honduras, we will now turn to the environmental applications and focus on the problematic of cold areas, high altitude and dangerous areas.

7 MONITORING OF HAZARDS, ENVIRONMENTAL AND AGRICULTURAL APPLICATIONS

Figure 7-1: The Randa rockslide failure (Wallis, Switzerland). The lower part is situated 1400m a.s.l. The height difference from the bottom to the top is more than 800m.

Due to the climate changes in the last decades and the circumstances that we have to deal with in Switzerland, e.g. various hazards, like rock falls, land slides and flooding and the local geomorphic conditions (narrow valleys etc.), this chapter is focusing on the monitoring of hazards and environmental applications in small-scale and large-scale areas using UAVs for data acquisition.

We will use our 3D flight planning tool for the documentation of a rockslide, use our UAVs under different flight modi and weather conditions, and test them at high altitude. Furthermore, we will use our in-house matching algorithm for difficult matching areas, such as strong shadows (rockslide) and repetitive pattern (maize field)

7.1 The rockslide Randa (Switzerland)

7.1.1 Rockslide Randa

The focus of the geological project Randa was to characterize the large scale rockslide in Randa (Wallis, Swiss Alps; see Figure 7-1). This rockslide will be used as an example of the ultimate evolutionary stages corresponding to the complete development of the basal shear surface(s) and internal rock mass deformation. The project Randa is imbedded into the large scale project "Rockslide Processes and Mechanisms: Progressive Development of Shear/Slide Surface in Rock Slopes" from the Engineering Geology Group of ETH Zurich, S. Loew and HazNETH: Research Network on Natural Hazards at ETH Zurich.

In order to understand this failure stage in a better way, the interrelationships between pre-existing tectonic fractures, subsequent tensile fracturing and shearing of intact rock bridges was investigated. Furthermore, for the understanding of the rock mass structure and kinematics during this evolutionary stage, the basal shear planes needed to be identified, and the internal rock mass deformation had to be studied. Finally the 3D time-dependent displacement field had to be measured more in detail using the UAV-image data and the generated DSM (Randa, 2009).

As a result of these aims, a high-resolution DSM with a spatial resolution of 10–20cm had to be generated and images with a footprint of 2-5cm in object space had to be acquired and oriented. Because of the non-nadir case and a difficult terrain, the standard aerial flight planning procedures could not be applied.

The lower part of the site was acquired with our UAV system Copter 1B in May 2007, equipped with a Nikon D2Xs. The whole site was later acquired by a manned helicopter in November 2007, using the Helimap system (Helimap, 2009), combining laser scanning and oblique images (Vallet, 2007, Vallet and Skaloud, 2004). The system is based on a Riegl LMS-Q240i-60 laser scanner for point cloud generation and a Hasselblad H1 camera with a Dos Imacon Xpress 22Mpix back, which is normally used for texture mapping. The system is coupled with a GPS/INS antenna, to obtain position and orientation during data acquisition. It can be installed on standard helicopters and is operated manually, and therefore can be tilted to allow an acquisition geometry almost perpendicular to the flank. This is a major advantage in steep terrain to avoid large geometric degradation (Skaloud J., et al., 2005). The CCD-sensor has a size of 49x37mm resulting in a pixel size of 9µm. Both sensors have a similar field of view (57° for the camera and 60° for the LiDAR). The IMU is a tactical-grade strapdown inertial system (iMAR LMS) with a very high measurement rate (up to 500Hz). The GNSS-signal is received by a carrier phase receiver. Main advantage of the system compared to conventional aerial systems lies in its image acquisition geometry. Due to the fact that the system can be tilted, the acquisition configuration can be adapted even for steep terrain. Oblique images have the same beneficial properties as nadir zenith images.

Using the two comparable systems, the autonomously flying model helicopter and the manned helicopter, at one site, allowed the analysis of the performance of the systems. Moreover, it is possible to compare and integrate the two data sets.

7.1.2 Flight planning

As mentioned above, for the recognition of features with a length of 10-20cm, an image scale of 1:4500 was selected which results in a pixel footprint of approximately 3cm. The distance to the cliff was defined to 230m, which is equal to the normally flying height above ground. Finally, the side and end lap were set to 75%. Using this high overlap along and across strip it was possible to avoid occlusions and gaps in the image data (see Figure 7-7). The flight velocity was defined to 3m/s, while the shutter speed was 1/1000s. Therefore, the influence of the image motion was negligible.

After defining these parameters, the most recent elevation model (extracted out of aerial images with a scale 1:25000) with the highest available point density was used. Therefore, the LiDAR data provided by swisstopo, with a point spacing of 2m, was selected. Using this data set and the available orthophoto (swissimage, swisstopo®) allowed the definition of the area of interest. The area was separated in three sections, using the inclination and aspect values of

the slope. After the definition of these sections, the flight planning was done in the 3D case, as described in section 4.2.1, and the inclined flight lines for the helicopter flight were generated. Finally, using this information the image acquisition points were determined and transferred to the navigation unit (wePilot1000) of the mini UAV-system. Due to the inclination of the plane the camera was mounted with a pitch angle of 15-30° (respectively for the individual sections) on the helicopter (see Figure 7-2).

Figure 7-2: Our copter 1B during a test flight with the inclined camera looking perpendicular to the flight direction.

Such precise planning was necessary due to the large distance between operator and mini UAV, which limited the visibility of the mini UAV. Furthermore, before flying along the predefined flight path, the mini UAV was tested at an altitude of 2400m a.s.l. in order to ensure that the engine of the helicopter would not fail due to low air pressure. This test was important, since the helicopter manufacturer set the maximum flying altitude to 1500m a.s.l.

7.1.3 Field work

7.1.3.1 UAV 2007

Since the Randa rockslide covers a height from 1400m – 2300m a.s.l. the mini UAV-system was tested at the Flueelapass (~2400m a.s.l., Graubuenden, Switzerland). For the flight at Flueelapass, weight dummies instead of the mounted camera were used on the helicopter. To enable the evaluation of the performance at such a height above mean sea level, the helicopter was started and switched to the assisted flying mode. In this mode the current parameters of

the engine were checked visually and saved on board of the helicopter. This specific test showed that the engine of our mini UAV-system already achieved the limit for the maximal turning moment of the engine. Therefore, to have a buffer, we decided to do the first flight only at the lower part of the rockslide (1400-1800m a.s.l., see Figure 7-1), while the upper part was to be covered by the Helimap flight.

As the illumination conditions were acceptable only in the morning, we decided to do the flight at Randa in the morning hours. In the afternoon strong shadows made the data processing more complicated, as a preprocessing of shadow areas had to be performed. Furthermore, the GPS-satellite availability was simulated in the preparation process. Thus, the existing elevation model of the surrounding (DHM25, swisstopo®) was integrated in a GPS sky plot software, which allowed the calculation of the accessible number of GPS and the postulated GDOP (Geometric Dilution Of Precision) value. Using this information, it was possible to have an approximate a-posteriori value for the accuracy of the GPS-position of the helicopter, which was crucial in such an environment.

Given that at the bottom of the site a large debris zone is situated (see Figure 7-1), the accessibility is quite complicated. Therefore, the start and landing point was defined close to a road at the bottom of the debris zone (see Figure 7-3). The field work itself was done in few minutes, where the longest part of the flight was the section from the starting point to the first image acquisition point and the way back. At the end of the first flight, the helicopter did a fast inexplicable turn along its own main axis. We therefore decided to stop the test and to evaluate the available flight data, which included high resolution images from the rockslide.
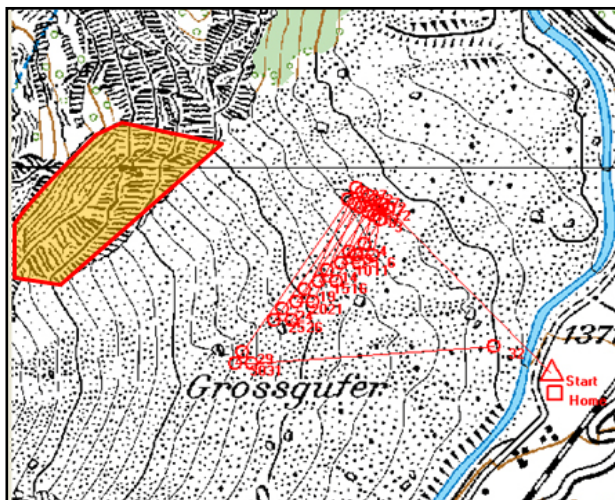
Figure 7-3: Screenshot of the ground control station software showing the flight lines of the Randa data acquisition. The orange shading shows the lower part of the Randa rock cliff.

147

The analysis of the unexpected turning of the UAV-system during the flight showed that the effect was caused by the fact that the neighboring points of the flight plan were defined to close to each other. Additionally, the effect occurred because the neighboring flight lines had a distance in horizontal and vertical direction, which caused a misinterpretation in the flight control software. Hence, during the flight, one predefined data acquisition point was skipped and the turning occurred during the flight at Randa. Based on this event, the flight control software was improved to handle autonomous flights flown with this type of configuration. Additionally, the analysis of the flight data showed that the system reached the limit for the maximal turning moment of the engine, similar to what occurred during the height test at Flueelapass.

7.1.3.2 Manned Helicopter 2007

Due to the mentioned problems with our UAV, we decided to document the site Randa completely using the Helimap system. Thus, in November 2007, both LiDAR data and high-resolution oblique images were acquired using the manned system. About 143 oblique aerial images were acquired together with the helicopter-based LiDAR data using the Hasselblad H1 camera. These photographs show a very high level of detail and cover an extent of about 300x250m^2 each. For normal use, the system relies on a Riegl LMS-Q240i-60 Laserscanner for point cloud generation. Data acquisition was done along nineteen horizontal flight lines that were arranged parallel to each other on different heights to cover the whole flank. The point cloud of this LiDAR data consists of $5.6 \cdot 10^6$ points and covers a total area of 3km^2 with a point density of 1-3pt/m^2 and vertical point accuracy better than 0.2m (Skaloud J., et al., 2005). These values were sub-optimal, since the planned point spacing was 10-20cm (see section 7.1.1). However the manned system allowed us to comprise the first analysis of the DSM and combine them with other measurement data (see section 7.1.5).

7.1.4 Photogrammteric processing

7.1.4.1 UAV images

The orientation of the images, which were acquired in the UAV field campaign 2007, was done in ISDM. Since no control point of the acquired area was visible, the images were oriented only relatively (see Table 7-2). These results were used for the processing of a DSM of the covered area. Figure 7-4 shows matching results of SAT-PP. For the complete covered area it was possible to extract grid, feature points and edges, even in the shadow areas. This was possible since the images were acquired in the early morning to avoid strong shadows.
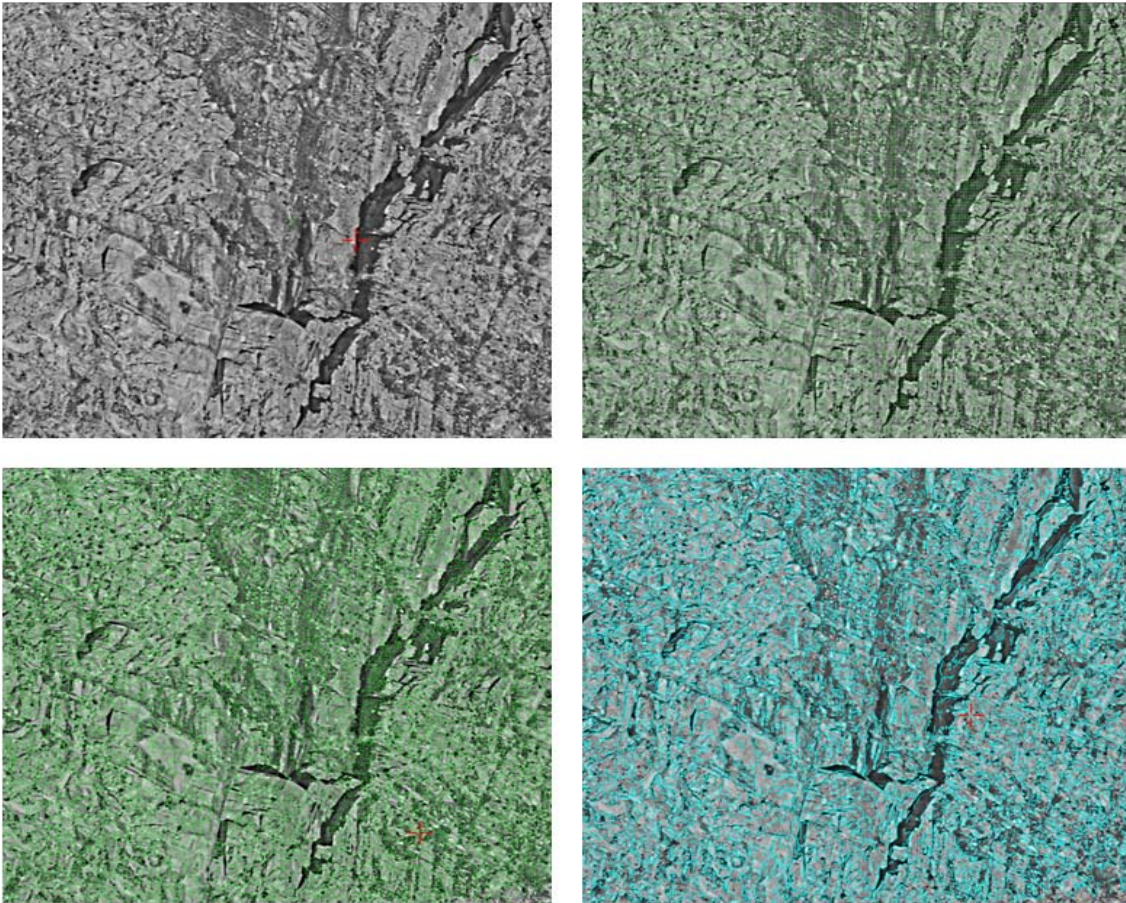
Figure 7-4: Matching results from SAT-PP of part of an image. Up: Preprocessed image (left) and matched grid points (right); Down: Extracted feature points (left) and edges (right).

7.1.4.2 LiDAR data

The raw data processing of the LiDAR data sets was done by Helimap System SA (Helimap, 2009). This processing included the fitting of flight lines and automated as well as manual filtering of ground points, outliers and artifacts. A detailed description is given in Skaloud J., et al., 2005 and Vallet, 2007.

The conversion of the processed LiDAR point cloud 2007 into a grid raster was done in the SCOP++ software (Inpho, 2009a) that is especially designed for processing large amounts of points.

Since all measurements of the geologists are done in the local Swiss coordinate system LV03 and further analyzed in ArcGIS (Version 9.1; ESRI, 2009), the 3D LiDAR data are transformed into 2.5D data. Thus, in the steep areas the data would be interpolated to a raster, which would result in a loss of information in the steep parts. Therefore, the DSM was visualized in Geomagic and an optimal view, perpendicular to the area of interest, was defined visually (see Figure 7-5). The rotation parameters around a defined point (For example point of gravity) were selected. Using an in-house developed tool, the point cloud

was rotated around the defined point. Since the aspect of the site has two mayor orientations, the point cloud was turned two times using separate rotation angles. The rotation parameters and the point for rotation are given in Table 7-1.

Table 7-1 : Parameter for the rotation of the DSM.

	Coordinates of the point for rotation in the LV03 system [m]			Rotation angles [°]		
	X	Y	Z	ω	φ	κ
Rotation 1	626143.437	107040.344	1994.010	10	60	0
Rotation 2	625863.375	107010.250	2147.610	50	60	0
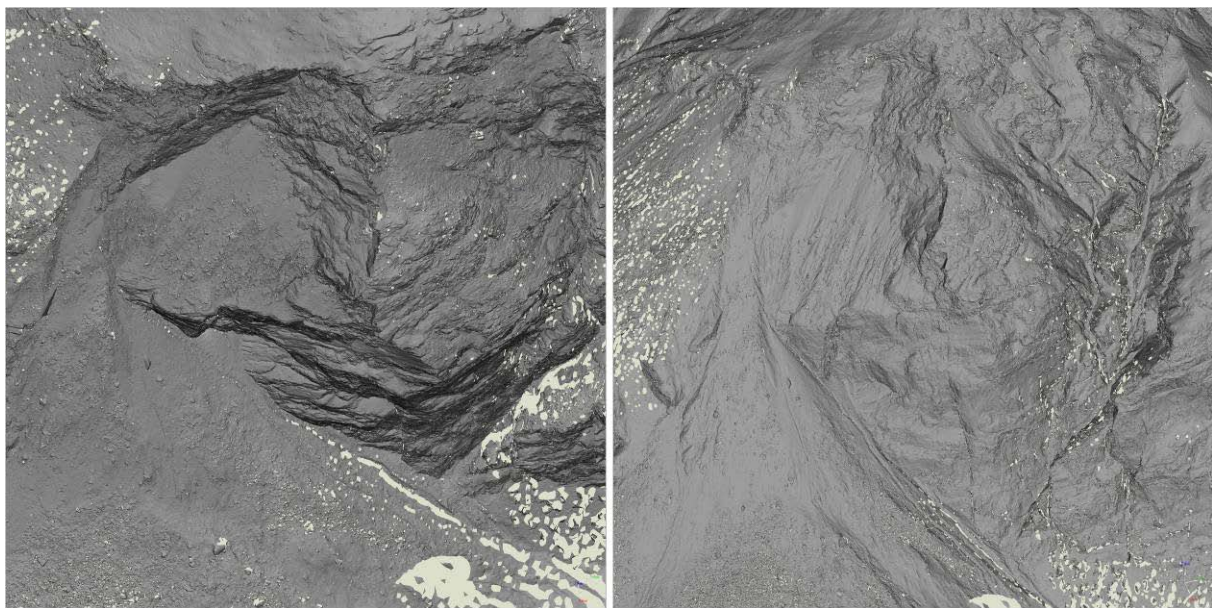
Figure 7-5: Left: Top down view in the LV03 coordinate system to the LiDAR-DSM visualized in Geomagic (V9; geomagic, 2009). Right: Rotated DSM following rotation 1 defined in Table 7-1.

7.1.4.3 Helimap images

The orientation of the oblique images was done in LPS and ISDM. Tie points were automatically and manually measured as well as visually checked in LPS.

From the GPS/INS measurements initial exterior orientation parameters were available. They even allowed stereo viewing of the images with a y-parallax, which results from the accuracy level of the GPS/INS-system. Therefore, by using only the given exterior orientation the processing of the images was not possible.

The GCPs were generated by precise geodetic measurements through the engineering company Geomatik AG (Geomatik, 2009 and Figure 7-6).
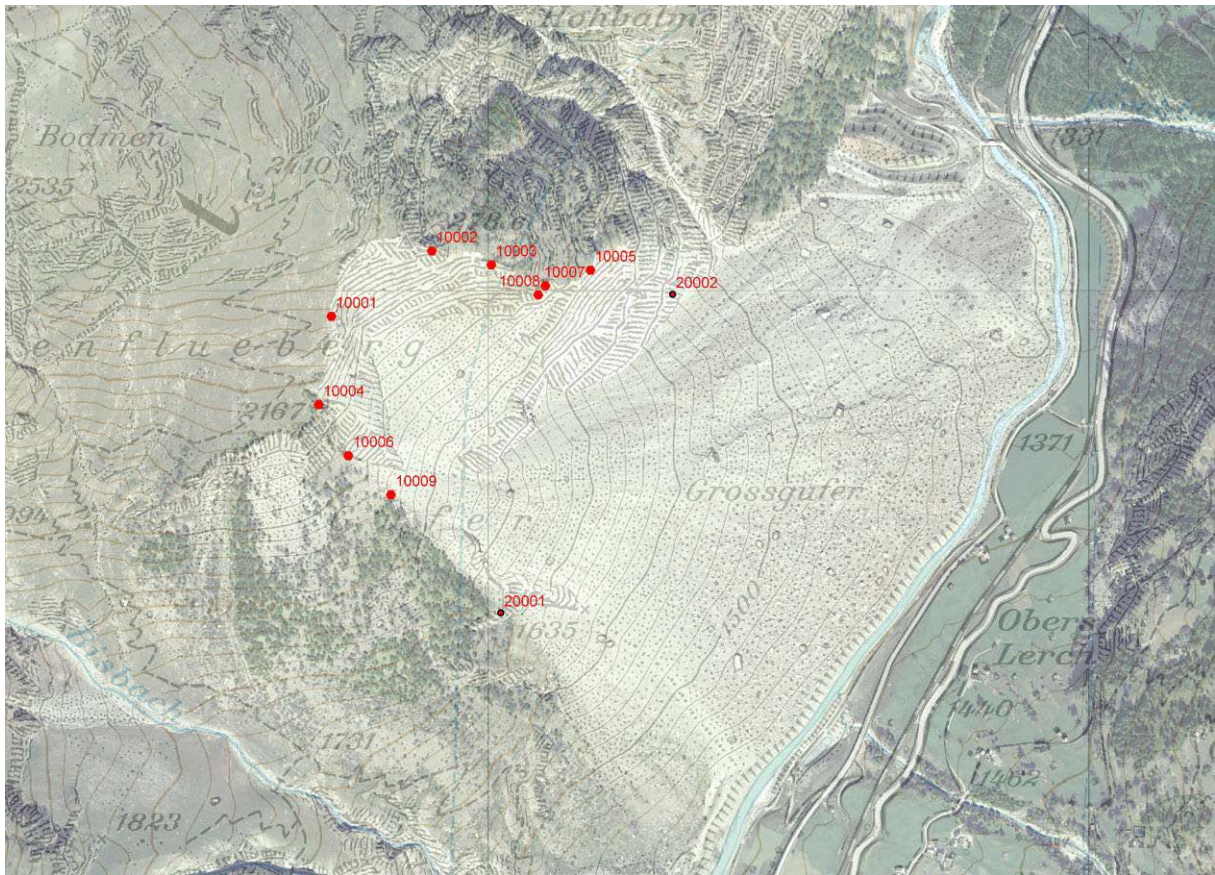
Figure 7-6: Overview of the available GCPs at the site Randa.

With LPS it was not possible to calculate an exterior orientation, neither with GCPs alone nor with supplementary exterior orientation information. The bundle block adjustment did not only terminate but also yielded very erroneous results (e.g. negative RMSE values). In our opinion the optimisation of the bundle adjustment or some basic implementation of it cannot cope with the oblique geometry that also is not constant over the whole block. The orientation angles change a lot between single images as the helicopter trajectory is not as stable as the one of a fixed-wing airplane and the helicopter position was adapted to the mountain (e.g. change of orientation to see otherwise occluded parts of the rock-face).

Unfortunately, in LPS no relative orientation can be calculated separately, therefore a relative orientation with ORIMA was attempted. Here, only single models could be calculated, the relative orientation of the whole block failed. Also tests with exterior orientation parameters, GCPs, free-network adjustment or minimal datum were unfruitful.

Therefore, a piece of software (interface) was written to transfer the tie points from the LPS image coordinates (in Pixel) to ISDM image coordinates (in µm). In this step, also different orientations and centers of the image coordinate system had to be taken into account. SAT-PP uses the top-left corner of a pixel as origin and the coordinate axes facing down and right whilst all these properties can be chosen freely in ISDM. Finally, using the software package

151

ISDM, the absolute orientation of the 54 images with 4 well identifiable GCPs was computed. The results of the orientation are shown in Table 7-2.

Table 7-2: Results of the orientation of the Helimap images in ISDM (ZI/Intergraph, 2009).

Block	σ_0	RMSE of GCPs			RMSE of image observation	
	[Pixel]	X [m]	Y [m]	Z [m]	x [µm]	y [µm]
UAV	4.07	/	/	/	1.98	2.01
Helimap	6.07	0.04	0.04	0.03	2.99	3.79

7.1.5 Comparison and data analysis

Using the acquired UAV-images (4-5cm GSD), a DSM of the lower part of the Randa rockslide with 15cm resolution was generated (see Figure 7-7). The complete site was documented with the Helimap system, with a pixel size of 6cm to 8cm. In comparison to the flight defined for the mini UAV-system, the Helimap flight was controlled by a pilot, who followed the flight lines with an accuracy of 30m. For the whole area the scale varied depending on the complexity of the terrain. It was also found that the Helimap system captured the cliff with an oblique field of view, which resulted in gaps in the data set. For the laser scan, the final point density was approximately 3pt/m^2 (see Figure 7-7).

The visual comparison of the extracted UAV-DSM and the LiDAR-DSM shows clearly that the fine structure of the cliff could be modeled from the UAV-DSM, while the LiDAR-DSM had large holes and less resolution (see Figure 7-7).

Figure 7-7: Left: Derived surface model from image matching, Middle: Zoom-in of an UAV-image, Right: Point cloud of Helicopter-based LiDAR projected on the derived surface model.
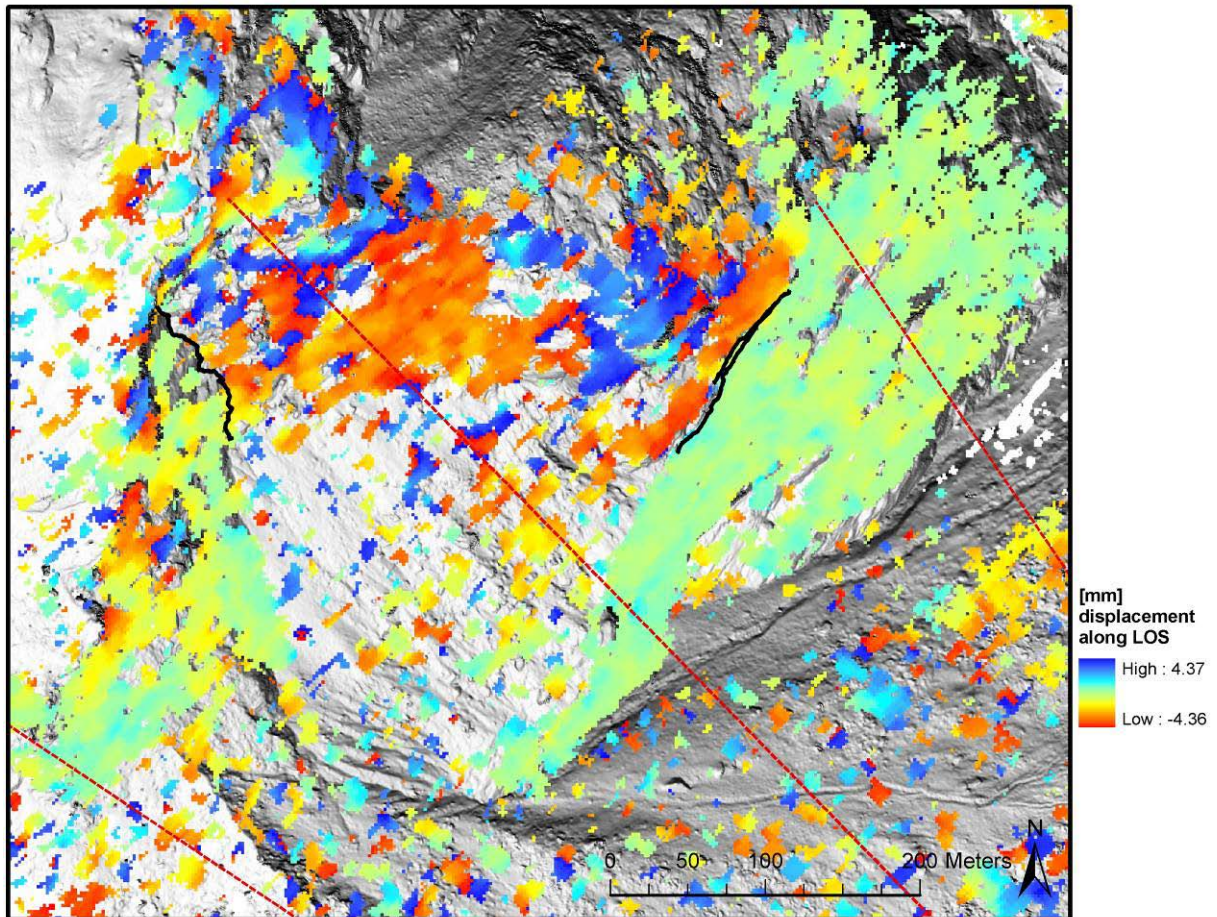
Figure 7-8: Measurements of a fracture visualized in the DSM overlaid with DINSAR measurements. The red dashed line shows the line of sight of the DINSAR measurements.

However, using the LiDAR DSM and the generated orthoimages, finally a complete 3D model was generated from the site Randa (see Figure 7-5). Using this data set, the geologist did the first measurements of fractures and shearing of intact rock and combined them with DINSAR (Tarchi, et al., 2003) measurements (see Figure 7-8). The Figure shows clearly that the measurement of the visible fracture (black lines) is correlated to the DINSAR measurements done by the Geology group at ETH Zurich (Randa, 2009).

7.2 Estimation of the volumetric changes of gravel-pits

This application is based on a study undertaken as part of a bachelor thesis at ETH Zurich in 2009 (Flury, 2009). The main task of this study was the evaluation of the suitability of a quadrotor for use in photogrammetry. Moreover, it was possible to transfer our flight planning into another flight control system. The data acquisition was accomplished in the assisted and autonomous flight modi. Although, the project on estimation of volume changes of gravel pits was a pilot study, it is a good example of how the generation of a workflow for the extraction of elevation models can be done for other objects, like the gravel pit (see Figure 7-9). This pilot study was done in cooperation with the companies omnisight (omnisight, 2009) and Lötscher Kies + Beton AG (Lötscher, 2009).

Figure 7-9: Panorama of the gravel pit taken from the UAV MD4-200 (microdrones, 2009b).

7.2.1 Demand for documentation of local movements

In Switzerland the mining of gravel pits has to be documented quarterly. This documentation is necessary, since the owners of lots of many gravel pit receive compensation in relation to the mining volume. Quite often the mining area is separated into several lots and owned by different proprietors. Furthermore, in a quarter the mining at a gravel pit is focused only at a specific local spot. Consequently, while only local movements have to be recorded, the documentation of the site using conventional aerial photogrammetry or laser scanning is too expensive.

Hence, in our pilot study, we were looking for an alternative to the traditional methods which would be available at a more favorable price. Additionally, the alternative data acquisition method should also be quickly applied, adaptable in parallel to the mining and able to be completed by employees of the operating company of the gravel pit.

7.2.2 Field work 2009

The dimensions of our pilot area were limited to 60m x 60m. The surface comprises moderate areas and steep flanks (see Figure 7-9). The GSD of a pixel was set to 5cm.

154

The quadrotor UAV, md4-200 of the company microdrones, was chosen for the field work, due to the fact that the owner of the operating company bought recently this particular quadrotor system. The md4-200 UAV is described in section 3.3.1.1. The UAV system can be equipped with several low-cost still-video cameras, which meet the payload limitation of maximal 200g.

For our field work in 2009 the Panasonic Lumix FX35 was used. The FX35 is a compact camera with a zoom lens of 25-100mm. Additionally, the camera features an integrated image stabilizer, a shutter speed of up to two milliseconds and a live-view video function. The camera was calibrated using the software package iWitness (iWitness, 2009), which allows a automated camera calibration using color coded targets.

For the absolute orientation during the flight, 10 GCPs were placed temporary and measured with the real-time GNSS measurement system GPS 1200 (Leica-Geosystems, 2009). The GCPs were constructed out of a wooden plate, with a white circle placed on top of a black background. The measurement accuracy of the GCPs was 2cm. The point coordinates were measured in half an hour field work.

The two flights, accomplished during the field work in February and April 2009, were done in the assisted and autonomous flight mode respectively. For the assisted flight modus, the quadrotor was flown in two predefined flying heights above ground level. Then, using the live-view modus, the operator steered the system to the defined acquisition points, checked the image overlapping on the screen and acquired two to three images per position. A single image per position would not have been sufficient, because the system was permanently adapting the position and orientation of the platform, due to wind conditions.

The flight planning of the autonomous flight was accomplished using the software mdCockpit. The predefined coordinates, using the 2.5D flight planning tool (see section 4.2.1), were manually typed into the software. Based on these coordinates, the flight path was generated in the software and the additional parameters for the flight were defined in the waypoint editor. After finishing the flight planning, the flight path was visually controlled in the 3D-view of the waypoint editor. The autonomous flight was again affected by extreme wind conditions. There may have also been some parameters, which may not have been selected carefully (For example: Number of images per acquisition point). Thus, the images were acquired more or less in an irregular order and only few images were used for the data processing (see Table 7-3).

7.2.3 Data processing

The data processing of the images was accomplished in LPS V9.1 and SAT-PP V1.0 for the image orientation and DSM generation respectively with an input weight for the GCPs of 2cm in planimetry and 3cm for the height component. Finally, the orthoimage was generated using LPS and the results were visualized using ArcScene.

The achieved accuracy of the orientation is shown in Table 7-3. The number of σ_0 was for all image blocks less than one pixel and the RMSE of the GCPs was a maximum of 14cm, which corresponds to three pixel in the image space. Due to the low image quality of the cameras, in some of the images the GCPs could not be defined correctly. This resulted in the 70m image blocks having an the observed accuracy of 3pixel maximal.

Table 7-3: Orientation values of the quadrotor images taken from the gravel pit in February and April 2009.

Flight	Block	σ_0	RMSE of GCP			RMSE of image observation	
		[Pixel]	X [m]	Y [m]	Z [m]	x [Pixel]	y [Pixel]
1	70m	0.92	0.09	0.09	0.06	0.80	0.83
	100m	0.70	0.01	0.03	0.02	0.50	0.51
2	70 m, 2 images	0.62	0.01	0.01	0.01	0.03	0.14
	70 m, 3 images	0.81	0.02	0.01	0.03	0.46	0.78

After image orientation, the elevation model of the site was generated using SAT-PP with a point spacing of 20cm. For the verification of the produced DSM in SAT-PP, a DSM was also generated using the software package LPS. While LPS and SAT-PP showed visually similar results, the LPS-DSM produced blunders in the steep parts and in the homogenous texture areas, like snow coverage. The differences between the LPS and SAT-PP DSMs can be explained by the different matching strategies implemented into the software packages and because of the standardized pre-processing of the images in SAT-PP. Thus, especially in shadow areas, like the steep parts, SAT-PP was able to extract more points than LPS.

7.2.4 Results

The extracted DSMs are visualized in Figure 7-11 and Figure 7-12, for flight one and two respectively. The second DSM covers only a smaller area, because the DSM was only extracted from one stereo pair. The visual comparison of the DSM shows that in the lower part in the DSM, where homogenous white snow coverage was present in the February images, small blunders occurred in the reconstructed surface. However, the main structures were reconstructed in both data sets.

Figure 7-10 shows the reconstructed textured 3D-model of the February flight.

Figure 7-10: Textured 3D model of the gravel pit visualized in ArcScene.
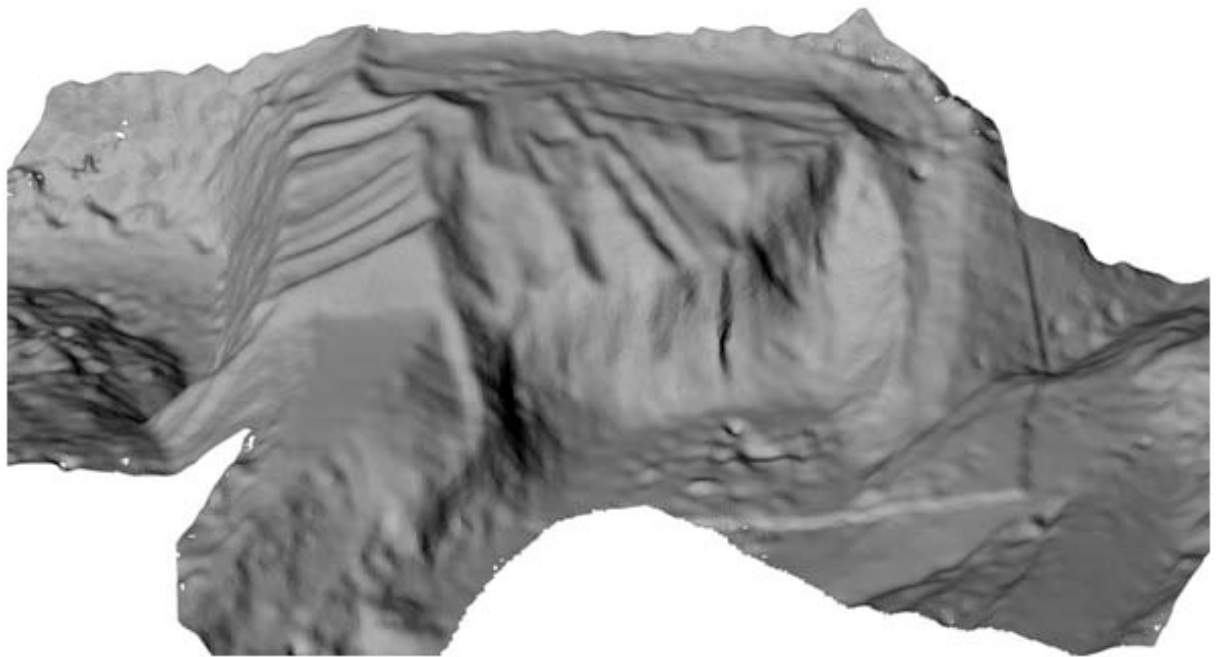
Figure 7-11: DSM1 (February 2009) image data generated with SAT-PP.
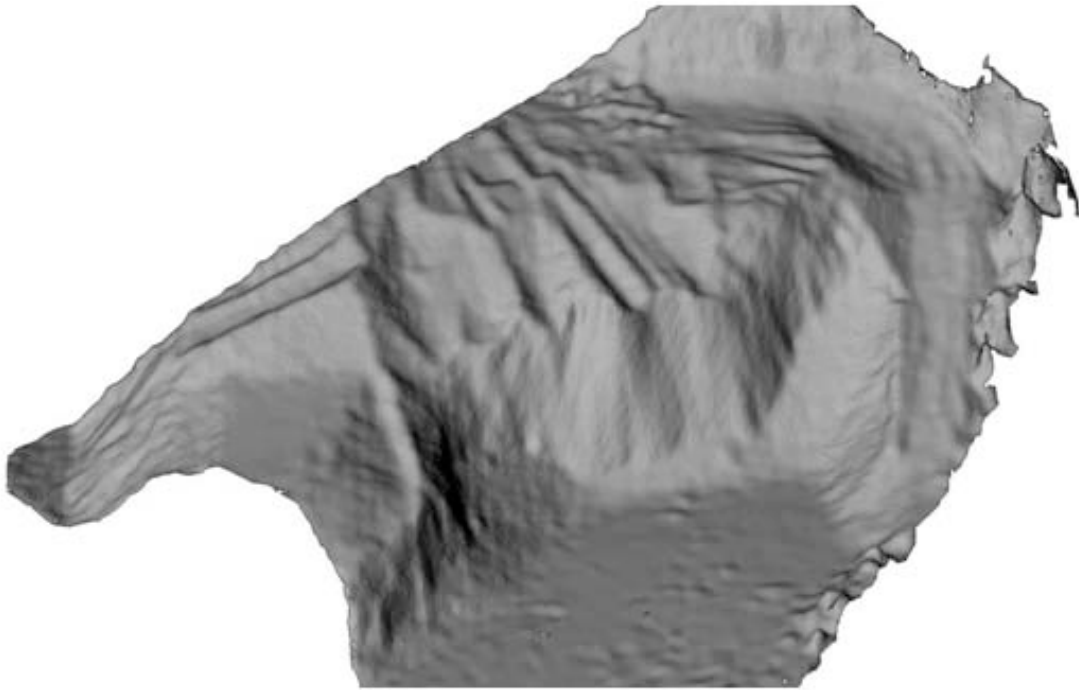
Figure 7-12: DSM2 (April 2009) image data generated with SAT-PP.

🟥	3.5m – 5.0m
🟧	2.0m – 3.5m
🟨	0.5m – 2.0m
🟩	-0.5m – 0.5m
🟦	-0.5m – -2.0m
🟦	-2.0m – -3.5m
⬛	-3.5m – -5.0m
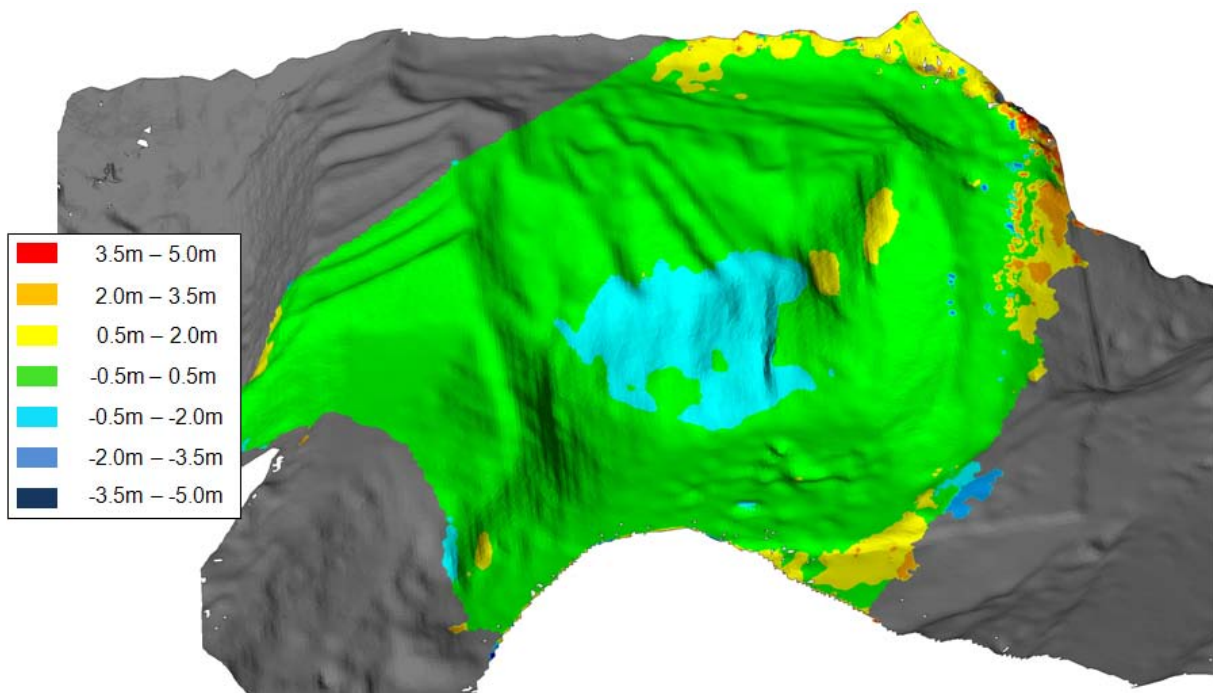
Figure 7-13: Comparison of the DSM1 and DSM2 of the gravel pit.

The comparison of the two DSMs using the software Geomagic Studio showed that both surfaces fit together, with an exception in the border areas of the images. Here, presumably matching errors occurred in the model. These errors can be avoided through cutting out the image area by 5-10 percent. In the steep part of the surface a digging zone between the February and April is visible. Using the calculated differences of the two surfaces and the

158

according size of the area, the volume change can be calculated. With an optimum measurement accuracy of the automatically extracted surface of factor two of the GSD, we can expect an accuracy in height of 10cm. This accuracy would approximately correspond to a volumetric accuracy of $10m^3$ for an area of 10m by 10m, which is in the range of the requested accuracy of the operating company. The achieved accuracy can be improved using a higher quality camera or by changing the image resolution, which would result in a larger number of images. However, increasing the number of images would not be worthwhile, since the processing cost would go up and the benefit for fast data acquisition would be compensated through the cost of data processing. Thus it is recommended to use higher quality cameras and to improve the flight performance of the system.

7.2.5 Conclusions

Data required for the documentation of a subset of a gravel pit was collected in the assisted flight modus by the operating company, while the autonomous flight was conducted using a predefined flight path. The flight parameters and acquisition points were predefined for all of the repeating flights. The processing of the image data, including image orientation and DSM extraction, was accomplished in 4-6 hours per model. Depending on the number of images, the processing time differed between the February and April data set. The software LPS has a self-explanatory workflow, which would allow the processing to be taken over by a surveying company. Since the quality of the DSM was not sufficient enough in LPS, it is recommended to use a more advanced DSM-matching strategy, as is implemented in SAT-PP.

Under optimal conditions, an accuracy of 2 pixels in height can be expected for the generated DSM of the bare ground, while in steep areas an accuracy of 2 pixel in height can be expected, while in steep areas the accuracy can go up to 5-8 pixel. Therefore, for the steep areas, additional stereo pairs have to be processed. The results can then be integrated into the surface model and the viewing angle for the data acquisition has to be adapted accordingly.

7.3   Agriculture: The maize field project

The maize field study was conducted to determine the extent to which topography can influence the rate of cross-pollination. The effect at short and medium distances between pollen donor and pollen receptor fields (0 – 17.5m) was investigated in the canton of Zurich, Switzerland, during 2005 and 2006. Specifically, we focused on the DSM generation of a vegetation area with high repetitive pattern and on the integration of the cross-pollination data with a surface model covering the vegetation (Vogler, et al., 2009). Cross-pollination was determined by means of a system of grain color markers consisting of white-grain and yellow-grain hybrids, functioning as the pollen receptor and pollen donor, respectively. The measurements of the slope inclination were based on aerial image data acquired by our model helicopter Copter 1B. The project was conducted in cooperation with the Institute of Plant Sciences at ETH Zurich, P. Stamp (IPW, 2009).

During the study it was possible to improve the data acquisition from the stop to the cruising points, which resulted in faster data acquisition. The data set acquired in 2006 was oriented using the GPS/INS values from the wePilot, as approximation for automated tie point extraction and image orientation.

7.3.1   Test sites

The two test sites were located in the canton of Zurich, Switzerland, in 2005 (A) and 2006 (B). Both sites are typical fields of the Swiss midlands, situated in an area with a mixture of woods, settlements and intensive agricultural areas of wheat, maize and grassland, upon a hilly topography.

The test sites were designed so we could focus on the influence of inclination on cross-pollination (Figure 7-17). The fields had an equal inclination of 3.4° (A, eastwards) and 6.8° (B, eastwards). In agricultural areas, steeper inclinations are susceptible to erosion. Site A had an area of 240 x 80m^2, with two white receptor areas (120 x 40m^2) and two yellow donor areas of the same size, arranged diagonally across it (Figure 7-14 and Figure 7-17). Six sampling blocks (15 x 20m^2), three with a downhill and three with an uphill orientation, were at the border of both receptor areas (Figure 7-17). Site B had an area of 80 x 170m^2. In experiment B, a receptor area (40 x 170m^2) was sown within two donor areas (Figure 7-17). Six sampling blocks (15 x 20m^2), three with a downhill and three with an uphill orientation, were arranged in the receptor area.
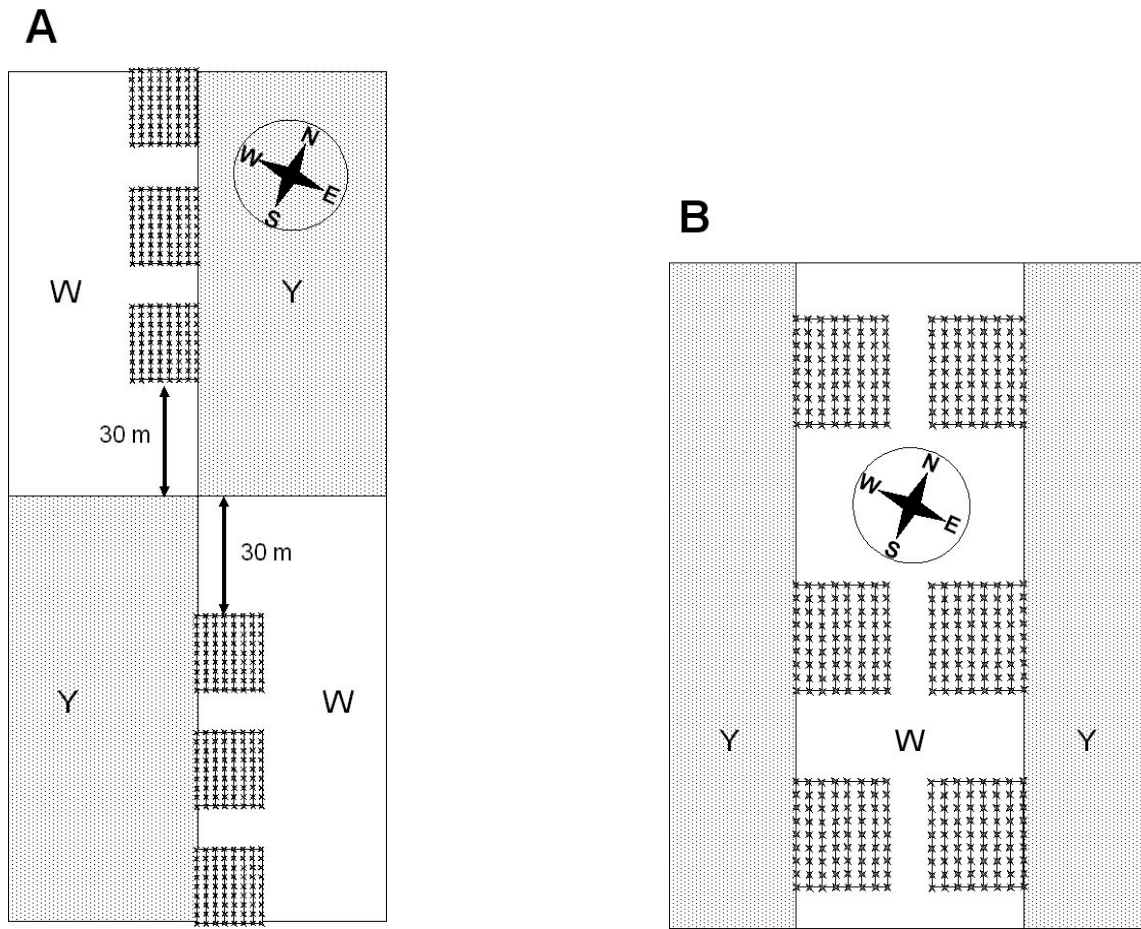
Figure 7-14: Field layouts of experiments A and B. Letters "Y" (yellow grain) and "W" (white grain) mark the positions of yellow donor and white grain receptor field parts in relation to the geographic direction. Stars represent sample points with five plants each (Vogler, 2009).

A portable weather station (Onset Computers, Pocasset, MA, USA) was installed about 200 m away from the test sites during the experiment. The direction of the wind and the wind speed were logged every two minutes at a height of about 3m above ground.

7.3.2 Photogrammetric data acquisition and measurements of plant heights

After anthesis, digital images were taken with a still-video camera (Canon D20) mounted on our Copter 1B.

Before image acquisition, the flight planning was conducted with the 2.5D tool (see 4.2.1). The flight parameters (Table 7-4) were set up depending on the selected UAV and camera system, the required image resolution of 3cm per Pixel, the maximum flying height of 100m above ground, and the along and across track overlap were set to 75%.

161

Table 7-4: Parameters for the flight planing.

Parameter	Value
Project parameter	
Image scale	1:4000
Side / end lap	75% / 75%
Flying height above ground	~ 80m
Camera Canon EOS 20D	
Focal length (calibrated)	20.665 mm, RMSE 1.5e-003mm
Pixel (Image format)	8.25 MPixels (3520x2344)
Parameters of the UAV system	
Image acquisition point	Stop points (Site A) Cruising points (Site B)
Flight mode	Autonomous
Flying velocity	3m/s

After defining the flight parameters, the area of interest was roughly identified in the Swiss National Map 1: 25,000 by swisstopo®. Based on the flight parameters mentioned above, a flight trajectory was calculated using the 2.5D flight planning tool and the generated 3D coordinates, the flying velocity and the flying mode were transferred to the flight control system. Then, the autonomous flight was done with the model helicopter Copter 1B. Following the flight trajectory in the stop mode for area A, the images were captured automatically at the predefined positions (Table 7-4 and Table 7-5) in cruising mode during the flight over area B. In the stop mode, the helicopter flew to stop points autonomously and the operator triggered the image by radio link, while in the cruising mode, data acquisition was totally autonomous. The images of area A were captured in 20 minutes (stop mode), while in the cruising flight mode, the images were all acquired in 5 minutes.

Table 7-5: Number of aerial images used for photogrammetric processing.

Experiment	Acquired aerial images / image strips	Aerial images / image strips used for processing
A	82/4	42/2
B	57/5	57/5

The images were oriented with the software packages LPS V9.0 and ISDM and a DSM was generated with the software SAT-PP V1.0. Finally, an orthoimage was produced by means of LPS.

For area A, two to three tie points were measured manually per stereo pair as initial values for the image triangulation, while for area B the initial values were calculated using the Kalman Filter in wePilot. A breeze caused a slight move of the leaves and the tassels of the plants during the data acquisition. Thus, the two to three manually measured tie points were, unfortunately, insufficient for 5 to 10% of the images and it was necessary to measure additional points manually for these images (Eisenbeiss, 2007). The measured tie points (site A) and the approximate positions of the camera (site B) were used as initial values for the automated extraction of tie points and triangulation. After image orientation, a DSM with a GSD of 10cm was generated automatically using SAT-PP. The visual check of the DSM showed that the main structures of the maize field could be reconstructed. However in some parts blunders in the DSM occurred, due to the moving leaves in the data acquisition (see Figure 7-15). With the generated DSM, an orthoimage (3cm grid size) was produced.
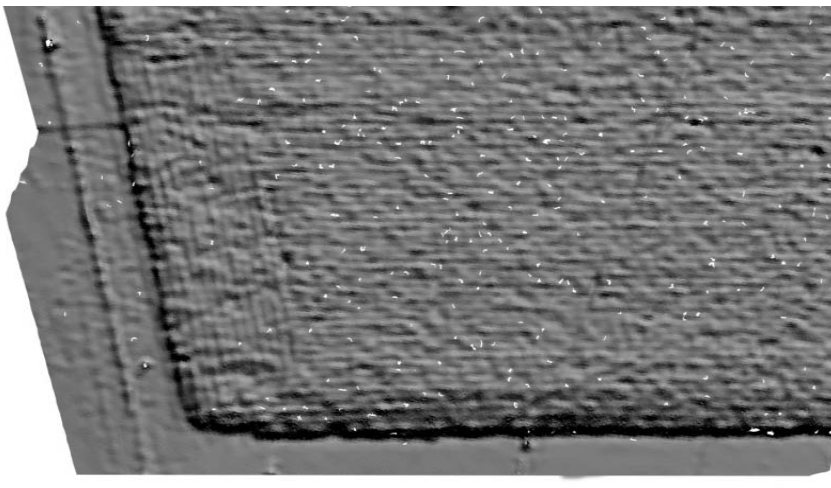
Figure 7-15: Part of the DSM of the maize field A showing the main structures of the field.

After image orientation, two procedures for measuring plant height were developed. In the first procedure, the measurements of plant height were done in the stereo measurement mode in LPS. This method resulted in the specific plants being easily identified. The height was determined manually by the operator. In the second procedure, the corresponding plants in the orthophoto were identified by the operator, while the heights were extracted automatically in ArcGIS (V9.1) using the generated DSM.

7.3.3 GIS data analysis

For the integration of the data into a database, the same data structure was defined for site A and B. Furthermore, analysis functions for one field were developed and tested and applied to the second field. The input data (Figure 7-16) and the data analysis are described below.
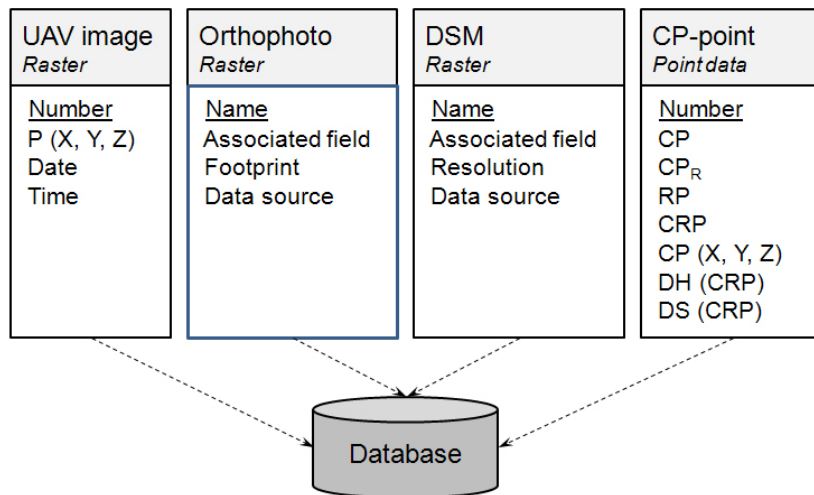
Figure 7-16: Schema for the GIS-database.

For each field the UAV images, orthophotos, DSMs and cross-pollination (CP) points were generated and integrated into the database. The UAV image was identified by the image number, while the coordinates (P (X, Y, Z) in the Swiss Coordinate System (CH1903)), and the date and time of image acquisition were defined as additional attributes. Name, associated field, footprint/resolution and data source are the attributes of the orthophoto and DSM, while the name of the file is the main attribute. The CP points are integrated as point data, which can be identified by the point number of cross-pollination. Each point has a CP (cross-pollination) value, an identifier for reference points (RP), corresponding reference point (CRP), coordinates (CP (X, Y, Z)) and the difference with respect to the reference point in planimetry (DS) and in height (DH). If the CP value is zero, the corresponding point is a reference point; therefore no data will be present under CRP, DS and DH. If the CP value is larger than zero, DS and DH are calculated (with respect to the CRP). DH is calculated as the difference in the height of a sample receptor plant compared to the closest donor plant (see equation 7-1).

$$DH = CRP(Z) - CP(Z) \cap DS = MIN \qquad 7\text{-}1$$

To calculate the correlation of relative cross-pollination (CP_r) and the difference in height of the pollen donor and pollen receptor (DH), cross-pollination was defined as the relative cross-pollination rate of one sample block to eliminate the influence of distance. The relative rate of cross-pollination is therefore defined

$$CP_r = Abs \left(average \left(CP_{row\,2-8} \right) \right) \qquad 7\text{-}2$$

where *Abs* is the absolute value, *average (CP row 2-8)* is the average cross-pollination of all sampling points in a sample block (except row 1) and *CP* is the cross-pollination rate at a single sampling point.

The statistical analyses of the correlation of DH and CP_r are described fully Vogler, et al., 2009.

7.3.4 Results analysis

In our experiment, we were able to improve the automated data processing of UAV images by integrating the observed coordinates of the flight trajectory into the direct georeferencing of the UAV image data. The differences of the planned and the observed positions, as well as the offsets calculated from the direct georeferencing are given in Table 7-6. The differences between the planned, observed and calculated projection centers confirm the accuracy level of the wePilot1000 given in Table 3-10.

Table 7-6: Comparison of the image acquisition points of the flight in 2006: Planned vs. Metadata (wePilot1000) and image orientation (oriented) vs. Metadata.

	Planned - wePilot			Oriented - wePilot		
	dX [m]	dY [m]	dZ [m]	dX [m]	dY [m]	dZ [m]
Mean	0.66	1.07	-4.44	-1.27	4.89	-4.25
σ	0.20	0.75	0.33	0.67	1.67	0.18

Furthermore, our experiment allowed the automatic measurement of absolute plant height (3D), and by using grain color markers, we were able to accurately assess the number of cross-pollinated grains of single plants (Bannert and Stamp, 2007). The measurement of tassel height by digital surface models is possible, because the UAV system generates high-resolution photos due the proximity to the object (see Vogler, et al., 2009).

Figure 7-17: Top (Experiment A) and bottom (Experiment B) figures show a screenshot of the 3D-model using the Swissimage orthoimage (swisstopo®) draped over the DHM25 (swisstopo®) combined with the orthoimage of the maize field and the position of the sampled receptor plants generated from the UAV images. Yellow donor areas are grey emphasized; the remaining areas are those of the white receptor maize.

The analysis done by Vogler, et al., 2009 showed that the rate of cross-pollination of receptor plants in downhill areas increased when the difference in height to the corresponding pollen donor plant also increased. The free downhill trajectory probably enhanced the movement of pollen over longer distances. Accordingly, the rate of cross-pollination was slightly higher in

these areas compared to those in fields in flat areas. In conclusion, a downhill increase of cross-pollination could indeed be proven. However, the effect of this factor seems to be weaker than that of others such as wind direction and velocity. Over longer distances (> 17.5 m) there was no effect of topography on cross-pollination (Vogler, et al., 2009).

7.4 Main achievements

In the chapter "Monitoring of hazards and environmental applications" we were able to show the high potential of UAV images for the documentation of large rock slide areas, such as Randa (Switzerland). The comparison of the extracted UAV-DSM with helicopter borne-LiDAR, showed that using UAV image data, one could reconstruct the detailed structure of the rock surface in high detail. This was a result of precise flight planning and the perpendicular field of view of the UAV system to the steep cliff. However, the experiment at Randa also showed the limitation of UAVs in high altitude Alpine areas. As the UAV could only operate at heights below 2000m, only a small part of the surface was reconstructed using the UAV-images. The complete surface had to be reconstructed with lower resolution out of the data acquired with a manned helicopter system.

In an additional example, we showed that it was possible to reconstruct a dense elevation model from images acquired by a low-cost compact camera mounted on a quadrotor. The results provided an estimation of the volume changes of a gravel pit, as an alternative to the airborne laser scanning and photogrammetry in small-scale areas. Additionally, we evaluated the performance of the assisted and autonomous flight modus of this quadrotor.

Finally, we generated dense elevation models of maize fields, which were used for the analysis of the pollen dispersal in maize. It was possible to integrate the observed trajectory into direct-georeferencing, which allowed us to improve the automation of the workflow of processing UAV images.

8 CONCLUSIONS AND PERSPECTIVES

Figure 8-1: UAVs: Ready for new tasks.

8.1 Conclusions

The work described in this thesis has resulted in a new understanding of UAVs, in particular their use as a photogrammetric data acquisition platform.

8.1.1 Literature review and classification of UAVs

For the first time, a comprehensive literature review of UAVs with respect to their use in photogrammetry, manually controlled and autonomously flying, was presented. This review described the early applications of unmanned aerial vehicles in photogrammetry, as well as the state of the art of current research in UAV photogrammetry. Based on the literature review and results of our real world applications, we formulated new classification methods for UAVs. We present our new classification to the photogrammetry community as a potential standard for the classification of UAVs used as photogrammetric measurement platforms.

Using the review and the formulated classification, users can select an appropriate UAV system, distinguishing between low-cost, open source, commercialized, manually and assisted controlled and autonomously flown UAVs. Depending on the application requirements, an appropriate UAV can then be selected based on its real-time capabilities and the accuracy of the integrated sensors.

The biggest limitation in using mini UAVs in photogrammetry is their weather dependency. Most of the available systems on the market are strongly influenced, by even light wind conditions. More recent UAV systems have a stabilization of the payload or the platform itself, thereby reducing the weather dependency. A drawback of these systems is that two persons, back-up pilot and operator, are generally needed for the UAV operation, since stabilized systems are more complex than non-stabilized. Furthermore, weather dependency is also an important issue in terms of insurance of the UAV system.

8.1.2 Workflow

In chapters 4 and 5 we proposed a workflow for the planning, generation and processing of UAV images. The developed workflow and tools allow the automation of the data processing. Particularly, the integration of the flight planning into the flight control system enables precise image data acquisition: "You know what you get".

This statement can be underlined by the analysis of the flight performance. Specifically, we analyzed the flight performance of model helicopters and provided examples for manually controlled flights, such as kites and balloons. It was clearly evident from our examples that a manually controlled UAV is not as stable as an assisted or autonomously controlled UAV system. Additionally, the different flight modi were shown to have a non-negligible influence

on the flight performance, which is related to the accuracy of the 3D trajectory of the UAV. Since the accuracies given by the system manufacturers are generally not verified, we set up a test field for the evaluation of UAVs at the Campus Hönggerberg (ETH Zurich) and applied a new automated independent method for the tracking of the 3D trajectory of UAVs. These results confirmed the accuracy values of our UAV system as specified by the system manufacturer.

Continuing the workflow for the photogrammetric data processing, we evaluated a number of different commercial photogrammetric software packages used for the orientation and DSM generation from UAV images. The study showed that not all software packages could be used in all possible applications of UAV photogrammetry. Quite often, only the combination of several packages enabled us to completely process the data set. These limitations of commercially available software packages result from the fact that they are designed for standard aerial images and cannot handle arbitrary image configurations.

In section 5.3 we showed results of a UAV-borne laser scanning using a LMS-Q160 (Riegl, 2009) integrated in a large scale UAV Scout B1-100 (Aeroscout, 2009) platform. The first results are quite promising for upcoming applications, while the 3D trajectory of the LiDAR data has to be improved and investigated further in future studies.

With the proposed workflow for the data acquisition and processing of UAV images, it is possible to firstly work in similar applications as in aerial and close range photogrammetry. Secondly, associated with the developments in automated flight planning tools and the improvement of the automated flight of UAVs, it is also possible to document areas faster and cheaper than with aerial and close range photogrammetry. Thirdly, using UAVs it is possible to fly closer (up to few meters) to objects than with manned systems, while the aerial view allows the data acquisition of objects which cannot be documented using terrestrial photogrammetry.

In contrast to the traditional aerial photogrammetry, UAV systems can operate autonomously. The coordinates in the flight planning are frequently defined relative to the start point, which allows flight planning independently from existing maps and coordinate systems. Finally, the capability of using UAVs in unaccessible and dangerous areas, and the improvements in the data processing open up new applications in photogrammetry.

8.1.3 Applications

As examples for the suitability of UAVs for a wide range of applications, particular in archaeological, cultural heritage, and environmental applications and monitoring of a rock slide were conducted in this thesis.

It was possible to generate dense and accurate elevation models with 5cm resolution for Copán, 10cm for Pinchango Alto and the Maize field study and ~15cm for the rockslide Randa from off-the-shelf SLR images. The generated elevation data was compared to manual measurements in stereoscopic images, terrestrial and air-borne laser scanning. Depending on the resolution of the image and laser data the generated elevation data are comparable, while the automated methods (image matching and laser scanning) provide denser and more accurate data than manual measurements. The main difference in our study between the laser DSM and the DSM produced using image matching was due to the locations of the applied sensors (aerial or terrestrial).

The example castle Landenberg showed the improvement of the particular flight planning for single object acquisition. In this example it was possible to use the flight planning tool "circle" successfully, which allowed us to generate images which covered the house roof and façade in one image strip. Therefore, it was possible to reduce the number of images which were necessary for the modeling and texturing of the castle.

Furthermore, in our case studies we could underline the great potential of low-cost UAVs for the fast data acquisition by non-experts. Using an easily controllable system, such as a quadrotor under good weather conditions, it is possible to acquire images using the assisted or automated operation mode, for the automated extraction of surface models of small areas like in our gravel pit project (60m x 60m).

The variety of applications also showed that UAVs are ready to be used under different environmental conditions worldwide. However, our tests showed that the maximum flying height, which depends on the type of UAV system and the environmental conditions (temperature, air pressure and wind), is so far an important limiting factor for some of the systems.

8.2 Perspectives

8.2.1 General remarks

The trend in UAV photogrammetry is moving towards the use of autonomous UAVs, since manually controlled systems are highly affected by environmental conditions.
Because of the automation of the UAV flight and the improvements in the automation of the workflow proposed here for data processing, UAVs can now be applied for practical applications. Additionally, low-cost UAVs and some of the M-class systems can be controlled during the flight mission by non-experts, though most of the M-class and L-class UAVs still

have to be controlled by an experienced operator. However, the regulations for UAVs in Switzerland and abroad have to be improved to facilitate more extensive use. Currently the regulations governing many UAV flights remain a grey area. For example, the L-class UAVs have to interact with the local air navigation service during the flight to avoid collisions with the regular air traffic. For flights over urban areas, the safe operation of the existing UAV systems has to be improved, e.g. by integration of two-way communication systems.

Future applications of UAVs, especially in Switzerland, will be in the Alps for the monitoring and documentation of local changes of glaciers, rock- and landslides and flooding events. Thereby, we have to distinguish between applications of high (cm level) accuracy, for example DSM and orthophoto production, and low (m level) accuracy applications, e.g. geotagging and mosaicking for quick overviews. The state of the art UAVs are ready for real-time image acquisition, while post processing is mandatory for applications requesting high accuracy.

8.2.2 *Potential of Low-cost UAVs*

The evaluated low-cost systems showed that these systems are easily controllable. The acquired data has a great potential to get a first overview of the area of interest. Moreover, our system showed also its usability for teaching. Students can easily be motivated and the whole workflow can be explained and demonstrated (see Grenzdörffer and Engel, 2008, Pueschel, et al., 2008). Thus in future work low-cost UAVs will be integrated as a fixed part in the photogrammetric education at ETH Zurich.

8.2.3 *UAVs for accurate 3D measurements*

Based on the results presented here, we believe that for future projects it would be desirable to be able to use a laser scanner and a camera mounted on a mini UAV, such as a L-class UAV for most applications, which require high resolution and accuracy. Exploiting the advantages of both sensors, a combined approach will yield more precise elevation models: The laser scanner creates highly dense point clouds in areas with low texture, while image data is advantageous for edge measurement and texture mapping. The existing flight planning tools would have to be extended for the combined data acquisition of LiDAR and image data. The most important factor for the combination of image and LiDAR data is the improvement of the accuracy of the flight trajectory of an UAV, which would lead to the real-time capability of data processing of such UAV platforms and the combined processing of the data. In this combination, first the images have to be oriented. In a second step using the enhanced image orientation the trajectory of the LiDAR data can be improved. Thirdly, the registered LiDAR point cloud can then be projected back into the images. Finally, in a combined adjustment the

trajectory can be further improved and a DSM can be generated both from the LiDAR and image data.

In addition to the combined systems also OM, M and L-class image-based systems can be used for precise measurements. It can be expected that differential GPS / GNSS systems and other sensors are getting more compact and the cost for the systems, related to the growing number of applications in the future, will become cheaper. So far for most of the existing UAV-systems the integrated low-cost INS is the limiting factor for high accuracy.

Finally, it can be stated that more UAVs will fly autonomously in the future, the 3D trajectory can be generated with higher accuracy and more systems will be stabilized. These improvements will turn UAV photogrammetry in to an almost autonomous photogrammetric measurement tool. These developments will give an important input for the further progress in the developments of the Digital Photogrammetry techniques and processes.

BIBLIOGRAPHY

AAAI, 2008. American Association for Artificial Intelligence corporate website, http://www.aaai.org, (accessed 04.16. 2008).

Abbeel, P., Coates, A., Quigley, M. and Ng, A. Y., 2007. An application of reinforcement learning to aerobatic helicopter flight, In: NIPS, 19.

Abdulla, Q. A., 2004. Photogrammetric platforms, In: Manual of Photogrammetry, Ed.: McGlone, J. C., American Society for Photogrammetry and Remote Sensing, Bethesda, Maryland, USA, 677-730.

Aber, J. S., Aber, S. W. and Pavri, F., 2002. Unmanned small-format aerial photography from kites for acquiring large scale, high-resolution, multiview-angle imagery, In: The International Archives of the Photogrammetry, Remote Sensing and Spatial Information Sciences, Pecora 15/Land Satellite Information IV/ISPRS Commission I/FIEOS, Denver, CO, USA.

Adobe, 2009. Adobe Photoshop CS4 corporate website, http://www.adobe.com/de/products/photoshop/compare/?sdid=DYWMG, (accessed June 6 2009).

Aeroscout, 2009. Aeroscout corporate website, http://www.aeroscout.ch/, (accessed 31 March 2009).

Aerotopol, 2009. Aerotopol corporate website, http://www.aerotopol.com/, (accessed May 12 2009).

Agouris, P., Doucette, P. and Stefanidis, A., 2004. Automation and digital photogrammetric workstations, In: Manual of Photogrammetry, Ed.: McGlone, J. C., American Society for Photogrammetry and Remote Sensing, Bethesda, Maryland, USA, 949-981.

Ahlfeldt, J., 2004. On Reconstructing and Performing Maya Architecture Temple 22, Copan, Honduras (AD 715)&#8221, Unpublished dissertation, Department of Art History and Archaeology, Columbia University, p. 596.

Akca, D., 2007. Least Squares 3D surface matching, Dissertation, Institute of Geodesy and Photogrammetry, ETH Zurich, Zurich, p. 92.

Altan, M. O., Celikoyan, T. M., Kemper, G. and Toz, G., 2004. Balloon photogrammetry for cultural heritage In: International Archives of the Photogrammetry, Remote Sensing and Spatial Information Sciences, XX ISPRS Congress, Istanbul, Turkey, XXXV-B5, 964-968.

ASL, 2009. Autonomous System Lab (ASL) corporate website, http://www.asl.ethz.ch/, (accessed June 5 2009).

Autodesk, 2009. Autodesk Maya corporate website, http://www.autodesk.de/adsk/servlet/index?siteID=403786&id=11473933, (accessed May 8 2009).

AWI, 2009. Sensitivity of permafrost in the arctic (sparc), Alfred-Wegner Institut for Polar and Marine Research corporate website, http://www.awi.de/en/research/young_investigators/helmholtz_university_young_investigators_groups/sensitivity_of_permafrost_in_the_arctic/, (accessed May 9 2009).

BACS, 2009. Bayesian Approach to Cognitive Systems (BACS) corporate website, http://www.bacs.ethz.ch/, (accessed June 4 2009).

BAE-Systems, 2009. Next-Generation Automatic Terrain Extraction (NGATE), Manuscript, p. 2.

Baltsavias, E. P., 1991. Multiphoto geometrically constrained matching, Dissertation, Institute of Geodesy and Photogrammetry, ETH Zurich, Zurich, p. 49.

Bannert, M. and Stamp, P., 2007. Cross-pollination of maize at long distance, In: Eur. J. Agron., 27, 44-51.

BAZL, 2001. Verordnung über Luftfahrt besonderer Kategorien (VLK), 748.941, 8.

Bellingham, J. S., Tillerson, M., Alighanbari, M. and How, J. P., 2003. Cooperative Path Planning for Multiple UAVs in Dynamic and Uncertain Environments, In: 42nd IEEE Conference on Decision and Control, Maui, Hawaii (USA).

Bendea, H. F., Chiabrando, F., Tonolo, F. G. and Marenchino, D., 2007. Mapping of archaeological areas using a low-cost UAV the Augusta Bagiennorum Test site, In: XXI International Symposium, Athens, Greece.

Bigras, C., 1997. Kite aerial photography of the Axel Heiberg Island fossil forest, In: American Society of Photogrammetry and Remote Sensing, First North American Symposium on Small Format Aerial Photography, University of Minnesota, USA, 147-153.

Blender, 2008. Blender, Open source 3D graphics creation website corporate website, http://www.blender.org/cms/Home.2.0.html, (accessed 04.29. 2008).

Brown, D. C., 1971. Close-range camera calibration, In: Photogrammetric Engineering, 37, 8, 855-866.

CAP, 2004. Unmanned Aerial Vehicle Operations in UK Airspace - Guidance, 722, 60.

Carlson, J., 1997. Kiteflying in freezer, In: The Aerial Eye, 3, 2, 6-7.

CASA, 2001. Unmanned Aircraft and Rockets, Civil Aviation Regulations, (CASA), C. A. S. A., p. 10.

Choi, K., Lee, I., Hong, J., Oh, T. and Shin, S. W., 2009. Developing a UAV-based rapid mapping system for emergency response, In: SPIE, Unmanned Systems Technology XI Orlando, FL, USA.

Choi, K., Lee, I., Shin, S. W. and Ahn, K., 2008. A Project Overview for the Development of a Light and Flexible Rapid Mapping System for Emergency Response, In: The International Archives of the Photogrammetry, Remote Sensing and Spatial Information Sciences, ISPRS Congress, Beijing, China, XXXVII. Part B1, 915-920.

Colomina, I., Blázquez, M., Molina, P., Parés, M. E. and Wis, M., 2008. Towards A New Paradigm for High-Resolution Low-Cost Photogrammetryand Remote Sensing, In: The

International Archives of the Photogrammetry, Remote Sensing and Spatial Information Sciences, ISPRS Congress, Beijing, China, XXXVII. Part B1, 1201-1206.

Coppa, U., Guarnieri, A., Pirotti, F. and Vettore, A., 2008. Accuracy Enhancement of Unmanned Helicopter Positioning with Low Cost System, In: The International Archives of the Photogrammetry, Remote Sensing and Spatial Information Sciences, ISPRS Congress, Beijing, China, XXXVII. Part B5, 843-849.

Cramer, M., 2001. Genauigkeitsuntersuchungen zur GPS/INS-Integration in der Aerophotogrammetrie, Deutsche Geodätische Kommission, München, p. 122.

Cui, H., Lin, Z. and Zhang, J., 2008. Research on Low Altitude Image Acquisition System, In: Computer And Computing Technologies In Agriculture, Volume I, Ed.: Li, D., Springer, Boston, USA, 95-102.

D. Shim, D., Chung, H., Kim, H. J. and Sastry, S., 2005. Autonomous exploration in unknown urban environments for unmanned aerial vehicles, In: AIAA GN&C Conference, San Francisco, California.

DGPF, 2009. Evaluierung digitaler photogrammetrischer Luftbildkamerasysteme corporate website, http://www.ifp.uni-stuttgart.de/dgpf/DKEP-Allg.html, (accessed May 25 2009).

Ebner, H., 1976. Self-calibrating block adjustment, In: International Archives of the Photogrammetry, Remote Sensing and Spatial Information Sciences, Congress of the International Society for Photogrammetry, Helsinki, Finland.

Eck, C., 2001. Navigation Algorithms with Applications to Unmanned Helciopters, Dissertation, Institute of Measurement and Control, ETH Zurich, Zurich, Switzerland, p. 175.

Egbert, J. and Beard, R. W., 2007. Road following control constraints for low altitude miniature air vehicles, In: American Control Conference, New York, U.S., 353-358.

Eisenbeiss, H., 2003. Positions- und Orientierungsbestimmung eines autonomen Helikopters - Vergleich zwischen direkter Georeferenzierung und Aerotriangulation mit Videobilddaten, Diploma Thesis, Institute for Photogrammetry and Remote Sensing, University of Technology Dresden, Dresden, p. 86.

Eisenbeiss, H., 2004. A mini unmanned aerial vehicle (UAV): System overview and image acquisition, In: International archives of photogrammetry, remote sensing and spatial information sciences, International workshop on processing and visualization using high resolution imagery, Pitsanulok, Thailand Vol. XXXVI-5/W1, on CD-Rom.

Eisenbeiss, H., 2007. Applications of photogrammetric processing using an autonomous model helicopter, In: Revue française de photogrammétrie et de télédétection, no 185, 51-56.

Eisenbeiss, H., 2008a. The Autonomous Mini Helicopter: A powerful Platform for Mobile Mapping, In: The International Archives of the Photogrammetry, Remote Sensing and Spatial Information Sciences, ISPRS Congress, Beijing, China, XXXVII. Part B1, 977-983.

Eisenbeiss, H., 2008b. A model helicopter over Pinchango Alto – comparison of terrestrial Laser scanning and aerial Photogrammetry, In: New Technologies for Archaeology: Multidisciplinary Investigations in Palpa and Nasca, Peru (Natural Science in Archaeology) Ed.: Reindel, M. and Wagner, G. A., Springer-Verlag Gmbh, Berlin, Heidelberg, 339-358.

Eisenbeiss, H., 2008c. UAV photogrammetry in plant sciences and geology, In: 6th ARIDA Workshop on "Innovations in 3D Measurement, Modeling and Visualization, Povo (Trento), Italy.

Eisenbeiss, H., Lambers, K. and Sauerbier, M., 2007. Photogrammetric recording of the archaeological site of Pinchango Alto (Palpa, Peru) using a mini helicopter (UAV), Figueiredo, A. and Velho, G. L.: Figueiredo, A. and Velho, G. L., in 33rd CAA Conference, 175-184.

Eisenbeiss, H., Lambers, K., Sauerbier, M. and Zhang, L., 2005. Photogrammetric documentation of an archaeological site (Palpa, Peru) using an autonomous model helicopter, In: International Archives of Photogrammetry, Remote Sensing and Spatial Information Sciences, CIPA, Torino, Italy, Vol XXXIV-5/C34, 238-243.

Eisenbeiss, H., Novák, D., Sauerbier, M., Chapuis, J. and Püschel, H., 2009a. Einsatz einer autonomen Plattform und der Irrlicht Engine für die 3D-Echtzeitvisualisierung am Beispiel von Schloss Landenberg, Luhmann, T. and Müller, C.: Luhmann, T. and Müller, C., in Verlag Herbert Wichmann, Oldenburger 3D-Tage, 390-396.

Eisenbeiss, H., Stempfhuber, W. and Kolb, M., 2009b. Genauigkeitsanalyse der 3D-Trajektorie von Mini-UAVs, In: Zukunft mit Tradition "29. Wissenschaftlich-Technische Jahrestagung der DGPF", Ed.: Seyfert, E., Deutschen Gesellschaft für Photogrammetrie, Fernerkundung und Geoinformation (DGPF) e.V., Potsdam, 407-417.

Eisenbeiss, H. and Zhang, L., 2006. Comparison of DSMs generated from mini UAV imagery and terrestrial laser scanner in a cultural heritage applications, In: International Archives of Photogrammetry, Remote Sensing and Spatial Information Sciences, ISPRS Commission V Symposium, Image Engineering and Vision Metrology, Dresden, Germany, XXXVI-Part5, 90-96.

Ellum, C. and El-Sheimy, N., 2006. New Strategies for integrating photogrammetric and GNSS data, In: International Archives of Photogrammetry, Remote Sensing and Spatial Information Sciences, Commission V Symposium 'Image Engineering and Vision Metrology, Dresden, Germany, XXXVI-Part5, 103-108.

EosSystemsInc, 2009. Photomodeler corporate website, http://www.photomodeler.com/indexd.htm?gclid=CJzQ9MaHsJoCFUQI3wod8EA3bw, (accessed May 9 2009).

ESRI, 2009. ArcGIS corporate website, http://www.esri.com/, (accessed May 18 2009).

Eugster, H., 2007. Georegistrierung mittels Minidrohnen erfasster Videosequenzen – Ansätze und Genauigkeitsanalyse, in DGPF Tagungsband, SGPBF, DGPF und OVG Dreiländertagung 2007, 637-648.

Eugster, H. and Nebiker, S., 2007. Geo-registration of video sequences captured from mini UAVs - approaches and accuracy assessment, In: International Archives of the Photogrammetry, Remote Sensing and Spatial Information Sciences, 5th Symposium on Mobile Mapping Technology, Padua, Italy.

Eugster, H. and Nebiker, S., 2008. UAV-Based Augmented Monitoring - Real-Time Georeferencing and Integration of Video Imagery with Virtual Globes, In: The International Archives of the Photogrammetry, Remote Sensing and Spatial Information Sciences, ISPRS Congress, Beijing, China, XXXVII. Part B1, 1229-1235.

EUROSDR, 2009. EuroSDR - a European Spatial Data Research Network corporate website, http://www.eurosdr.net/start/, (accessed May 25 2009).

Everaerts, J., 2008. The Use of Unmanned Aerial Vehicles (UAVS) for Remote Sensing and Mapping, In: The International Archives of the Photogrammetry, Remote Sensing and Spatial Information Sciences, ISPRS Congress, Beijing, China, XXXVII. Part B1, 1187-1192.

Everaerts, J., Lewyckyj, N. and Fransaer, D., 2004. Pegasus: Design of a Stratospheric Long Endurance Uav System for Remote Sensing, In: International Archives of Photogrammetry, Remote Sensing and Spatial Information Sciences, ISPRS Congress, Istanbul, Turkey, XXXV, Part B2, 29-33.

Fash, W. L., 1991. Scribes, Warriors and Kings, Thames and Hudson Ltd., London, p. 192.

Fiberteck, 2009. Fiberteck, INC. corporate website, http://www.fibertek.com/, (accessed June 6 2009).

Flury, G., 2009. Volumenabschätzung eines Kiesabbau- und Deponiegebietes mittels UAV-Bilddaten Bachelor Thesis, Institute of Geodesy and Photogrammetry, ETH Zurich, Zurich, p. 36.

Fotinopoulos, V., 2004. Balloon photogrammetry for archaeological surveys, In: International Archives of the Photogrammetry, Remote Sensing and Spatial Information Sciences, XX ISPRS Congress, Istanbul, Turkey, XXXV-B5, 504-507.

Fransaer, D., Lewyckyj, N., F., V. and J., E., 2004. Pegasus : Business Model for a Stratospheric long Endurance Uav System for Remote Sensing, In: International Archives of Photogrammetry, Remote Sensing and Spatial Information Sciences, ISPRS Congress, Istanbul, Turkey, XXXV, Part B2, 625-629.

Gaisecker, T., 2006. Pinchango Alto e 3D archaeology documentation using the hybrid 3D laser scan system of RIEGL, In: Recording, Modeling and Visualization of Cultural Heritage, Ed.: Baltsavias, E., et al., Taylor & Francis, London, 459-464.

Gawronski, J. H. G. and Boyarsky, P. V., 1997. Northbound with Barents: Russian-Dutch integrated archaeologic research on the Archipelago Novaya Zemlya, Uitgeverij Jan Mets, Amsterdam, p. 255.

Geocopter, 2009. Geocopter corporate website, http://geocopter.nl/, (accessed April 8 2009).

geomagic, 2009. geomagic corporate website, http://www.geomagic.com/de/products/, (accessed May 19 2009).

Geomatik, 2009. Laus Aufdenblatten Geomatik AG corporate website, http://www.geomatik-ag.ch/, (accessed 18 May 2009).

Gerke, M., 2008. Dense Image Matching in Airborne Video Sequences, In: The International Archives of the Photogrammetry, Remote Sensing and Spatial Information Sciences, ISPRS Congress, Beijing, China, XXXVII. Part B3b, 639-644.

GIS-Obwalden, 2009. GIS Obwalden corporate website, http://www.gis-ow.ch, (accessed May 19 2009).

Gomez-Lahoz, J. and Gonzalez-Aguilera, D., 2009. Recovering traditions in the digital era: the use of blimps for modelling the archaeological cultural heritage, In: Journal of Archaeological Science, 36, 1, 100-109.

Gonzalez, J. P., Nagy, B. and Stentz, A., 2006. The Geometric Path Planner for Navigating Unmanned Vehicles in Dynamic Environments, In: Proceedings ANS 1st Joint Emergency Preparedness and Response and Robotic and Remote Systems, Salt Lake City (Utah), USA.

GoogleEarth, 2009. Google Earth corporate website, http://earth.google.com/, (accessed May 2 2009).

Grenzdörffer, G. and Engel, A., 2008. Eine vergleichende Untersuchung von zwei Micro-UAV's – Perspektiven für die aktuelle und kostengünstige Geoinformationsgewinnung, In: GIS, 1/2008, 17-25.

Grenzdörffer, G., Engel, A. and Jütte, K., 2008a. Low-cost UAV's in der Land- und Forstwirtschaft – Eine vergleichende Untersuchung von zwei Mini-UAV's, In: Seyfert, E., DGPF-Jahrestagung 2008, Oldenburg, Germany, 27-36.

Grenzdörffer, G., Engel, A. and Teichert, B., 2008b. The Photogrammetric Potential of Low-Cost UAVS in Forestry and Agriculture, In: The International Archives of the Photogrammetry, Remote Sensing and Spatial Information Sciences, ISPRS Congress, Beijing, China, XXXVII. Part B1, 1207-1213.

Gruen, A., 1985. Adaptive least squares correlation: a powerful image matching technique, In: South African Journal of Photogrammetry, Remote Sensing and Cartography, 14, 3, 175-187.

Gruen, A., 1999. Photogrammetrische Aufnahmen der Geoglyphen von Nasca, Palpa und San Ignacio, In: Nasca - Geheimnisvolle Zeichen im Alten Peru, Ed.: Rietberg, M., Museum Rietberg, Zurich, Switzerland, 5-14.

Gruen, A., Cocard, M. and Kahle, H.-G., 1993. Photogrammetry and Kinematic GPS: Results of a High Accuracy Test, In: Photogrammetric Engineering & Remote Sensing, 59, 11, 1643-1650.

Gruen, A., Zhang, L. and Visnovcova, J., 2001. Automatic reconstruction and visualization of a complex Buddha tower of Bayon, Angkor, Cambodia, in DGPF, 21. Wissenschaftlich-Technische Jahrestagung der DGPF, "Photogrammetrie-Fernerkundung-Geoinformation: Geodaten schaffen Verbindungen", 289-301.

Haala, N., 2005. Multi-Sensor-Photogrammetrie, Habilitation, Fakultät für Bau- und Umweltingenieurwissenschaften, Universität Stuttgart, München 2005, p. 103.

Haarbrink, R. B. and Eisenbeiss, H., 2008. Accurate DSM production from unmanned helicopter systems, In: International Archives of Photogrammetry, Remote Sensing and Spatial Information Sciences, ISPRS Congress, Beijing, China, XXXVII. Part B1, 1259-1264.

Haarbrink, R. B. and Koers, E., 2006. Helicopter UAV for photogrammetry and rapid response, In: International Archives of Photogrammetry, Remote Sensing and Spatial Information Sciences, ISPRS Workshop of Inter-Commission WG I/V, Autonomous Navigation, Antwerp, Belgium.

Hagenbach, M. and Wanner, P., 2009. Digital Elevation Models of restored river corridors by means of motorised paragliders, Bachelor Thesis in Environmental Science, ETH Zurich, Zurich, Switzerland, p. 113.

Hanusch, T., 2008. A new texture mapping algorithm for photorealistic reconstruction of 3D objects, In: International Archives of the Photogrammetry, Remote Sensing and Spatial Information Sciences, ISPRS Congress, Beijing, China, XXXVII. Part B5-2, 699-705.

Heipke, C., 1999. Automatic Aerial Triangulation: Results of the OEEPE-ISPRS Test and Current Developements, in Wichmann, Photogrammetric week, 177-191.

Helimap, 2009. Helimap corporate website, http://www.helimap.ch/Deutsch/ger_index.html, (accessed May 25 2009).

Herwitz, S. R., Leung, J. G., Higgins, R. G. and Dunagan, S. E., 2002. Remote command-and-control of imaging payloads using commercial off-the-shelf technology, in IGARSS, Geoscience and Remote Sensing Symposium, 2726-2728.

Hirobo, 2009. Hirobo corporate website, http://model.hirobo.co.jp/, (accessed March 11 2009).

Hoffmann, G. M., Rajnarayan, D. G., Waslander, S. L., Dostal, D., Jang, J. S. and Tomlin, C. J., 2004. THE STANFORD TESTBED OF AUTONOMOUS ROTORCRAFT FOR MULTI AGENT CONTROL (STARMAC), in 23rd Digital Avionics System Conference, 12.E.4- 121-10.

Hohmann, H. and Vogrin, A., 1982. Die Architektur von Copan, Akademische Druck- u. Verlagsanstalt, Graz, Australia, p. 182.

Hongoh, D., Kajiwara, K. and Honda, Y., 2001. Developing Ground Truth Measurement System using RC Helicopter and BRDF Model in Forest Area, In: Asian Association on Remote Sensing, 22nd Asian Conference on Remote Sensing, Sigapore, ??

Hongxia, C., Zongjian, L. and Guozhong, S., 2007. Non-metric CCD Camera Calibration for Low Attitude Photogrammetric Mapping, in IEEE, Electronic Measurement and Instruments, 2007. ICEMI '07. 8th International Conference on, 2: 689-696.

Horcher, A. and Visser, R. J. M., 2004. Unmanned Aerial Vehicles: Applications for Natural Resource Management and Monitoring, In: Council on Forest Engineering Annual Meeting, Hot Springs (AR), USA.

i3D-viewer, 2009. i3D Virtual Globe corporate website, http://www.fhnw.ch/habg/ivgi/forschung/i3d, (accessed March 11 2009).

ifp, 2009. Photogrammetric test site Vaihingen/Enz, Institute for Photogrammetrie, University Stuttgart corporate website, http://www.ifp.uni-stuttgart.de/forschung/photo/test_site/vaihingen.htm, (accessed May 25 2009).

IGI-Systems, 2009. IGI-Systems corporate website, http://igi-systems.com/index.htm, (accessed May 12 2009).

IHAH, 2009. 3D Archaeology and Cultural Heritage Management in Honduras corporate website, http://www.ihah.hn/taller3d.html, (accessed June 6 2009).

Imbach, B. and Eck, C., 2009. Autonomer UAV Helikopter für Vermessung und industrielle Anwendungen_Luhmann, T. and Müller, C.: Luhmann, T. and Müller, C., in Herbert Wichmann, 8. Oldenburger 3D-Tage, 384-389.

Inpho, 2009a. Inpho Scop++ corporate website, http://www.inpho.de/index.php?seite=index_scope, (accessed May 19 2009).

Inpho, 2009b. Match T DSM corporate website, http://www.inpho.de/index.php?seite=index_match-t, (accessed May 25 2009).

Intergraph/ZI, 2009. Intergraph Photogrammetry corporate website, http://www.intergraph.com/photo/, (accessed May 12 2009).

IPW, 2009. Institute of Plant Sciences at ETH Zurich (IPW) corporate website, http://www.ipw.ethz.ch/, (accessed May 25 2009).

Irrlicht, 2009. Irrlicht engine corporate website, http://irrlicht.sourceforge.net/, (accessed June 3 2009).

ISPRS, 2004. Congress Proceedings, In: International Archives of the Photogrammetry, Remote Sensing and Spatial Information Sciences, XX ISPRS Congress, Istanbul, Turkey.

ISPRS, 2006. Congress Proceedings, In: International Archives of the Photogrammetry, Remote Sensing and Spatial Information Sciences, ISPRS Mid-term Syposia, .

iWitness, 2009. iWitness Close Range Photogrammetry corporate website, http://www.iwitnessphoto.com/, (accessed June 6 2009).

Jang, H. S., Lee, J. C., Kim, M. S., Kang, I. J. and Kim, C. K., 2004. Construction of national cultural heritage management system using rc helicopter photographic syrveying system, In: International Archives of Photogrammetry, Remote Sensing and Spatial Information Sciences, ISPRS Congress, Istanbul, Turkey, XXXV, Part B5, 473-478.

Jizhou, W., Zongjian, L. and Chengming, L., 2004. Reconstruction of buildings from a single UAV image, In: International Archives of Photogrammetry, Remote Sensing and Spatial Information Sciences, ISPRS Congress, Istanbul, Turkey, XXXV, Part B8, 940-943.

Johnson, G. W., Meisner, D. E. and Johnson, W. L., 1990. Aerial Photography of the Nazca Lines, In: The Lines of Nasca, Ed.: Aveni, A., F., Memoirs of the American Philosophical Society, Philadelphia, 273-283.

Jütte, K., 2007. Innovative Methoden der Überwachung der Kiefergroßschädlinge in Mecklenburg-Vorpommern, Höppner, K.: Höppner, K., in Land Brandenburg, Aktuelle Aspekte zur Bewirtschaftung und Ökologie der Kiefer im nordostdeutschen Tiefland, 1-38.

Jütte, K., 2008. Vergleich verschiedener low-cost Luftbildaufnahmesysteme sowie Einsatz von Drohnen: Grenzen und Möglichkeiten, in Bayerische Landesanstalt für Wald und Forstwirtschaft Der gepixelte Wald - Fachtagung zur Forstlichen Fernerkundung

Kaaniche, K., Champion, B., Pegard, C. and Vasseur, P., 2005. A vision algorithm for dynamic detection of moving vehicles with a UAV, In: IEEE International Conference on Robotics and Automation, 1878-1883.

Karras, G. E., Mavromati, D., Madani, M., Mavrelis, G., Lymperopoulos, E., Kambourakis, A. and Gesafidis, S., 1999. Digital orthophotography in archaeology with low-altitude non-metric images, In: International Archives of Photogrammetry & Remote Sensing, WG V/2 & 5 "Photogrammetric Measurement, Object Modeling and Documentation in Architecture and Industry", Thessaloniki, Greece, XXXII-5/W11, 8-11.

Kerle, N., Heuel, S. and Pfeifer, N., 2008. Real-time data collection and information generation using airborne sensors, In: Geospatil information Technology for Emergency Response, Ed.: Zlatanova S and Li, J., Taylor & Francis, London, UK, 43-74.

Kersten, T., 1999. Digital Aerial Triangulation in Production - Experiences with Block Switzerland, in Wichmann, Photogrammetric week, 193-204.

Kersten, T., Przybilla, H. J. and Lindstaedt, M., 2006. Integration, Fusion und Kombination von terrestrischen Laserscannerdaten und digitalen Bildern, In: DIN Deutsches Institut für Normung e.V. und Humboldt-Universität zu Berlin, Anforderungen an geometrische Fusionsverfahren, Berlin, Germany.

Kirschner, H. and Stempfhuber, W., 2008. The Kinematic Potential of Modern Tracking Total Stations - A State of the Art Report on the Leica TPS1200+, Stempfhuber, W. and Ingensand, H.: Stempfhuber, W. and Ingensand, H., in MCG, 51-60.

Kise, M., Rovira-Más, F. and Zhang, Q., 2005. A stereovision-based crop row detection method for tractor-automated guidance, In: Biosystems Eng, 90, 357-367.

Kraus, K., 2007. Photogrammetry - Geometry from Images and Laser Scans, Walter de Gruyter, Goettingen, Germany, p. 459.

Kupferschmidt, D., 2008. Viviendo entre dos Horizontes en el Intermedio Tardío, In: Arqueología de Palpa, Perú: Períodos Nasca, Horizonte Medio e Intermedio Tardío, Ed.: Reindel, M. and Lambers, K., Forschungen zur Archäologie Außereuropäischer Kulturen, Wiesbaden, .

Laliberte, A., S., Winters, C. and Rango, A., 2007. Acquisition, orthorectification, and classification of hyperspatial UAV imagery, In: Fourth Annual Symposium: Research Insights in Semiarid Scosystems, RISE, University of Arizona, Tucson.

Lambers, K., 2006. The geoglyphs of Palpa, Peru: documentation, analysis, and interpretation, Aichwald, Bielefeld, Germany, p. 177.

Lambers, K., Eisenbeiss, H., Sauerbier, M., Kupferschmidt, D., Gaisecker, T., Sotoodeh, S. and Hanusch, T., 2007. Combining photogrammetry and laser scanning for the recording and modelling of the late intermediate period site of Pinchango Alto, Palpa, Peru, In: J. Archaeol. Sci., 34, 1702-1710.

Lee, I., 2002. Perceptual Organization of Surfaces, Dissertation, Ohio State University, Columbus, Ohio (US), p. 178.

Leica-Geosystems, 2009. Leica-Geosystems corporate website, http://www.leica-geosystems.com/ch/de/lgs_7491.htm, (accessed May 19 2009).

Leica, 2009. Leica Geosystems corporate website, http://www.leica-geosystems.com/ch/de/lgs_7491.htm, (accessed May 11 2009).

Lin, Z., 2008. UAV for mapping - low altitude photogrammetry survey, In: The International Archives of the Photogrammetry, Remote Sensing and Spatial Information Sciences, ISPRS Congress, Beijing, China, XXXVII. Part B1, 1183-1186.

Lötscher, 2009. Lötscher Kies + Beton AG corporate website, http://www.loetscher-kiesbeton.ch/, (accessed June 6 2009).

Luhmann, T., Robson, S., Kyle, S. and Harley, I., 2006. Close Range Photogrammetry - Principles, Methods and Applications, Whittles Publishing, p. 510.

Marks, A. R., 1989. Aerial photography from a tethered helium filled balloon, In: The Photogrammetric Record, 13, 74, 257-261.

Masahiko, N., 2007. UAV borne mapping system for river environment, In: 28th Asian Association of Remote Sensing Conference, Kuala Lumpur, Malaysia.

Mavionics, 2009. Mavionics corporate website, http://www.mavionics.de/, (accessed March 11 2009).

Microdrones, 2009a. Manual MDCockpit, In: Kreuztal, Germany.

microdrones, 2009b. microdrones corporate website, http://www.microdrones.com/, (accessed March 11 2009).

Mikrokopter, 2009. Mikrokopter corporate website, http://www.mikrokopter.de/ucwiki/, (accessed April 8 2009).

Miyatsuka, Y., 1996. Archaelogical real time photogrammetric system using digital still camera, In: The International Archives of the Photogrammetry, Remote Sensing and Spatial Information Sciences, XVIII ISPRS Congress, Vienna, Austria, XXXI-B5, 447-452.

Mori, M., Masahiro, S., Akamatsu, Y., Yamana, R. and Yahara, T., 1996. Discussion on the automatic measurement of traffic flow by video camera mounted on balloon, In: International Archives of the Photogrammetry, Remote Sensing and Spatial Information Sciences, ISPRS Congress, Vienna, Austria, XXXI, B5, 378-381.

Nackaerts, K., Everaerts, J., Choi, R., Delauré, B., Van Achteren, T. and Biesemans, J., 2008. Calibration Strategy for the Medusa Camera System, In: The International Archives of the Photogrammetry, Remote Sensing and Spatial Information Sciences, ISPRS Congress, Beijing, China, XXXVII. Part B1, 1247-1252.

Nagai, M., Chen, T., Ahmed, A. and Shibasaki, R., 2008. UAV Borne Mapping by Multi Sensor Integration, In: The International Archives of the Photogrammetry, Remote Sensing and Spatial Information Sciences, ISPRS Congress, Beijing, China, XXXVII. Part B1, 1215-1221.

Nagai, M., Shibasaki, R., Manandhar, D. and Zhao, H., 2004. Development of digital surface and feature extraction by integrating laser scanner and CCD sensor with IMU, In: International Archives of the Photogrammetry, Remote Sensing and Spatial Information Sciences, XX ISPRS Congress, Istanbul, Turkey, XXXV-B5, 655-659.

Nebiker, S., Annen, A., Scherrer, M. and Oesch, D., 2008. A Light-Weight Multispectral Sensor for Micro UAV - Opportunities for Very High Resolution Airborne Remote Sensing, In: The International Archives of the Photogrammetry, Remote Sensing and Spatial Information Sciences, ISPRS Congress, Beijing, China, XXXVII. Part B1, 1193-1199.

Nebiker, S., Christen, M., Eugster, H., Flückiger, K. and Stierli, C., 2007a. Integrating mobile geo sensors into collaborative virtual globes - design and implementation issues, In: International Archives of the Photogrammetry, Remote Sensing and Spatial Information Sciences, 5th International Symposium on Mobile Mapping Technology MMT'07 Padua, Italy, XXXVI-5/C55, Book & CD.

Nebiker, S., Christen, M., Eugster. H, Flückiger, K. and Stierli, C., 2007b. Integration von mobilen Geosensoren in kollaborative virtuelle Globen, In: DGPF Tagungsband Dreiländertagung der SGPBF, DGPF und OVG: Von der Medizintechnik bis zur Planetenforschung - Photogrammetrie und Fernerkundung für das 21. Jahrhundert, FHNW Muttenz, Switzerland, 189-198.

Newhall, B., 1969. Airborne camera: The world from the air and outer space, Hasting House, Trowbridge & London, p. 144.

Niethammer, U., Rothmund, S. and Joswig, M., 2009. UAV-based remote sensing of the slow moving landslide Super-Sauze, In: Landslide processes, Ed.: CERG Editions, Strasbourg, 69-74.

Niranjan, S., Gupta, G., Sharma, N., Mangal, M. and Singh, V., 2007. Initial Efforts toward Mission-specific Imaging Surveys from Aerial Exploring Platforms: UAV, In: GIS development, Map World Forum, Hyderabad, India.

Nordberg, K., Farnebäck, G., Forssén, P.-E., Granlund, G., Moe, A., Wiklund, J. and Doherty, P., 2002. Vision for a UAV helicopter, In: Workshop on aerial robotics, Lausanne, Switzerland.

Noth, A., Bouabdallah, S., Michaud, S., Siegwart, R. and Engel, W., 2004. Sky-Sailor Design of an Autonomous Solar Powered Martian Airplane, In: 8th ESA Workshop on Advanced Space Technologies for Robotics, Noordwick, Netherlands.

Noth, A., Siegwart, R. and Engel, W., 2007. Autonomous Solar UAV for Sustainable Flights, In: Advances in Unmanned Aerial Vehicles, Ed.: Valavanis, K. P., Springer, Tampa, Florida, USA, 377-406.

omnisight, 2009. omnisight GmbH corporate website, http://www.omnisight.ch/, (accessed June 6 2009).

Otto, G. P. and Chau, T. K. W., 1988. A "Region-Growing" Algorithm for Matching of Terrain Images., In: 4th Alvey Vision Club, University of Manchester, UK.

Paparazzi, 2009. Paparazzi: The free autopilot corporate website, http://paparazzi.enac.fr/wiki/Main_Page, (accessed April 8 2009).

Patias, P., Saatsoglou-Paliadeli , C., Georgoula, O., Pateraki, M., Stamnas, A. and Kyriakou, N., 2007. Photogrammetric documentation and digital representation of the macedonian palace in Vergina-Aegeae, In: CIPA, XXI International CIPA Symposium, Athens, Greece, ??

Pettersson, P.-O. and Doherty, P., 2004. Probabilistic roadmap based path planning for autonomous unmanned aerial vehicles, In: 14th Int'l Conf. on Automated Planning and Scheduling, Whistler, British Columbia, Canada.

Poli, D., 2005. MODELLING OF SPACEBORNE LINEAR ARRAY SENSORS, Dissertation, Institute of Geodesy and Photogrammetry, Zurich, p. 216.

Przybilla, H.-J. and Wester-Ebbinghaus, W., 1979. Bildflug mit ferngelenktem Kleinflugzeug, In: Bildmessung und Luftbildwesen, Zeitschrift fuer Photogrammetrie und Fernerkudung, 47, 5, 137-142.

Pueschel, H., Sauerbier, M. and Eisenbeiss, H., 2008. A 3D model of Castle Landenberg (CH) from combined photogrammetric processing of terrestrial and UAV-based images, In: The International Archives of the Photogrammetry, Remote Sensing and Spatial Information Sciences, ISPRS Congress, Beijing, China, Vol. XXXVII. Part B8, 93-98.

Puri, A., 2004. A Survey of Unmanned Aerial Vehicles (UAV) for Traffic Surveillance, Internal Report, Department of Computer Science and Engineering, University of South Florida, Tampa, FL, USA, p. 29.

Randa, 2009. Randa rockslide corporate website, (accessed May 18 2009).

Record, 2009. Record: REstored COrridor Dynamics (Record) corporate website, http://www.cces.ethz.ch/projects/nature/Record, (accessed May 2 2009).

Reidelstuerz, P., Link, J., Graeff, S. and Claupein, W., 2007. UAV (unmanned aerial vehicles) für Präzisionslandwirtschaft. 13. Workshop Computer-Bildanalyse in der Landwirtschaft & 4. Workshop Precision Farming, In: Bornimer Agrartechnische Berichte, 61, 75-84.

Reindel, M., 2005. Pinchango Alto: a gold miner's settlement in Palpa, southern Peru, In: Wars and conflicts in prehispanic Mesoamerica and the Andes, Brussels, 90-98.

Reindel, M. and Isla Cuadrado, J., 1999. Ausgrabungen in Los Molinos und La Muña: Ergebnisse der Grabungskampagne 1998 des Archäoloschen Projektes Nasca-Palpa. Süd-

Peru, In: Jahresbericht der Schweizerisch-Lichtensteinischen Stiftung für Archäologische Forschung im Ausland, Ed.: Zurich/Vaduz, 123-152.

Reindel, M., Isla Cuadrado, J. and Lambers, K., 2002. Abschließende Untersuchungen zu Geoglyphen und Siedlungen in Palpa, Südperu. Ergebnisse der Feldkampagne 2001 des Archäologischen Projektes Nasca-Palpa, In: Jahresbericht der Schweizerisch-Liechtensteinischen Stiftung für Archäologische Forschungen im Ausland Ed.: Zurich / Vaduz, 37-54.

Richards-Rissetto, H., 2009. Using Valley-Wide GIS for Archaeological Analysis and a Google SketchUp Model of Ancient Copan, In: 3D Archaeology and Cultural Heritage Management in Honduras, Copan, Honduras.

Riegl, 2009. Riegl corporate website, http://www.riegl.com/, (accessed 1 April 2009).

Ries, J. B. and Marzolff, I., 2003. Monitoring of gully erosion in the Central Ebro Basin by large-scale aerial photography taken from a remotely controlled blimp, In: CATENA, 50, 2-4, 309-328.

Rockwell, 1996. C-MIGITS II - Integrated GPS-INS (Rockwell international), Manuscript, p. .

Roeoesli, C., 2009. Processing of UAV-images: Samoilov Island, Russia, Institute of Geodesy and Photogrammetry, ETH Zurich, Zurich, p. 46.

RolleiMetric, 2009. RolleiMetric corporate website, http://www.rollei-metric.com/index.php?id=12&page=home&lang=en, (accessed May 12 2009).

Rovira-Más, F., Zhang, Q. and Reid, J. F., 2005. Creation of three-dimensional crop maps based on aerial stereoimages, In: Biosystems Eng, 90, 251-259.

Sasiadek, J. Z. and Duleba, I., 2000. 3D Local Trajectory Planner for UAV, In: Journal of Intelligent and Robotic Systems, 29, 191-210.

Sauerbier, M., 2008. Virtual Flight Over the Nasca Lines – Automated Generation of a Photorealistically Textured 3D Model of the Pampa de Nasca, In: New Technologies for Archaeology: Multidisciplinary Investigations in Palpa and Nasca, Peru (Natural Science in Archaeology), Ed.: Reindel, M. and Wagner, G. A., Springer-Verlag Gmbh, Berlin, Heidelberg, 307-320.

Sauerbier, M., 2009. 3D Virtual Reconstruction and Visualization of Complex Architectures, In: International Archives of Photogrammetry, Remote Sensing and Spatial Information Sciences, Proceedings of the 3rd ISPRS International Workshop 3D-ARCH 2009, Trento, Italy, XXXVIII-5/W1, on DVD.

Sauerbier, M. and Lambers, K., 2003. A 3D model of the Nasca lines at Palpa (Peru), In: International Archives of the Photogrammetry, Remote Sensing and Spatial Information Sciences, International Workshop on Visualization and Animation of Reality-based 3D Models, Tarasp, Switzerland, XXXIV-5/W10, CD-ROM.

Sauerbier, M., Schrotter, G., Eisenbeiss, H. and Lambers, K., 2006. Multi-resolution image-based visualization of archaeological landscapes in Palpa (Peru), Campana, S. and Forte, M.: Campana, S. and Forte, M., in Oxford: Archaeopress, From Space To Place: Proceedings of the 2nd International Conference on Remote Sensing in Archaeology, 353-359.

Scherer, S., Singh, S., Chamberlain, L. and Saripalli, S., 2007. Flying Fast and Low Among Obstacles, In: IEEE International Conference on Robotics and Automation, Rome, Italy.

Scheritz, M., Dietrich, R., Scheller, S., Schneider, W. and Boike, J., 2008. High Resolution Digital Elevation Model of Polygonal Patterned Ground on Samoylov Island, Siberia, Using Small-Format Photography, In: United states permafrost association, 9th International Conference on Permafrost, University of Alaska, Fairbanks, USA, 1589-1594.

Schwidefsky, K. and Ackermann, F., 1976. Photogrammetrie, Teubner, Stuttgart, Germany, p. 384.

Sick, 2009. Sick sensor intelligence corporate website, http://www.sick.de/de/de.html, (accessed June 6 2009).

Skaloud, J., 1999. Problems in Direct-Georeferencing by INS/DGPS in the Airborne Environment, In: International Archives of the Photogrammetry, Remote Sensing and Spatial Information Sciences, ISPRS Workshop on Direct versus indirect methods of sensor orientation, Barcelona, Spain.

Skaloud J., Vallet, J., Keller, K., Vessière, G. and Kölbl, O., 2005. Helimap: Rapid Large scale Mapping Using Handheld LiDAR/CCD/GPS/INS Sensors on Helicopters, In: ION GNSS Congress, Long Beach, California (USA).

Skarlatos, D., Theodoridou, S. and Glabenas, D., 2004. Archaeological surveys in Greece using radio-controlled helicopter., In: FIG Working Week, Athens, Greece.

Skyline, 2009. Skyline Terra Exporer corporate website, http://www.skylinesoft.com/SkylineGlobe/corporate/home/index.aspx?, (accessed May 9 2009).

Sotoodeh, S., 2006. Outlier detection in laser scanner points cloud, In: International Archives of the Photogrammetry, Remote Sensing and Spatial Information Sciences, Proceedings of the ISPRS Commission V Symposium'Image Engineering and Vision Metrology', Dresden, Germany, XXXVI, PART 5, 297-302.

Sotoodeh, S., Novak, D., Sauerbier, M., Scaradozzi, D., Caiti, A., Conte, G., Zanoli, S. M., Drap, P., Chapman, P., Pascoal, A. M., Long, L. and Hanke, K., 2008. UPGRADE and IMODELASER: Tools and Best Practice for 3D Data Acquisition and Processing for CH in Different Environments, In: Rome Event 2008 of the EPOCH Network of Excellence in Open Cultural Heritage Rom, Italy.

Spatalas, S., Tsioukas, V. and Daniil, M., 2006. The use of remote controlled helicopter for the recording of large scale urban and suburban sites, In: Culture of Representation, Xanthi, Greece.

Steffen, R. and Förstner, W., 2008. On Visual Real Time Mapping for Unmanned Aerial Vehicles, In: The International Archives of the Photogrammetry, Remote Sensing and Spatial Information Sciences, ISPRS Congress, Beijing, China, XXXVII. Part B3a, 57-62.

Stempfhuber, W., 2004. Ein integritätswahrendes Messsystem für kinematische Anwendungen, Deutsche Geodätische Kommission, München, p. 131.

Stempfhuber, W. and Kirschner, H., 2008. Kinematische Leistungsfähigkeit von zielverfolgenden Tachymetern - Ein Beitrag zum Stand der Technik am Beispiel des Leica TPS1200+, In: Allgemeine Vermessungs-Nachrichten (AVN), 06/2008, 216-223.

Stöllner, T. and Reindel, M., 2007. Vorspanische Goldgewinnung im Bereich von Palpa-Nasca. Bericht über eine einwöchige Prospektionskampagne an der Südküste Perus, In: Der Anschnitt, 1/2007, 2-12.

Sugiura, R., Noguchi, N. and Ishii, K., 2005. Remote-sensing Technology for Vegetation Monitoring using an Unmanned Helicopter, In: Biosystems Engineering, 90, 4, 369–379.

Surveycopter, 2009. Surveycopter corporate website, http://www.surveycopter.fr/, (accessed March 11 2009).

swisstopo, 2005. Näherungslösungen für die direkte Transformation CH1903 <--> WGS84 4.

Tarchi, D., Casagli, N., Fanti, R., Leva, D. D., Luzi, G., Pasuto, A., Pieraccini, M. and Silvano, S., 2003. Landslide monitoring by using ground-based SAR interferometry: an example of application to the Tessina landslide in Italy, In: Engineering Geology, 68, 15-30.

Thamm, H. P. and Judex, M., 2006. The "Low cost drone" - An interesting tool for process monitoring in a high spatial and temporal resolution, In: The International Archives of the Photogrammetry, Remote Sensing and Spatial Information Sciences, ISPRS Commission VII Mid-term Symposium "Remote Sensing: From Pixels to Processes", Enschede, the Netherlands, XXXVI part 7, 140-144.

Theodoridou, S., Tokmakidis, K. and Skarlatos, D., 2000. Use of Radio-Controlled Model Helicopters in archaeology Surveying and in Building Construction Industry, In: International Archives of the Photogrammetry, Remote Sensing and Spatial Information Sciences, XIX ISPRS Congress, Amsterdam, The Netherlands, XXXIII-B5, ??

Thrun, S. a. D., Mark and Haehnel, D., 2003. Scan Alignment and 3D Surface Modeling with a Helicopter Platform, In: International Conference on Field and Service Robotics, Lake Yamanaka, Japan.

Tokmakidis, K., Ito, J., Mamoto, E. and Mori, F., 1998. Detail Surveys with Close-Range Photogrammetry in Archaeological Sites, in International Archives of the Photogrammetry, Remote Sensing and Spatial Information Sciences, Commission V Symposium "Real-Time Imaging and Dynamic Analysis", ??

Tokmakidis, K. and Scarlatos, D., 2002. Mapping excavations and archaeological sites using close range photos, In: International Archives of the Photogrammetry, Remote Sensing and Spatial Information Sciences, Commission V Symposium "Close-Range Imaging, Long-Range Vision", Corfu, Greece, XXXIV part 5, ??

Trisirisatayawong, I. and Cheewinsiriwat, P., 2004. Automatic Flight Planning for Unmanned Aerial Vehicle Utilizing GIS Analysis on Digital elevation Model, In: Asian Conference on Remote Sensing, Chiang Mai, Thailand, 1, 179-183.

UAVP, 2009. UAVP: Universal aerialvideo platform corporate website, http://uavp.ch/moin, (accessed April 8 2009).

Vallet, J., 2007. GPS-IMU and LiDAR integration to aerial photogrammetry: Development and practical experiences with Helimap System®, In: Dreiländertagung 27. Wissenschaftlich-Technische Jahrestagung der DGPF, Muttenz, Switzerland, 649-658.

Vallet, J. and Skaloud, J., 2004. Development and experiences with a fully-digital handheld mapping system operated from a helicopter, In: The International Archives of the

Photogrammetry, Remote Sensing and Spatial Information Sciences, XX ISPRS Congress, Istanbul, Turkey, XXXV, Part B, 791-796.

van Blyenburgh, P., 1999. UAVs: and Overview, In: Air & Space Europe, I, 5/6, 43-47.

Verhoeven, G. J. J., 2009. Providing an archaeological bird's-eye view - an overall picture of ground-based means to execute low-altitude aerial photography (LAAP) in Archaeology, In: Archaeological Prospection, 9999, 9999, n/a.

Vexcel, 2009. Vexcel corporate website, http://www.vexcel.com/, (accessed May 12 2009).

Visiongain, 2009. The Unmanned Aerial Vehicles (UAV) Market 2009-2019, Internal Report, p. 123.

Visnovcova, J., Zhang, L. and Gruen, A., 2001. Generating a 3D model of a Bayon tower using non-metric imagery, In: Asian Journal of Geoinformatics, 2, 1, 11-18.

Vito, 2009. Vito, UAV Flights corporate website, http://isprs.vgt.vito.be/uav/Testflights.html, (accessed June 2 2009).

Vogler, A., 2009. Simulation of transgenic pollen dispersal at short distances in maize (Zea mays L.), Dissertation, Institute of Plant breeding, ETH Zurich, Zurich, Switzerland, p. 115.

Vogler, A., Eisenbeiss, H., Aulinger-Leipner, I. and Stamp, P., 2009. Impact of topography on cross-pollination in maize (Zea mays L.). In: European Journal of Agronomy, 31, 99-102.

Vozikis, E., 1983. Analytical methods and instruments for mapping from balloon photography, In: The Photogrammetric Record, 11, 61, 83-92.

Wanzke, H., 1984. The Employment of a hot-air ship for the stereophotogrammetrc documentation of antique ruins, In: International Archives of the Photogrammetry, Remote Sensing and Spatial Information Sciences, ISPRS Congress, Rio de Janeiro, XXV-5, 746-756.

Warner, E., S., Graham, R. W. and Read, R. E., 1996. Small format AERIAL PHOTOGRAPHY, Whittles Publishing, Caithness (Scotland), UK, p. 348.

weControl, 2009. weControl corporate website, http://www.wecontrol.ch/, (accessed March 11 2009).

Wendel, J., Meister, O., Schlaile, C. and Trommer, G. F., 2006. An integrated GPS/MEMS-IMU navigation system for an autonomous helicopter, In: Aerospace Science and Technology, 10, 527-533.

Wester-Ebbinghaus, W., 1980. Aerial Photography by radio controlled model helicopter, In: The Photogrammetric Record, 10, 55, 85-92.

Whittlesley, J. H., 1970. Tethered Balloon for Archaeological Photos, In: Photogrammetric Engineering, 36, 2, 181-186.

WITAS, 2009. WITAS - The Wallenberg Laboratory for research on Information Technology and Autonomous Systems corporate website, http://www.ida.liu.se/ext/witas/, (accessed April 8 2009).

Wzorek, M., Land´en, D. and Doherty, P., 2006. GSM Technology as a Communication Media for an Autonomous Unmanned Aerial Vehicle, In: 21th UAV Systems Conference, Bristol.

Yahama, 2009. Yahama, Sky systems corporate website, http://www.yamaha-motor.co.jp/global/about/business/sky/index.html, (accessed March 11 2009).

Yasuda, Y. and Miyatsuka, Y., 2001. Archaeological 3D visualization for Chinese fortress sites, In: GIS Development, http://www.gisdevelopment.net/application/archaeology/general/archg0015.htm, (accessed May 19 2009).

Yundong, W., Qiang, Z. and Shaoqin, L., 2008. A Contrast among Experiments in Three Low-altitude Unmanned Aerial Vehicles Photography: Security, Quality & Efficiency, In: The International Archives of the Photogrammetry, Remote Sensing and Spatial Information Sciences, ISPRS Congress, Beijing, China, XXXVII. Part B1, 1223-1227.

Zhang, C., 2008. An UAV-based photogrammetric mapping system for road condition assessment, In: The International Archives of the Photogrammetry, Remote Sensing and Spatial Information Sciences, ISPRS Congress, Beijing, China, XXXVII. Part B5, 627-631.

Zhang, C., 2009a. Photogrammetric processing of low-altitude UAV imagery, In: ASPRS, ASPRS 2009 Annual Conference, Baltimore, Maryland (U.S.).

Zhang, C., 2009b. UAV-based remote sensing of road conditions, In: ASPRS, ASPRS 2009 Annual Conference, Baltimore, Maryland (U.S.).

Zhang, L., 2005. Automatic digital surface model (DSM) generation from linear array images, Dissertation, Institute for Geodesy and Photogrammetry, ETH Zurich, Zurich, Switzerland, p. 219.

Zhao, H. and Qi, Y., 2008. The Error Analysis and Correction Method Research of the Attitude Data for the UAV Remote Sensing Images, In: The International Archives of the Photogrammetry, Remote Sensing and Spatial Information Sciences, ISPRS Congress, Beijing, China, XXXVII. Part B1, 1243-1246.

Zhou, G., Li, C. and Cheng, P., 2005. Unmanned aerial vehicle (UAV) real-time video registration for forest fire monitoring, In: IEEE International, Geoscience and Remote Sensing Symposium, 1803-1806.

ZI/Intergraph, 2009. ZI/Intergraph corporate website, http://www.intergraph.com/global/de/photo/, (accessed May 19 2009).

Zischinsky, T., Dorfner, L. and Rottensteiner, F., 2000. Application of a new Model Helicopter System in Architectural Photogrammetry, In: International Archives of Photogrammetry, Remote Sensing and Spatial Information Sciences, ISPRS Congress, Amsterdam, the Netherlands, XXXIII, B5/2, 959 - 965.

Zwicker, M., 2000. Photogrammetrische Auswertung der Siedlung Pinchango im Gebiet Palpa (Peru), Diploma Thesis, Institute of Geodesy and Photogrammetry, ETH Zurich, Zurich, p. 29.

Appendix A – Classification of UAV photogrammetry
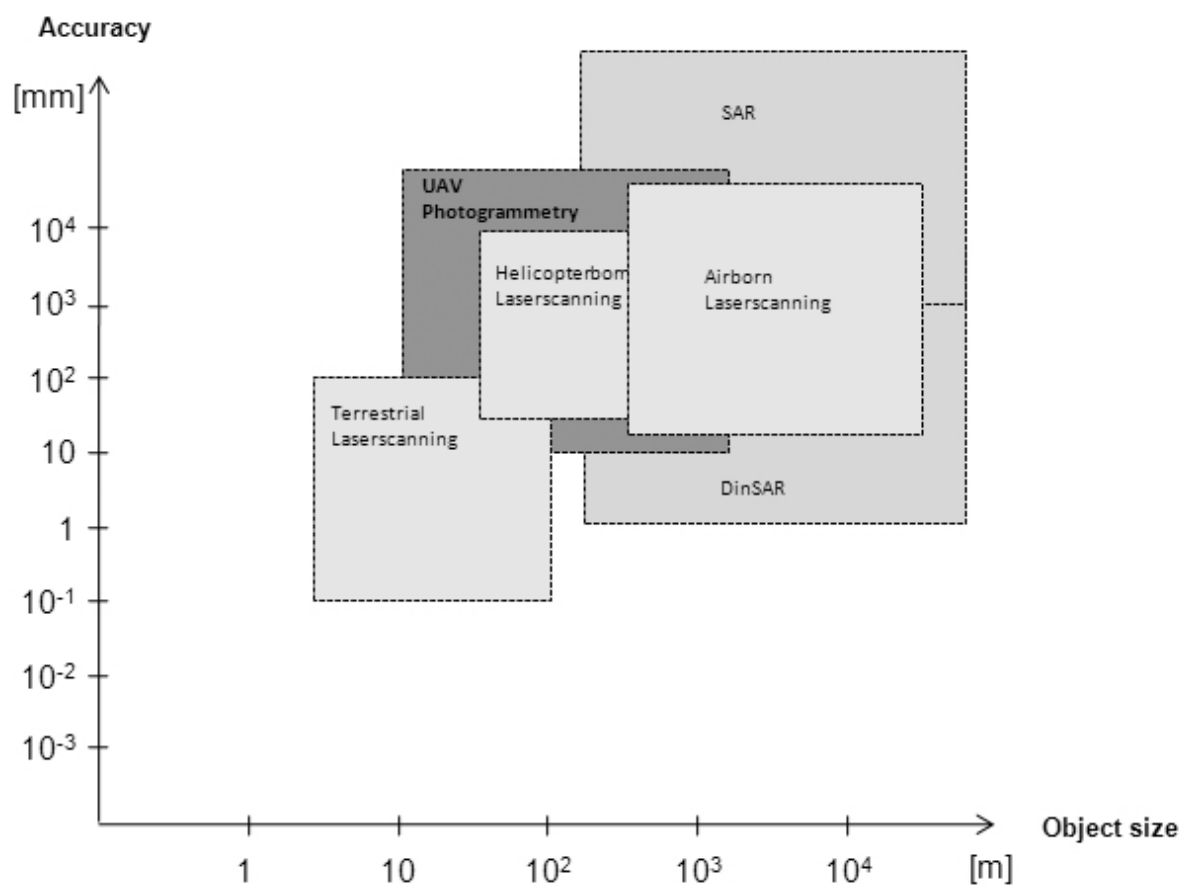
Figure A-1: The accuracy of measurement methods in relation to the object/area size. Extension to Figure 1-2.

Appendix B – Webpages related to UAVs

Table B-1: Overview of the variety of research groups, companies and open source groups related to UAVs.

| Name	Type	webpage
Aeroscout	Company	http://www.aeroscout.ch/
Aerovista	Company	http://www.aerovista.ch/
Bluebird Aero System Ltd	Company	http://www.bluebird-uav.com/
Henseleit Helicopters	Company	http://www.henseleit-helicopters.de/
orbit, geospatial technologies	Company	http://www.orbitgis.com/
US Navy Begins Development of VTUAV	Company	http://www.vtol.org/uavpaper/NavyUAV.htm
Yahaha, Aeronautics	Company	http://www.yamaha-motor.co.jp/global/about/business/sky/index.html
Airrobot	Company	http://www.airrobot.de/
Ascending Technologies	Company	http://www.asctec.de
Draganfly	Company	http://www.rctoys.com/rc-toys-and-parts/DF-SAVS/RC-HELICOPTERS-DRAGANFLYER-SAVS.html
Flying-Digicam	Company	http://www.flying-digicam.de/index.htm
Fuji Heavy Industry, Subaru	Company	http://www.fhi.co.jp/english/
Geocopter	Company	http://geocopter.nl/
HighKopter.de	Company	http://highkopter.de/
Intellicopter	Company	http://www.intellicopter.de/
microdrones GmbH	Company	http://www.microdrones.com
Micropilot	Company	http://www.micropilot.com/
Novadem	Company	http://www.novadem.com/
omnisight	Company	http://www.omnisight.ch/
Schiebel	Company	http://www.schiebel.net/
SwissUAV	Company	http://www.swiss-uav.com/swiss-uav/index.php
weControl	Company	http://www.wecontrol.ch
XeD-Shop	Company	http://www.x3d-shop.de/
Yahama	Company	http://www.yamaha-motor.co.jp/global/about/business/sky/index.html
International Aerial Robotics Competition	Competition	http://iarc.angel-strike.com/
UAV forum	Forum	http://www.uavforum.com/
Mikrokopter	Open source	http://www.mikrokopter.de
Paparazzi - The free Autopilot	Open source	http://paparazzi.enac.fr
UAVP	Open source	http://ng.uavp.ch/moin
DLR	Research Institut	http://www.dlr.de/ft/en/desktopdefault.aspx/tabid-1377/1905_read-3350/
Ithaca UAV project	The Centre of Excellence	http://www.ithaca.polito.it/projects/uav.php
Aerospace Robotics Laboratory, Stanford University	University	http://sun-valley.stanford.edu/arl.html
Carnegie Mellon University	University	http://www.ri.cmu.edu/projects/project_93.html
Georgia Tech Mobile Robot Lab	University	http://www.cc.gatech.edu/ai/robot-lab/research.html
Institut für Theoretische Elektrotechnik und Systemoptimierung (ITE)	University	http://www.ite.uni-karlsruhe.de/
Institut Geomatika	University	http://www.ideg.es/eng/
Link collection Gordon Petrie	University	http://www.weblinks.spakka.net/db/0
Micro Air Vehicle Computer Vision Platform	University	http://pixhawk.ethz.ch/
Projekt RCS²	University	http://www.dualservers.com/rc-videoflight/
The JAviator Project	University	http://cs.uni-salzburg.at/javiator/index.php
TU-Berlin	University	http://pdv.cs.tu-berlin.de/MARVIN/
UAV ETHZ	University	http://www.uav.ethz.ch/
UAV Photogrammetry	University	http://www.photogrammetry.ethz.ch/research/heli/index.html
Universities of the German Armed Forces, Munich	University	http://www.unibw.de/lrt13_2/Forschung/Projekte/UAVPF
USC Autonomous Flying Vehicle Project, Robotic Embedded Systems Laboratory, Southern California	University	http://www-robotics.usc.edu/~avatar/
Virtual Monitoring (ViMo), Fachhochschule Nordwestschweiz	University	http://www.fhnw.ch/habg/ivgi/forschung/vimo
Waterloo Aerial Robotics Group	University	http://www.ece.uwaterloo.ca/~warg/index.html
WITAS	University	http://www.ida.liu.se/ext/witas/

Appendix C – mdCockpit
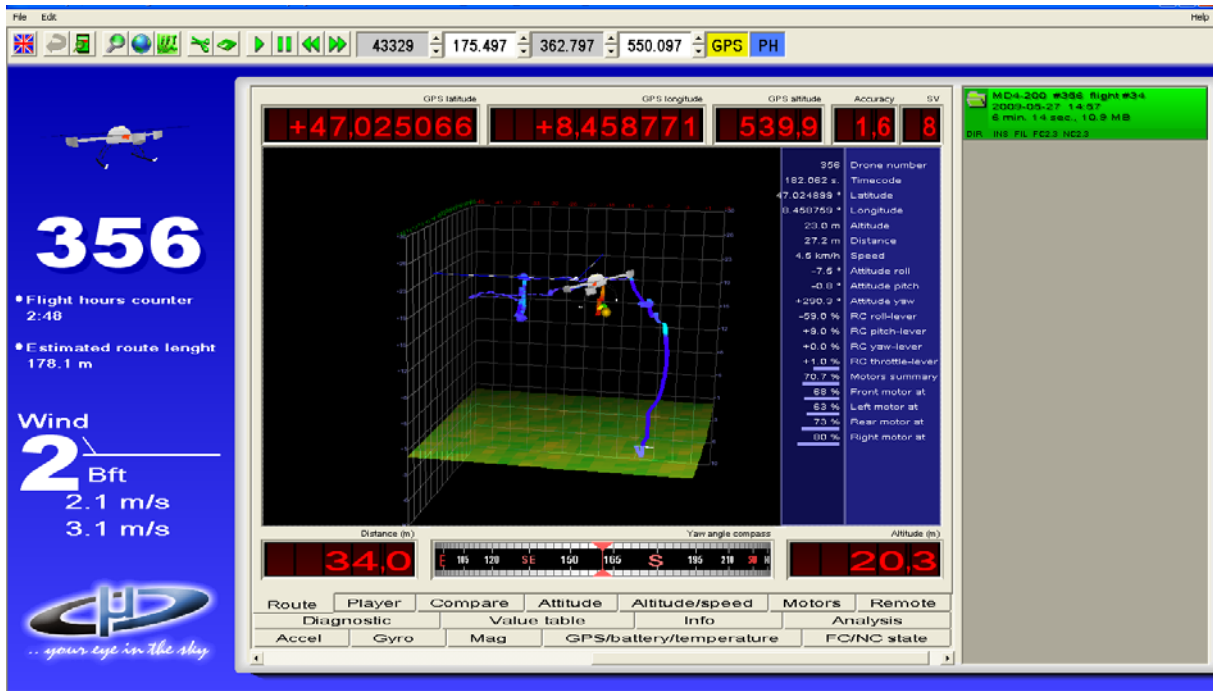
Figure C-1: Snapshot of the mdCockpit, SD-Card controller showing the flight trajectory and the attribute values of a particular point of the flight path.
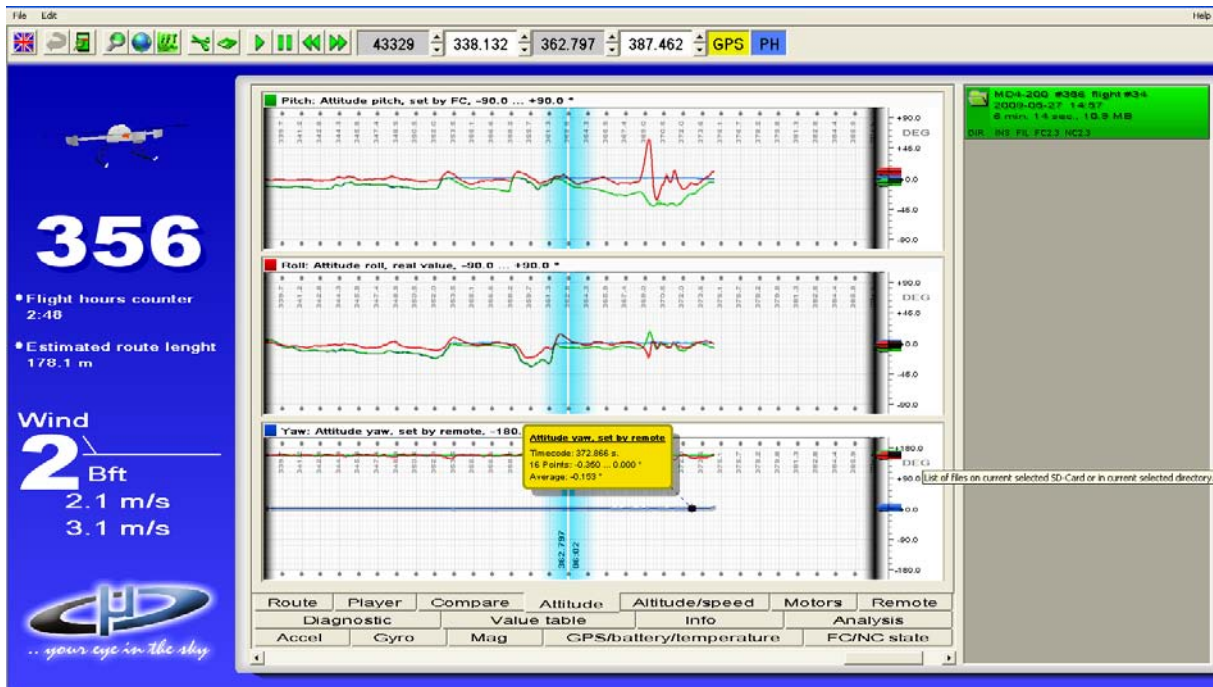

Figure C-2: Snapshot of the mdCockpit, SD-Card controller showing the reference and the measured values of the rotation angle.
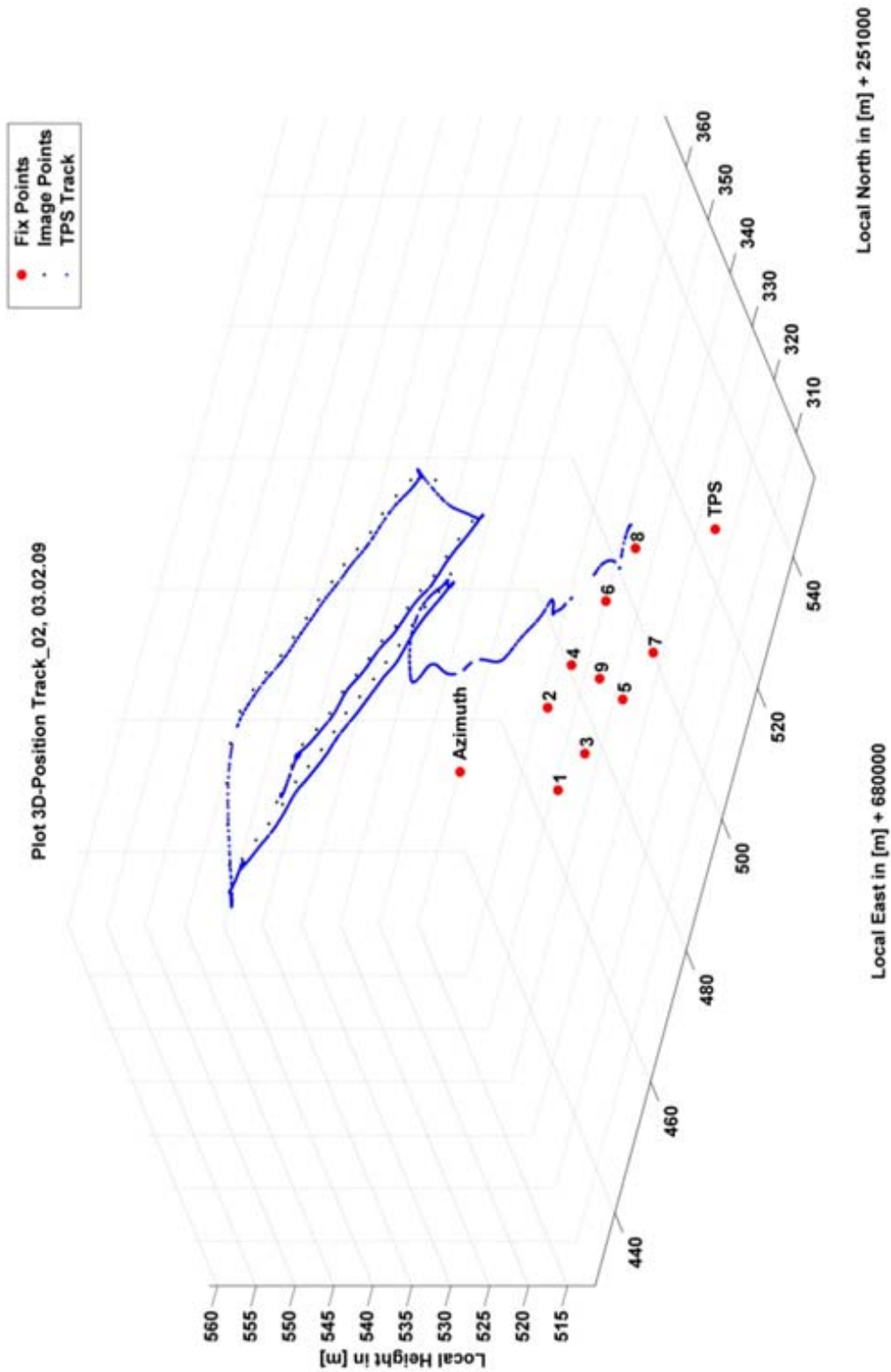
Appendix D – Flight trajectories tracking UAV

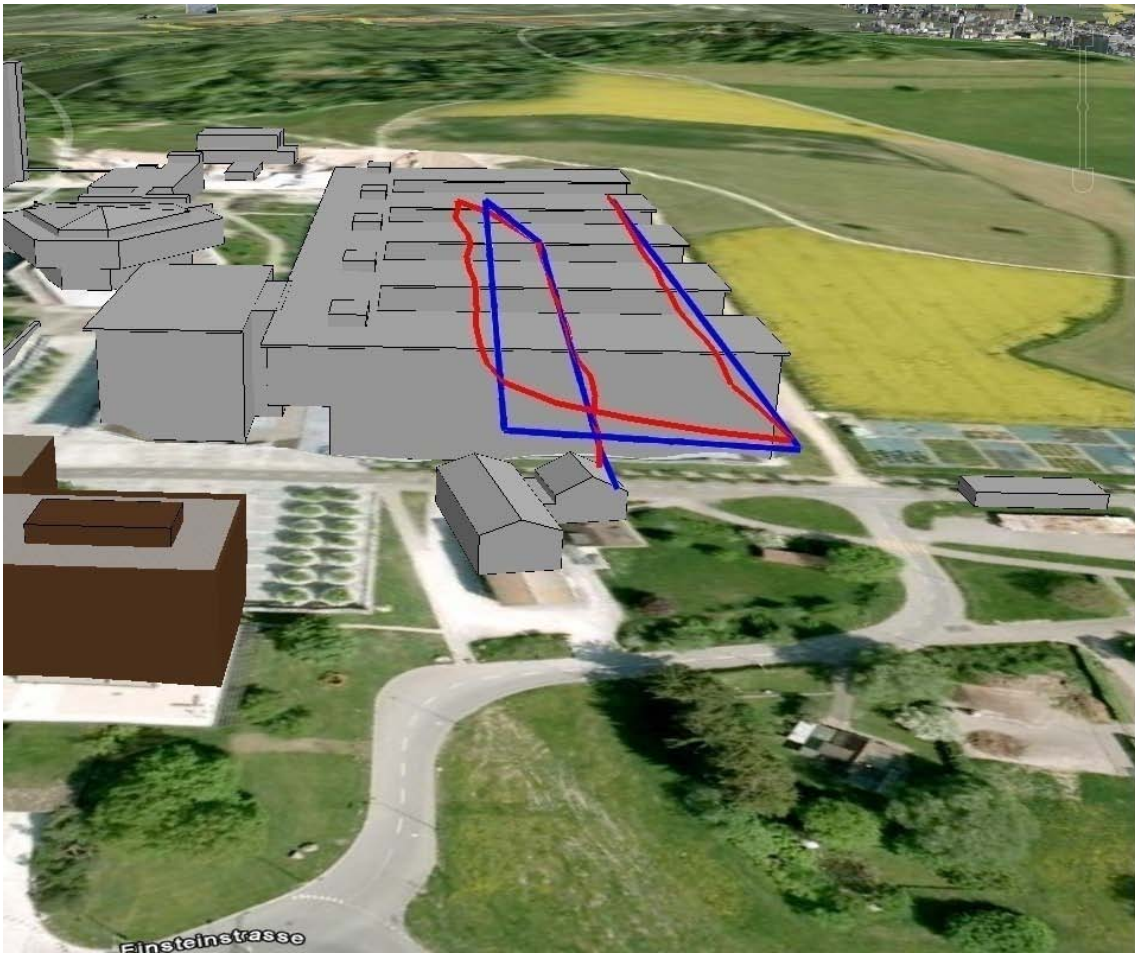**Figure D-1: 3D differences between the GPS observation and the tachymeter tracking Flight 2.**

Figure D-2: Flight trajectory planned vs. observed trajectory (wePilot1000-10g/N).

Appendix E – Accuracy INS systems

Sensor	Bias (mg)	acc. Bias (m/s2)	misalignment in mrad	axis gyro drift in deg/hr	Position error in m due bias after [s]		Position error in m due misalignment error after [s]		Position error in m due gyro drift after [s]	
					10	1000	10	1000	10	1000
Honeywell HG 1700	1	0.00981	0.1	1	0.49	4905	0.4905	4905	0.0079	7926.7
Crossbow IMU400CD-100	12	0.11772			5.89	58860			0.2854	285361.3
IMU 600 - Fiber Optic Gyro	0.05	0.00049	0.1	0.01	0.02	245.25	0.4905	4905	0.0001	79.3
The Litton LN200 system	0.3	0.00294	0.2	0.07	0.15	1471.50	0.9810	9810	0.0006	554.9
Examples for typical sensors										
Navigation-Grade (INS-IMU)	0.05	0.00049		0.015	0.02	245.25			0.0001	118.9
Tactical Grade (IMU or ISA)	0.2	0.00196		0.1	0.10	981			0.0008	792.7
Consumer Grade (sensory or ISA)	100	0.98100		100	49.05	490500			0.7927	792670.4
	500	4.90500		3600	245.25	2452500			28.5361	28536133.3

Figure E-1: Accuracy estimation of INS stand alone systems.
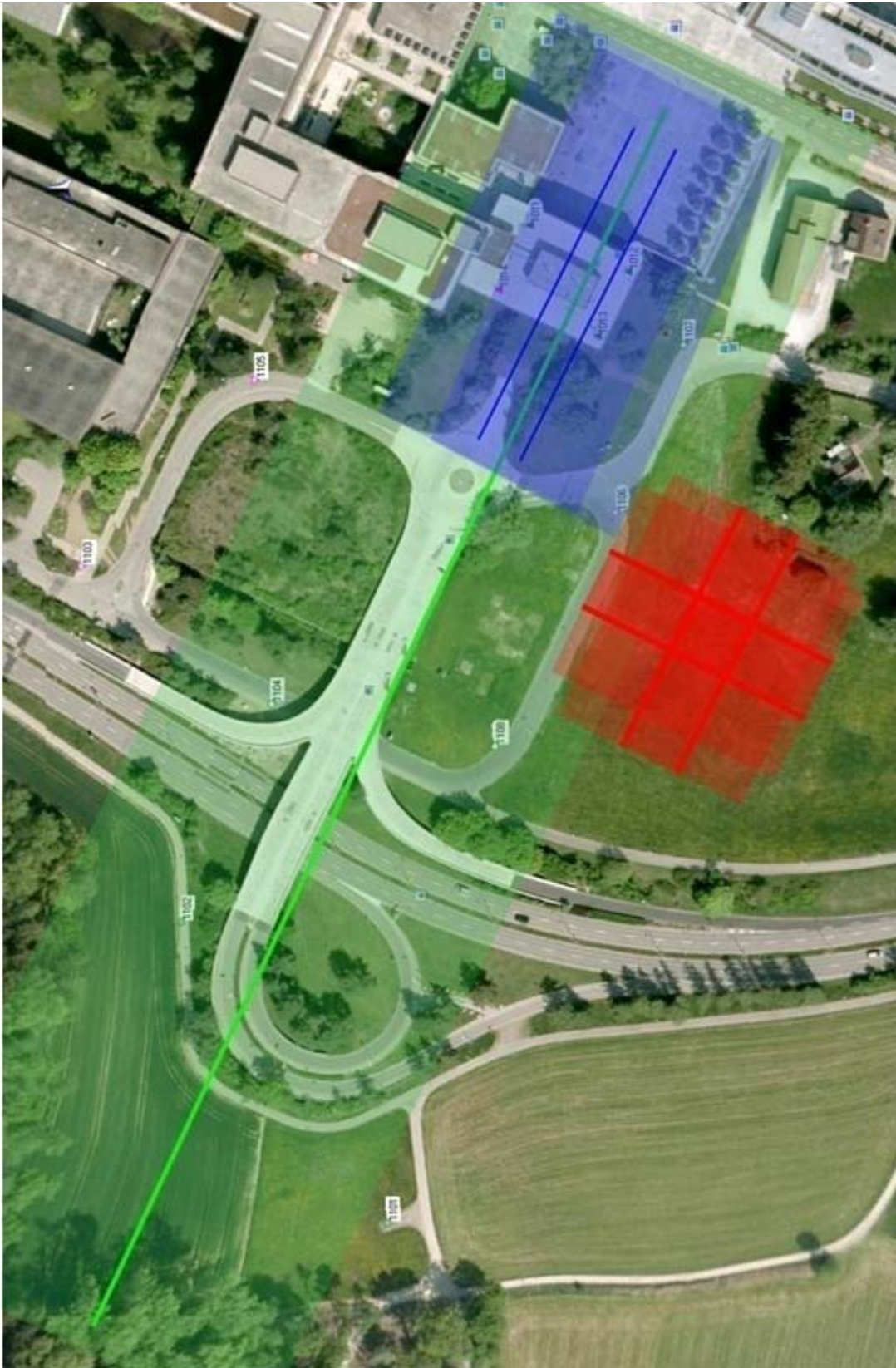
Appendix F – Test field Hönggerberg
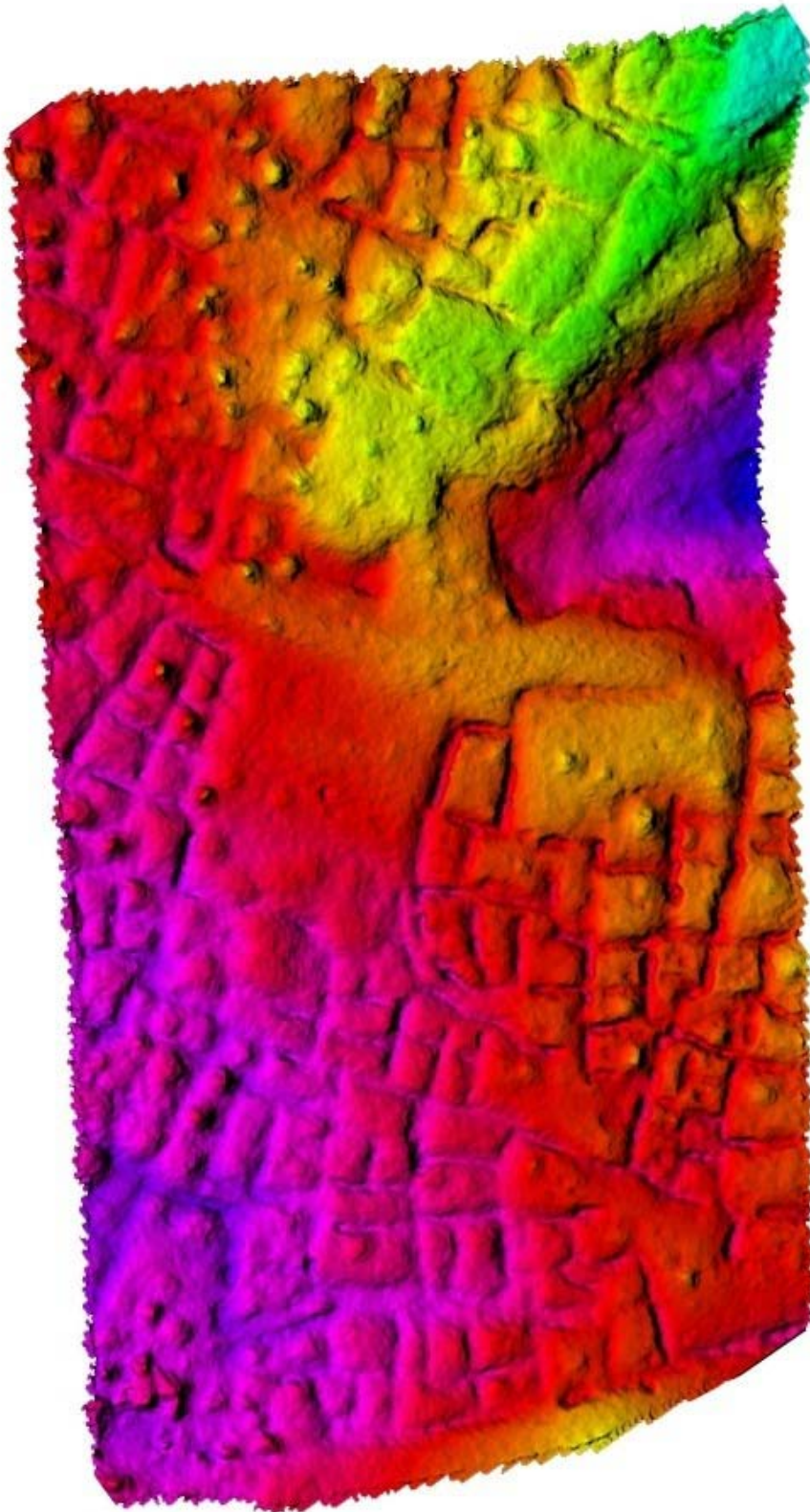

Figure F-1: Test field Hönggerberg.

Figure F-2: LiDAR test field during the data acquisition.

Appendix G – Extracted DSM Pinchango Alto

Figure G-1: Color-coded SAT-PP-DSM of the central part of Pinchango Alto.

CURRICULUM VITAE

Dipl.-Ing. Henri Eisenbeiss
Institute of Geodesy and Photogrammetry
ETH Zurich
CH-8093 Zurich

Personal:

Date of birth: December 31st, 1977
Nationality: German

Work history:

2003 to date:	PhD Candidate Doctor of Sciences expected completion 2009.
2008 to date:	Co-Chair of the ISPRS Working Group I/V - UVS for Mapping and Monitoring Applications.
Position since 2005:	Lecturer at ETH Zurich.
Position since 2004:	Lecturer for Postgraduate Course in Spatial Information Systems at ETH Zurich.
2003-2004:	Attended Postgraduate Course in Spatial Information Systems at ETH Zurich.
Position since 2003:	Teaching and Research Assistant at the "Chair of Photogrammetry and Remote Sensing" ETH Zurich.
2003:	Freelancer for Milan Flug GmbH, Schwarze Pumpe, Germany
2002:	Studies of Health GIS and UAVs at WITAS (The Wallenberg laboratory for research on Information Technology and Autonomous Systems) at Linkoeping University, Sweden.
1997-2003:	Studies of Geodetic Sciences at University of Technology Dresden (Germany) with major subjects of the study Photogrammetry/Remote Sensing and Science of Surveying.

Publications:

40 publications at conferences, in journals and book chapters since 2004. A complete list of publications is available at: http://www.photogrammetry.ethz.ch/general/persons/henri_publ.html

Projects:

Close-Range Photogrammetry:

Copan: 3D Modelling of Temple 22 (Honduras), 3D Modeling of the pre-Inca site Pinchango Alto (Peru) with terrestrial laserscanning and UAV images, Automated processing of UAV-images for the analysis of Pollen dispersal in maize (Switzerland), Landenberg (Switzerland), Accuracy analysis of the 3D-trajectory of UAVs using Tachymeter Tracking (Switzerland), Implementation of a LiDAR system into an UAV-system (Switzerland), Progressive Rockslope Failure, Phase III (Randa, Switzerland), Zurich relief in the 18th century (Switzerland)

Remote Sensing, Satellite and Aerial Photogrammetry:

3D Modeling of Machu Picchu (Peru), Processing of high-resolution satellite images, Determination of forest border lines from remote sensing data (Switzerland), Calibration and validation of ALOS/PRISM images, SAT-PP (Satellite Image Precision Processing), Evaluation of landslide potential in southern Ecuador (Tambo region), Integrating agronomic and socioeconomic aspects of reversing soil degradation by tropical legume tree by GIS analysis, Walapane (Sri Lanka), Monte Rosa east face (Switzerland), Cogear (Switzerland)

Teaching:

Eye Learn: An Interactive WEB based e-Leaning Environment in Photogrammetry and Remote Sensing

Awards:

2008:	Youth Forum Best Paper Award for "A 3D model of Castle Landenberg (CH) from combined photogrammetric processing of terrestrial and UAV-based images at the XXI ISPRS Congress, 2008 (together with Hannes Püschel and Martin Sauerbier).
2007:	Hansa Luftbild Preis 2007 for the best paper in the PFG Journal 2006 (together with Emanuel Baltsavias and Li Zhang).

Languages:

Native language:	German
Foreign languages:	English (highly competent written and oral)
	Russian, French &Swedish (basic knowledge)